

Analysis of the fatigue performance of adhesively bonded wood joints

Gaspard A. Clerc

Vollständiger Abdruck der von der Ingenieur fakultät für Bau Geo und Umwelt der Technischen Universität München zur Erlangung des akademischen Grades eines

Doktor-Ingenieurs (Dr.-Ing.)

genehmigten Dissertation.

Vorsitzender:

Prof. Dr.-Ing. Stefan Winter

Prüfende der Dissertation:

1. Prof. Dr. ir. Jan Willem G. van de Kuilen
2. Prof. Dr.-Ing. habil. Dr. h. c. Peter Niemz, ETH Zurich
3. Prof. Dr.-Ing. habil. Christian U. Große

Die Dissertation wurde am 08.06.2020 bei der Technischen Universität München eingereicht und durch die Ingenieur fakultät Bau Geo Umwelt am 12.10.2020 angenommen

Si la barbe faisait le sage, les chèvres seraient toutes docteurs.

Contents

1	Introduction	12
1.1	Background and research gap	12
1.2	Research objectives and thesis structure	13
1.3	Specific research objectives	14
2	Wood Bonding	18
2.1	Material	18
2.2	Anatomy of the bond line	19
2.3	Bonding mechanisms	21
2.4	Fracture under Quasi-static loading	23
2.4.1	Introduction	23
2.4.2	Strain Energy Release Rate	23
2.4.3	Stress intensity factor	24
2.4.4	Mode of rupture	25
2.5	Fatigue and fatigue fracture in wood and adhesively bonded wood . . .	27
2.5.1	Introduction	27
2.5.2	Strength degradation under cyclic loading	28
2.5.3	Crack propagation under cyclic-fatigue loading	31
2.6	Wood anatomy in a fracture mechanics context	33
3	Main investigation	38
3.1	Paper I - Influence of humidity and frequency on the energy dissipation in wood adhesives	38
3.2	Paper II - Reaction kinetics investigation in relation to the influence of humidity on fatigue behavior of wood lap joints	56
3.3	Paper III - Adhesive wood joints under quasi-static and cyclic fatigue fracture Mode II loads	86

3.4	Paper IV - Feasibility study on Hartman-Schijve data analysis for mode II fatigue fracture of adhesively bonded wood joints	119
3.5	Paper V - Fractography combined with unsupervised pattern recognition of acoustic emission signals for a better understanding of crack propagation in adhesively bonded wood	150
4	Additional Investigations	174
4.1	Modification of the surface properties to improve the fatigue resistance	174
4.2	Influence of the sample size on the fatigue life	174
4.3	Use of fracture mechanics for design of bonded joints	176
4.4	Application of the fatigue model on additional data sets	177
4.4.1	Comparison with fatigue design according to EC5	177
4.4.2	Application of the fatigue model on glued in rods fatigue experiment	178
5	Synthesis	182
5.1	Main findings	182
5.2	Potential for future research	183
5.3	Recommendation for fatigue testing	184
5.4	Closing words	185
6	References	186
7	Acknowledgment	192
8	Curriculum Vitae	193
9	List of Publications and Conference Papers	194

Nomenclature

1C-PUR One component polyurethane

A Maximum Energy release rate value in $[J/m^2]$

a Crack length in $[mm]$

a, b Fatigue Coefficients given in Eurocode 5: Design of timber structures

AE Acoustic Emission

A_r Area

C Compliance in $[m/N]$

C, m Experimentally determined constants for Paris equation

CFRP Carbon Fiber Reinforced Polymer

D, β Experimentally determined constants for Hartmann-Schijve equation

DMA Dynamical Mechanical Analysis

E Elastic Modulus

ELS End-Loaded Split

ENF End-Notched Flexure

EPI Emulsion-Polymer-Isocyanate

ERR Energy Release Rate

EWP Engineered wood product

F External work of load

CONTENTS

- G Physical value of Energy Release Rate in $[J/m^2]$
- G_{max} Maximum energy release rate measured in one cycle
- G_{min} Minimum energy release rate measured in one cycle
- G_{thr} Threshold energy release rate
- GLT Glued Laminated Timber
- GiR Glued in rods
- HCF High cycle fatigue
 - IC Intercell failure
 - IW Intrawall failure
- K Stress intensity factor $[N/m^{3/2}]$
- K_c Critical stress intensity factor
- k_{fat} Reduction factor for fatigue design given in Eurocode 5: Design of timber structures
- LCF Low cycle fatigue
- LEFM Linear Elastic Fracture Mechanics
- LVL Laminated Veneer Lumber
- MF Melamine Formaldehyde
- MUF Melamine Urea Formaldehyde
- N Number of cycle
- PRF Phenol Resorcinol Formaldehyde
- PUR Polyurethane
- P Load in $[N]$
- R_c Crack resistance
- R R-ratio, ratio of min stress/max stress

CONTENTS

TW Transwall failure

U Strain Energy

UF Urea Formaldehyde

W Surface Energy

w Width

WFP Wood Fracture/Failure Percentage

β_k Geometry parameter

σ_k Far Field Stress

ν Poisson's constant

σ_l Minimum stress

σ_{up} Maximum stress

σ_m Average stress

σ_0 Endurance limit

κ Constant for fatigue design given in Eurocode 5: Design of timber structures

Φ Shift Parameter for fatigue Model (see Paper II)

Λ Slope Parameter for fatigue Model (see Paper II)

Additional specific nomenclature are given at the start of the paper in the main investigation section.

Summary

Wood, as natural composite material, is generally considered to have a good resistance against fatigue loading due to its fibrous structure and viscoelastic properties. Nowadays, timber structures are generally an assemblage of several wood pieces adhesively bonded and the influence of the adhesive on the fatigue performance remains largely unknown. The influence of the adhesive properties (stiffness, presence of fibers, type of adhesive system) on the fatigue performance was investigated in this thesis. The first hypothesis was to investigate if ductile adhesives are able to dissipate a higher amount of energy per loading cycle compared to brittle adhesives. This amount of dissipated energy would not participate to damage accumulation in the bond line. This hypothesis was investigated in paper I on pure adhesive film samples and verified on adhesively bonded wood lap-shear samples in paper II. The results showed that samples bonded with ductile adhesives are able to sustain a higher number of cycles than samples glued with brittle adhesive systems. This is probably due to a more homogeneous stress distribution for the ductile adhesively bonded samples. In paper II, a new fatigue model has been developed to analyze experimental fatigue results. This model is a combination of a physical and a statistical model which allows to describe the behavior at low and high relative strengths, i.e., for the complete lifetime of the specimen. For lap-shear samples, the strength degradation with increasing number of loading cycles takes place through an accumulation of micro-damages. The loading situation, however, is different if a macro crack is present in the sample. Indeed, the modulus and strength degradation during the fatigue loading will be the result of the propagation of cracks. The influence of the adhesive properties on the crack growth was investigated in paper III and paper IV. In both papers, the sample chosen is a 4-point End-Notched Flexure specimen (4-ENF), where the crack propagation occurs in Mode II (shearing). In paper III, it was shown that the crack propagation of adhesively bonded wood joints can be described using the Paris equation. In paper IV, the domain of application of the Paris equation was expanded using the modified Hartman-Schijve equation which, for

the first time, was applied to successfully describe the fatigue fracture of adhesively bonded wood joints. It was shown in paper III and paper IV that the brittle adhesive systems have generally a slower speed of crack propagation at similar applied stress level compared to ductile adhesives. The addition of fibers to the adhesive was also shown to increase the performance of the ductile adhesive. The reason for the better performance of the brittle adhesives are investigated in paper V. A new fractography technique combined with an unsupervised pattern recognition of Acoustic Emission signals with source location was developed. With this, it was shown that in samples glued with the brittle adhesive system, the crack does not propagate in the adhesive layer but at the interface with the wood or directly in the wood. Crack propagation hence results in a slower crack speed at higher energy release rate due to the higher wood/adhesive adhesion. Hence, it appears that the development of a high-performance adhesive for fatigue loading is a complex topic as the choice of adhesive properties depend on the presence of cracks and loading situation. Further developments should investigate the modification of the surface properties of the bond line to increase the adhesion of the wood with the adhesive, allowing to combine the advantage of a ductile adhesive with a crack propagation at the wood interface.

Zusammenfassung

Holz als natürlicher Verbundwerkstoff gilt wegen seiner faserartigen Struktur und den viskoelastischen Eigenschaften allgemein als resistent gegenüber Ermüdungsbelastung. Heutzutage bestehen Holzstrukturen meist aus einem Verbund mehrerer, verklebter Holzteile und der Einfluss des Klebers auf das Ermüdungsverhalten ist weitgehend unbekannt. Die vorliegende Dissertation untersucht den Einfluss von Klebereigenschaften (Steifigkeit, Faseranteile, Klebstofftyp) auf das Ermüdungsverhalten. Eine erste Hypothese für die Untersuchung war, ob duktile Klebstoffe mehr Energie pro Lastzyklus dissipieren können als spröde Kleber. Diese dissipierte Energie würde dann nicht zur Schädigungsentwicklung in der Klebfuge beitragen. In der Publikation I wurde diese Hypothese für reine Klebstoff-Prüfkörper in Form dünner Filme untersucht und in Publikation II mittels verklebter Zugscherprüfkörper verifiziert. Die Ergebnisse zeigten, dass mit duktilen Klebern verklebte Prüfkörper eine höhere Anzahl Lastwechsel aushalten als jene mit spröden Klebstoffen. Dies ist wahrscheinlich auf eine homogenere Spannungsverteilung in den duktil verklebten Prüfkörpern zurückzuführen. In Publikation II wurde ein neues Modell zur Beschreibung des experimentell beobachteten Ermüdungsverhaltens entwickelt. Dieses kombiniert ein physikalisches mit einem statistischen Modell, damit das Verhalten bei vergleichsweise niedrigen wie auch höheren Belastungen und somit für die gesamte Lebensdauer des Prüfkörpers dargestellt werden kann. In Zugscherprüfkörpern wird die Abnahme der Festigkeit mit zunehmender Anzahl Lastzyklen durch Zunahme von Mikroschädigung bewirkt. Die Belastungsart ändert allerdings, falls im Prüfkörper ein makroskopischer Riss existiert. Tatsächlich resultiert die Festigkeitsabnahme während Ermüdungsbelastung aus Risswachstum. Der Einfluss der Klebstoffeigenschaften auf die Rissausbreitung wurde in den Publikationen III und IV untersucht. In beiden Publikationen wurde der sogenannte 4-Punkt End Notched Flexure (4-ENF) Prüfkörper (End-gekerbter Biegebalken) gewählt, bei dem Rissausbreitung in Mode II (Scherung) erfolgt. In Publikation III wurde gezeigt, dass die Rissausbreitung in verklebten Holzverbunden mit der Paris-

Gleichung beschrieben werden kann. In Publikation IV wurde der Anwendungsbereich der Paris-Gleichung mittels der modifizierten Hartman-Schijve-Gleichung erweitert, die hier zum ersten Mal erfolgreich für die Beschreibung des Bruchverhaltens unter Ermüdungsbelastung genutzt wurde. In den Publikationen III und IV wurde gezeigt, dass spröde Klebstoffe bei vergleichbarem Lastniveau im Vergleich mit duktilen Klebstoffen generell eine langsamere Rissausbreitungsgeschwindigkeit zeigen. Die Beigabe von Fasern in den Kleber führte ebenfalls zu einer Verbesserung des Verhaltens duktiler Klebstoffe. Die Gründe für das bessere Verhalten spröder Klebstoffe wurden in Publikation V untersucht. Es wurde eine neue fraktografische Methode kombiniert mit unüberwachter Mustererkennung von Schallemissionssignalen mit Quellenortung entwickelt. Damit wurde gezeigt, dass in Prüfkörpern mit sprödem Klebstoff der Riss sich nicht im Kleber, sondern an der Grenzfläche mit dem Holz oder sogar im Holz ausbreitet. Rissausbreitung ergibt daher, wegen der höheren Adhäsion von Holz und Kleber, eine niedrigere Rissausbreitungsgeschwindigkeit bei höherer Energiefreisetzungsrate. Daher scheint die Entwicklung von Hochleistungsklebstoffen für Ermüdungsbelastung ein komplexes Thema zu sein, da die Wahl der Klebstoffeigenschaften von dem Auftreten von Rissen sowie der Belastung abhängen. Weitere Entwicklungen sollten Modifikation der Oberfläche der Klebfuge studieren, um die Adhäsion von Holz mit dem Kleber zu erhöhen, was erlauben würde, den Vorteil duktiler Klebstoffe mit Rissausbreitung an der Grenzfläche zu Holz zu kombinieren.

1. Introduction

1.1 Background and research gap

The use of adhesives is essential for the wood industry as it allows to assemble small wooden elements into large engineered wood products through different bonding processes. Recently, new challenging timber structures have been designed and produced around the world, for example the Mjosa Tower in Brumunddal near Oslo with a height of 85.4 meters and the Hoho Vienna tower with a height of 84 meters. Such structures, due to their size and/or domain of application are exposed to extraordinary loading conditions. Especially, the influence of cyclic load due to winds are higher so that fatigue effects may become more prominent. Currently, the wind loads are considered as static loads for the structures mentioned above. Cyclic or dynamic loads can cause damage accumulation over long time period, those effects are only considered (according to EN 1995-2 Section 6.2 for bridges) for parts of bridges and connections that are subject to frequent stress changes due to traffic or wind loads. In this standard only few connection types are defined, glued bonds are not specified and hence the influence of the adhesive is not considered.

An adhesive accepted for an application in structural engineering wood products has to fulfill the requirements given in EN 302 (for phenolic and amino plastic adhesives) and in EN 15425 (for one-component polyurethane (1C-PUR) and emulsion-polymer-isocyanate (EPI) adhesives). These standards examine the performance of the adhesive exposed to dead load, live load, weathering, climate extremes and interactions of the previous mentioned effects by means of accelerated aging tests. The requirements for live loads do not demand any test under cyclic loading (only variable humidity conditions), implying that the requirements for an adhesive are only based on tests realized under quasi-static loading. This supposes that the properties of the adhesive under cyclic loads are correlated to the properties obtained under quasi-static loading.

In (Smith et al., 2003), a literature review found no clear influence of the adhesive on the fatigue performance of Engineered wood product (EWP). However (Bachtiar et al., 2017), showed that the performance of adhesives under cyclic fatigue loading could not be predicted from tests performed under quasi-static loading and that rigid and brittle adhesive systems are performing better under low cycle, high amplitude fatigue (LCF) whereas ductile adhesives tend to perform better under high cycle, low amplitude fatigue (HCF). The reason, explaining the influence of the adhesive properties on the performance of the wood joints loaded under cyclic fatigue loading remained unclear and required further investigation.

1.2 Research objectives and thesis structure

The main research objective was to understand which adhesive properties influence the fatigue performance of the adhesively bonded wood. The goal of these investigations is to develop an understanding of the adhesive wood bonding performance under cyclic loads, and to improve the knowledge of the fatigue phenomenon in adhesively bonded wood joints with a possible application in a design guideline. This dissertation provides a broad collection of experiments examining different mechanical aspects of bonded wood loaded under cyclic loading.

In paper I, the hypothesis presented by (Bachtiar et al., 2017) that ductile adhesives with a low modulus of elasticity are dissipating a higher amount of energy for each cycle than brittle and stiff adhesives is investigated on adhesive film samples only under cyclic loading and variable relative humidity. In paper II, the results obtained in paper I, for adhesive film samples are compared to adhesively glued specimens. Specifically, the stress-cycles curves (S-N) of glued lap-shear samples are determined for different wood moisture contents. The failure of the lap-shear samples used in paper II occurs through accumulation of micro-damages in highly stressed zones. This raises the question if the influence of the adhesive system is similar if macro-damages (crack) are a priori present in the sample. This questions was studied in papers III and IV, where the influence of the adhesive system on the damage propagation is examined by investigating the rate of crack propagation and energy release rate under cyclic fatigue loading for three adhesive systems. In paper V, a new fractography technique is combined with acoustic emission signals measured during crack propagation to explain the different behavior observed between the adhesive systems.

1.3 Specific research objectives

- **Paper I:** Influence of humidity and frequency on the energy dissipation in wood adhesives
 - Objectives: the hypothesis that *ductile adhesives with a low modulus of elasticity are dissipating a higher amount of energy for each cycle than brittle and stiff adhesives* is investigated. If ductile adhesive dissipate a higher amount of energy into heat during each cycle, this energy cannot participate to the crack propagation and may explain the better fatigue performance of ductile low elastic modulus adhesive systems.
 - Method: In order to avoid the influence of the wood (and its variability) adhesives only were tested using a Dynamical Mechanical Analysis (DMA). Samples of five different adhesive systems are exposed to cyclic loading under three different ambient moisture levels (35%, 65% and 85% relative humidity).
 - Main Results: It is shown that 1C-PUR adhesives dissipate more of the stored energy than Melamine Formaldehyde (MF) and Phenol Resorcinol Formaldehyde (PRF) adhesives. Humidity increases the dissipative processes in all PUR adhesives, especially in the polyamide fiber filled adhesive. PRF adhesive is less influenced by humidity until 85% R.H. While for all other tested adhesives the dissipative processes generally increase with higher humidity. The damping of the investigated MF adhesive increases with increasing humidity. The influence of the frequency on the energy dissipation is low for all tested adhesives in the investigated frequency range. Further fatigue tests with glued wood samples are needed to confirm the results observed on the free standing adhesive films.

- **Paper II:** Reaction kinetics in relation to the influence of the humidity on fatigue behavior of wood lap joints
 - Objectives: the hypothesis that *ductile adhesives with a low modulus of elasticity are dissipating a higher amount of energy for each cycle than brittle and stiff adhesives* is examined for adhesively bonded samples. Also, the hypothesis that *addition of fibers slow down the crack propagation and therefore improve the*

fatigue lifetime is tested on specimens glued with three different adhesives two 1C-PUR and one PRF adhesive.

- Methods: Both 1C-PUR adhesives are based on the same prepolymer with the only difference that small polyamide fibers are added to one of the adhesive (HB110). Lap-shear samples are first tested under quasi-static loading to determine their maximal strength. Then, the number of cycles prior to the rupture of the sample is measured for each sample tested under cyclic loading at approximately 30-50-85% of the mean maximal strength and at different moisture levels.
 - Main Results: The results point out that 1C-PUR adhesive without fibers can sustain more load cycles for a similar relative stress compared to the other tested adhesives. It is also observed that for high ambient moisture levels, the adhesion between the wood and the 1C-PUR is degraded, whereas it remains relatively constant for the PRF adhesive system. The correlation between the fatigue performance and the amount of energy dissipated is not sufficient to explain why the ductile 1C-PUR adhesives are performing best. If this were the case, the HB 110 adhesive containing the fibers would have the best performances (as it has the highest tan delta value in paper I). Here, the adhesive without fibers is performing better.
- **Paper III:** Adhesive wood joints under quasi-static and cyclic fatigue fracture Mode II loads
 - Objectives: In paper II, only samples without obvious defect or crack are tested. This represents a type of fatigue where microdamages accumulate until forming a macro crack which then propagates until the failure of the specimen. In paper II, only a very limited crack propagation can be observed due to the very unstable crack propagation. The presence of cracks (due to delamination or swelling/shrinking effect) is very common in real timber structures and should be specifically investigated. For this reason, this specific aspect of fatigue, the crack propagation under fatigue loading is examined in this paper.
 - Method: Adhesively bonded wood samples glued with the same adhesive tested in paper I and paper II (two 1C-PUR adhesives and one PRF) are tested under four points end-notched flexure quasi-static and cyclic fatigue loading at 5 Hz

- Main results: In the case of crack propagation, it seems that the higher adhesion of the brittle adhesive allows for the crack to propagate in the wood at a slower rate and higher energy (this hypothesis is later examined in paper V). Indeed, the brittle rigid adhesive system is performing better than the ductile 1C-PUR adhesives. A further result obtained in this paper is that the fatigue crack propagation of adhesively bonded wood joints can be described using the Paris equation based on a fracture mechanics approach.
- **Paper IV:** Feasibility study on Hartman-Schijve data analysis for mode II fatigue fracture of adhesively bonded wood joints
 - Objectives: Despite being successful for describing the fatigue crack propagation, the Paris equation (presented in paper III) has several limitations. To extend its range of application, the feasibility of applying the Hartman-Schijve equation to wood joints is investigated and published here for the first time ever.
 - Method: The same crack propagation data presented in paper III is examined using the Hartmann-Schijve equation.
 - Main Results: It is shown that this equation can be successfully applied to the analysis of the crack propagation data and that it confirms the results obtained in paper III. Also, a discussion about the application of the modified Hartman-Schijve equation in a design guideline is presented.
- **Paper V:** Fractography combined with unsupervised pattern recognition of acoustic emission signals for a better understanding of crack propagation in adhesively bonded wood
 - Objectives: Which layer in the bond line is more favorable for a crack propagation is discussed. The question is whether a crack propagation in the wood-adhesive interface is favorable in terms of energy and/or speed of crack propagation compared to a propagation at the adhesive interface.
 - Method: The acoustic emission signals obtained during the crack propagation are monitored and classified using an unsupervised pattern recognition algorithm. The classification clusters are compared with the different type of failure observed with a new fractography method.

- Main Results: It is shown that, a crack propagation in the wood interface (corresponding to link 6-7 in 2.1) is generally slower as more obstacles have to be overcome for the crack to grow through the complex wood anatomical structures. The addition of fibers in the adhesive had a similar but lesser effect.

2. Wood Bonding

2.1 Material

In all the experiments presented in this thesis, beech wood (*Fagus sylvatica* L.) is used as testing species. Even though spruce (*Picea abies* L.) is the most used species for manufacturing glued laminated timber (GLT) elements, beech wood is generally preferred for adhesive testing. This is mainly due to the higher strength of beech wood compared to spruce. Due to the low strength of spruce, the fracture of the sample is always located in the wood and not in the adhesive, and hence limits the loading of the bond line. Due to the use of beech wood for manufacturing the lap-shear samples, it was decided to use the same species for all the tests. The same three adhesives are tested in each experiment to be able to compare the effects and results in a systematic way. These adhesives come from two different adhesive systems:

- Phenol Resorcinol Formldehyde adhesive - The Aerodux 185 with hardener HRP 155 is one of the oldest industrial adhesive systems on the market. It was already used during the second world war for the manufacturing of airplanes plywood and remains in use today. Airplane components are subject to high dynamic loads (Müller et al., 2004). It represents therefore a good point of comparison to estimate the performance of other adhesives loaded under cyclic loading. It is one of the best performing adhesives for structural wood bonding, and, hence, it is often used as reference to compare the performance of other adhesives (Kläusler et al., 2013), (Clerc et al., 2017). The main disadvantage of this adhesive, aside from the dark brown color, is that it contains a high amount of formaldehyde which is carcinogenic. For this reason, the GLT manufacturers are looking for alternatives in order to avoid exposing their employees to formaldehyde.
- One-Component-Polyurethane adhesives. Two 1C-PUR adhesives were used in this dissertation, the HB 110 and the VN 3158, both produced by Henkel AG.

1C-PUR adhesives represent an interesting alternative to PRF due to the absence of Volatile Organic Compound (VOC) in the formulation and their relative ease of use (no mixing is required). An overview of the research on 1C-PUR adhesive for hardwood gluing was published by (Luedtke et al., 2015) However, their performance under high moisture conditions is not yet as good as that of PRF adhesives. The HB 110 is approved for usage in load bearing structures, the VN 3158 is however an experimental adhesive which is not certified. The VN 3158 adhesive is based on the same prepolymer as the HB 110 with the only difference between both systems being that the HB 110 contains short polyamide fibers (approx. length of 500 μm and width of 50 μm) and the VN 3158 not. 1C-PUR was used to investigate the influence of fibers on the fatigue properties.

2.2 Anatomy of the bond line

In this chapter an overview of wood adhesive bonding is presented. A bond line is an assemblage of two wood lamellas with an adhesive layer in between. Depending on the model approaches, this adhesive layer is divided into three sub-layers, the middle cohesive and the outer adhesion layers. (see Fig. 2.1). In the cohesive layer, only the portion of the adhesion layer without any contact with the wood is considered. The two adhesion layers are defined as the layers in contact with the cohesive layer of the adhesive and the wood adherent layer.

It is likely that adhesive molecules will have different properties depending on whether they are bonding with similar adhesive molecules or with the wood substrate (Ren and Frazier, 2012). The model presented by (Marra, 1992) proposed a chain like analogy to describe the fracture of the bondline. In this model the bond line is divided into 9 different layers (see Fig. 2.1) inferring that the bond is only as good as the weakest link in the chain. Link 1 is the pure adhesive phase, unaffected by the substrates and assumed to be homogeneous. Links 2 and 3 represent the adhesive boundary layer that may have cured under the influence of the substrates and is no longer homogeneous. Links 4 and 5 represent the interface between the boundary layer and the substrate and constitute the “adhesion” mechanism. Links 6 and 7 represent wood cells that have been modified by the process of preparing the wood surface and/or the bonding process itself. For example, surface preparation techniques such as sanding, planing or flaking will cause small damages in the wood cells, likely increasing the potential of failure in the bond at that location. Finally, links 8 and 9 represent the unmodified wood. In a

classically designed adhesive bond the weakest link should be the wood, meaning that failure of the bond should happen in the links 8 and 9. This was extensively discussed by (Hass et al., 2012) (Kläusler et al., 2014) as for longitudinal tensile lap-shear samples, only a weak correlation exists between percentage of wood failure and strength of the bond. This point is further discussed in paper V. A simplification of the Marra Model was proposed by (Habenicht, 2009), that divides the bond line into 3 sub-layers. This model is presented in Fig. 2.1.

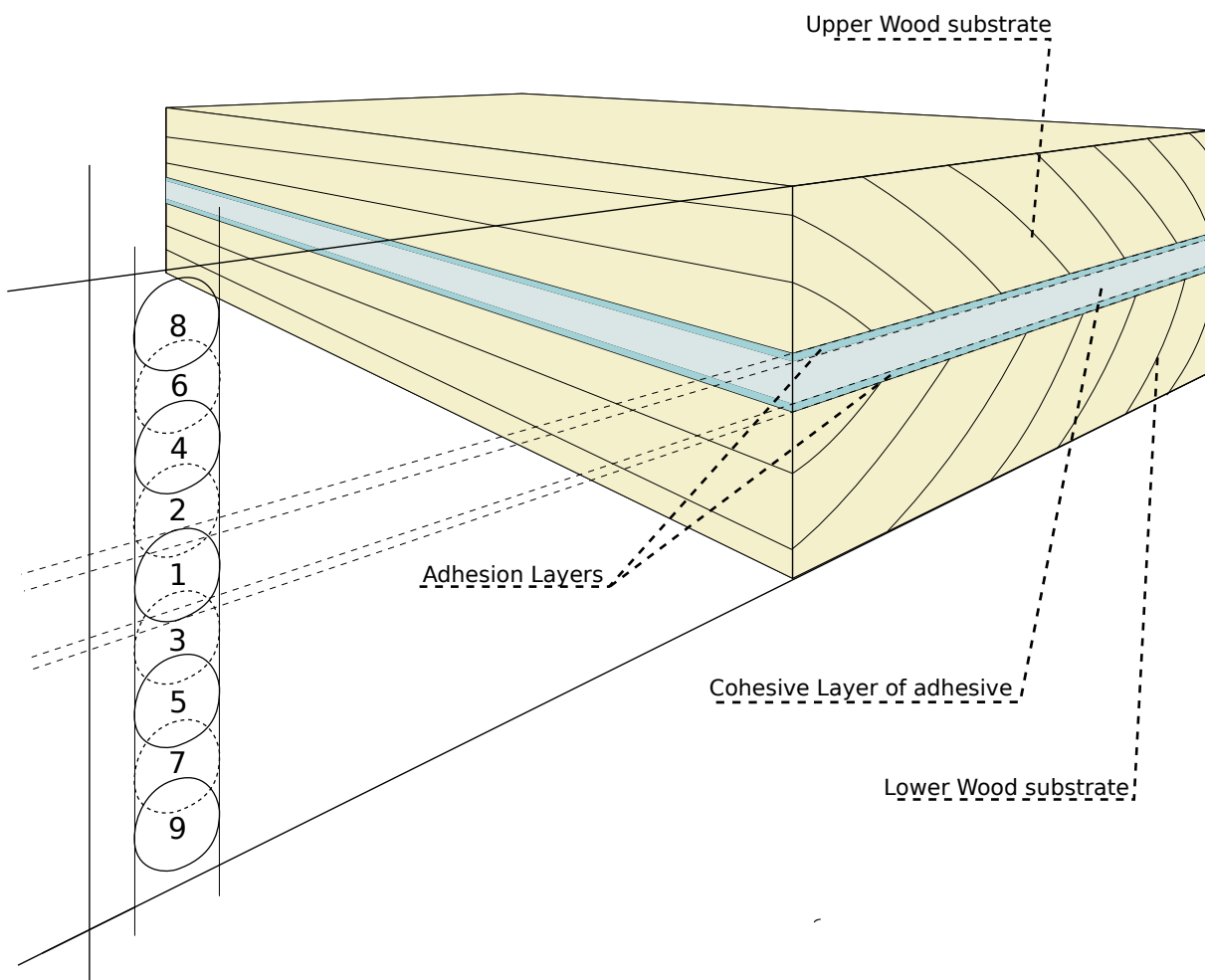


Figure 2.1 – Anatomy of the bond line with cohesive layer, adhesion layers and lower and upper wood substrate corresponding to 9 layers model from (Marra, 1992) depicted on the left

The chain-like analogy used to describe rupture in both above described models, can also be used as analogy to understand the behavior of the bond line under fatigue loading. Indeed, each layer has to contribute in order for the bondline to sustain a given stress. This analogy was used by (Clerc et al., 2017) to study the ageing behavior under moisture-temperature combination of the bond line and by (Kläusler et al., 2013) to

study the influence of the moisture in static application. In both papers, adhesive film samples were manufactured to study the influence of one parameter on the cohesive properties of the bond line without influence of the wood. This approach was discussed by (Ren and Frazier, 2012) who noted that the morphology of the adhesive is changed in contact with the wood and that therefore studying only film samples could lead to wrong conclusions. For this reason, adhesive film testing is an important addition to obtain a better understanding of wood bonding, but only together with bonded specimen testing, a comprehensive understanding of bonding of wood can be obtained. In the case of this thesis, the first question was to examine the influence of the cohesive properties of the adhesive on the fatigue behavior. It was supposed that ductile adhesives with a low elastic modulus dissipate a higher amount of energy per loading cycle and hence have better performance. This hypothesis was examined in paper I. These results were then compared with two different types of bonded wood specimen in article II and III, IV respectively.

2.3 Bonding mechanisms

Several mechanisms are used to explain the adhesive bonding of the wood.

- Adhesive penetration: It is important to distinguish the macropenetration, i.e. the penetration and fixation of the adhesive in the cavities and pores of the wood and the micropenetration, the penetration of the adhesive in the cell wall of the adherent. The importance of the macropenetration has been overstated in the past (Habenicht, 2009). Today, chemical and physical interactions and micropenetration are considered to be more significant. (Hass et al., 2012)
- Physical forces: These bonds are based on the physical affinity between the molecules of the adherent and adhesive. The Van der Waals forces include dispersive forces, dispersion forces and dipole-dipole interactions. The strongest secondary bonds are hydrogen bonds, which are most likely involved in the adhesion of wood and adhesives. These forces are typically relatively weak compared to ionic and covalent bonds, as they do not result from a chemical bond, they are also more susceptible to disturbance for example under influence of moisture.
- Covalent forces: They are chemical bonds in which atoms share electron pairs. This is the type of interaction that provides the highest binding force. As a result,

its use in the development of adhesives has always been privileged. A covalent bond is possible between the hydroxyl groups in the wood and some adhesive components such as isocyanate, aldehyde and epoxy.

The strength of the bond line is given by the type and number of molecules and their interaction between the adhesive and the adherent as well as temperature, moisture and stress state. For example, for 1C-PUR adhesives, the bonding is mainly due to physical forces, no covalent bonds are formed. These physical forces are reversible and one issue of 1C-PUR adhesives is that the reaction of the isocyanate with water is quicker than with any of the other hydroxyl-containing compounds, and when water is present, hence the water-isocyanate reaction dominates all others (Weaver and Owen, 1995). Furthermore, 1C-PUR adhesives are mainly only bonding on the surface of the wood cells, no penetration in the wood cell walls was observed by (Hass et al., 2012). On the contrary, PRF adhesives infiltrate the cell wall and they are also suspected to form primary bonds with the wood cell wall polymers (Kamke and Lee, 2007), (Yelle and Ralph, 2016). A detailed description of the chemical formulation of 1C-PUR can be found in (Clauss et al., 2011) and in (Habenicht, 2009) for phenol resin adhesives.

2.4 Fracture under Quasi-static loading

2.4.1 Introduction

The mechanics of materials is based on the concept of stress and strain theory. This simple and elegant approach has laid the foundation of classical structural engineering for several hundred years. And yet, in many practical situations, this model must be refined as in stress theory the influence of material defects is not directly considered. Indeed, using the stress theory, the materials is generally simplified as a continuum in which stress is homogeneously distributed. However, once heterogeneity or defects are present this is no longer the case. The first mechanical consideration of the influence of defects on the strength of material was published by Griffith (Griffith, 1921), hence laying the foundation of fracture mechanics. In this chapter the concepts of fracture mechanics are presented and applied to bonded wood, first considering a quasi-static loading and then the influence of cyclic fatigue loading.

Fracture mechanics can be approached with two different ways, the **strain energy release rate**, which is based on the global energy balance of Griffith and the **stress intensity factor**, which is based on the local stress distribution around a crack tip. Both approaches are summarized in the next section.

2.4.2 Strain Energy Release Rate

In a closed system, if an elastic body is deformed by an external load, there is elastic strain energy stored in the body in addition to the change in the potential energy of the load system. In this approach, the presence of a crack is accounted for in the energy balance by the surface energy of the crack areas. According to Griffith, if a crack is to grow, the total energy must either be reduced or unchanged. This may be written in terms of system equilibrium:

$$\frac{d}{dA}(F - U) = \frac{dW}{dAr} \quad (2.1)$$

where dAr is the incremental change in crack area (Ar), F the external work of load, U the strain energy and dW is the increment in surface energy (W) associated with the crack formation. In linear elastic fracture mechanics, the left-hand side is commonly referred to strain energy release rate G and the right-hand side as crack resistance R . G and R both have units of energy per unit area (e.g. J/m^2). G can be interpreted as

the energy available to grow a crack of the size of a unit area, while R_c is the energy required for propagation of a unit area of crack. Generally, the crack growth condition is written in terms of a critical strain energy release rate (ERR) G_c , which should be a material constant and independent on the sample geometry. G can be calculated for an elastic body subjected to load or displacement control using equation:

$$G = \frac{1}{2w} P^2 \frac{dC}{da} \quad (2.2)$$

where w is the width of the sample, P the load, C the compliance and a the crack length.

2.4.3 Stress intensity factor

In this approach, instead of considering the global energy state of a structure before and after the crack growth, only the local stress state at the crack tip is considered. A fracture criterion can hence be obtained which is a function of the specimen geometry, applied load and crack length:

$$K = \beta_k \sigma_k \sqrt{a} \quad (2.3)$$

where β_k is a dimensionless geometry parameter, σ_k is the far field stress and a is the crack length. The stress intensity factor (K) units are stress times the square root of length (e.g. $Nm^{-3/2}$). Once, K reaches a critical value K_c (defined as the critical stress intensity factor) a crack in the material will grow. K_c is also often referred to as fracture toughness of a material. This stress intensity factor approach was developed for assessing crack growth in metals (simplified as homogeneous isotropic materials). In the case of wood, the anisotropy and inhomogeneity of the material must be considered to determine the stress concentration at the crack tip. Furthermore, as noted by (Smith et al., 2003), the stress intensity factor approach assumes a nominally sharp crack tip, which is not necessarily the case for wood, where the crack tip in the complex structure of the material often cannot be defined as clearly as in homogeneous materials (van der Put, 2007). As wood is a natural composite material, the approach chosen in this thesis relies on the strain energy release rate. It should however be emphasized that both approaches, which are basically predicting the fracture strength of a particular structure should be equivalent. The following equation allows to reconcile the two

approaches:

$$G = \frac{K^2}{E} \quad (\text{for plane stress})$$

$$G = (1 - \nu^2) \frac{K^2}{E} \quad (\text{for plane strain})$$
(2.4)

with ν the poisson coefficient, E the modulus of elasticity.

2.4.4 Mode of rupture

The G and K values are generally expressed according to different basic modes (I,II,III) of crack opening. Each mode corresponds to a given type of load application, as shown in Fig. 2.2,

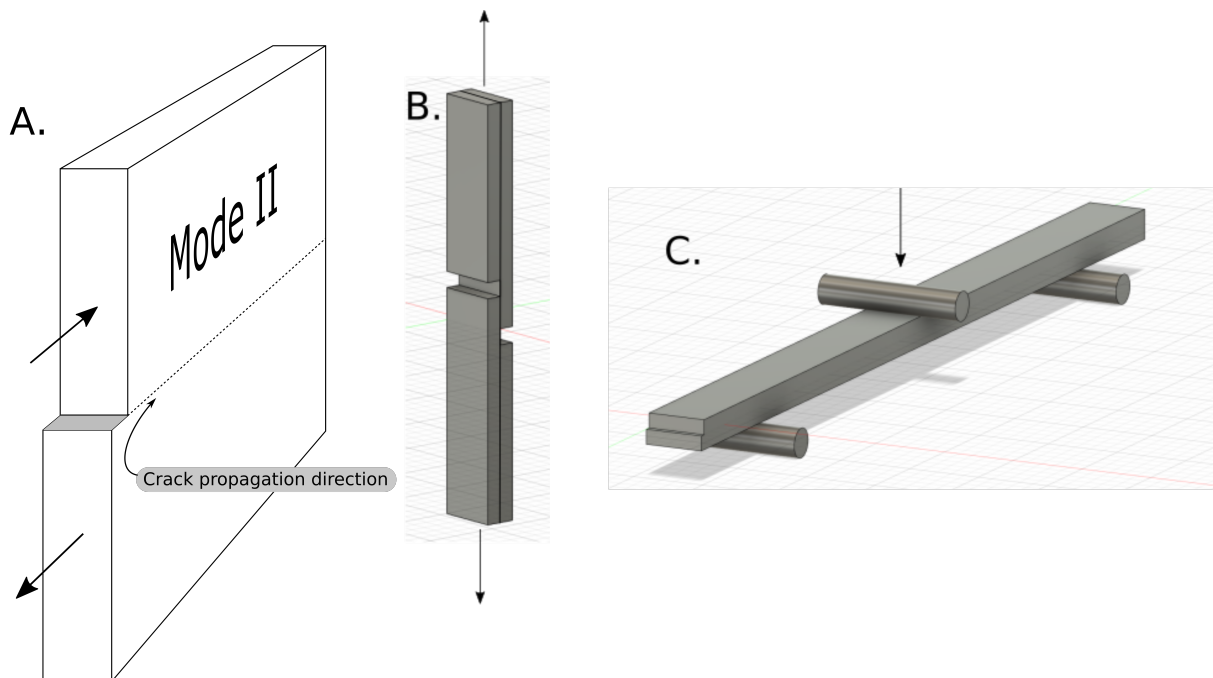


Figure 2.2 – A. Schematic drawing of load distribution corresponding to Mode II loading, B. Sample geometry of tensile shear stress sample used in paper II, C. End-notched flexure sample used in paper III and IV.

- Mode I is the opening mode, where the crack grows due to a tensile stress normal to the plane of the crack
- Mode II is the sliding mode, where the crack grows due to shear stress acting parallel to the plane of the crack and perpendicular to the crack front

- Mode III is the tearing mode, here the crack grows due to shear stress acting parallel to the plane of the crack and parallel to the crack front

Mode I is the most studied mode for most materials and also for wood. In wood structures, due to the significant anisotropy, strength in the radial, tangential direction is only 1% of that in the longitudinal direction (Niemz and Sonderegger, 2017). For this reason, mode I fracture perpendicular to the grain has received the most attention from engineers and wood scientists (Yoshihara and Satoh, 2007), (Xavier et al., 2011), (Rhême et al., 2013), (Ammann and Niemz, 2015b). This has as consequences that during the design of timber structures, load application perpendicular to the grain is avoided or should at least be minimized (Smith et al., 2003). Furthermore, considering a Glued Laminated Timber (GLT) beam loaded in bending, the main tensile stress occurs in the lower lamella of the beam. In this case, the adhesive has no influence on the design of the beam as the maximal stress occurs in the wood. If the beam is shorter, however, shear stresses become predominant and, in this case, the highest stress could occur in the bondline. Also, if a delamination or damage is already present in the bondline, due for example to inhomogeneous adhesive application or high moisture/temperature loads, high shear stresses will appear at the crack tip due to the non-linear stress distribution. For these reasons, the main investigations of this thesis focus on the study of the G properties obtained under Mode II loading as it seems more relevant for the performance of the adhesive. Mode III loading was not studied in this thesis, as it represents a less common loading situation for typical timber engineering structures. Nonetheless, its study using a similar setup as presented by (Yoshihara, 2005) could be relevant to better understand the effect of differential swelling and shrinking of the wood on the adhesive in glulam.

The G value obtained under Mode II must be directly associated to a wood property with specific orientation of the wood. With three axes of symmetry (longitudinal, radial and tangential) nine different G values exist for one type of mode loading. The complete characterization of the fracture toughness of wood would therefore imply to obtain 27 different G values for accounting for the different direction of load application considering the different wood growth axes.

The application of fracture mechanics to wood lacks a standardized testing method. This is especially true for Mode II where it is quite complex to obtain a pure mode II stress at the tip of the crack in an anisotropic material. Several geometries have been investigated by different authors to obtain pure Mode II loading (Smith et al., 2003). A comparison of different test methods applied on bonded joints between Carbon Fibre

Reinforced Polymers (CFRP) was recently published (Pérez-Galmés et al., 2018), which concluded that End-Loaded Split (ELS) test method is the most suitable method to measure the mode II fracture toughness. This test method provides large and stable crack propagation regions, it requires however a complex test fixture in comparison with the 4 point end-notched-flexure (4-ENF) test method 2.2. This method has been used to characterize laminated composite such as CFRP and adhesively bonded wood under quasi-static and cyclic loading (Martin and Davidson, 1999), (Yoshihara and Satoh, 2007). Its manufacturing is straightforward. It is however affected by friction at the adhesive layer. This effect was estimated to be negligible in the 3-ENF specimen and increased to 5.1% in the 4-ENF by (Schuecker and Davidson, 2000), who also noted that if the compliance calibration method is used as data reduction method, frictional effects will likely be overestimated. This effect remains relatively small compared to the coefficient of variation of wood properties, which is around 20%. In reality, no pure Mode I or II loading exist, and generally a combination of different modes or mixed-mode loading is encountered. This amount is however very low for 4-ENF samples, but can vary depending on the crack propagation path. (Ammann and Niemz, 2015a) examined the influence of mixed-mode fracture toughness of PRF and PUR adhesives bond lines in European beech wood, showing that the toughness of PRF and 1C-PUR bond joints performed similarly as plain wood. (Ammann and Niemz, 2015a) also noted that the failure of PRF joints was mainly located in the wood, whereas for 1C-PUR the failure was located at the adhesive interface, which confirm the results shown in paper II. This was also noted in (Ammann and Niemz, 2014), who also showed that the loading rate was positively correlated with the fracture energy for bonding joints glued with 1C-PUR, MUF and PRF. (Ammann and Niemz, 2015b) also investigated the fracture energy of glued bond joints in Mode I for 1C-PUR and PRF adhesive and (Xavier et al., 2011) for epoxy adhesive.

2.5 Fatigue and fatigue fracture in wood and adhesively bonded wood

2.5.1 Introduction

Fatigue is the process of progressive localized permanent structural change occurring in materials exposed to sustained and fluctuating loading which may culminate in crack formation and growth or complete fracture after sufficient number of fluctuations.

Typically, fatigue failure occurs at a stress intensity lower than that required to cause in-elastic behavior or fracture under monotonic loading. In this thesis, two different aspects of fatigue will be investigated. First, the strength degradation of a specimen, without macroscopic defects, under cyclic fatigue loading will be investigated. Then, the crack propagation under cyclic fatigue loading, where the energy and number of cycles needed to grow a macroscopic crack (artificially created) will be observed. Both approaches will be specified in the following sections.

2.5.2 Strength degradation under cyclic loading

Wood and wood based products are also affected by the fatigue phenomenon. In this case, damage initiates as micro cracks which eventually aggregate leading possibly to macrocracks or failure.

Due to the absence of macrodefects, LEFM cannot be directly applied. In this case, a more empirical approach is generally chosen where the number of cycles until failure of the sample at a defined relative stress is observed. First the mean maximum strength is obtained by quasi-static tests on a number of specimens. Then, a new sample is loaded under cyclic fatigue at a given percentage of this previously defined mean ultimate strength. The number of cycles until rupture is then noted. By repeating this approach at several load levels, the S-N (stress cycle diagram) is obtained as shown for example in Figure 2.3.

It is generally observed that with decreasing stress level $\sigma_{up,i}$, the number of cycles until failure increases. Once a sufficiently low stress level is applied, even a large number of cycles (often exceeding several millions, i.e., beyond the number of cycles experienced during the life-time of the part or structure for which the specimen is tested) will not yield rupture. This stress level is often interpreted as endurance limit hypothetically requiring an infinite number of cycles to failure. The existence of such a limit in composite materials or wood, is, however, still debated. The assumption of an endurance limit is a reasonable working hypothesis (similar as ERR threshold value) (Smith et al., 2003). This value depends on the type of loading, the type of specimen, the moisture content, the R-ratio and the loading frequency.

Influence of R-ratio and type of loading Table 2.1 presents a range of results from different studies about the fatigue properties of wood for different types of loading, R-ratio and loading frequency according to (Forest Products Laboratory, 1989). Most of the studies were done with a R-ratio of 0.1, meaning that the stress σ_l is 10% of the

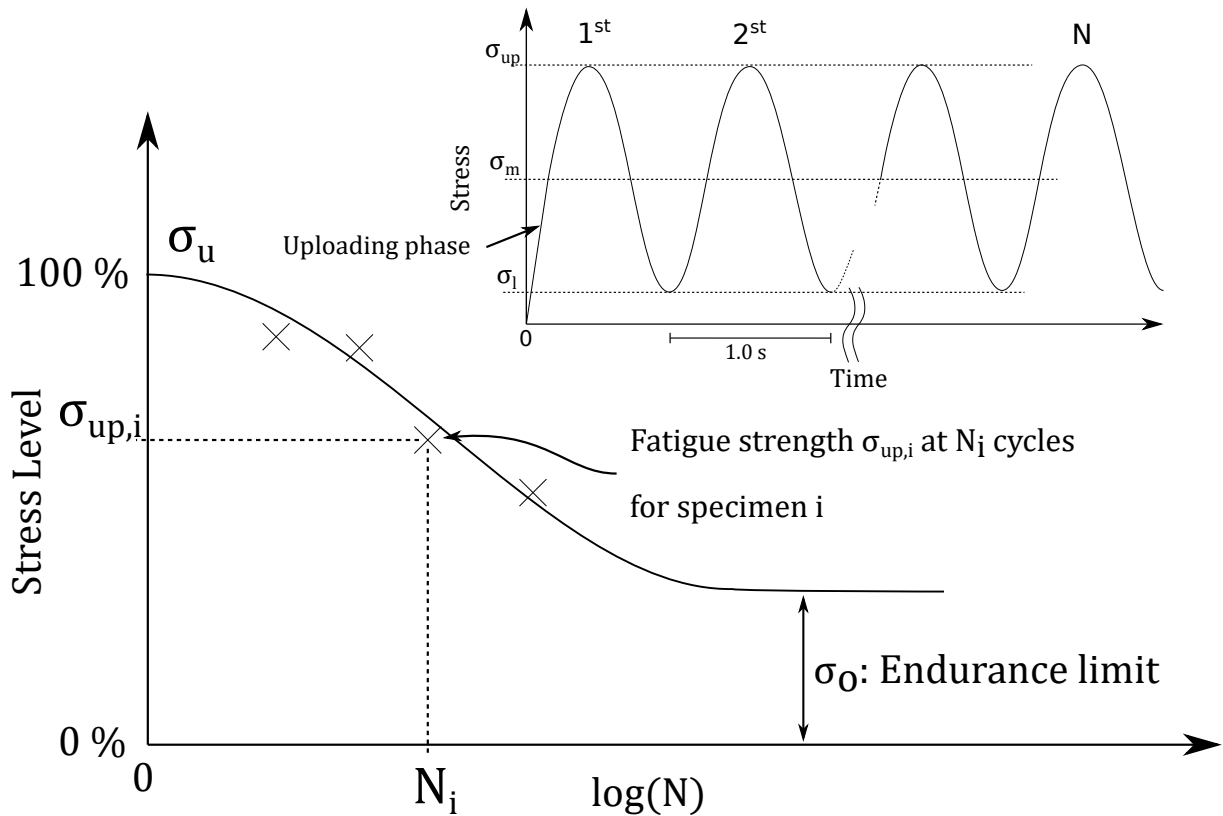


Figure 2.3 – Example of fatigue test data representation, the specimen i was tested at a stress level $\sigma_{up,i}$ until rupture after N_i cycles. In this example, a specimen was tested using a sinusoidal function with an R-ratio of $R = \frac{\sigma_l}{\sigma_{up}}$

maximum stress σ_{up} . The peak stress level, expressed as a percentage of estimated static strength, is associated with the fatigue life time in millions of cycles. In the first three lines of table 2.1, the effect of the R-ratio is demonstrated. The fatigue flexure strength decreases as R-ratio range decreases. This was also confirmed by (Tsai and Ansell, 1990), which studied the effect of R-ratio on $\sigma - N$ curves for sliced African mahogany LVL loaded in flexure, demonstrating that as the R-ratio approaches unity (which corresponds to static stress), the fatigue life increases. On the other hand, fully reversed load results in the shortest fatigue life. For other types of loading, it can be noted that fatigue strength is slightly lower in shear than in tension parallel to the grain. Also, fatigue strength in compression parallel to the grain is high compared with other properties. The influence of different waveforms studied by (Okuyama et al., 1984), demonstrated that square waves are the most damaging due to their highest stressing rate and longest residence period.

Table 2.1 – Influence of the Type of loading, R-ratio and Loading frequency on the peak stress level and fatigue life according to (Forest Products Laboratory, 1989)

Type of loading	R-ratio	Loading Frequency [Hz]	Peak stress level [%]	Fatigue life, N (10 ⁶ cycles)
Flexure	0.45	30	45	30
	0.0	30	40	30
	-1.0	30	30	30
Tension	0.1	15	5	30
	≈0.0	40	60	3.5
Compression	0.1	40	75	3.5
Shear	0.1	15	45	30

Influence of the loading frequency According to (Forest Products Laboratory, 1989), no clear relation has been established between the effect of the loading frequency and the fatigue strength. However, (Okuyama et al., 1984) showed that the number of cycles to failure increase with increasing loading frequency for compression and tension. This was confirmed by (Clorius et al., 2000) which also demonstrated the opposite for compression perpendicular to the grain where it was noted that the number of cycles to failure decreases with increased frequency. (Bach, 1975) noted that for compression parallel to the fiber the time to failure is inversely proportional to the loading frequency. (Clorius, 2002) concludes that the effect of frequency should be considered with the interaction of the duration of load and the loading direction. The loading frequency must be selected to avoid an increase of the specimen temperature which could modify the specimen properties. (Clerc et al., 2017) noted a modification of 1C-PUR adhesive properties (increase of rigidity) after several weeks exposure at a temperature of 70°C. The temperature resistance of the adhesive is however dependent of the exact chemical formulation. The wood substrate properties show little influence to a temperature increase below 100°C. (Myslicki, 2016) proposed a short-time procedure at a frequency of 5 Hz without temperature increase in the wood. It should however be mentioned that a higher loading frequency means a higher average loading rate which could possibly also influence the fatigue strength. For bridges, pedestrians induce frequencies in the range of 0.8-2 Hz (Ingólfsson et al., 2012), whereas for cyclic wind loads the frequencies are in the range of 0.01 to 1.0 Hz (Hirsch and Bachmann, 1995). In paper III and IV a loading frequency of 5 Hz is chosen while in paper II the samples are loaded with a frequency of 1 Hz.

Influence of the adhesive The influence of the adhesive on the fatigue strength is also a discussed point. Based on flexural fatigue results (Tsai and Ansell, 1990) concluded that solid wood and laminated wood do not fundamentally differ in fatigue behavior. This point is however discussed by (Sterr, 1963) who observed that the fatigue strength of laminated beams is 23 % higher than solid beams, density and moisture being equal. Also, the influence of the type of adhesive is not evident, (Ota and Tsubota, 1967) Ota and Tsubota suggested that the type of resin does not affect the fatigue behavior, while (Tsai and Ansell, 1990) mentioned that urea resin to be marginally better than phenol resin on laminated Japanese cypress. In the context of this thesis, no experiment was designed to compare solid wood and laminated wood. As nowadays, most of the timber structures are composed of GLT or LVL elements, it was decided to focus solely on the influence of the type of adhesive on the fatigue behavior. More recently, (Aicher and Stapf, 2010) showed that lumber finger joints glued with a one-component polyurethane are sensible to the fatigue phenomenon under constant or cyclic loading but that once released from loading the residual strength of run-out specimens (2 million cycles) is equal to the quasi-static strength prior to testing.

2.5.3 Crack propagation under cyclic-fatigue loading

In Linear Elastic Fracture Mechanics (LEFM) under monotonic loading, crack propagation occurs once the crack tip stress intensity reached the critical value for this material. Under cyclic-fatigue loading, however the crack growth happens at a value well below the critical value (K or G). The fracture mechanics approach consists in relating the change in crack length da over a number of load cycles dN to the range of stress intensity factor, this relationship can take the form of:

$$\frac{da}{dN} = f(\Delta K) \quad (2.5)$$

where a is the crack length, N is the number of cycles at a range intensity factor ΔK . In equation 2.5, da/dN is as the crack length growth per load cycle. Intuitively it can be expected, that the greater the stress range at similar absolute stress, the faster the crack grows. Using this simple empirical assumptions, different types of functions can be used to model equation 2.5. (Paris and Erdogan, 1963) compared different crack propagation laws and proposed a relatively simple power model to describe crack

propagation:

$$\frac{da}{dN} = C(\Delta K)^m \quad (2.6)$$

where C and m are experimentally determined constants. The original formulation of equation 2.6 used the stress intensity range ΔK as it was mainly applied on metals. For composites, as stated earlier, the use of the strain energy release rate is generally preferred. From a fracture mechanics point of view, the stress intensity factor is proportional to the square root of the energy release rate $K \approx \sqrt{G}$ according to equation 2.4. Several formulations are commonly used, G_{max} (maximum ERR), G_{min} (minimum ERR), $\Delta G = G_{max} - G_{min}$ or $\frac{G_{max}}{G_{min}}$. In Figure 2.4, a typical fatigue crack growth diagram is shown. The x-axis represents the energy release rate. The y-axis ($\frac{da}{dN}$) is the crack increment over one cycle. Both axis are displayed using on a logarithmic scale. Generally, this diagram is separated into three distinct regions:

- Region I: For low energy release rate, the crack increment becomes smaller leading to an asymptotically small crack growth. The value G_{thr} is defined as the threshold ERR below which no crack growth occurs.
- In region II the crack growth is linear (if both axes are plotted in a logarithmic scale). The Paris equation can be applied only in this region.
- Region III: for high energy release rate, the crack increment per cycle increases leading to the rupture. The ERR value A correspond to the maximum ERR measured during one quasi-static test.

Paper III in the main investigation section explores the applicability of the Paris equation to adhesively bonded wood.

The Paris equation is only valid to describe the stable crack growth in region II of the fatigue test. No information can be gained on the behavior in fast/slow crack growth regions. An estimation of the G_{thr} value would be especially valuable for design purpose in order to estimate the ERR below which no crack propagation occurs. To extend the Paris-equation beyond the linear fatigue crack growth range, (Hartman and Schijve, 1970) proposed a new equation for the study of aluminum alloys which was changed by (Jones et al., 2012) as modified Hartman-Schijve (HS) equation to represent Mode I, Mode II, and later Mode I/II delamination growth in composites, according to equation 2.7.

$$\frac{da}{dN} = D \left(\frac{\sqrt{G_{max}} - \sqrt{G_{thr}}}{\sqrt{1 - \sqrt{G_{max}/A}}} \right)^\beta \quad (2.7)$$

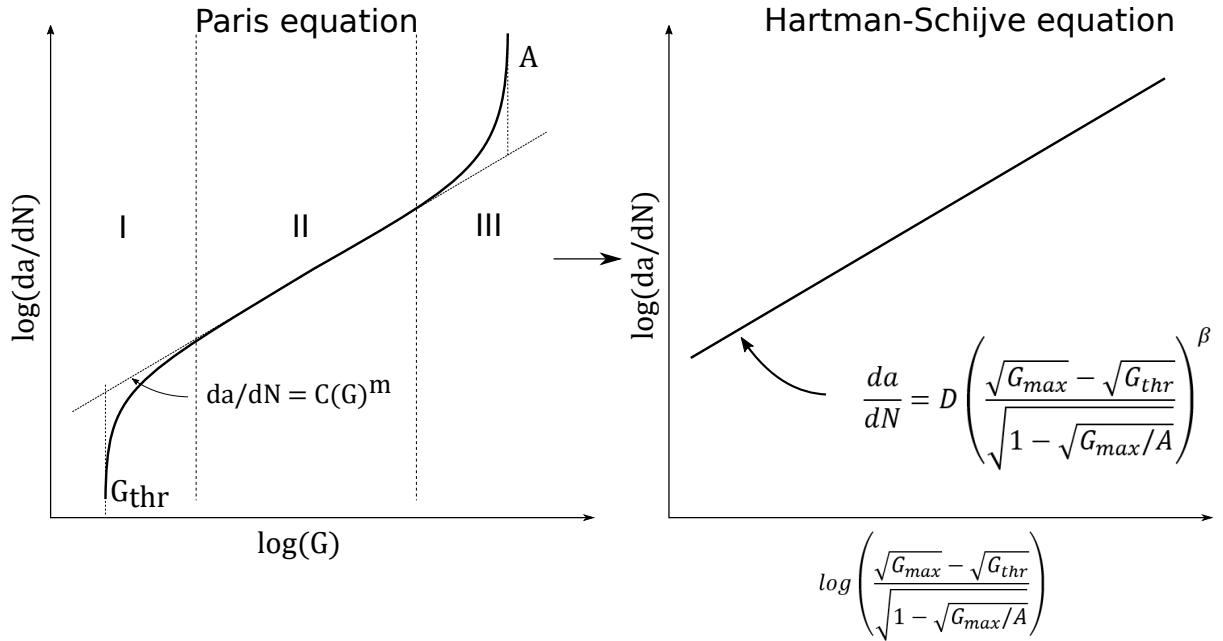


Figure 2.4 – Typical fatigue crack-growth diagram with three distinct crack growth regions: Region I, small ERR leading to asymptotic small crack growth, Region II: linear crack growth, Region III: high ERR leading to rupture

where a is the crack length, N the number of cycles, G_{max} the maximum ERR measured during one cycle, G_{thr} the threshold ERR value, A the maximum ERR value and D , β being fit parameters. Using the HS-equation, the complete data set can directly be used for analysis. In comparison, data analyzed with the Paris equation should be carefully chosen so that only the linear part of crack growth is analyzed. However, a more refined data reduction method is needed to be able to estimate the four parameters for the HS-equation with sufficient accuracy (instead of two for the Paris equation). Furthermore, two of the HS-equation (A and G_{thr}) have a physical meaning as described above, whereas the parameters of the Paris-equation are only fit parameters. The application of the Paris equation and of the Hartman-Schijve equation to crack propagation in adhesively bonded wood is specifically examined and further developed in paper III and IV respectively.

2.6 Wood anatomy in a fracture mechanics context

In this section, a brief description of the wood anatomy is given with an emphasis on its influence on the failure mechanisms. Three types of fractures can be observed at the wood cell level: intercell, intrawall, and transwall, as illustrated in Figure 2.5.

Intercell failures (IC) occurs at the middle lamella and represents the separation of cells. Intrawall failure (IW) refers to failure within the secondary wall, most often at the secondary wall S2/S1 interface. When the fracture path cuts across the wall, the failure is described as transwall (TW). Several authors suggest that different failure modes exist between static and fatigue loading. For compression loading, (Kollmann, 1968) noted a typical failure pattern due to the buckling of tracheids. A similar failure pattern was observed by (Tsai and Ansell, 1990) on the compression side of Khaya laminates bending specimen. In tension, the fatigue damages are more difficult to distinguish from quasi-static damages. The main weakness in the wood cellular structures is in the transverse to the grain direction. Under tensile loading, small defects in the wood can generate shear loading which can then result in slippage between and within the cell wall layers, cracking in secondary wall layers and longitudinal splitting along the grain. High density changes in the interfaces latewood-earlywood are likely to generate such failures, as observed by (Tsai and Ansell, 1990) on Sitka specimens. They also also noted that the possible failure mechanism of wood under tension loading still needs to be investigated. The previous observations were however all recorded for softwood. In hardwoods, failure results in an extremely complex fracture surface with transwall failure that follows the S2 microfibril angles in cells having a thick S2 layer. (Smith et al., 2003).

Additionally, the influence of the bond line on the failure mechanisms must be considered. The study of the failure modes of glued in rods in LVL and glulam showed that with increasing glue-line thickness, the percentage of failure at the resin-rod interface (for a 2mm glue-line thickness) (Madhousi and Ansell, 2004) increases. The highest percentage of wood failure was observed for a 0.5mm glue-line thickness, the authors noted ruptured cells due to splitting under fatigue loading. However, 0.5mm is still relatively thick in comparison to a max 0.1 mm glue-line thickness, common for surface bonding in glulam. Also, a comparison of the failure mechanisms observed for glued in rods with surface gluing should consider that higher local stresses in the vicinity of the rod are obtained. In Figure 2.6, two examples of the influence of the adhesive and the wood anatomy on the crack propagation path are shown.

The samples shown in 2.6 are lap-shear specimens according to EN 302-1. In Figure 2.6, the original adhesive is shown in dark blue for the 1C-PUR and in black for the PRF. After failure, the samples were re-bonded using an adhesive with a fluorescent additive. The cross-section of the sample was then observed under a UV-microscope, the crack line is shown in light blue. Hence, it can be seen that the crack tends to follow weak

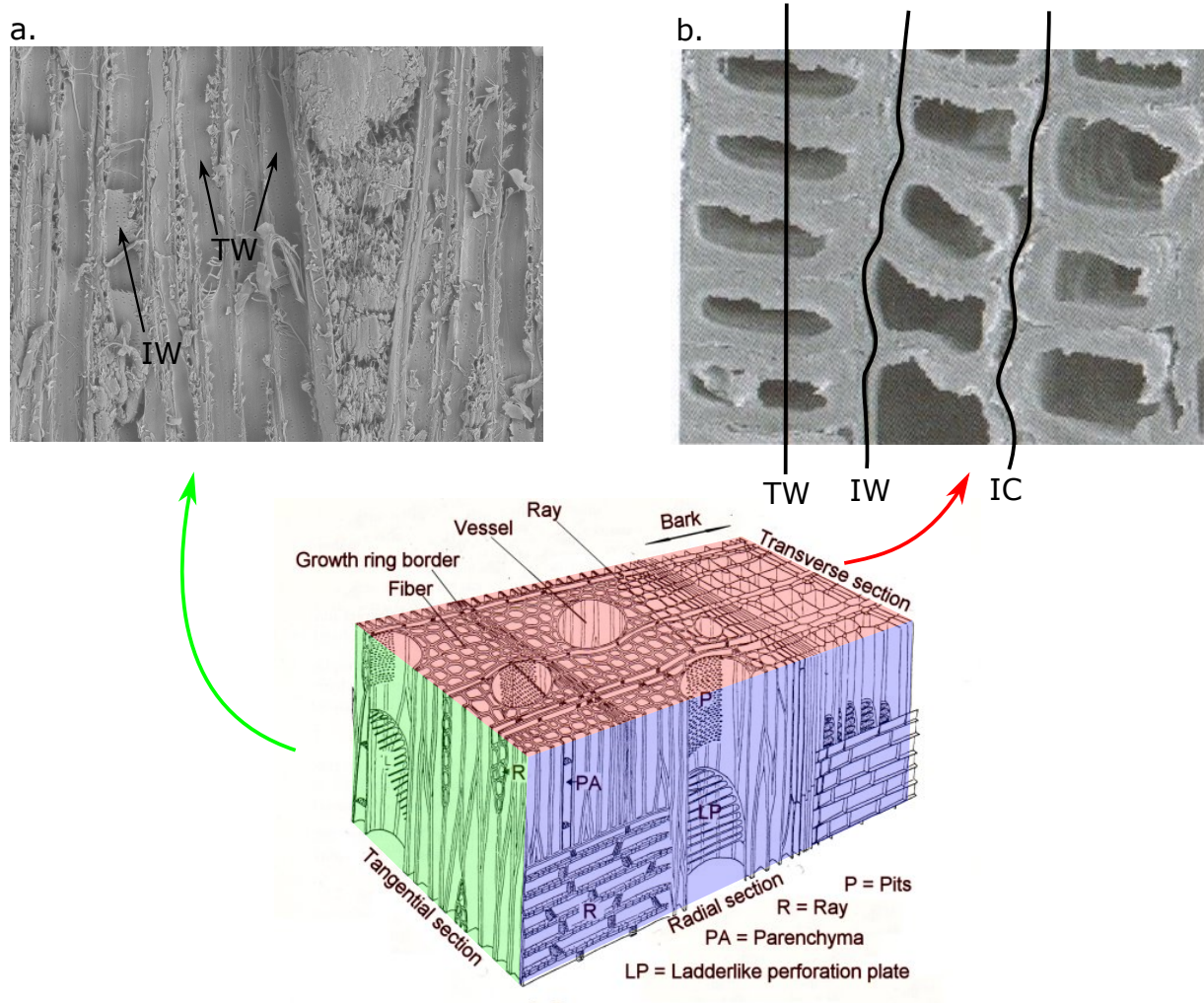


Figure 2.5 – a. Example of crack Intrawall and Transwall (TW) failure in Beech wood - b. Example of Transwall, Intrawall (IW) and Intercell (IC) failure (acc. to (Smith et al., 2003) for spruce) Main anatomical cuts for beech wood

points of the wood anatomy, for example zones with a high concentration of vessels. Further, it is possible to observe multiple fracture lines. These examples also show that different fracture layers are possible for the same samples, with a crack propagating through the cohesive layer, then the adhesive and the wood for the same sample. It should however be noted that the influence of the wood anatomy is possibly exaggerated compared to beech samples as ash wood is a ring-porous hardwood. In beech wood the vessel distribution is more diffuse porous, whereas for ash wood most of the vessels are concentrated at the annual ring transition. One common difficulty in the study of fracture behavior is that description of the fracture can only be done once the sample has failed. It is hence difficult to understand which mechanisms are leading to the failure and how the damages accumulate. Recent investigations combined fractography

analysis with Acoustic Emission (AE) measurement to gain a better understanding of the damage development (Baensch, 2015). AE testing is based on analyzing acoustic waves caused by rapid stress changes in materials. This technique is highly sensitive, quasi-nondestructive, with a high-time resolution ($\mu s - ms$) and has been applied successfully to in-service inspection as well as material characterization (Ando et al., 2006), (Bertolin et al., 2020). An overview of investigation using Acoustic emission in delamination investigation is presented by (Bohse and Brunner, 2008). In comparison with industrial composites, few studies use AE for damages characterization of wood samples and even less for adhesively bonded wood. A more detailed state of the art summary of the use of AE to characterize wood and bonded wood fracture can be found in paper V.

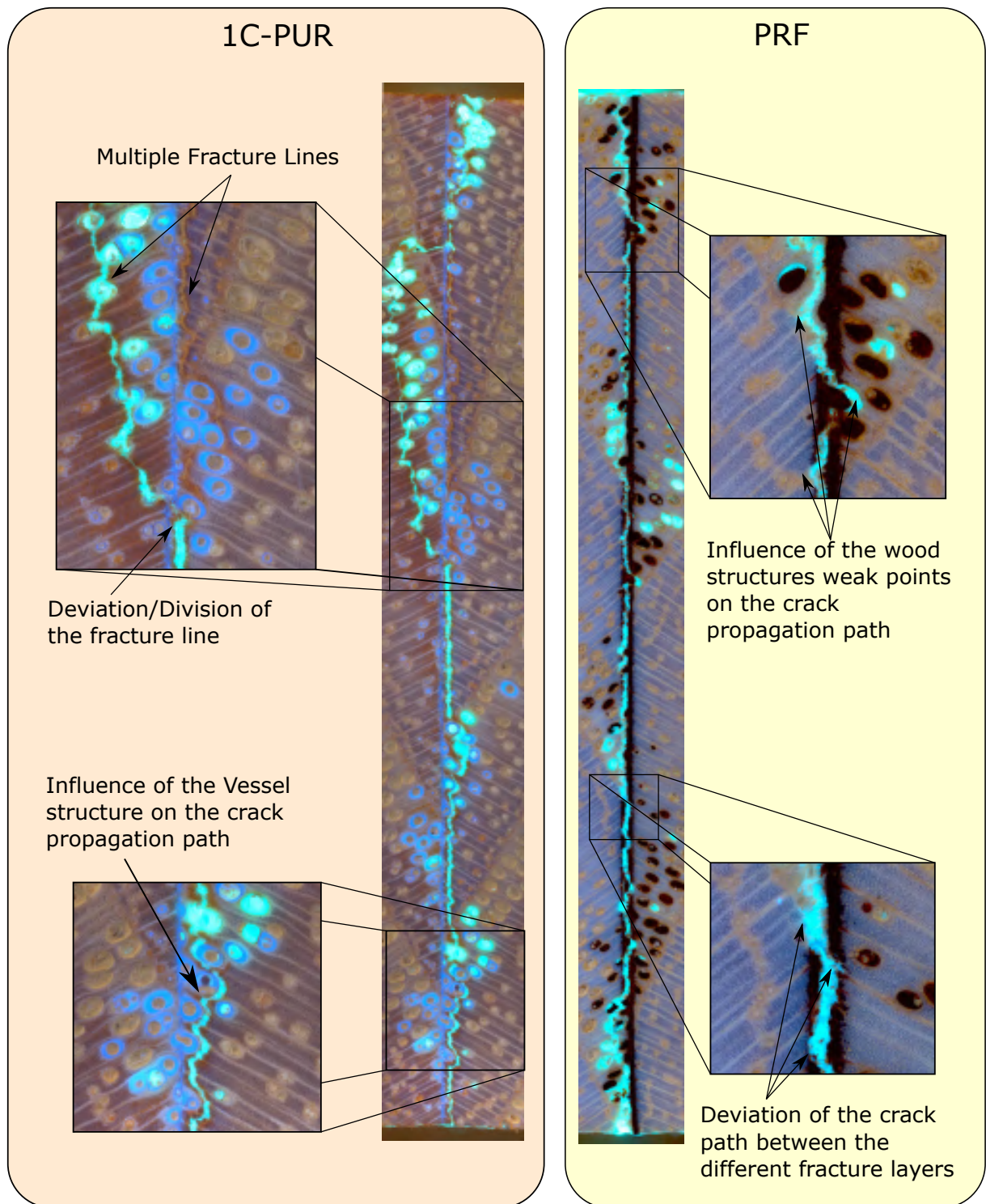


Figure 2.6 – Influence of the adhesive system on the crack propagation path in ash Wood. On the right side, the PRF system original adhesive is shown in black and on the left side the 1C-PUR original adhesive in dark blue. The crack path is shown with a light blue fluorescent adhesive.

3. Main investigation

3.1 Paper I - Influence of humidity and frequency on the energy dissipation in wood adhesives

Paper I

International Journal of Adhesion and Adhesives 92 (2019) 99-104

Influence of humidity and frequency on the energy dissipation in wood adhesives

Tina Künniger^{a,*}, Gaspard Clerc^{b,d,*}, Sébastien Josset^c, Peter Niemz^b, Frédéric Pichelin^b, Jan Willem G. van de Kuilen^d

- a. Empa, Swiss Federal Laboratories for Materials Science and Technology
Laboratory for Applied wood Materials
Überlandstrasse 129
CH-8600 Dübendorf

- b. Bern University of Applied Sciences
Architecture, Wood and Civil Engineering
Solothurnstrasse 102
CH-2500 Biel

- c. Henkel & cie. AG
Industriestrasse 17a
CH-6203 Sempach Station
Switzerland

- d. Technical University of Munich
Wood Technology Munich
Winzererstrasse 45
DE-80797 München

*Joint first author

Abstract

In this paper, the frequency dependent energy dissipation of typical wood adhesive under cyclic stress was studied on film adhesive samples. Three moisture-curing one component polyurethane (1C-PUR) adhesives with relative ductile behavior, one melamine formaldehyde (MF) and one phenol formaldehyde resorcinol (PRF) adhesives both with a more brittle behavior were prepared to study the viscoelastic properties at different relative air humidities (RH). Dynamic Mechanical Analysis (DMA) in tensile mode was used to determine loss modulus, storage modulus and loss factor Tan Delta on free standing adhesive films. It has been shown that 1C-PUR adhesives dissipate proportional more of the stored energy than MF and PRF adhesives. Humidity increased the dissipative processes in all PUR adhesives, especially in the polyamide fiber filled adhesive. PRF adhesive is less influenced by humidity. While for all other tested adhesives the dissipative processes generally increased with higher humidity, humidity decreased the damping of the investigated MF adhesive. The influence of the frequency on the energy dissipation is low for all tested adhesives in the investigated frequency range. Further fatigue tests with glued wood samples are needed to confirm the results observed on the free standing adhesive films.

Keyword

Adhesives for wood, Dynamic mechanical analysis, Fatigue, Energy dissipation, 1C-PUR

Introduction

The fatigue behavior of wood caused by alternating mechanical and environmental impacts was the topic of many researches during the 1900–1940 years (Kollmann 1951). Afterwards a dwindling interest in studying the dynamical properties of wood could be noticed since wood was slowly replaced by metal and composite materials. Nowadays, timber construction is gaining in interest and more ambitious construction projects are envisaged such as high multi-storey buildings and wind turbines. For such projects, knowledge about the behavior of construction timber exposed to dynamical excitation is essential. Although the behavior of wood during fatigue has been studied (Kollmann 1951, Bonfield & Ansell 1991) the behavior of glued wood under dynamic stress has been hardly investigated (Müller et al. 2004). It was shown (Müller et al. 2004)

that the fatigue behavior of glued wood specimen seems to depend on the adhesive properties. Brittle adhesives with high modulus of elasticity (MOE) perform better under high intensity and low cycle fatigue (LCF), while ductile adhesives with low MOE are more suitable for low intensity and high cycle fatigue (HCF). However, the nature of interaction between wood and adhesive during fatigue testing is understood less clearly. A classification of wood adhesives has been proposed (Frihart 2009) where wood adhesives are classified not only according to their chemical but also their mechanical behavior. This classification resulted in two different groups: The in-situ polymerized group containing the relatively rigid, highly cross-linked polymers such as UF, MF, MUF, PF and PRF and a second group, the pre-polymerized adhesive containing the flexible polymers such as PUR and PVAc. Generally, MOE values of amino resin adhesives' are higher than those of phenolic adhesives, while in comparison PUR adhesives exhibit the lowest range of MOE values (Konnerth et al. 2006, Konnerth et al. 2007). An overview of adhesive mechanical properties can be found in Ref. (Stoeckel et al. 2013). Wood adhesives, as viscoelastic material, produce hysteresis energy during fatigue. Some of the dissipated energy is released as heat, but most is absorbed in the sample, raising its temperature. At low frequency, the increase of the temperature is negligible. But at higher frequency-excitation the temperature of the specimen may exceed the glass transition temperature of Hemicellulose and Lignin wood component (Sandberg et al. 2013) and therefore change its behavior from glassy to rubbery properties. One component polyurethane (1C-PUR) adhesives are characterized by significantly lower stiffness and hardness compared to amino- and phenoplastic resins, such as melamine formaldehyde (MF) and phenol resorcinol formaldehyde (PRF) system, but absorb more deformation energy and show ductile failure behavior leading to lower wood failure percentage (Clauß et al. 2011). The application of more ductile adhesives in glued laminated timber should allow an increasing fatigue performance caused by a higher energy dissipation of the adhesive. Assuming that the fatigue failure will result in crack initiation and propagation (Dao & Dicken 1987), it can be hypothesized that, while dissipating a higher amount of energy by deformation, this released energy will not contribute to crack propagation and finally to the failure of the bondline. Dynamical Mechanical Analysis (DMA) is an efficient method to characterize the energy dissipation of cured adhesive film samples. The DMA allows examining the influence of the frequency of excitation, the temperature of the polymer as well as the moisture content of the polymer on the energy dissipation of the cured adhesive. DMA in tensile mode showed interesting results on PVAc film samples (López-Suevos & Frazier

2006), where an influence of the frequency on the loss factor Tan Delta was shown. The maximal energy dissipation occurred at 1 Hz. In addition to the frequency, the moisture content of the wood also influences the mechanical properties of the wood adhesive compound (Kollmann 1951), and therefore should be considered. Kläusler et al. investigated the influence of humidity on the tensile strength and tensile E-modulus of different wood adhesives (Kläusler et al. 2013). The tests on 1C-PUR, MF and PRF wood adhesive showed a distinct influence of moisture on the tensile strengths and MOE. Generally, by increasing the relative humidity a softening of the adhesive was observed, whereby phenolics and structural amino resin showed highest sensitivity (Stoeckel et al. 2013). In this study, the energy dissipation of brittle and ductile adhesives is investigated using DMA in tensile mode. Three different 1C-PUR, one MF and one PRF adhesive were chosen for DMA testing under defined climatic conditions. As the frequency of oscillation in timber construction is generally low, only the energy dissipation at low frequency (0.1 Hz–10 Hz) was considered. In order to understand the specific performance of the different adhesives excluding the influence of wood, only cured, free standing adhesive films were produced and tested in this study.

Material and method

Adhesives

Five commercially available wood adhesives were chosen: 3 different 1C-PUR, 1 MF and 1 PRF. For the one component polyurethane (1C-PUR) adhesive system, LOCTITE HB 110 PURBOND (short: HB 110) was selected containing polyamide fibers. The second PUR-type, VN 3158 is based on the same polymer as the HB 110 but was prepared without fibers to differentiate the influence of the adhesive polymer and the fiber. Additionally, the LOCTITE HB S309 PURBOND (short: HB S309) was used as a commonly available 1C-PUR adhesive with a different polymer formulation than the HB 110. For the Melamine Formaldehyde (MF) system, the GripPro Design adhesive A002 was chosen, mixed with a ratio of 100:50 with the hardener H002. For the Phenol Resorcinol Formaldehyde (PRF) adhesive, the Aerodux 185 was chosen, mixed with a ratio of 100:20 with the hardener HRP 155.

Preparation of cured film samples

1C-PUR (HB S309, HB 110 and VN 3158) cast sheets of approximately 100 μm thickness were produced using a film applicator under low humidity conditions in a dry box (< 10% RH). The low relative humidity allows slow curing of the adhesive and therefore helps to reduce the formation of gas (CO_2) bubbles. After curing at least one week at 20 °C and 65% R.H, the film samples were punched out using a stamping tool. MF and PRF adhesive films were processed at 20 °C and 65% R.H using a film applicator. The samples were punched out before complete curing of the adhesive, approx. 2–3 h after mixing of the components. For DMA testing the films were cut into rectangle specimen with a width of 6 mm. Afterwards specimen were randomly separated into 3 batches for conditioning at 20 °C and 35%, 65% and 85% RH respectively. All samples were conditioned for a minimum of two weeks before testing. Prior to DMA tests the thickness of the specimen was measured. MF ($147 \pm 15 \mu\text{m}$), PRF ($234 \pm 19 \mu\text{m}$) and HBS 309 ($76 \pm 12 \mu\text{m}$) showed relatively uniform film thickness while VN 3158 ($99 \pm 46 \mu\text{m}$) and HB 110 ($103 \pm 26 \mu\text{m}$) varied widely due to the difficulties during preparation.

Dynamic mechanical analysis (DMA)

Viscoelastic properties of cured adhesive films were investigated with a DMA Q800 including DMA-RH Accessory (TA Instruments, New Castle, USA). The DMA-RH Accessory allows mechanical properties of a sample to be analyzed under controlled and/or varying conditions of both relative humidity and temperature. Free standing polymer films were assessed via film-tension mode at a constant temperature of 20 °C and three different humidity conditions 35%, 65% and 85% RH (according to the preconditioning of the samples; as described in section 2.2). After the sample was placed in tension between a fixed and moveable clamp the DMA-RH Accessory chamber were closed to reach the set temperature and relative humidity. A dictated starting point of 0% RH and a fixed humidity ramp rate of only 2% RH per minute required an equilibration time of at least 5 min before starting the measurement. All tests were conducted as frequency sweeps from 0.1 Hz to 10 Hz and 0.1% strain as a level within the linear response. For each sample group, three separate measurements were taken to generate an average DMA response. Presented data for MF and PRF adhesives were measured with this *Test routine 1*. The results of PUR films measured with routine 1 showed high standard deviation and anomalies, probably due to insufficient curing of the films during storage under low air humidity conditions. Therefore, a second test

routine was set up. For *Test routine 2* PUR films were conditioned at 20°C and 85% RH before the DMA test. Samples were assessed again via film-tension mode as frequency sweeps from 0.1 Hz to 10 Hz, with 0.1% strain and at a constant temperature of 20°C. In contrast to the procedure described above, every single sample was measured at the three different humidity conditions (35%, 65% and 85% RH) in a row using the RH step mode. After achieving the chamber condition of 20°C/85% RH the first frequency sweep was conducted at 85% RH. Afterwards the humidity was decreased to 65% RH and the sample equilibrated 600 min before the next frequency sweep. The humidity was decreased further to 35% RH, and finally the sample equilibrated 600 min before the last frequency sweep. For each PUR group, three separate measurements were taken to generate an average DMA response. Only samples measured with *Test routine 2* were used for the main experiment. Additionally, specimens of HB 110 and VN 3158 adhesives were investigated with a DMA RSA III (TA Instruments, New Castle, USA). The free standing polymer films were assessed via film-tension mode in the temperature range of -100°C to +150°C with a heating rate of 2 °C/min at 1 Hz frequency and 0.1% strain amplitude. The temperature corresponding to the peak value of loss modulus E'' vs. Temperature curve was taken as the dynamic glass transition temperature (T_g) as recommended in the standard ASTM D 4065-94.

Fourier transform infrared spectroscopy (FTIR)

Based on the assumption that some of the PUR films were not fully cured before DMA tests, the degree of curing for the different PUR adhesive films was monitored by FTIR. Spectra were recorded on a Tensor 27 (Bruker, USA) in the range of 4000-500 cm^{-1} with 32 scans per measurement. All recorded spectra were normalized to the reference peak at 1600 cm^{-1} , which corresponds to the aromatic ν (C=C) peak and does not participate in the reaction. Particular attention was paid to the characteristic peak at 2250–2270 cm^{-1} , which is indicative of the isocyanate stretching vibrations (–NCO–). An obvious peak in these ranges indicates an incomplete consumption of isocyanate and therefore an unfinished or insufficient curing process.

Results and discussion

According to ISO 6721-1:2011 (E) the storage modulus E' is the real part of the complex modulus and proportional to the maximum energy stored during a loading cycle. E'

represents the stiffness of a viscoelastic material. The loss modulus E'' is the imaginary part of the complex modulus and proportional to the vibrational energy dissipated into heat during one loading cycle, while the loss factor $\tan \Delta$ is commonly used as a measure of the damping as the ability of relaxation and recovery of the polymer chains after deformation.

Influence of humidity on the viscoelastic properties

The average storage modulus, loss modulus and loss factor $\tan \Delta$ measured at constant temperature of 20 °C and at 1 Hz frequency are presented in Figs. 1–3 respectively. The influence of the humidity is shown for each adhesive. Rigid adhesives such as MF and PRF show higher storage and loss moduli, compared to the PUR adhesives, because of their generally aromatic nature of the backbone, their high degree of cross-linking and therefore their limited ability of deformation. PUR adhesives with more flexible backbones allow easier deformation, measurable in lower storage and loss moduli. Against expectation the fibre-reinforced 1C-PUR adhesive HB 110 shows the lowest storage modulus, also compared to the not reinforced 1C-PUR adhesives. A lower storage modulus after incorporation of the fibers indicates a reduced cohesive energy between macromolecular chains and an insufficient interfacial bonding between fiber and polymer. With increasing humidity adhesives are less stiff, seen as a clear decrease of all storage moduli (Fig. 1), due to the plasticizing effect of water. The strongest plasticizing effect shows HB 110 with a decrease of 37% after increasing the relative humidity from 35% to 85%. The storage modulus of MF and PRF decreased by 25%, while the moduli of the unfilled 1C-PUR adhesives decreased by 18%. There is only a slight influence of moisture on the loss moduli of all 1C-PUR adhesives and also on PRF (Fig. 2), while the loss modulus of the MF adhesive declined by nearly 40%. A declined E'' value indicates a decrease of the vibrational energy dissipated into heat during one loading cycle. The average loss factor $\tan \Delta$ (damping) measured at a frequency of 1 Hz is presented in Fig. 3. The damping gives the balance between the elastic phase and viscous phase in a polymeric structure. HB 110, the fiber-reinforced adhesive, shows the highest $\tan \Delta$ value, which indicatives the best damping behavior, while all other adhesives are more elastic, represented by a lower $\tan \Delta$ value. Ester linkages and urethane linkages of polyurethanes can undergo hydrolysis, which leads to chain scission. The free volume increases and allows an easier sliding of the chain segments (Kovačević et al. 1993). This trend was more obvious for HB 110, compared to the not

fiber filled PUR adhesives. The observed difference is probably due to high sensitivity of polyamide fibers to humidity as investigated by Ref. (Parodi et al. 2018). The damping of PRF was less influenced by humidity, due to the good hydrolysis resistance of the C–C bonds between the phenolic part and formaldehyde (Dunky & Niemz 2002). A contrary behavior has been observed for the amino-resin. Hydrolyses on MF also leads to scission of polymer-melamine crosslinks, but followed by the formation of melamine-melamine crosslinks, which are much more rigid than the polymer-melamine ether linkages (Bauer 1986). As a result, dissipative processes and also the damping capacity are decreasing.

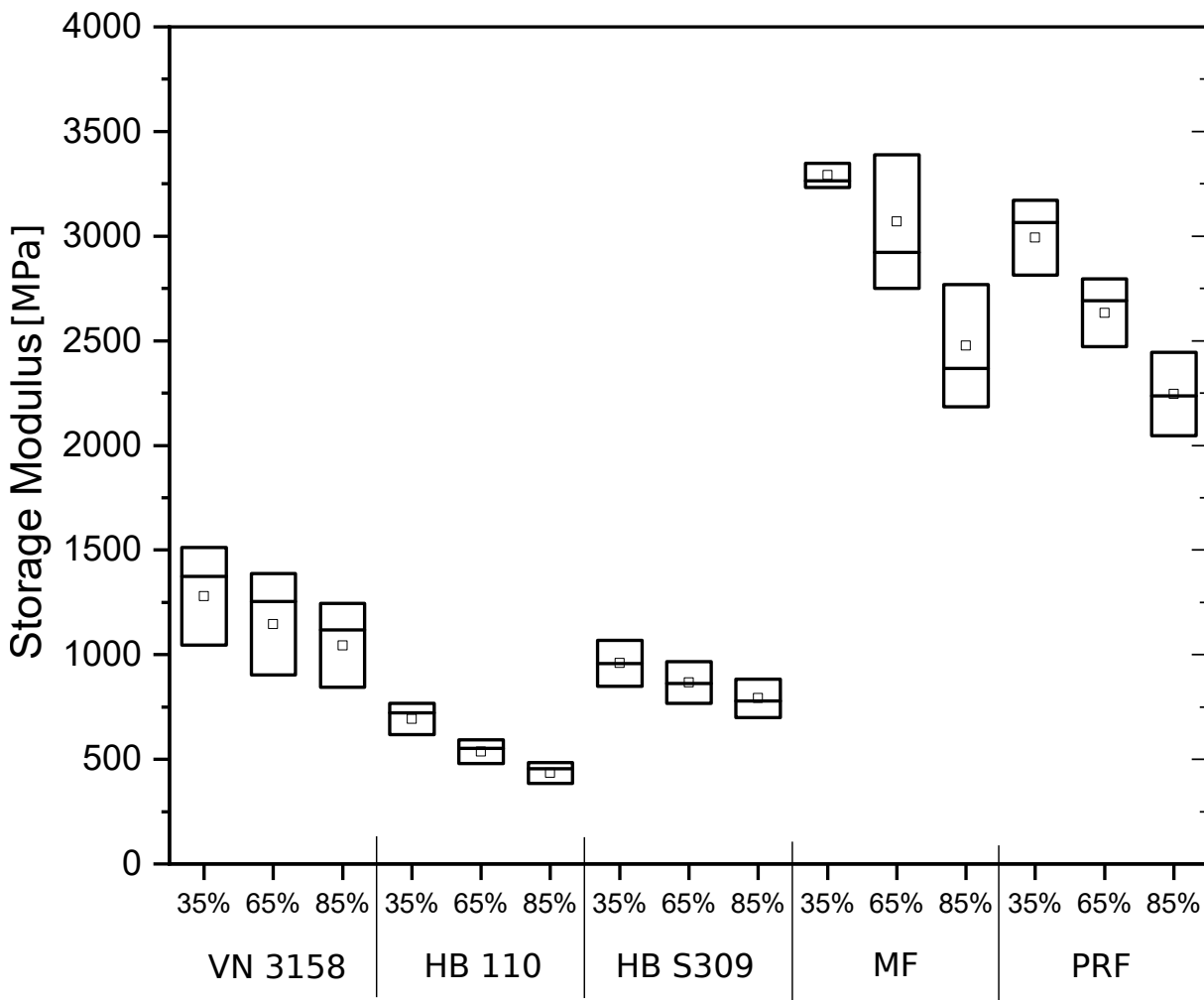


Figure 1 – Storage Modulus at 1 Hz frequency and 20 °C for all adhesives at 35%, 65% and 85% RH (□ mean, - median, □ standard deviation).

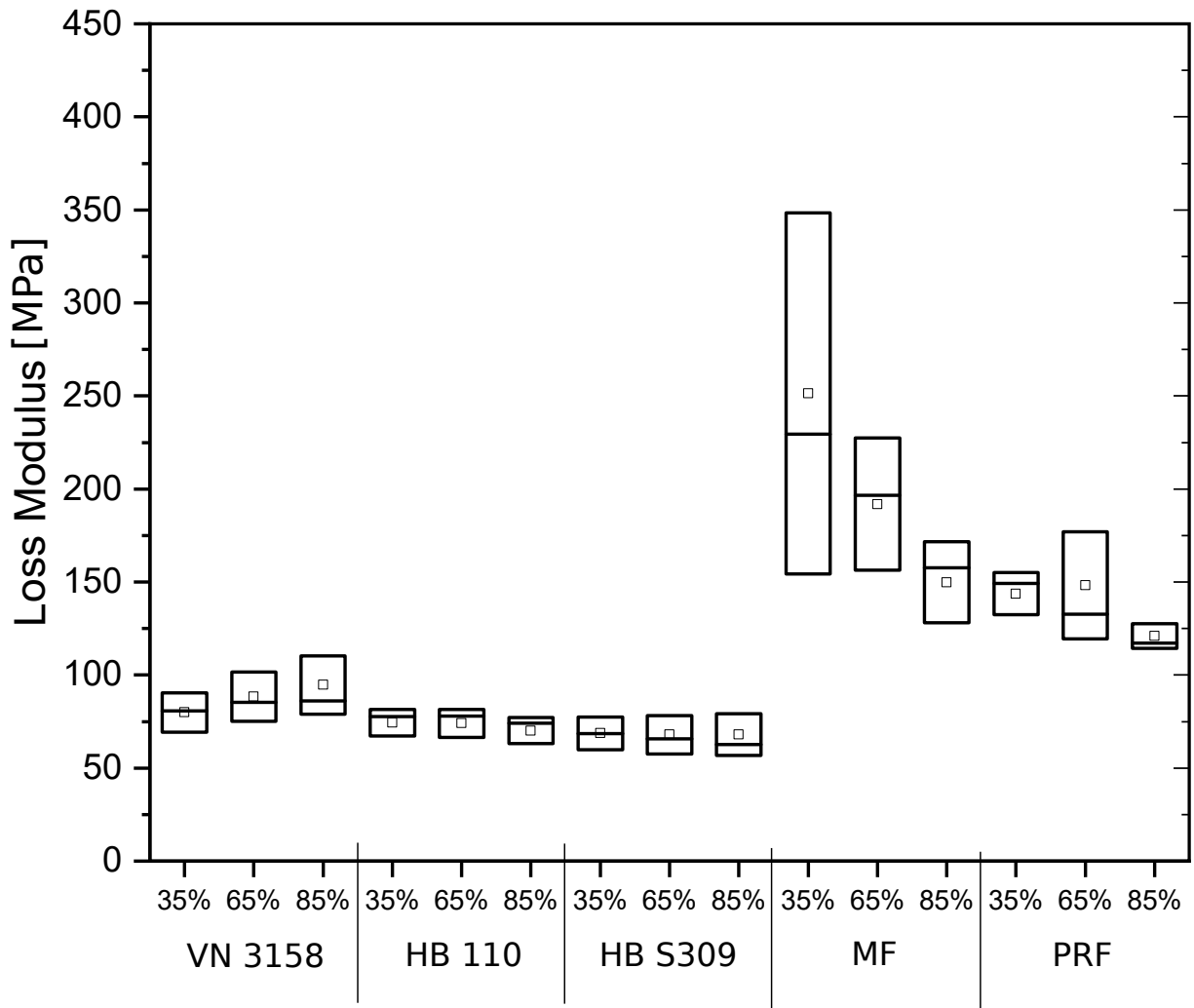


Figure 2 – Loss Modulus at 1 Hz frequency and 20 °C for all adhesives at 35%, 65% and 85% RH (□ mean, - median, □ standard deviation).

Influence of the frequency on the viscoelastic properties

The loss factor Tan Delta measured in the range of 0.1 Hz–10 Hz at constant temperature of 20 °C is presented in Fig. 4. Every mean value curve consists of 3 single measurements each. The influence of the frequency on the energy dissipation is small in the investigated frequency range. Except MF all other adhesives show an unchanged trend over the frequency range, irrespective of whether they were tested in dry or humid condition. The dissipation predominantly decreases slightly with increasing frequency. The dissipation behavior of MF adhesive changed, depending on the moisture content of the sample and the relative humidity of the surrounding. While the dissipation of the dry samples (35% RH) increased with increasing frequency, a decrease was measured

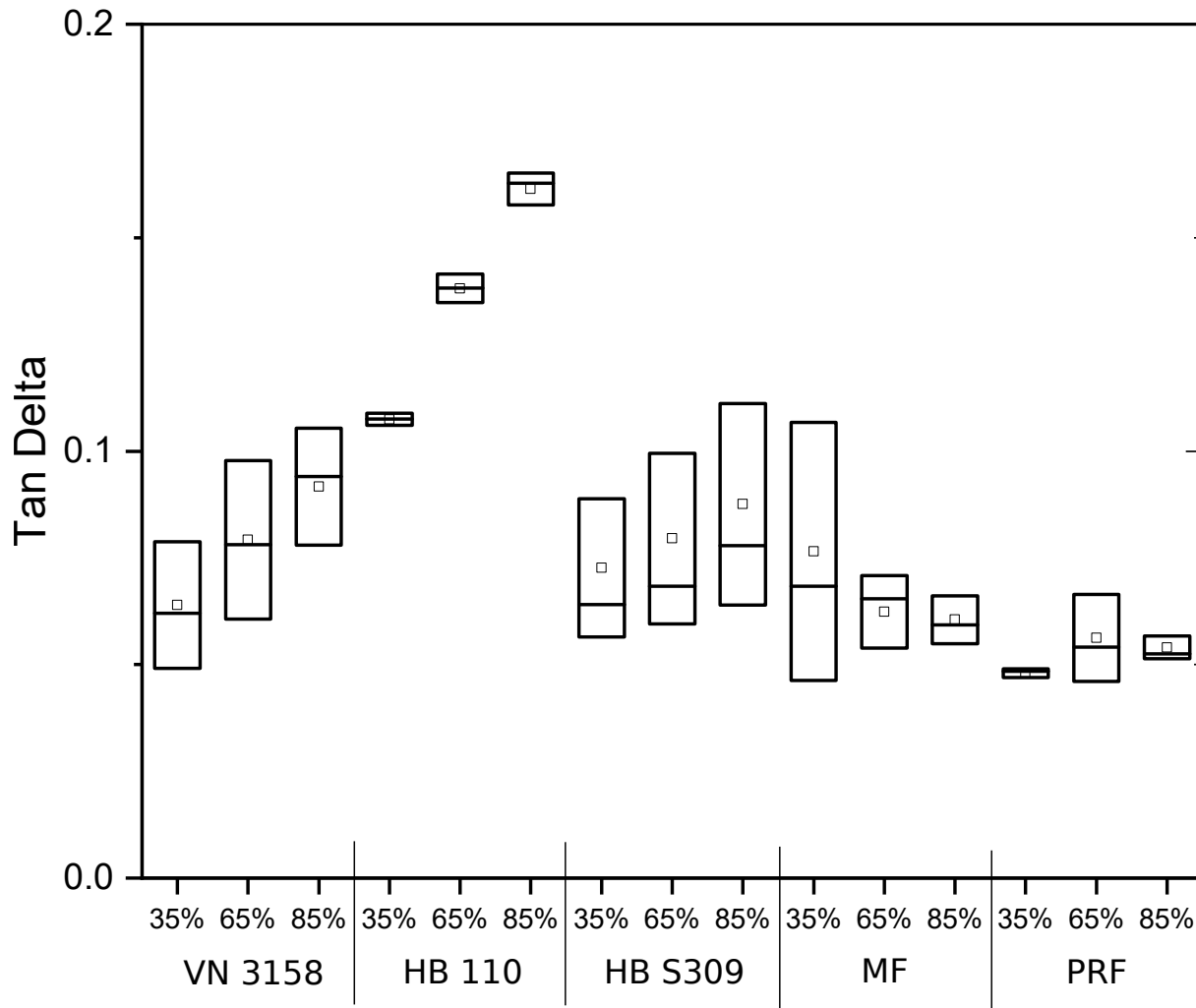


Figure 3 – Tan Delta at 1 Hz frequency and 20 °C for all adhesives at 35%, 65% and 85% RH (□ mean, - median, □ standard deviation).

for the moist samples (65% and 85% RH). The influence of the frequency is being superimposed by the influence of the humidity.

Effect of fibers on the dissipation behavior

HB 110, a 1C-PUR adhesive reinforced with polyamide fibers and VN 3158, the same polymer without fibers as a reference were tested to investigate the effect of the fibers on the dissipation behavior. All samples were conditioned at 20 °C and 65% RH before test. The transition temperatures of these adhesives are shown in Fig. 5. The glass transition of the soft segment at a temperature of about -80 °C is not influenced by the addition of polyamide fibers. A second transition visible at 54 °C for VN 3158 can be assigned to the transition of the hard segment. The incorporation of fibers into the polymer

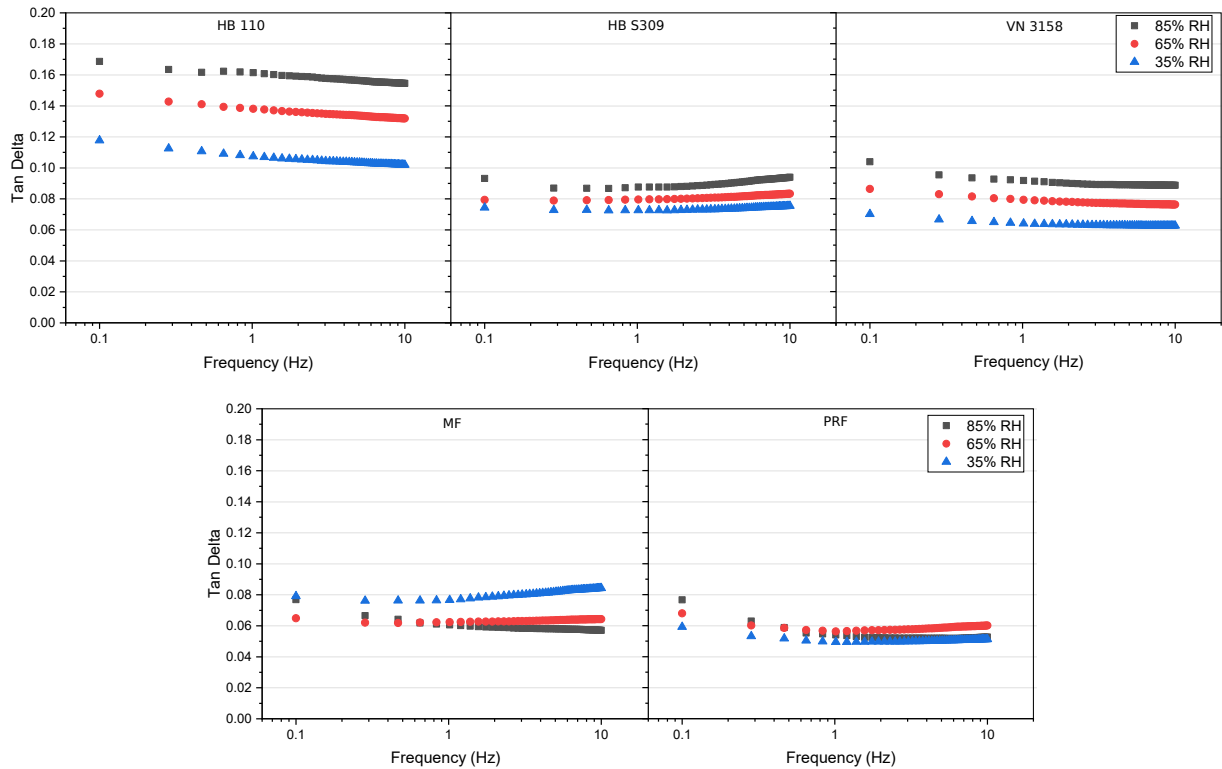


Figure 4 – Influence of the frequency on the loss factor Tan Delta for all adhesives at 35%, 65% and 85% RH.

matrix leads to a significant decrease of the transition temperature from 54 °C to -7 °C. This is an indication of an increased free volume and a reduction of cohesive energy between macromolecular chains. Furthermore, results let suppose, that the interfacial bonding between fibers and polymer is low. Results show that in this particular case the addition of fibers allows higher energy dissipation in the temperature range of -30 °C up to around 50 °C, while above 50 °C fibers improve the thermal stability of the PUR adhesive.

Fourier transform infrared spectroscopy (FTIR)

Results of PUR films measured with *Test routine 1* showed high standard deviation and anomalies as Fig. 6 exemplifies. Despite the expected decrease of the storage modulus due to plasticizing effect of water, samples stored and tested in 85% relative humidity showed the highest storage modulus. That is probably due to expected insufficient curing of the films during storage under low air humidity conditions (35% and 65% RH). To verify this suspicion, FTIR spectra were measured on thinner and thicker VN 3158 samples (Fig. 7). Particular attention was paid on the characteristic peak at

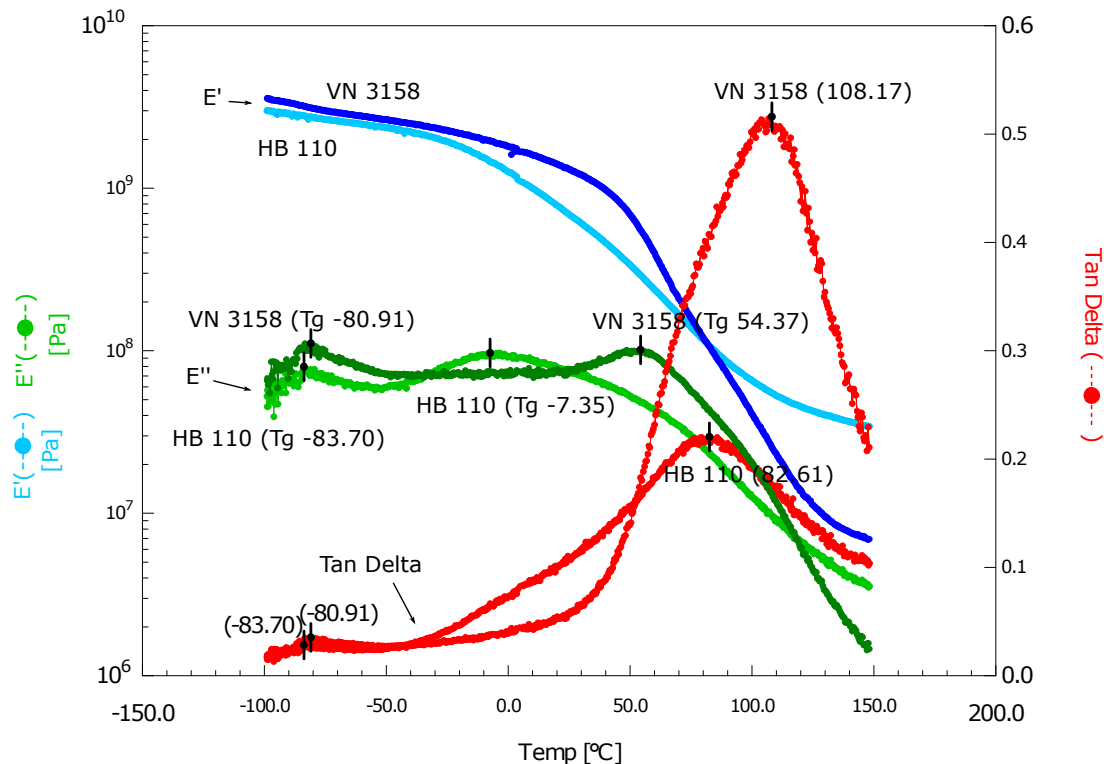


Figure 5 – Storage Modulus at 1 Hz frequency and 20 °C for the adhesive VN 3158 at 35%, 65% and 85% RH (□ mean, - median, □ standard deviation).

2250–2270 cm^{-1} which is indicative of the isocyanate stretching vibrations ($-\text{NCO}-$). All samples stored at 20 °C/35% RH showed a clear peak at 2270 cm^{-1} . This indicates an incomplete consume of isocyanate and therefore an unfinished or insufficient curing process, which probably resulted in the observed low storage moduli as seen in Fig. 6. In contrast all samples stored at 20 °C/85% RH showed no peak in this region. Samples which were stored at 20 °C/6% RH showed some film thickness dependence. While thin specimen seemed to be complete cured with no peak at 2270 cm^{-1} , a slight peak could be detected for all thicker specimen. It seems, that there is a surplus of isocyanate in the adhesive films for 1C-PUR adhesives that does not react or only very slowly at room temperature. Only exposure to relative high air humidity or temperatures will allow a complete reaction of isocyanates. This effect has already been observed by Clerc et al. (2017) on adhesive films and by Kläusler et al. (2013) on glued wood samples. Measurements of the Tan Delta values over the complete frequency range on insufficient cured samples, reveal a Tan Delta value approximatively 15% lower than fully cured samples. All samples revealing a insufficient curing were excluded from the main experiment.

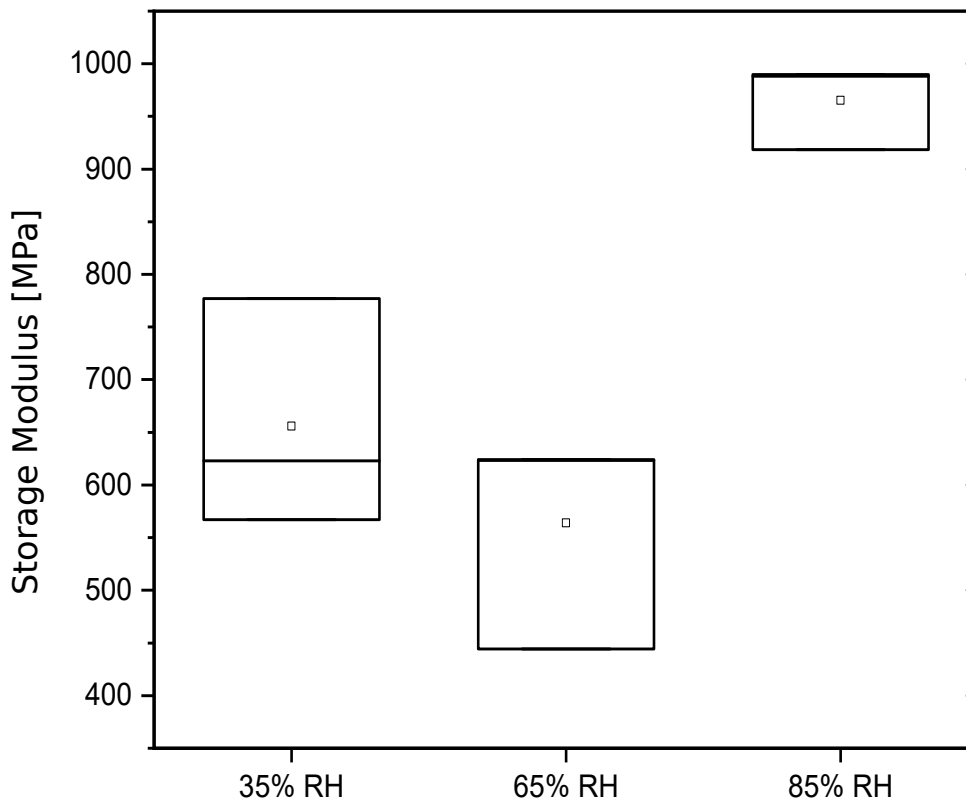


Figure 6 – Storage Modulus at 1 Hz frequency and 20 °C for the adhesive VN 3158 at 35%, 65% and 85% RH (□ mean, - median, □ standard deviation).

Conclusion

The energy dissipation of 5 different adhesives was tested using DMA. The influence of frequency and relative humidity was investigated on three 1C-PUR adhesives, one MF and one PRF adhesive. More brittle adhesives such as MF and PRF show bigger absolute Storage moduli and Loss moduli than the 1C-PUR adhesives. The fiber filled 1C-PUR adhesive has the best damping behavior, conspicuous by the highest Tan Delta values, compared to all other tested adhesives. PRF showed the lowest damping behavior. The high energy dissipation of the 1C-PUR is best explained by the ductile mechanical properties of the adhesive. The lower elastic modulus of such adhesive is due to a less dense polymer network, which allows greater deformation. During these deformations, the long polymer chains will dissipate heat through friction. In comparison, the more brittle adhesive such as MF and PRF, are storing a higher amount of elastic energy in their denser polymer network but release a smaller amount of energy in friction. Humidity increased the dissipative processes in all PUR adhesives due to hydrolysis of the polymer chains. This effect was particularly strong for the fiber filled adhesive HB

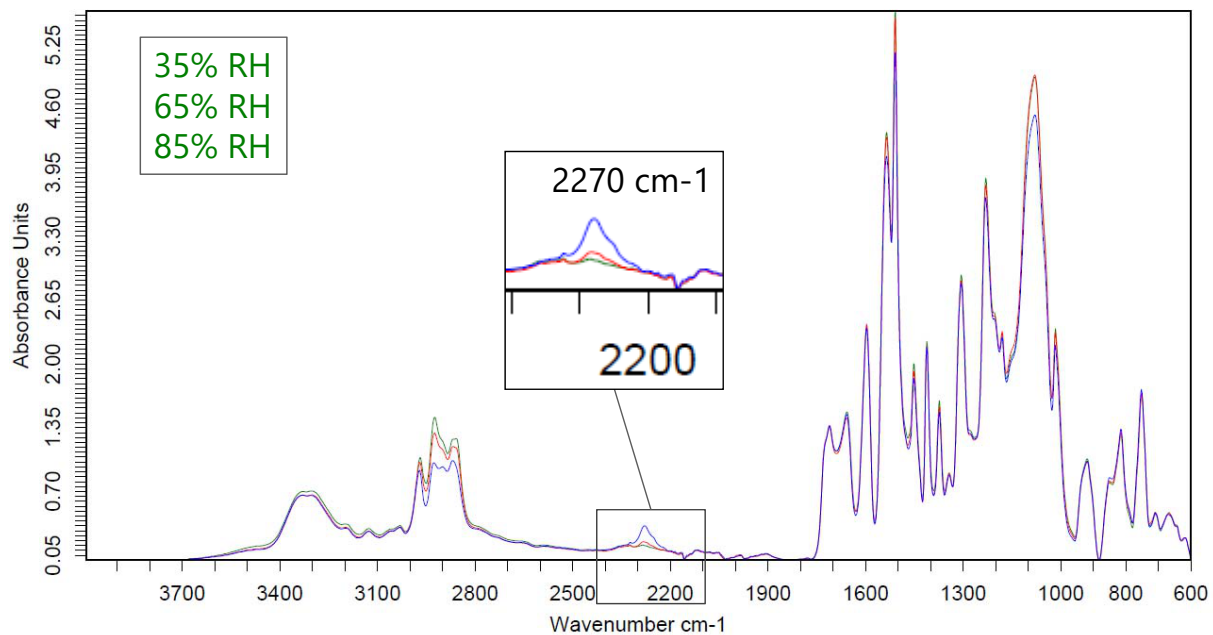


Figure 7 – Representative FTIR spectra of thin VN 3158 specimen (normalized to reference peak at 1600 cm^{-1}); . Samples were stored at 20 °C and different humid conditions (35%, 65%, 85% RH).

110. Dissipative processes of PRF were less influenced by humidity, attributable to the good hydrolysis resistance of the C–C bonds. A different behavior has been observed for the amino-resin, where higher moisture leads to decreased dissipative processes due to the formation of melamine-melamine crosslinks. The influence of the frequency on the energy dissipation was low in the investigated frequency range. A uniform tendency for all adhesives could not be observed. All adhesives showed slightly different behavior with increasing frequency. One corollary to the high ductility of 1C-PUR is that such adhesives are more sensible to creep effect than brittle adhesives. As mentioned by Ref. (Frangi et al. 2004), creep can be a limiting factor especially at higher temperature for structural application. Therefore, any further increase of the ductility of the adhesive in order to improve the fatigue performance should be done considering the influence of creep. General attention should be paid on the curing condition of free PUR films. FTIR measurements confirmed an unfinished or insufficient curing process, especially of thicker samples, which were stored at low humid conditions (35% RH). As reported by Ref. (Sandberg et al. 2011), the properties of cured adhesive depend on multiple factors, such as temperature, humidity and curing time. Furthermore, significant changes in wood adhesive polymerization were observed by Ref. (Ren & Frazier 2013) between adhesive polymerized in wood or in plain films due to wood-adhesive interactions. The obtained results shall therefore be considered with caution and applicable for

the adhesives. However, a good correlation is generally found between tests done on polymer films and directly in the bond line (Konnerth et al. 2006, Stoeckel et al. 2013). In accordance with the obtained results, 1C-PUR, especially fiber reinforced 1C-PUR adhesives are an interesting alternative to amino and phenol resins in cyclic fatigue loaded structures, due to their higher energetic dissipation. The obtained results confirm that PUR obtained longer fatigue life as MUF and PRF adhesive (Bachtiar et al. 2017). However, further testing is needed to explain the better performance of brittle adhesives in low cycle fatigue (LCF) when compared to PUR adhesive. The application of the obtained results to wood bonding should be done carefully as the combined system is more complex with regard to energy dissipation and fatigue. Further tests are needed to investigate the energy dissipation and fatigue behavior of wood samples glued with the tested adhesives.

Acknowledgment

The authors thank the Swiss Innovation Agency - Innosuisse for the financial support (Project 18958.1), as well as Henkel AG for providing 1C-PUR adhesives.

References

1. Kollmann F. (1951) *Technologie des Holzes und der Holzwerkstoffe*. Berlin: Springer.
2. Bonfield PW, Ansell MP. (1991) Fatigue properties of wood in tension, compression and shear. *J Mater Sci*;26(17):4765–73.
3. Müller Ulrich, Müller Helmut, Teischinger Alfred (2004). Durability of wood Adhesives in 50 year old aircraft and glider constructions. *Wood Res*;49(3):25–33.
4. Bachtiar EV, Clerc G, Brunner AJ, Kaliske M, Niemz P. (2017) Static and dynamic tensile shear test of glued lap wooden joint with four different types of adhesives. *Holzforschung*;71(5):391–6.
5. Frihart CR. (2009) Adhesive groups and how they relate to the durability of bonded wood. *J Adhes Sci Technol*;23(4):601–17.

6. Konnerth J, Jäger A, Eberhardsteiner J, Müller U, Gindl W. (2006) Elastic properties of adhesive polymers. II. Polymer films and bond lines by means of nanoindentation. *J Appl Polym Sci*;102(2):1234–9.
7. Konnerth J, Gindl W, Müller U. (2007) Elastic properties of adhesive polymers. I. Polymer films by means of electronic speckle pattern interferometry. *J Appl Polym Sci*;103(6):3936–9.
8. Stoeckel F, Konnerth J, Gindl-Altmutter W. (2013) Mechanical properties of adhesives for bonding wood—a review. *Int J Adhesion Adhes*;45:32–41.
9. Sandberg D, Haller P, Navi P. (2013) Thermo-hydro and thermo-hydro-mechanical wood processing: an opportunity for future environmentally friendly wood products. *Wood Mater Sci Eng*;8(1):64–88.
10. Dao KC, Dicken DJ. (1987) Fatigue failure mechanisms in polymers. *Polym Eng Sci*;27(4):271–6.
11. Clauß S, Gabriel J, Karbach A, Matner M, Niemz P. (2011) Influence of the adhesive formulation on the mechanical properties and bonding performance of polyurethane prepolymers. *Holzforschung*;65(6):835–44.
12. López-Suevos FE, Frazier C. (2006) Rheology of latex films bonded to wood: influence of cross-linking. *Holzforschung*;60(1):47–52.
13. Kläusler O, Clauß S, Lübke L, Trachsel J, Niemz P. (2013) Influence of moisture on stress–strain behaviour of adhesives used for structural bonding of wood. *Int J Adhesion Adhes*;44:57–65.
14. Konnerth J, Stöckel F, Müller U, Gindl W. (2010) Elastic properties of adhesive polymers. III. Adhesive polymer films under dry and wet conditions characterized by means of nanoindentation. *J Appl Polym Sci*;118(3):1331–4.
15. Kovačević V, Šmit I, Hacı D, Sućeska M, Mudri I, Bravar M. (1993) Role of the polyurethane component in the adhesive composition on the hydrolytic stability of the adhesive. *Int J Adhesion Adhes*;13(2):126–36.
16. Parodi E, Peters GWM, Govaert LE. (2018) Prediction of plasticity-controlled failure in polyamide 6: influence of temperature and relative humidity. *J Appl Polym Sci*;135(11):45942.

17. Dunky M, Niemz P. (2002) Holzwerkstoffe und Leime: technologie und Einflussfaktoren. Berlin, Heidelberg: Springer Berlin Heidelberg. Imprint; Springer.
18. Bauer DR. (1986) Melamine/formaldehyde crosslinkers: characterization, network formation and crosslink degradation. *Prog Org Coating*;14(3):193–218.
19. Clerc G, Brülisauer M, Affolter S, Volkmer T, Pichelin F, Niemz P. (2017) Characterization of the ageing process of one-component polyurethane moisture curing wood adhesive. *Int J Adhesion Adhes*;72:130–8.
20. Frangi A, Fontana M, Mischler A. (2004) Shear behaviour of bond lines in glued laminated timber beams at high temperatures. *Wood Sci Technol*;38(2):119–26.
21. Ren D, Frazier CE. (2013) Structure/durability relationships in polyurethane wood adhesives: neat films or wood/polyurethane composite specimens? *Int J Adhesion Adhes*;45:77–83.

3.2 Paper II - Reaction kinetics investigation in relation to the influence of humidity on fatigue behavior of wood lap joints

Paper II

Holzforschung 74 (2020) 865-880

Reaction kinetics investigation in relation to the influence of humidity on fatigue behavior of wood lap joints

Gaspard Clerc^{1,3}, Thomas Lüthi², Peter Niemz¹, Jan Willem G. van de Kuilen^{3,4}

1. Bern University of Applied Sciences
Architecture, Wood and Civil Engineering
Solothurnstrasse 102
CH-2500 Biel

2. Empa, Swiss Federal Laboratories for Materials Science and Technology
Center for X-ray Analytics
Überlandstrasse 129
CH-8600 Dübendorf

3. Technical University of Munich
Wood Technology Munich
Winzererstrasse 45
DE-80797 München

4. Faculty of Civil Engineering and Geosciences
Delft University of Technology
Delft, the Netherlands

Abstract

It is generally assumed that the properties of wood against fatigue are good, but little is known about the properties of adhesively bonded wood, which represents today most of the wood-based products. Lap-shear samples glued with three common wood adhesives (two ductile one component polyurethane system and one brittle phenol resorcinol adhesive) were tested under cyclical loads at three different climates (20°C, 35%-50%-85% relative humidity). For the analysis of the data, an empirical model based on reaction kinetics was developed. In addition, a probabilistic model was used to estimate the endurance limit and the expected run-outs lifetime. Both models were combined to accurately model fatigue at high and low relative stress intensity. It was shown that ductile one component polyurethane (1C-PUR) adhesives perform better than brittle adhesive system under dry climates (35%-50% R.H.). However, for higher relative humidity, the brittle phenol resorcinol formaldehyde (PRF) adhesive showed better performance, most probably due to a better wood-adhesive adhesion in wet climate. An average endurance limit for tensile shear stresses between 20%-48% of the mean tensile shear strength was estimated for the tested adhesives. It was shown that the model parameters could be linked to fundamental physical constants through the reaction kinetics approach, however, further research are needed to correlate these parameters to specimen specific quantities.

Keyword

Wood Adhesive, S-N curves, Fatigue modelling

Nomenclature

A_f Cross section of a flow unit

C, B Reaction rate constant

E_a Activation energy

F_1, F_2, \dots, F_n Generic name for coefficients of the Foschi and Yao Model

h Plank's constant

- k Loading rate
- k_b Boltzmann's constant
- n_1, n_2 Work terms of the activation's energy
- N Number of cycles
- N_0 Threshold cycles limit
- N_i, σ_i Number of cycles and stress of failure for specimen i
- N_m Number of bonds
- R Gas Constant
- T Absolute temperature [K]
- TSS Tensile shear strength [MPa]
- W, W_b, W_f Work due to external constrains
- γ_b Maximum localized strain deformation
- α Damage index ($\alpha = 0$ in undamaged state, $\alpha = 1$ at failure)
- α_c Accumulated damage during the uploading phase
- λ, δ, β Location, scale and shape parameter of a Weibull distribution
- Δ Shape parameter of equation 12
- γ_f Jump of flow segment at activation
- ϵ Strain
- σ Stress
- σ_f Mean stress on the flow unit
- σ_u Ultimate tensile shear strength
- σ_{up} Upper strength limit in cyclic test
- σ_l Lower strength limit in cyclic test

σ_0 Endurance limit

$\Delta\sigma$ Stress range

Φ Shift parameter of equation 12

Introduction

The accumulation of cyclic loads over longer periods of time may lead to damage of the structure at stress levels below the structural design strength. This fatigue phenomenon also impacts wood and was well studied until the end of Second World War, where this field of study lost interest due to the advent of composite materials and light metals (Tsai and Ansell 1990). Even though the study of the influence of the adhesive properties on the quasi-static properties of wood-glued joints is a field that has already been well studied (Stoeckel et al. 2013), few recent papers have specifically investigated the influence of different type of adhesive on the fatigue performance of bonded wood. Recently, (Bachtiar et al. 2017) showed that adhesives with different elastic moduli have led to different fatigue performances, which were not obvious under quasi-static loading conditions. The brittle adhesive systems (melamine-urea-formaldehyde, (MUF), fish and bone glue) seem to perform well under high intensity, low cycle fatigue (LCF) while the more ductile adhesive (1C-PUR) system perform better under low intensity, high cycle fatigue (HCF). It is possible that the ductile 1C-PUR dissipate a higher amount of strain energy into heat, which is consequently not available for damage accumulation (Künniger et al. 2019). Even though different adhesion phenomena are observed depending on the chemicals nature of the adhesive systems, it remains generally valid that brittle tested adhesives possess a denser interconnected polymer network, responsible for the high elastic modulus and providing also basically more connecting points to the wood, resulting in a better adhesion and to a higher wood fracture percentage (Bachtiar et al. 2017). It remains however unclear how the wood moisture content, type of loading and the type of adhesive influence the shape of the Stress-Cycle number curve (S-N curve) especially for high cycle fatigue. The influence of increased humidity on adhesively bonded wood lap-joint loaded under quasi-static loading has already been well studied (Kläusler et al. 2013). For all types of adhesives, a decrease in the shear strength is generally observed with increasing wood moisture content. Under cyclic fatigue loading, only a mild sensitivity of the fatigue strength to moisture content was noted by (Lewis 1962) on plain wood. Due to the difficulty

of obtaining fatigue data for very high number of cycles, fatigue models are used to extrapolate the data outside the test range assuming a given material's behavior. The majority of models used for the derivation of Stress-Cycle curves (S-N curves) from experimental data are to some extent based on empirical assumptions (Smith et al. 2003). Analyzing fatigue results is a notorious difficult task due to the scatter (for same load levels a variation of 2 order of magnitude is common) and to the low number of samples. In this paper a new model based on reaction kinetics was developed to specifically analyze the results of cyclic fatigue testing and facilitate the comparison of the different wood adhesives. In order to obtain a realistic depiction of low-cycle fatigue phenomena, a probabilistic model was used to estimate the endurance limit and the lifetime of run-out specimen (samples which did not fail during the tests). The goal of this paper is to compare the performance of three different wood adhesives under cyclic fatigue loading, in order to determine which adhesive, and corresponding adhesive properties, seem optimal to sustain fatigue loads.

Fatigue Modeling

Derivation of the fatigue damage model based on reaction kinetics approach

Krausz and Eyring described long term effects in materials on the basis of a reaction kinetics approach (Krausz and Eyring 1975). The principle of this approach is that in a solid, molecules occupy equilibrium positions and are vibrating about the minimum of the free energy potential. In the absence of mechanical stress, there is no movement of the solid or parts of solid as there are on average as many jumps to the right or to the left of the energy barrier (Fig 1, A.). When the molecules are displaced from the equilibrium positions by an applied stress (Fig 1, B.), the potential energy is increased. This means that the potential energy surface is changed, making the reaction more probable, decreasing the barrier height with W_f in forward direction and increasing the barrier height with W_b in backward direction. Where $W = W_b + W_f = \sigma A_f \lambda_f$ represents the work of the external constrains. In Fig 1. the influence of a tensile stress σ on the potential energy of a flow unit A_f is demonstrated using a simple tensile test example. It shall be noted, that flow unit can represent molecules, groups of molecules or filaments, fibrils etc.

Caulfield (Caulfield 1985) applied this approach on wood assuming a single energy

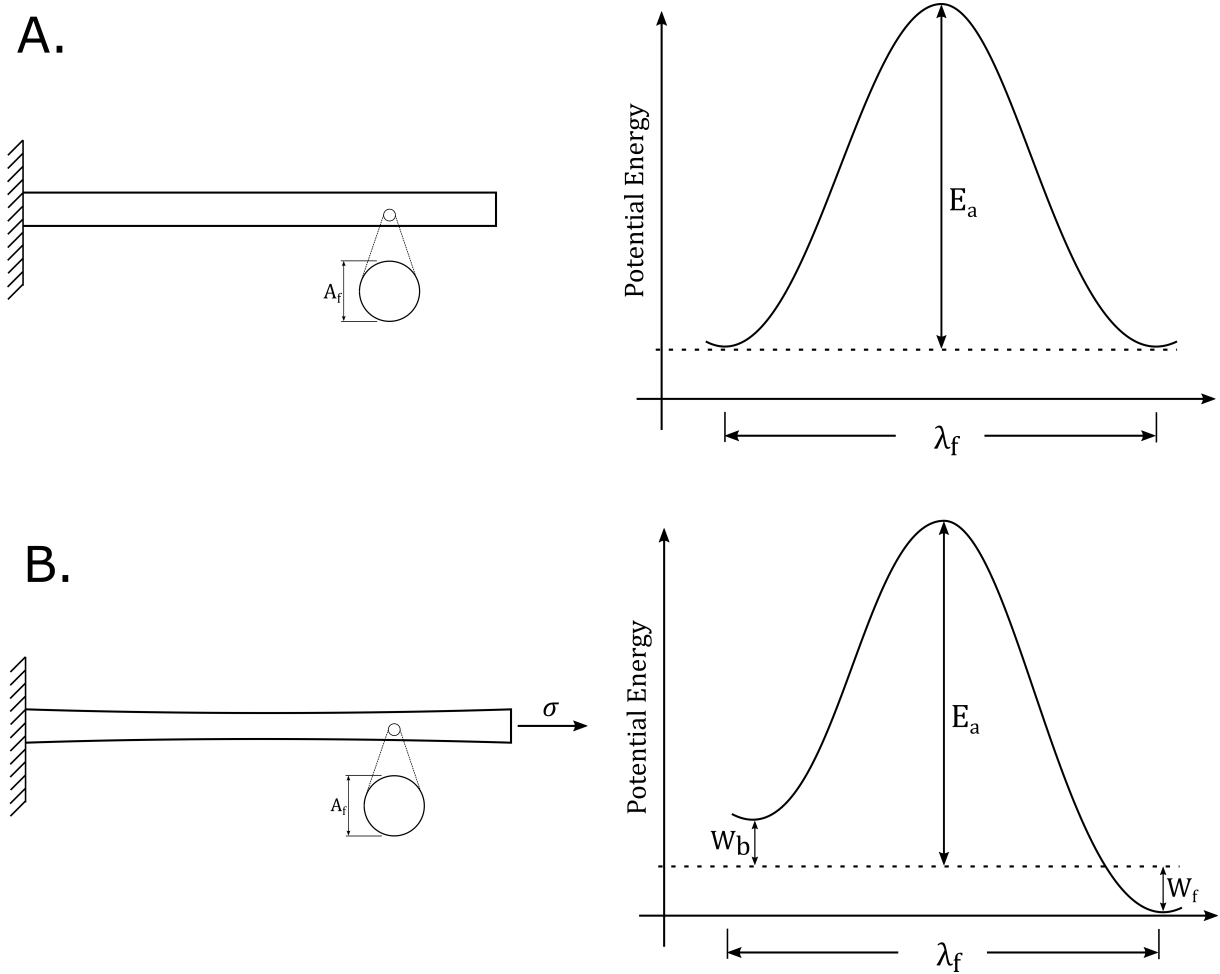


Figure 1 – A. For a material with no external stress, the potential energy barrier is symmetrical, meaning the tendency for a flow unit (A_f) to jump the barrier E_a is the same in either direction. B. Once this material is exposed to a stress (σ), the potential energy barrier is distorted by the external work W_b and W_f and the tendency for flow unit to jump over λ_f in the direction of the applied stress is greater than in the opposite direction

barrier obtaining equation:

$$N = \frac{hy_b}{k_b T \lambda_f} \exp\left(\frac{E_a}{RT} - \frac{\lambda_f A_f}{2k_b T} \sigma\right) \quad (1)$$

where k_b is the Boltzmann's constant, T the absolute temperature, h the Planck's constant, E_a is the activation energy, λ_f is jump of the flow segment, A_f the cross section of a flow segment, R the Gas constant and σ the applied stress. This model assumes that for a constant stress over time, the material will creep until a localized strain deformation (y_b) is reached, at which point in time the specimen will fail. Van der Put used a similar approach, extending the theory using a multiple set of energy barriers,

showing the applicability to describe both creep and damage phenomena (van der Put 1986), (van der Put 1989). For high levels of stress, as in the case of fatigue loading and crack growth, the bond breaking equation can be simplified and written as follows:

$$\frac{d\epsilon}{dt} = (C + B\epsilon) \left(\frac{\sigma - \sigma_0}{\sigma_u} \right)^n \quad (2)$$

Where ϵ is the strain associated with linear flow (C) and plastic flow ($B\epsilon =$ damage development) and t is the time. Parameters B and C are reaction rate constants describing how many flow units jump over the energy barrier given by equation:

$$C, B = \frac{k_B T}{h} \exp\left(\frac{-E_a}{RT}\right) \quad (3)$$

where E_a is the activation energy for the different reaction rate constants and n is the work term of the activation energy, which describe how much the energy barrier is shifted under the influence of a mechanical stress: $n = \frac{\sigma_f \lambda_f}{N_m k_b T}$ where σ_f is the part of the mean stress on the flow units, λ_f the jump of the flow segment at activation and N_m is the number of flow units per unit area, see also (Krausz and Eyring 1975), $\sigma - \sigma_0$ is the effective stress on the flow units, σ_0 is the endurance limit (also called threshold stress level) below which no damage occurs, σ_u is the ultimate strength .

In an independent way (Barrett and Foschi 1978) developed an empirical model assuming that the damage propagation is function of the applied stress and current damage. This state variable model is shown in the following equation:

$$\frac{d\alpha}{dt} = F(\sigma(t), \alpha) \quad (4)$$

Where α is the damage index ($\alpha = 0$ in undamaged state, $\alpha = 1$ at failure), $\sigma(t)$ the applied stress at time t and α is the current damage. The above equation can then be written in form of a power series expansion which can then be expressed as the following model (Barrett and Foschi 1978):

$$\frac{d\alpha}{dt} = F_1(\sigma - \sigma_0)^{F_2} + F_3\alpha \quad (5)$$

With F_1, F_2, F_3, F_4 being parameters without assigned physical meaning and σ_0 the endurance limit. The first term on the right-hand side describes that the damages accumulate for load higher than the endurance limit, however this model had an unwanted feature, due to the F_3 parameter in the second term on the right-hand side, it

will always lead to failure (van de Kuilen 1999). Later this model was further developed and improved by (Foschi and Yao 1986) :

$$\frac{d\alpha}{dt} = F_1[\sigma - \sigma_0\sigma_u]^{F_2} + F_3[\sigma - \sigma_0\sigma_u]^{F_4}\alpha \quad (6)$$

It appears that the form of Equation 6 is equivalent to Equation 2, when the plastic strain ϵ is considered as damage formation:

$$\frac{d\alpha}{dt} = C[\sigma - \sigma_0\sigma_u]^{n_1} + B[\sigma - \sigma_0\sigma_u]^{n_2}\alpha \quad (7)$$

where n_1 and n_2 are different work term of activation energy corresponding to different processes (van der Put 1989). Thus, the Foschi & Yao equation can be explained by the physical parameters of equation 2. Equation 7 can then be integrated to obtain the number of cycles until fracture for a given stress, assuming a Time – Load cycle equivalence ($N_i \approx \sum \sigma t_i$):

$$N(\sigma) = \frac{1}{B[\sigma - \sigma_0\sigma_u]^{n_2}} \ln \left[\frac{B + C[\sigma - \sigma_0\sigma_u]^{n_2-n_1}}{\alpha_c B + C[\sigma - \sigma_0\sigma_u]^{n_2-n_1}} \right] \quad (8)$$

The value for α_c which represents the accumulated damage during the uploading phase in an (equivalent) creep test, can be approximated by (Yao and Foschi 1993):

$$\alpha_c = \left(\frac{\sigma - \sigma_0}{1 - \sigma_0} \right)^{n_1+1} \quad (9)$$

The value for C can be approximated by (Yao and Foschi 1993):

$$C \approx \frac{k(n_1 + 1)}{[\sigma_u(1 - \sigma_0)]^{(n_1+1)}} \quad (10)$$

where k is the loading rate. Foschi and Yao (1986) assumed that the four fitting parameters (B, C, n_2, n_1) of equation 8 are positives, independent random variables with log normal distributions. The estimation of the parameter is useful in order to simplify the model as they allow to judge which damage process is predominant. For a specific usage in cyclic fatigue testing, the average loading rate, k , is oscillating constantly with an average value close to zero. For this reason, it results that the C coefficient in equation 10 is very small and can be neglected. Considering this, equation 8 can be simplified into:

$$N(\sigma) = \frac{1}{B[\sigma - \sigma_0\sigma_u]^{n_2}} \ln \left[\left(\frac{(1 - \sigma_0\sigma_u)}{(\sigma - \sigma_0\sigma_u)} \right)^{n_1+1} \right] \quad (11)$$

This model is actually a combination of two terms, the first term $\frac{1}{B[\sigma - \sigma_0\sigma_u]^{n_2}}$ which has the same form as the Madison Model (Wood 1947) multiplied with the second term $\ln\left[\left(\frac{1-\sigma_0\sigma_u}{\sigma-\sigma_0\sigma_u}\right)^{n_1+1}\right]$ accounting to the non-linear damage accumulation near the ultimate strength. For each term, the parameters n_2 and n_1 should be adjusted to the relative influence of both processes. However, mathematically the expression $(n_1 + 1) \cdot \ln\left[\left(\frac{1-\sigma_0\sigma_u}{\sigma-\sigma_0\sigma_u}\right)\right]$ is equivalent to $\ln\left[\left(\frac{1-\sigma_0\sigma_u}{\sigma-\sigma_0\sigma_u}\right)^{n_1+1}\right]$. As any strictly positive number can be obtained by multiplying two numbers, only one parameter is needed to model the influence of the parameter B and n_1 such as $\Phi = \frac{n_1+1}{B}$. Therefore, if these parameters are obtained through a fitting process, it is not directly possible to account for the relative importance of both terms as there is an infinity of B and n_1 value resulting in the same Φ . For this reason, the final equation was simplified to contain only three fitting parameters (Φ , Λ and σ_0).

$$N(\sigma) = \Phi[\sigma - \sigma_0\sigma_u]^{-\Lambda} \cdot \ln\left[\left(\frac{1 - \sigma_0\sigma_u}{\sigma - \sigma_0\sigma_u}\right)\right] \quad (12)$$

As shown in Figure 2, each parameter has a clear influence on the shape of the S-N curve. The Φ parameters influencing the shift of the S-N curve along the cycles axis without modifying the slope of the curve, the Λ parameters influencing the slope of the S-N curve and the σ_0 parameter representing the asymptotic behavior of the S-N curve for $N \rightarrow \text{Inf}$, e.g. the endurance limit.

Interpretation of the physical meaning of the parameters Φ and Λ :

Using the van der Put model to derive the value of the coefficient gives the following estimation:

$$\Phi = \frac{(n_1+1)}{B} = \left(\frac{\sigma_{f,1}\lambda_{f,1}h}{(N_{m,1}k_b^2T^2} + \frac{h}{k_bT})\right)\exp\left(\frac{E_a}{RT}\right)$$

and Λ to:

$$\Lambda = n_2 = \frac{\sigma_{f,2}\lambda_{f,2}}{N_{m,2}k_bT}$$

from these equations, the coefficients $\sigma_{f,1}$, $\lambda_{f,1}$, $N_{m,1}$, E_a , $\sigma_{f,2}$, $\lambda_{f,2}$, $N_{m,2}$ are unknown and should be determined through fitting to the data. As previously explained, it is mathematically not possible to distinguish the influence of the work term n_1 and the activation energy term B , for the same reason it is not possible to directly distinguish the influence

of the different coefficient listed above. However, the equation 12 can be used as an analogy to give insight in the fatigue phenomena. For example, with increasing temperature, the parameter Φ and Λ will decrease, meaning that the S-N curve will shift to the left and the curve will become steeper. In term of reaction kinetics, this means that with increasing temperature, the probability of a molecule to shift its energetic level is increased hence increasing the rate of damage accumulation, and therefore decreasing the lifetime of the specimen. The influence of temperature on time to failure of adhesively bonded specimens has been clearly shown in (Knorz et al. 2018) shifting the time-to-failure line to the right at elevated temperatures. Also, as it could be expected, having a higher activation energy or higher flow unit strength will increase the lifetime of the specimen. It is recognized however that for wood, even though activation energy is generally related to bond slip (in contradiction to primary bond breakage), determination of activation energy will always lead to a 'mean' value because the large variety of molecules (cellulose, hemicellulose and lignin).

Parameters estimation

In equation 12, the parameters Φ , Λ and σ_0 should be fitted to the data. The fitting parameters of the Model 2 were obtained through minimization of the function:

$$\sum_{i=1}^n (\log(N(\sigma_i)) - \log(N_i))^2 \quad (13)$$

Where n is the number of tested samples, N_i and σ_i the number of cycle and respectively the load level until rupture of the considered sample. Using equation 13 to obtain the fitting parameters will always result in an endurance limit (sometimes also named fatigue limit) of zero. Meaning that any load, no matter how small, will ultimately lead to the failure of the specimen. The existence of a fatigue limit is well established for metal, it remains however unclear if such a limit exist for wood (Nielsen 2000a). Several authors estimated an endurance limit for a specific loading type and type of specimen, for example (Kyanka 1980) estimated an endurance limit around 35-50% of the maximal bending stress for wood and wood composites, (van der Put 1989) estimated an endurance limit around 35 % of the maximal load, whereas (Ogawa et al. 2017) predicted an endurance limit of 60% of the maximal load level for compression loading perpendicular to the grain of Japanese cypress. But ultimately, all above mentioned endurance limit values are resulting from extrapolation of a mathematical model out of the range of experimental data and should therefore only be considered as

estimation. Nevertheless, it seems that assuming an endurance limit for wood and wood composites is an acceptable working hypothesis (Smith et al. 2003). For fatigue models based on Foschi and Yao, the endurance limit is understood as a fitting parameter or as an external constant which should be chosen according to a given reference. As explained previously, if the endurance limit is set as fitting parameter, its value will be minimized to zero. This is also the case in the Damaged Visco-elastic Material theory of (Nielsen 2000a, 2000b) which predicts that material such as wood will fail irrespective of an endurance limit. Ultimately, the estimation of an endurance limit with mechanical/empirical models outside the testing range without clear expectations of the behavior of the wood at such loads is bound to be imprecise. Concerning this issue, an interesting approach consists in using a probabilistic fatigue model (Castillo and Fernández-Canteli 2009). This model is based on a modified three-parameters Weibull distribution, in which the cumulative distribution for fatigue lifetime at a given stress range and the cumulative distribution for the stress range at a given lifetime are not independent and must satisfy a compatibility condition. Fulfilling this compatibility conditions allows to establish a functional equation $F(N, \sigma_{Delta\sigma})$ in the form a Weibull model, as shown under equation 14:

$$F(N, \Delta\sigma) = 1 - \exp \left[- \left(\frac{(\log N - N_0)(\log \Delta\sigma - \sigma_0) - \lambda}{\delta} \right)^\beta \right]; \quad (14)$$
$$(\log N - N_0)(\log \Delta\sigma - \sigma_0) \geq \lambda$$

Where N_0 is the threshold cycle limit, σ_0 is the endurance limit. λ, δ, β are location, scale and shape Weibull parameters, respectively. This model was validated for metal fatigue tests (Koller et al. 2009) and for concrete (Castillo and Fernández-Canteli 2009), as the basic assumptions of this model are also valid for composites, its validity should extend to composites material such as wood. Using equation 14 to fit the data allows to obtain an estimation of the endurance limit. This estimated value can then be used as constant σ_0 in equation 12.

Dealing with run-out

Due to practical limitation it is often not possible to test each sample until failure, especially for low stress values. For this reason, a maximal lifetime was fixed (here at 1.2E6 cycles) upon which samples were defined as run-out. Dealing with such samples is a complex question as the obtained number of cycles is less than the real

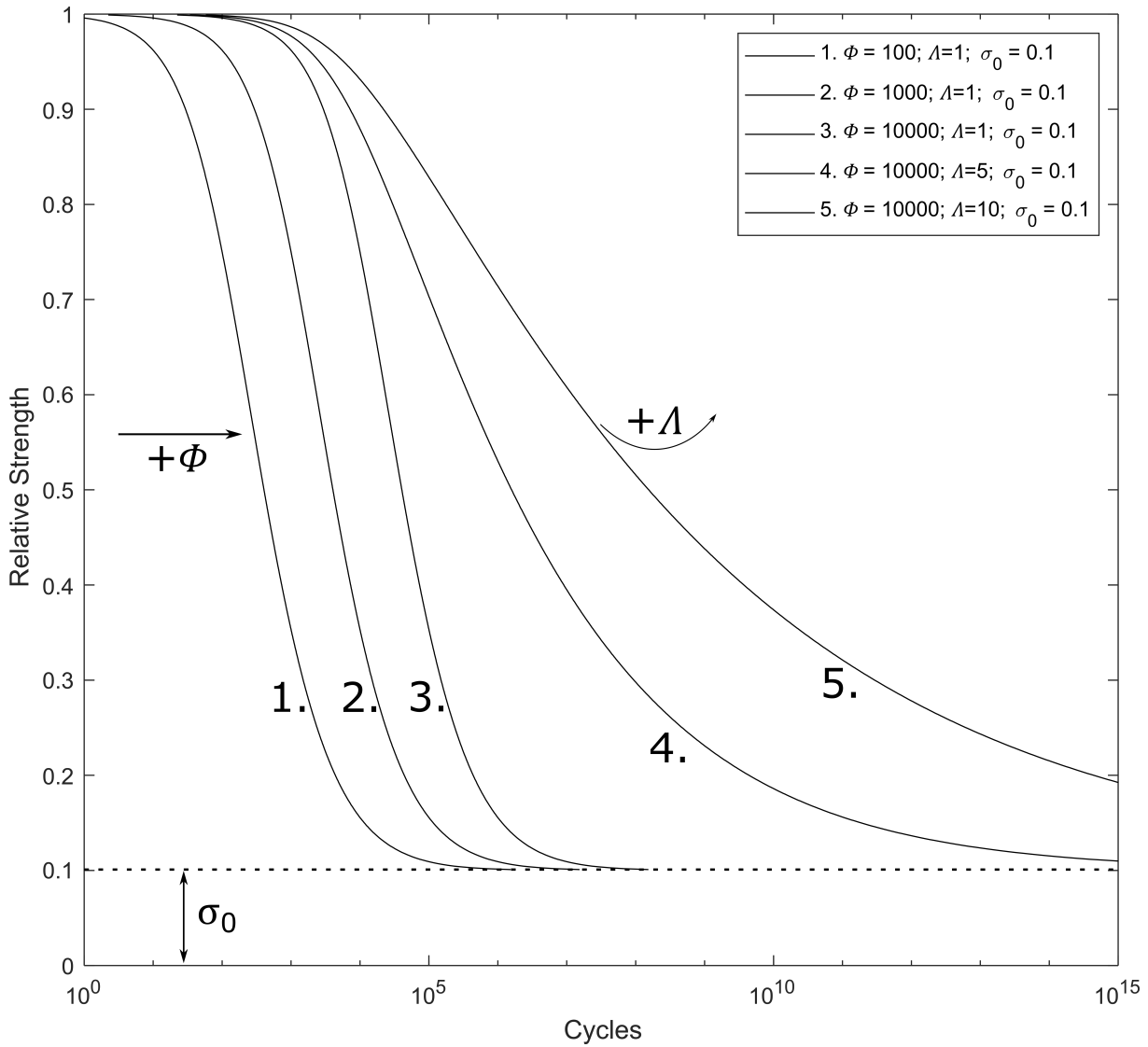


Figure 2 – Influence of the three fit parameters of equation 12 on the shape of the S-N curve. For increasing C value, the S-N curve shift to the right along the cycles axis while keeping the same slope. For increasing D-value, the slope decreases. The endurance limit σ_0 represent the asymptote for $N \rightarrow \infty$

number of cycles until rupture (supposing the sample will fail). Using the probabilistic fatigue model, it is possible to estimate the number of cycles for which the sample would have failed. The process consists in determining the model parameters (given in equation 14) considering only the samples without run-outs. Using these parameters, the estimated failures values of the run-outs are obtained. Then, the model parameters are re-estimated using the data associated with real failures plus the expected ones associated with the run-outs. The two last steps are then repeated until convergence of the process takes place, which means that the transformed run-outs lifetimes are from the same distribution as the samples associated with failures. A complete and

detailed description of the determination process is outside of the scope of this article, but can be found in (Castillo and Fernández-Canteli 2009). For the present analysis, the software Pro-Fatigue (Fernández-Canteli et al. 2014) was used to determine the endurance limit and the lifetime of transformed run-out.

Material and Method

Sample manufacturing

Beech wood (*Fagus sylvatica* L.) was used for manufacturing the samples. Samples were produced according to (EN 302-1:2013). The wood lamellas were first planed to a thickness of 10 mm and stored for at least a week in 20°C, 65% relative humidity (R.H). Then, the lamellas were planed to a thickness of 5 mm prior to the bonding. Two different 1C-PUR adhesives were chosen, the LOCTITE HB 110 PURBOND and the VN 3158. Both adhesives have the same formulation with the only exception that small polyamide fibers were added to the adhesive HB 110. The Phenol Resorcinol Formaldehyde (PRF) Aerodux 185 from DYNEA was used as a reference. The bonding was performed according to the parameters described in Table 1. After curing, the samples were stored for one week at a climate of 20°C and 65% relative humidity again before being cut to the geometry described in 3. The samples were randomly divided in three batches according to the three tested climates (20°C 35% R.H, 20°C, 50%. RH and 20°C 85% R.H.). The samples were kept at least two weeks in each climate prior to testing, so that a difference smaller than 0.1% of the weight was measured over 24 hours. The average wood moisture content for each climate is given in table 2.

Table 1 – Gluing parameters for the two 1C-PUR adhesives (HB 110 and VN 3158) and for the PRF (Aerodux 185) adhesive

Adhesive	Hardener	Glue Spread [g/m ²]	Mixt. ratio [Adh./Hard.]	Pressing time [h]	Press. [MPa]	CAT [min]
HB 110	-	180	-	10	0.8	10
VN 3158	-	180	-	10	0.8	10
Aerodux 185	HRP 155	340	100/20	10	0.8	30

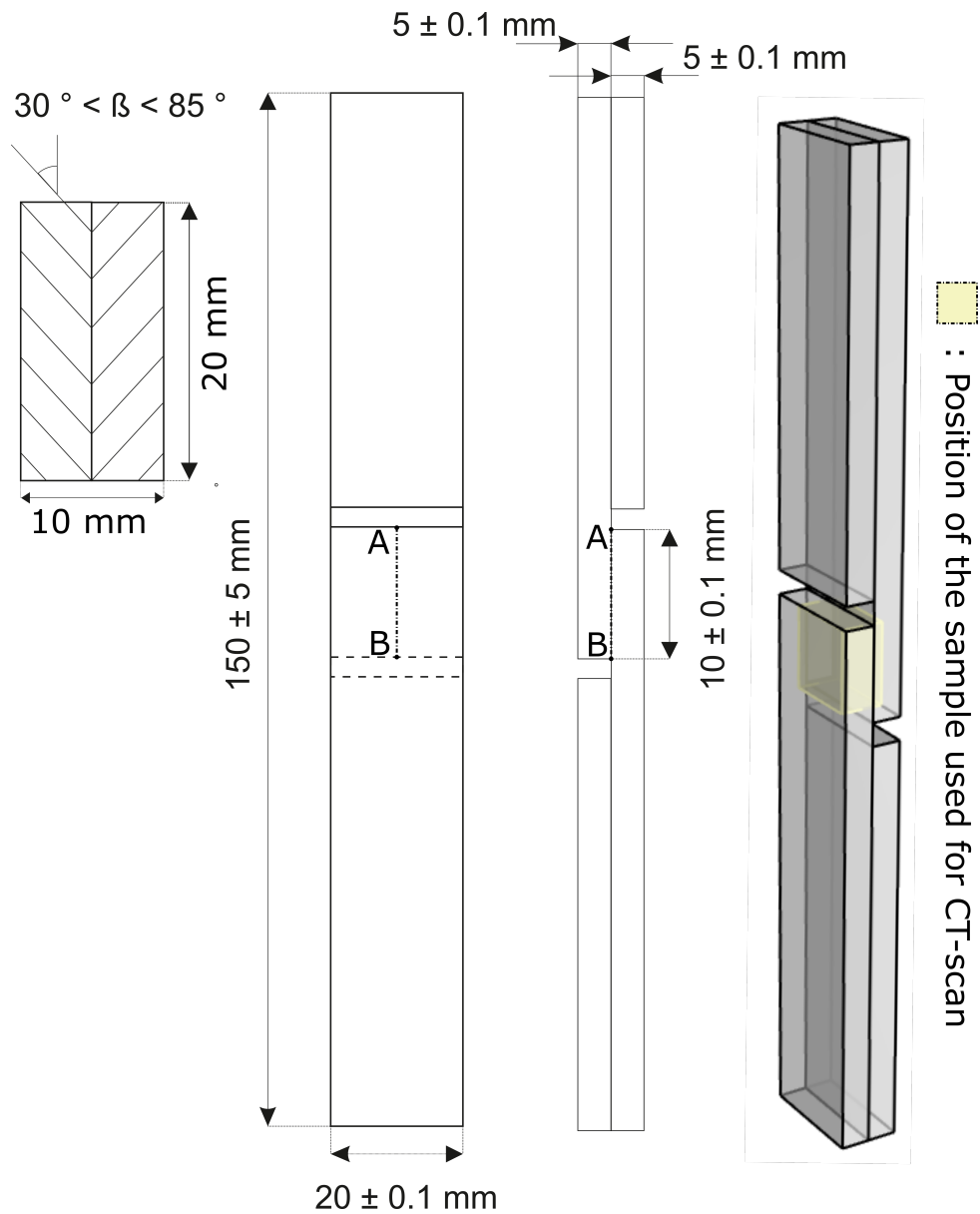


Figure 3 – Geometry of lap-joint samples according to (EN 302-1:2013) – Left: cross section, Right: 3D-view with position of the samples used for the CT-scan analysis – Path A-B shown for plotting the shear strength in figure 8.

Mechanical testing

The tensile longitudinal shear strength was first measured for each series and for each climate to serve as reference for the relative shear strength used in the cyclic tests. The samples were loaded until failure with a loading rate of 2 kN/min chosen in accordance with (EN 302-1:2013). All testing took place inside a chamber directly connected to a climatic chamber so that the chosen testing climate could be controlled and kept

Table 2 – Average wood moisture content (WMC) \pm standard deviation for the three tested climates. WMC was determined according to EN 13183-1

Climate	Wood Moisture Content [%]
20°C, 35% R.H.	8.0 \pm 0.1
20°C, 50% R.H.	10.3 \pm 0.1
20°C, 85% R.H.	19.2 \pm 0.2

constant during the entire experiment. The maximal force reached during the test was used as value for calculating the shear strength by dividing it by the shear stressed surface (10x20 mm²). The wood fracture percentage was determined for each specimen tested under quasi-static or fatigue cyclic loading according to (EN 302-1:2013). The cyclic tests were conducted at a frequency of 1 Hz to avoid any temperature increase of the sample. The chosen R-ratio (which is the minimum peak stress divided by the maximum peak stress $R = \frac{\sigma_l}{\sigma_{up}}$) was 0.1 with a maximal stress values ranging from 90% to 30% of the mean maximal shear short term strength (see table 3). The tests were performed on a Walter und Bai servo-hydraulic testing machine equipped with load cell of 20 kN with an accuracy of 0.1%

Preparation of sample for micro CT-scan

Micro CT-scan of the glue line were realized on run-out samples and non-tested samples glued with the PRF and the HB 110 adhesive. Small specimen (10 mm length, 5 mm height and 10 mm width) were cut in the central section of the samples (see Fig. 2). Each cross section was sanded to obtain a smooth cross-section surface. The CT images were acquired with an in-house built micro CT system based on a Viscom X9160-TXD microfocus X-ray tube in transmission mode and a Perkin Elmer XRD 1621 CN3 ES detector with 2048 x 2048 pixels using CsI (Tl) as scintillation material. The 3D tomograms were acquired in cone beam mode at 50 kV tube voltage and 120 μ A beam current with 1440 projections at a geometrical magnification of roughly 30 x, resulting in a voxel size of approximately 6.5 μ m³. The acquisition time was roughly 20 minutes; an influence on the sample due to the radiation can be excluded. For the best resolution of the interesting zone, the samples orientation was chosen in a way that the glue plane was perpendicular to the rotation axes and along the centerline of the radiographic projection. The reconstruction was performed with an in-house built software based on

the often-used Feldkamp algorithm (Feldkamp et al. 1984). Analysis of the tomographic data were realized using the ImageJ software library (Schindelin et al. 2012), (Schmid 2010).

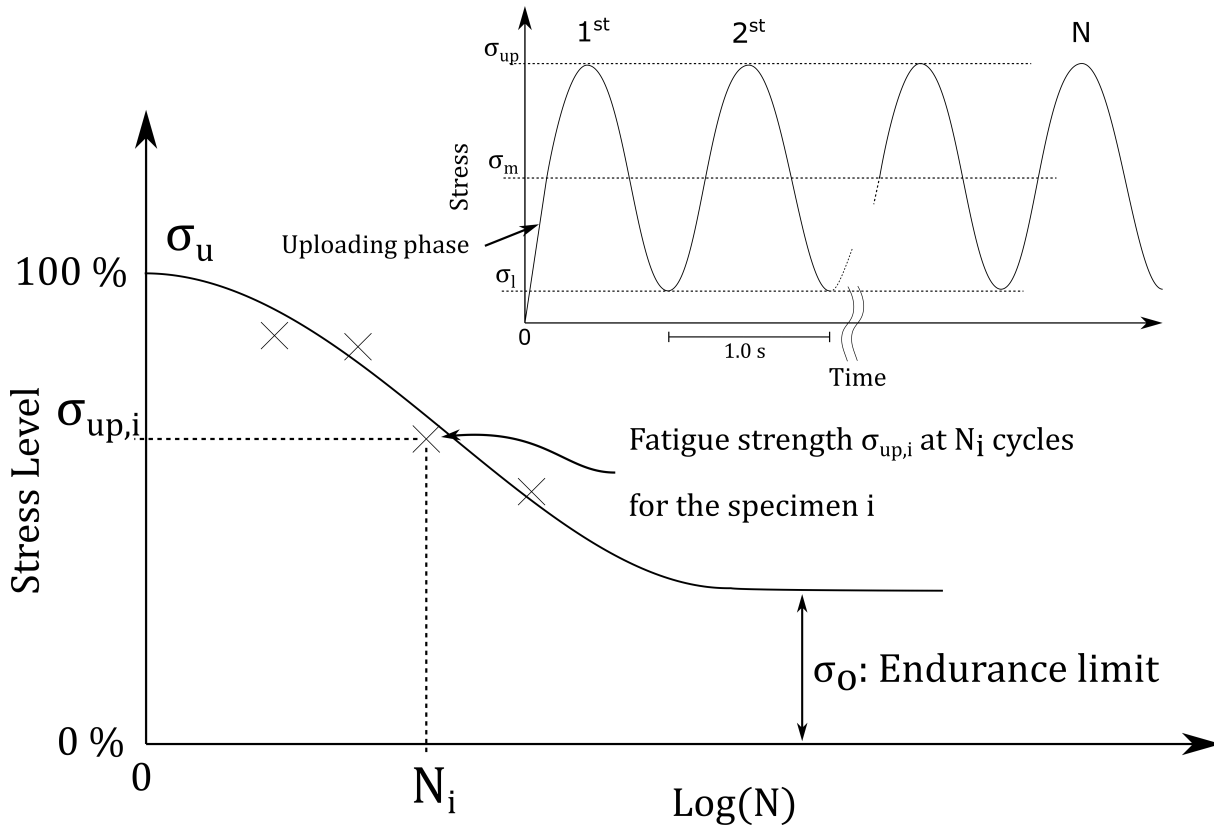


Figure 4 – Geometry of lap-joint samples according to (EN 302-1:2013) – Left: cross section, Right: 3D-view with position of the samples used for the CT-scan analysis – Path A-B shown for plotting the shear strength in figure 8.

Results

Short term tensile shear strength

The longitudinal tensile shear strength (TSS) results obtained at 35%, 50% and 85% R.H. for the three tested adhesives are shown in Table 3. These results show that for relatively dry climates (35% and 50% R.H.), no significant differences (t-test with $p=0.05$) in TSS exist between the tested adhesives. However, for high relative humidity, the performances of the 1C-PUR adhesive decline abruptly. This decline of performance is probably due to bad affinity between the wood and the 1C-PUR adhesive in high ambient moisture climate as observed by (Kläusler et al. 2013).

Table 3 – Tensile shear strength (TSS) [MPa] average value \pm one standard deviation and average Wood Fracture Percentage (WF) measured at three different relative humidity for the three tested adhesives. (Number of samples per series $n = 8$)

	R.H. = 35%		R.H. = 50%		R.H. = 85%	
	σ_u [MPa]	WF [%]	σ_u [MPa]	WF [%]	σ_u [MPa]	WF [%]
HB 110	13.7 \pm 1.9	20	14.7 \pm 0.9	0	9.5 \pm 1.7	0
VN 3158	11.6 \pm 1.3	0	14.0 \pm 1.3	0	7.3 \pm 1.0	0
PRF	14.5 \pm 0.8	100	14.8 \pm 0.9	100	12.4 \pm 1.7	100

Cyclic Fatigue

Table 4 – Average Wood Fracture Percentage (WFP) measured at three different relative humidity climate for the three adhesives tested under fatigue cyclic loading

	R.H. = 35%	R.H. = 50%	R.H. = 85%
	WF [%]	WF [%]	WF [%]
HB 110	30 \pm 40	30 \pm 40	30 \pm 40
VN 3158	30 \pm 40	30 \pm 40	30 \pm 40
PRF	30 \pm 40	30 \pm 40	30 \pm 40

The wood fracture percentage (WF) for all specimen tested under quasi-static loading is given in table 3 and in table 4 for samples loaded under cyclic fatigue. The type of loading has no noticeable difference on the wood fracture percentage. For the PRF specimen, the fracture was on average located in the link 6-7 of the Marra Model (Marra 1992). Which correspond to wood cell fracture located in the vicinity of the adhesive layer. For the VN adhesive almost no wood fracture was observed, the fracture layer corresponds the link 4-5 of the Marra model (Marra 1992) which correspond to an adhesion failure between the boundary layer and the wood substrate. The same type of fracture is observed for the HB 110. For both 1C-PUR adhesive (VN 3158 and HB 110) increasing wood moisture content decreases the wood fracture percentage, whereas no influence was observed for the PRF adhesive.

As shown in Figure 5, HB 110 and PRF samples tested at a relative humidity of 35% show a relatively similar behavior, the Λ coefficient for the HB 110 and PRF is around 6-8 whereas the Φ coefficient is three times higher for the HB 110. In comparison the VN adhesive has a very low Φ coefficient but a very “flat” S-N curves as demonstrated

Table 5 – Fitting coefficients (Φ , Λ , σ_0) values obtained for the three tested adhesive system at the different relative humidity obtained from equation 12

Adhesive	Relative Humidity	Φ	Λ	σ_0
PRF	35%	18.1	8.0	0.20
	50%	30.4	2.8	0.22
	85%	0.2	8.2	0.41
HB 110	35%	58.0	5.8	0.28
	50%	597.1	2.9	0.25
	85%	77.4	7.4	0.28
VN 3158	35%	0.02	13.4	0.43
	50%	4362.2	5.4	0.22
	85%	57.3	2.8	0.48

by the high Λ coefficient. Also, the endurance limit of the VN adhesive is clearly higher than for the PRF and HB 110 adhesive.

The samples tested at a relative humidity of 50% are shown in Figure 6. Again, the adhesive VN 3158 is performing better than the other system. Between the three adhesive systems, a factor 10 is observed between the three corresponding Φ coefficient, which means that for equivalent stress level, the adhesive VN 3158 can sustain 10 times more cycles than the adhesive HB 110 which can sustain 10 times more cycles than the PRF adhesive. The slope (given by the coefficient Λ) is almost identical for the HB 110 and PRF samples, whereas the VN 3158 adhesive demonstrates a less steep slope. The endurance limit is very similar between the system with an average around 3.3 ± 0.3 MPa.

The samples tested at a relative humidity of 85% are shown in Figure 7. The three adhesive systems S-N curves are quite similar due to the fact that the obtained results are very near. It should be reminded that at this relative humidity the short-term strength of the PRF is approx. 35% higher than for the 1C-PUR adhesives (see table 3). Using this relative scale, it appears, that contrary to the other climate, the slope coefficient Λ of the VN3158 is lower than the other adhesive systems. It should also be noted, that the LCF part of the S-N curve for the PRF adhesive is mostly determined by one run-out sample.

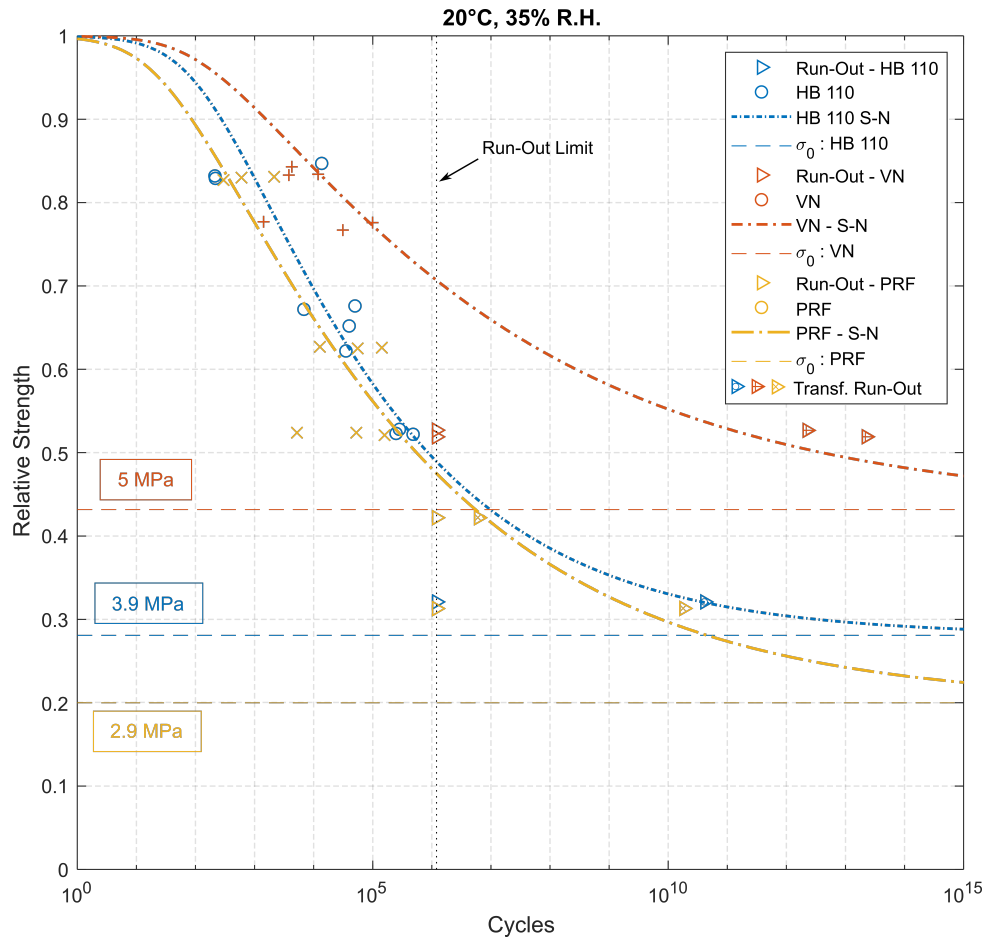


Figure 5 – S-N curves obtained at a climate of 20°C, 35% R.H. All points on the right of the Run-Out Limit are transformed Run-Outs (estimations obtained using the probabilistic model). The relative strength refers to the quasi-static strength (table 3) of each adhesive system. The absolute endurance limit strength value is given in a text box for each adhesive system.

Discussion

Influence of the adhesive's properties

For a relative humidity of 35% and 50%, both 1C-PUR adhesives can run a higher number of cycles for the same relative strength as than the PRF adhesive. Even though the difference are small between the HB 110 and PRF adhesive at a R.H. = 35%, the higher endurance limit of the HB 110 seem to confirm the hypothesis of (Bachtiar et al. 2017), that ductile adhesives such as both 1C-PUR are performing better under low cyclic fatigue. This hypothesis should however be confirmed with additional samples especially at a relative humidity of 35%. For higher humidity the performances of both 1C-PUR (adhesive HB 110 and VN 3158) decrease rapidly. This is certainly

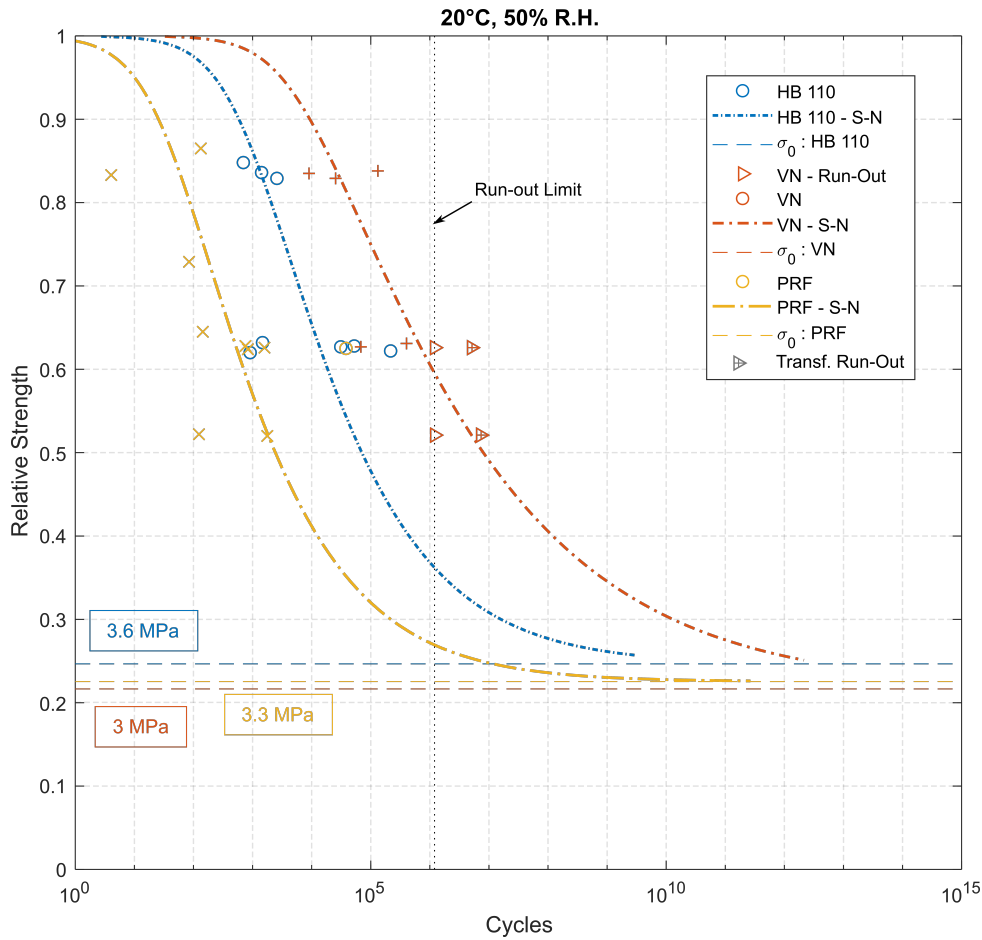


Figure 6 – S-N curves obtained at a climate of 20°C, 50% R.H. All points on the right of the Run-Out Limit are transformed Run-Outs (estimation obtained using the probabilistic model). The relative strength refers to the quasi-static strength (table 3) of each adhesive system. The absolute endurance limit strength value is given in a text box for each adhesive system .

due to the strength degradation of 1C-PUR under high humidity climate (Kläusler et al. 2013). This seems to be confirmed by the lower slope coefficient Φ (figure 6) for the VN adhesive and to the decreasing WFP (table 4) observed under high relative humidity. This contrasts with figure 5 and 6, where the average slope of the VN adhesive was generally less steep compared to the other adhesive system, this indicates that damages accumulate more rapidly for high ambient moisture content in comparison with the adhesive HB 110 which seems less impacted. One possible explanation, which should be verified in further tests, could be that fibers in the HB 110 adhesive which have a different humidity sensibility create a more heterogenous adhesive matrix with increased energy dissipation as measured by (Künniger et al. 2019). This increase in energy dissipation over the VN adhesive could compensate the reduced adhesion and

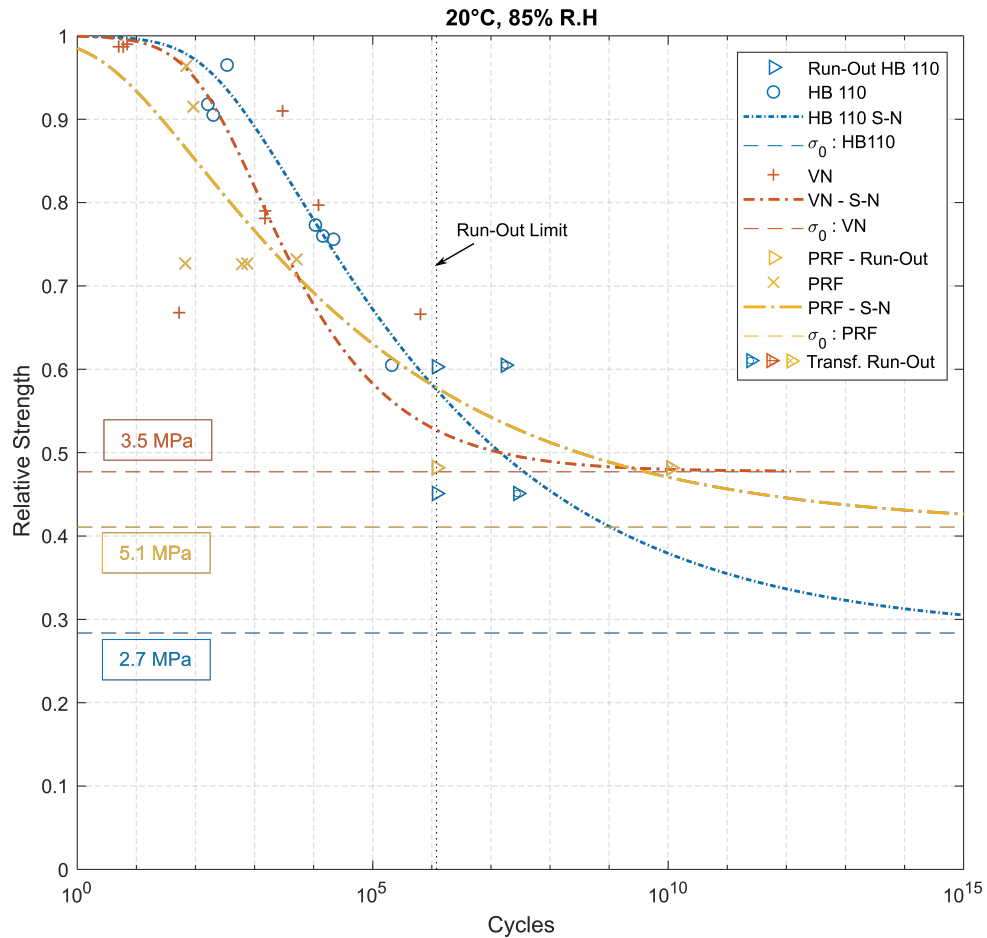


Figure 7 – S-N curves obtained at a climate of 20°C, 85% R.H. All points on the right of the Run-Out Limit are transformed Run-Outs (estimation obtained using the probabilistic model). The relative strength refers to the quasi-static strength (table 3) of each adhesive system. The absolute endurance limit strength value is given in a text box for each adhesive system.

results in slightly better performance for the HB 110 for cyclic loading at high moisture levels.

Influence of the sample geometry

The geometry used for the sample production is convenient and relatively easy to manufacture also it represents a standard testing geometry used for wood adhesive certification. However, Finite Element Analysis have shown (see Fig. 8) that the exact stress distribution is non-homogeneous and influenced by the adhesive modulus of elasticity (Hering 2011)

Furthermore, as seen in Fig. 8, for adhesives with a high elastic modulus, the stress peaks along the notches are higher than for adhesive with a lower elastic modulus. This

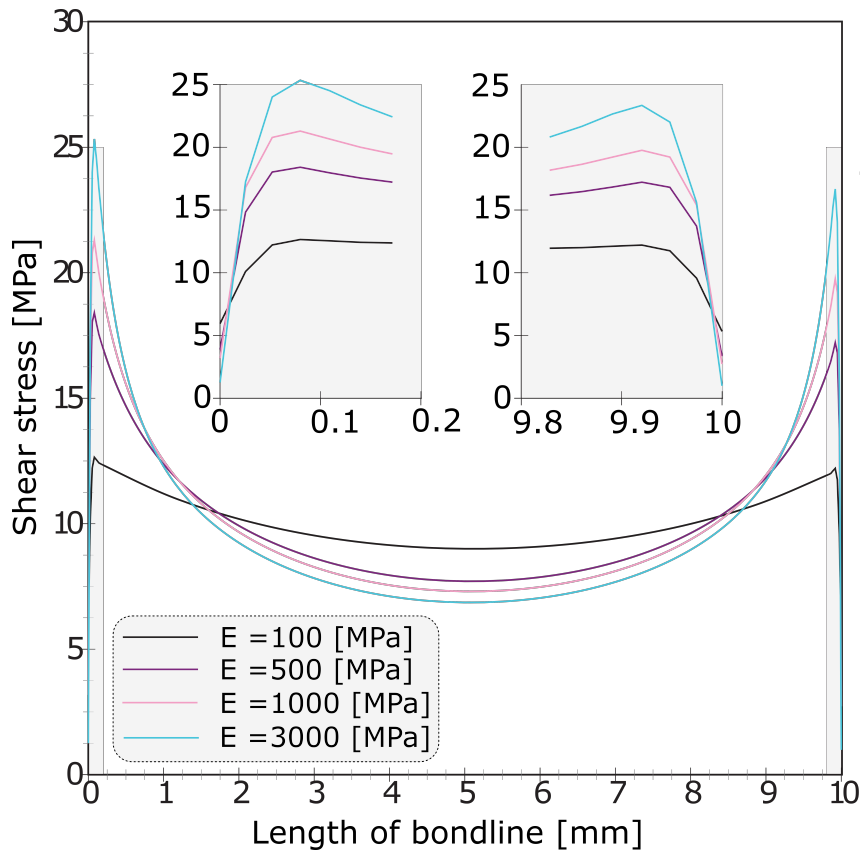


Figure 8 – Shear stress distribution along path AB (see fig. 3) in the bondline for various adhesive elastic modulus (E) values – A 500 [MPa] elastic modulus correspond approximately to the rigidity of the HB 110, 1000 [MPa] to the adhesive VN 3158 and 3000 [MPa] to the adhesive PRF (Künniger et al. 2019). Figure and data adapted from (Hering, 2011).

implies, that rigid adhesive such as the PRF adhesive will demonstrate higher stress concentrations than 1C-PUR adhesives. This is generally beneficial during quasi-static test as a more similar rigidity between the adhesive and the wood helps to obtain a better distribution of the stress into the wood. But it seems that in the case of cyclic loading, micro-damages accumulate more quickly in those highly stressed zones, eventually leading to the failure of the sample. Figure 9 presents a section of a run-out sample glued with the PRF-adhesive. As shown in the false color representation a small crack is visible on one extremity of the run-out sample. The depth of the crack was estimated to be around 0.5 mm, which correspond approximately to the zone where the stress concentrations are the highest as shown in Fig. 8 (Hering 2011). In comparison, no sign of a crack could be seen for the 1C-PUR glued samples and for the non-tested PRF samples (images not shown). However, due to the limited resolution of $6.5 \mu\text{m}^3$, the existence of microcracks below this size cannot be ruled out.

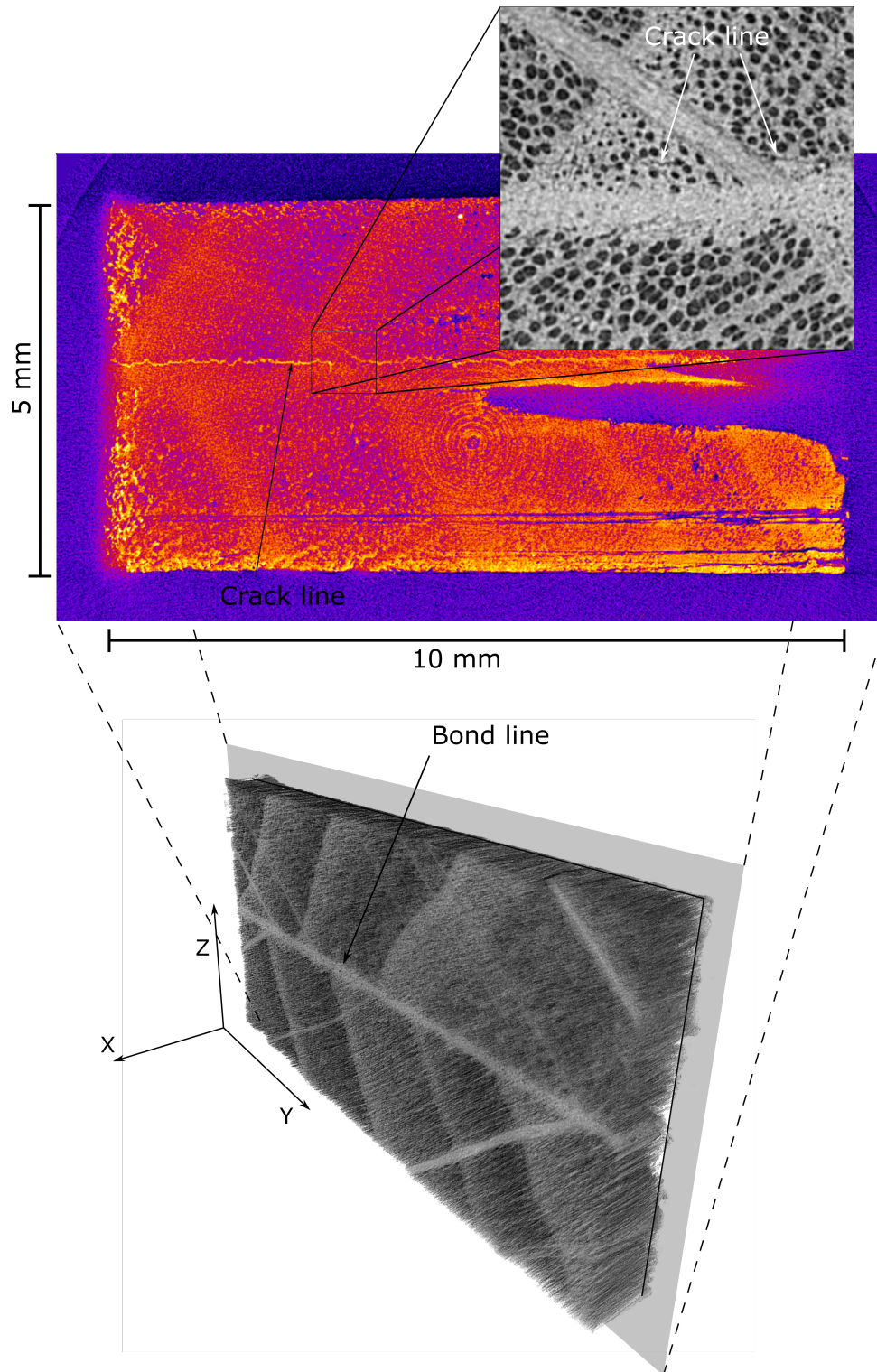


Figure 9 – Example of micro-CT scan result on one run-out PRF sample showing a small crack - 3D representation and false colors detailed view of the crack line on a cross-section of $10 \times 5 \text{ mm}^2$ – X-axis correspond to the longitudinal axis of the specimen, Y-axis to the width and Z-axis to the height of the specimen- the high density white line in the false color view is due to mineral particles incusted in the crack from the sanding process. As shown in the insert, the crack is still visible below the sample surface.

The data presented in this paper are showing that it is not possible to extrapolate directly the cyclic fatigue performance from quasi-static test. Indeed, during QS-test (at a climate of 20°C, 35% R.H and 50% R.H), the performance of the three adhesives are relatively similar. But under cyclic loading important differences between the adhesive systems emerge. It was shown, that 1C-PUR adhesive with a ductile behavior have better performance in dry moisture conditions than the more brittle PRF adhesive system. However, the decrease of the performance in higher moisture conditions is probably more due to the poor adhesion of 1C-PUR to the wood in high ambient moisture conditions, than to a modification of the dynamical properties of the adhesive. For these climates, the decrease of the tensile shear strength and the fact that no wood fracture was observed on the 1C-PUR clearly indicates an adhesion failure of the specimen. Indeed, as shown by (Künniger et al. 2019) the tan delta value of the 1C-PUR adhesive is increasing with the ambient moisture conditions, meaning that the performance of the 1C-PUR should continue to improve over the PRF adhesive (which displays a very constant tan delta value over the tested rel. humidity range). As this is not the case, it can be hypothesized that the cohesive properties of the adhesive have only a limited influence on the dynamical performance. An improvement of the adhesion between wood and adhesive, especially at higher relative humidity, while maintaining a relative low adhesive elastic modulus could be a promising development path for new adhesive system.

Influence of the relative humidity on the fatigue strength

The influence of the relative humidity on the adhesive PRF tested under cyclic fatigue is shown in figure 10. A steeper curve is observed for the 50% R.H. climate compared to the 35%. which would indicate a faster damage accumulation for high ambient moisture. This trend is however not confirmed at a climate of 85% R.H. Indeed, here a less steep S-N curve and a higher endurance limit are obtained. A similar behavior is observed for the adhesive HB 110. In terms of model approach, both strength and activation energy of molecular flow are lower at high humidity which should imply a considerable reduction of the fatigue lifetime as observed between the 35% and 50% R.H- climate. Additional tests are needed to confirm the obtained S-N curve to understand if the different fatigue behavior observed at high humidity is due to different type of failure process, possibly due to a saturation of wood cell with humidity. (Lewis 1962) noted a mild sensitivity of fatigue strength for plain timber between air dry and green wood

where, on average, a steeper slope was observed for air dry and treated wood compared to green wood with a possible higher endurance limit for green wood.

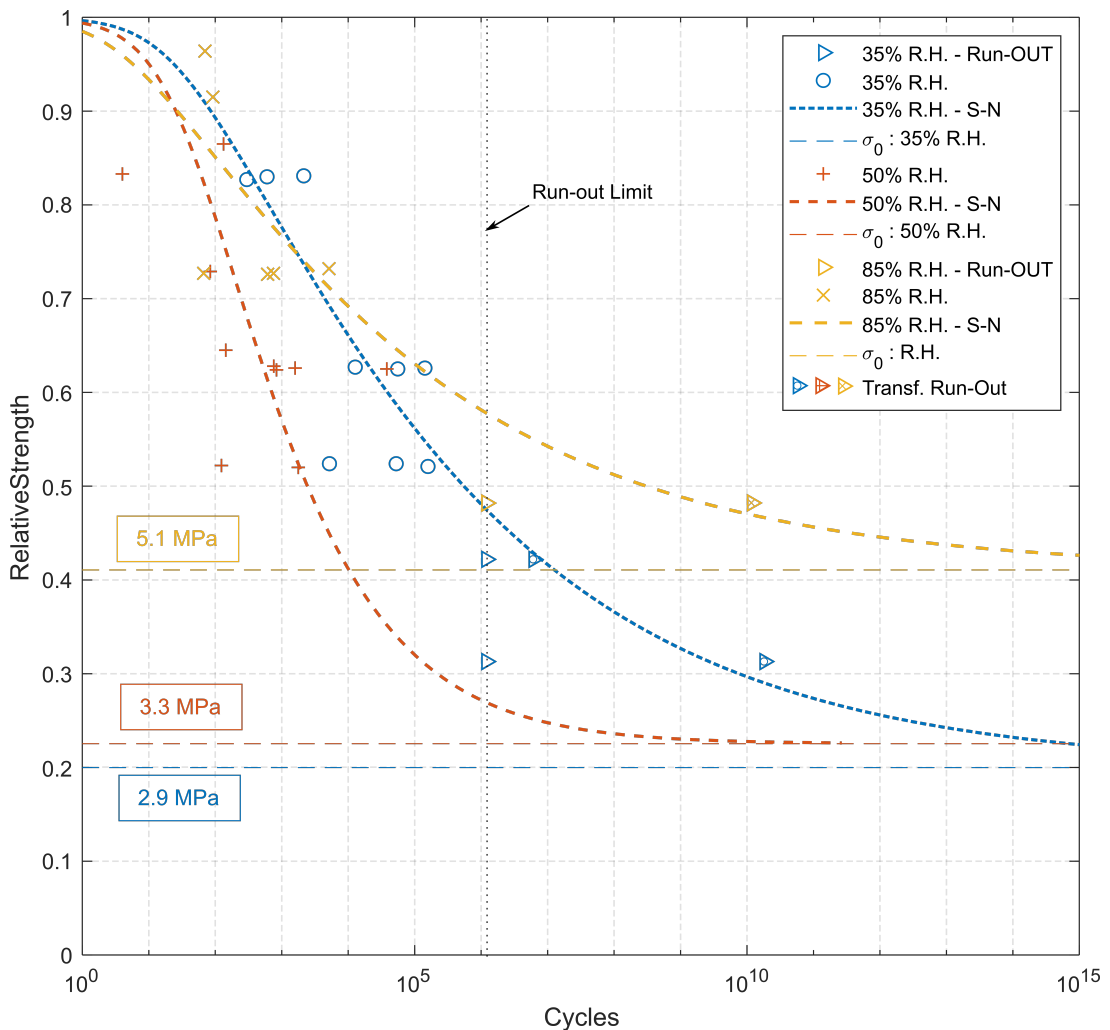


Figure 10 – Influence of three different relative humidity (35%-50%-85% R.H.) climates on the fatigue life of samples glued with the PRF adhesive. The relative strength refers to the quasi-static strength (table 3) of each adhesive system. The absolute endurance limit strength value is given in a text box.

It was noted that the endurance limit was not systematically influenced by the ambient moisture conditions. Indeed, the endurance limit was between 20-48 % (table 5) of the maximal load i.e. around 600 N or 3 MPa. This is in the same order as the value of 0.35 given in (van der Put 1989) for fatigue of wood and in (van de Kuilen 1999) for constant load in connections with a high shear stress levels under the fasteners, but clearly lower than for long term loads in wood, where this value is around 0.5 to 0.6. It seems therefore that the use of a probabilistic model to determine the endurance limit give satisfactory result compared to literature values. The endurance limit of the

data presented by (Bachtiar et al. 2017) for MUF and the 1C-PUR adhesive tested at 23°C, 50% R.H. was estimated to be 19% and 26% of the ultimate strength respectively. Which is in the same range as the data presented here.

Conclusion

A new general empirical model has been developed based on reaction kinetics for analyzing fatigue experiment. This model is able to describe the fatigue of adhesively bonded wood joints at low and high relative stress level using only three parameters which have a direct and clear influence on the determined S-N curves. A probabilistic model was used in an attempt to determine the endurance limit of bonded wood and estimate the fatigue lifetime of run-out samples. The obtained estimations seem to be realistic assumption of the endurance limit compared to literature values. This approach was used here on bonded wood specimen but could be applied to other material. It was shown that parameters Φ and Λ could be correlated with fundamental physical constant through the reaction kinetics approach, which provide a helpful analogy for understanding Stress-Cycle (S-N) curves. However, further researches are needed to be able to correlate these parameters with the sample properties (such as, for example, moisture content, type of wood, fibers orientation type of adhesive). It was shown, that for low relative humidity (35% and 50% R.H.) one component polyurethane (1C-PUR) adhesives can sustain a higher number of cycles for similar relative strength with an overall smaller damage accumulation rate than phenol resorcinol formaldehyde (PRF) adhesive. For high relative humidity (85% R.H.), the adhesion between the 1C-PUR adhesives and the wood is reduced leading to a decrease of the ultimate strength of the 1C-PUR samples compared to the PRF adhesive. In cyclic fatigue test at 85% R.H., the damage accumulation rate was higher for 1C-PUR adhesives compared to the PRF adhesive, which was attributed to the lower adhesion of 1C-PUR adhesives to the wood. The obtained results show that ductile adhesives, such as 1C-PUR, can run a higher number of cycles for a similar relative strength than brittle adhesive. It was hypothesized that this is due to the higher energy dissipated per cycle and to the more homogenous stress distribution along the glue line, delaying micro-damage accumulation.

Acknowledgement

The authors would like to express their thanks to Martin Lehmann who provided insight and expertise that greatly assisted the research and to Martin Otti for the support in performing the laboratory tests. The authors would also like to thank Innosuisse for the financial support (Project Nr.18958.1), as well as Henkel AG for providing 1C-PUR adhesive.

References

1. Bachtiar, E.V., Clerc, G., Brunner, A.J., Kaliske, M., Niemz, P. (2017) Static and dynamic tensile shear test of glued lap wooden joint with four different types of adhesives. *Holzforschung* 71(5):391-396
2. Barrett, J.D., Foschi, R.O. (1978) Duration of load and probability of failure in wood. Part I. Modelling creep rupture. *Canadian Journal of Civil Engineering* 5(4):505–514
3. Castillo, E., Fernández-Canteli, A. (2009) *A Unified Statistical Methodology for Modeling Fatigue Damage*. Springer Netherlands, Dordrecht
4. Caulfield, D.F. (1985) A chemical kinetics approach to the duration-of-load problem in wood. *Wood and Fiber Science* 17(4):504–521 EN 302-1:2013. Adhesives for load-bearing timber structures - Test methods - Part 1: Determination of longitudinal tensile shear strength
5. Fernández-Canteli, A., Przybilla, C., Nogal, M., Aenlle, M.L., Castillo, E. (2014) ProFatigue: A Software Program for Probabilistic Assessment of Experimental Fatigue Data Sets. *Procedia Engineering* 74:236–241
6. Feldkamp, L.A., Davis L.C. and Kress J.W. (1984): Practical cone-beam algorithm. *Journal of the Optical Society of America A* 1(6):612-619
7. Foschi, R.O., Yao, Z.C. (1986) Another Look at three duration of load models. International Council for Building Research Studies and Documentation Working Commission W18 - Timber Structures CIB-W18/19-9-1 Meeting 19 Florence, Italy.

8. Hering, S. (2011) Charakterisierung und Modellierung der Materialeigenschaften von Rotbuchenholz zur Simulation von Holzverklebungen, PhD Thesis ETH Zürich, Switzerland
9. Kläusler, O., Clauß, S., Lübke, L., Trachsel, J., Niemz, P. (2013) Influence of moisture on stress–strain behaviour of adhesives used for structural bonding of wood. *International Journal of Adhesion and Adhesives* 44:57–65
10. Knorz, M., Schmid, P., van de Kuilen, JW., Klaus. R. (2018) Time to Failure Testing in Shear of Wood–Adhesive Bonds under Elevated Temperatures. *Forest Products Journal* 68(4):383-389
11. Koller, R., Ruiz-Ripoll, M.L., García, A., Fernández-Canteli, A., Castillo, E. (2009) Exerimental validation of a statistical model for the Woehler field corresponding to any stress level and amplitude. *International Journal of Fatigue* 31(2):231–241
12. Krausz, A.S., Eyring, H. (1975) *Deformation kinetics*. John Wiley & Sons
13. Künniger, T., Clerc, G., Josset, S., Niemz, P., Pichelin, F., van de Kuilen, J.W.G. (2019) Influence of humidity and frequency on the energy dissipation in wood adhesives. *International Journal of Adhesion and Adhesives* 92:99-104
14. Kyanka, G.H. (1980) Fatigue properties of wood and wood composites. *International Journal of Fracture* 16(6):609–616
15. Lewis, W.C. (1962) Fatigue resistance of quarter-scale bridge stringers in flexure and shear. US Forest Product Laboratory, Madison , WI, USA Report No: 2236.
16. Marra, A.A. (1992) *Technology of wood bonding: Principles in practice*. Van Nostrand Reinhold, New York
17. Nielsen, L.F. (2000a) Lifetime and residual strength of wood subjected to static and variable load. Part I: Introduction and analysis. *Holz als Roh- und Werkstoff* 58(1-2):81–90
18. Nielsen, L.F. (2000b) Lifetime and residual strength of wood subjected to static and variable load. Part II: Applications and design. *Holz als Roh- und Werkstoff* 58(3):141–152

19. Ogawa, K., Shimizu, K., Yamasaki, M., Sasaki, Y. (2017) Fatigue behavior of Japanese cypress (*Chamaecyparis obtusa*) under repeated compression loading tests perpendicular to the grain. *Holzforschung* 71(6):499-504
20. Schindelin, J., Arganda-Carreras, I., Frise, E., Kaynig, V., Longair, M., Pietzsch, T., Preibisch, S., Rueden, C., Saalfeld, S., Schmid, B., Tinevez, J.-Y., White, D.J., Hartenstein, V., Eliceiri, K., Tomancak, P., Cardona, A. (2012) Fiji: an open-source platform for biological-image analysis. *Nature methods* 9(7):676–682
21. Schmid, B., Schindelin, J., Cardona, A. (2010) A high-level 3D visualization API for Java and ImageJ. *BMC Bioinformatics* 11:274
22. Smith, I., Landis, E., Gong, M. (2003) *Fracture and fatigue in wood*. Wiley, Chichester
23. Stoeckel, F., Konnerth, J., Gindl-Altmutter, W. (2013) Mechanical properties of adhesives for bonding wood—A review. *International Journal of Adhesion and Adhesives* 45:32–41
24. Tsai, K.T., Ansell, M.P. (1990) The fatigue properties of wood in flexure. *Journal of Materials Science* 25(2):865–878 van de Kuilen, J.W.G. (1999) *Duration of Load Effects in Timber Joints*. Ph.D., TU Delft, The Netherlands
25. van der Put, T.A.C.M. (1986) *Reaction kinetics of bond exchange of deformation and damage processes in wood*. International Council for Building Research Studies and Documentation Working Commission W18 - Timber Structures CIB-/W18/19-9-1 Meeting 19 Florence, Italy
26. van der Put, T.A.C.M. (1989) *Deformation and damage process in wood*. Ph.D., TU Delft, The Netherlands
27. Wood, L.W. (1947) Behavior of wood under continued loading. *Engineering News-Record* 139(24):108–111
28. Yao, F.Z., Foschi, R.O. (1993) Duration of load in wood: Canadian results and implementation in reliability-based design. *Canadian Journal of Civil Engineering* 20(3):358–365

3.3 Paper III - Adhesive wood joints under quasi-static and cyclic fatigue fracture Mode II loads

Paper III

International Journal of Fatigue 123 (2019) 40–52

Adhesive wood joints under quasi-static and cyclic fatigue fracture Mode II loads

Gaspard Clerc ^{a,d}, Andreas J. Brunner ^b, Sébastien Josset ^c, Peter Niemz ^a, Frédéric Pichelin ^a, Jan Willem G. van de Kuilen ^d

a. Bern University of Applied Sciences
Architecture, Wood and Civil Engineering
Solothurnstrasse 102
CH-2500 Biel

b. Empa, Swiss Federal Laboratories for Materials Science and Technology
Mechanical Systems Engineering
Überlandstrasse 129
CH-8600 Dübendorf

c. Henkel & cie. AG
Industriestrasse 17a
CH-6203 Sempach Station

d. Technical University of Munich
Wood Technology Munich
Winzererstrasse 45
DE-80797 München

Abstract

This paper investigates the energy release rate (ERR) in Mode II in-plane shear during delamination propagation under quasi-static and cyclic fatigue fracture loading with the 4-point end notched flexure (4-ENF) fracture test specimen. Wood joints bonded with three different adhesives, one rather brittle phenol resorcinol formaldehyde (PRF) and two different one component polyurethane (1C-PUR) adhesives with relatively low modulus of elasticity were tested in order to investigate the influence of the adhesive properties on the damage propagation under quasi-static and cyclic fatigue loading. A simple reduction method based on the specimens' compliance was used to calculate the crack growth and the energy release rate during the test. Additionally, an automated analysis method was developed estimating the energy of crack initiation from quasi-static test results. This shall avoid introducing additional scatter due to operator-dependent, manual analysis. It was shown that the three tested adhesives are displaying similar ERR values under quasi-static loading. Under cyclic fatigue fracture loading, the more brittle PRF samples are showing a slower crack growth rate for similar energy release rate in comparison with the 1C-PUR adhesives. The proposed testing method, applied to adhesively bonded wood joints, has been shown to give satisfactory results. This can be used for the development of new adhesives with increased performance regarding fatigue delamination growth. The automated data analysis has potential for application on other materials under cyclic Mode II fatigue fracture loads.

Keyword

Wood, Adhesive Joints, Fatigue crack growth, 4-ENF, Mode II

Nomenclature

a crack length

N number of cycles

N_{max} maximum number of cycles

K stress intensity factor

C, m fitting coefficients for the Paris equation

G_{max} maximum energy release rate measured during one cycle

$G_{II,max}$ maximum energy release rate in Mode II measured during one cycle

G_{thr} energy release rate threshold value

C_c compliance corrected according to setup rigidity

C_0 compliance calculated with a load of $P = 200\text{N}$

a_0 initial crack length

E_x Young's modulus of elasticity

I second moment of inertia

B width of the sample

H height of the sample

P_1 begin of the tests at a load of 20N during quasi-static loading

P_{NL} non-linear point during quasi-static loading

$P_{5\%}$ load at 5% increased compliance during quasi-static loading

P_{MAX} maximum load value during quasi-static loading

QS quasi-static tests

Introduction

Adhesively bonded joints play an increasingly important role in construction with composite materials, and, hence, specifically also in civil engineering structures made of wood materials (Vallée et al. 2016). Characterizing and comparing the performance of different types of adhesives under various load cases is essential for designing safe and durable wooden structures. A recent comparison between four types of adhesives used in glued wood lap joints (Bachtiar et al. 2017) had indicated that cyclic tensile shear fatigue loads yielded differences among the four adhesives that had not become apparent in quasi-static tensile lap shear tests. This type of test is often considered as a benchmark for adhesive performance in the wood-sector. However, despite its relative simplicity, lap-shear tests fail to determine useful adhesive properties (Tannert

et al. 2012) due to the complex multi-axial loading state. Also, no precise observation of the damage propagation can be made as a brittle failure is typically observed. In comparison, methods based on fracture energy (energy needed to fracture a unit area of the adhesive layer) offer an approach for quantifying the fracture behavior. The study of the energy release rate for wood bonding has already been investigated by numerous authors. Barret and Foschi (1977) introduced the geometry of the end-notch flexure (ENF) test to study the quasi-static Mode II fracture toughness evaluated as energy release rate (ERR) of wood in shear. The ENF specimen (as shown in Fig. 1) consists of two adherents partially joined with an adhesive layer. The non-glued part of the specimen is considered as starter crack, even though the crack tip (boundary between the glued zone and non-glued zone) is not necessarily a sharp crack tip. Often, the fracture toughness is investigated under mode I where the crack propagation is due to a tensile opening in the direction normal to the adhesive layer (Amman and Niemz 2015, Martin and Davidson 2013 and Watson et al. 2013). Despite the comparatively simpler testing procedure, mode I loading is not representative of the majority of the stresses occurring in wood glued beams. Indeed, as the strength of the wood is very weak perpendicular to the wood fibers, timber engineers try to avoid exposing the beam, or more generally, the material to such stresses. However, cracks induced by moisture stresses are generally due to a mixed mode loading (Niemz and Sonderegger 2017). Yoshihara and Ohta (2000) introduced the measurement of mode II fracture toughness (GII) of wood using the three-point bending end notched flexure test (3-ENF). One issue with using 3-ENF samples is that the crack propagation is usually stable only if the initial crack length is at least 0.7 times half the span length. Another concern for obtaining the crack growth resistance curve by the 3-ENF test is the measurement of crack length during the test. This is considered difficult for samples loaded in-plane shear (mode II) as the crack propagates without a clear opening. Yoshihara (2004) proposed another method using the four-point bend end-notched flexure test (4-ENF) to overcome the minimum crack length criteria and to extend the crack length range to the complete length between the upper loading noses. To overcome the need to measure the crack length during the test, Moura et al. (2006) suggested to derive the crack length and the ERR from the compliance of the specimen, i.e., the measured load and displacement data. In this paper, a similar method has been used to calculate the crack length from the compliance data using the Bernoulli Beam theory (Martin and Davidson 2013). Methods based on the compliance to calculate the crack length allow to consider the different Fracture Process Zones (de Moura et al. 2006) due to the

different adhesive ductility but often need additional tests to determine the required material properties. Using the Bernoulli Beam theory, only the Elastic Modulus in the longitudinal direction (E_x) is needed to derive the energy release rate (ERR). Here, the authors choose to calculate E_x directly from the mechanical test data in an elastic zone prior to the crack propagation. Using this method, no further tests were needed and the crack length and ERR could be calculated directly. It shall, however be noted, that with this method the influence of shear stresses on the deformation of the sample is not accounted for. However, the influence of the shear deformation was considered to be small due to the 4-point bending setup and the rather slender sample geometry. This method for calculating the crack length during the test, was compared to visual observations and acoustic emission signals to identify the advancement of the crack tip.

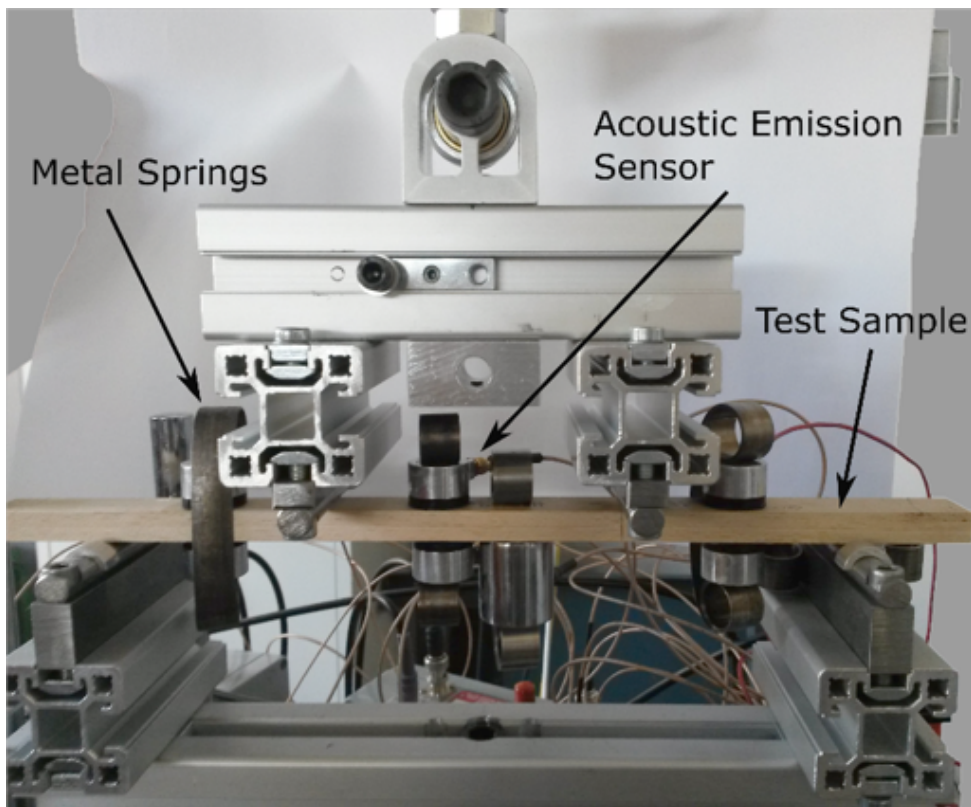


Figure 1 – Machine setup used for the experiment with the articulated head of support and the acoustic emission sensors mounted on the specimen.

Few researchers have addressed the performance of glued wood joints exposed to fatigue fracture testing. Previous works seem to focus mainly on the fatigue behavior of fiber reinforced wood composite (Jia and Davalos 2004, Qiao and Hu 2004) which are only a relatively marginal product compared to glued laminated timber. This

lack of interest is probably explained by the still common opinion encountered in the timber industry that wood itself is not prone to fatigue. Despite having good performance against fatigue, wood material can be expected to have similar fatigue performance as composite materials. Due to composition of the wood, i.e. cellulose fibers embedded in a lignin matrix, wood can be considered as a natural composite. In comparison with industrial composite, the formation of the wood cannot be controlled which generally implies a larger scatter in the results due to a larger variability in the intrinsic properties of the material. Also, considering only the performance of the wood is nowadays insufficient as wood is generally associated with adhesive to obtain the desired geometry and performance. Moreover, the influence of the glue properties on the performance of the wood adhesive joint remains vastly unknown. It is generally believed, that a fracture of the adherent is preferable for wood structures, as the glue should be stronger than the adherent. But this implies the use of rather brittle adhesives which generally perform poorly in terms of fatigue crack propagation (Hsieh et al. 2010). More ductile adhesives, however could provide a higher energy dissipation and a higher plasticity which would positively influence the fatigue lifetime of the bonded glue joint. For assessing, the influence of the adhesive properties on the cyclic fatigue fracture performance of the wood-adhesive joint, the crack growth related to the stress range per cycle was investigated using the same 4-ENF samples as in the Quasi-Static (QS) tests. Paris and Erdogan (1963) showed that a simple power model (Eq. (1)) can be used to describe the relation between the stress intensity factor range to a subcritical crack growth under cyclic fatigue load.

$$\frac{da}{dN} = C\Delta K^m \quad (1)$$

where ΔK is the stress intensity range, a the crack length, N the number of cycles, C and m fitting coefficients. This model can be visualized as a straight line (corresponding to the linear crack propagation zone) if the crack growth rate and the stress intensity range are plotted on a double logarithmic scale. A similar representation where the maximum energy release rate G_{max} instead of the stress intensity factor per cycle is used, is shown in Eq. (2)

$$\frac{da}{dN} = CG_{max}^m \quad (2)$$

This representation is convenient to use as it is often easier to calculate the ERR for inhomogeneous materials than the stress intensity factor. However, Eq. (2) is physically

erroneous since the ERR (G) is related to \sqrt{K} . Both models from Eqs. (1) and (2) are purely empirical and the parameters used are not directly related to physical mechanisms. Also, this model, only describes the linear part of the relation between the crack growth rate and the stress intensity factor range. It gives no information about the crack propagation leading to ultimate failure or concerning the existence of threshold ERR values where the crack growth rate becomes very small. Indeed, for small $\log(G)$ values, the $\log\left(\frac{da}{dN}\right)$ will become very small, hence approaching a ERR threshold value G_{thr} , under which no crack growth should occur (Pascoe et al. 2013, Kim et al. 2018). On the other hand, for large $\log(G)$ values approaching the quasi-static ERR, the $\log\left(\frac{da}{dN}\right)$ increases asymptotically. To determine the influence of the adhesive properties on the performance of the wood-adhesive joint a direct comparison of the energy needed for crack propagation was done under quasi-static and cyclic mode II fatigue fracture load using a brittle phenol formaldehyde system adhesive system compared to a rather ductile one component polyurethane adhesive. The use of ductile adhesives such as 1C-PUR tested here, generally implies a crack propagation in the bond line. To avoid a too fast crack propagation due to the very homogenous matrix of the adhesive, the addition of small polyamide fibers in the adhesive matrix to increase the fatigue fracture performance was investigated. The analysis of the results was done using an automated program (written with MATLAB R2018a) in order to simplify the analysis and minimize the scatter due to human factor. The aim of this article is hence to better understand the influence of the adhesive properties on the mode II cyclic fatigue fracture performance of the bond line and to improve the understanding of the main failure mechanisms and their causes in wood-adhesive joints.

Material and method

Preparation of the samples

Beech wood (*Fagus sylvatica* L.) with a mean density of 714 kg/m³ measured after storing the wood in a 20 °C, 65% R.H. climate was used for the tests. The wood has no defects such as knots and grain deviation. The length, the width and the height of the specimens correspond, respectively, to the longitudinal, tangential and radial wood orientation (average annual ring orientation of $13.7 \pm 5^\circ$). Planks were first planed to a thickness of 10 mm, a width of 150mm and a length of 700 mm. The planks were stored for at least two weeks in a climate of 20 °C and 65% relative humidity before planing to

a thickness of 5mm and then cut transversally in half. Before the adhesive bonding, a 15 μm thick fluoropolymer (ETFE230N) foil was applied between the lamellae on the first 120mm to simulate a starter crack. Three adhesives are compared in the tests, the first a relatively brittle phenol resorcinol formaldehyde (PRF, trade name «Aerodux 185») (PRF) and two ductile one component polyurethane (1C-PUR) adhesives with a low Modulus of Elasticity (MOE) (Kläusler et al. 2013). These two 1C-PUR adhesives are based on the same polymer, with the difference that additional short polyamide fibers were introduced in the adhesive matrix of the LOCTITE HB 110 PURBOND (HB 110) while absent in the LOCTITE VN 3158 (VN 3158). The gluing of the two lamellae was done approximately 3–4 h after the planing according to the gluing parameters described in Table 1 below. Once cured, the front-position of the foil was referenced as position of the crack tip and the crack length was cut to 110 mm. The samples were then cut to a width of 20mm and a length of 317 mm. The adhesively bonded wood joints were stored for several days in the test climate of 23 °C and 50% relative humidity before testing. The thickness of the adhesive layer was measured with a Leica DMLM/P optical microscope, for the HB 110 and VN 3158 adhesive the average thickness was $30 \pm 5 \mu\text{m}$ and $100 \pm 20 \mu\text{m}$ for the PRF adhesive, respectively. These differences between both adhesive systems are realistic and comparable to real glued laminated timber.

Table 1 – Gluing parameter used for the three different adhesives

Adhesive	Hardener	Glue spread [g/m^2]	Mixture ratio [Adh./Hard.]	Press. time [h]	Pressure [MPa]	CAT [min]
HB 110	-	180	-	10	0.8	10
VN 3158	-	180	-	10	0.8	10
Aerodux 185	HRP 155	340	100/20	10	0.8	30

Testing procedure

The machine used for the test was a servo-hydraulic test machine (type 1237 Instron) equipped with a 1 kN load cell with a load and displacement accuracy of at least 1% of the measured value. The head of the support, as shown in Fig. 1, was fully articulated to prevent any moment in the fixture apparatus. The quasi-static tests were performed under displacement control at 1 mm/min, three samples were tested for the VN adhesive and four samples for the PRF and HB 110 adhesive. For the

cyclically loaded samples, three samples for each adhesive were tested at a frequency of 5 Hz under displacement-control until reaching 40,000 cycles or until a low crack growth ($< 10^{-4}$ mm/cycle) was reached. The average displacement value was fixed to a deformation of 13.36 mm corresponding approximately to the average force of 400 N observed at the NL-Point. The amplitude of the test was fixed to ± 2.1 mm which corresponds approximately to a force of ± 200 N. The displacement ratio was set to 0.7 and kept constant for all samples. Also, Teflon was sprayed on the sample for assuring a low friction between the sample and the machine support. Selected quasi-static and cyclic fatigue fracture tests under mode II loading have been monitored with Acoustic Emission (AE). AE equipment (type AMSY-6) and preamplifiers (type AEP-3 with a band-pass between 30 and 1000 kHz), both from Vallen Systeme GmbH with 150 kHz resonant sensors (type SE-150M from Dunegan Engineering Corporation) have been used. Data acquisition settings were: acquisition threshold 40 dBAE, duration discrimination time 400 μ s, and a rearm time of 1 ms. Two AE sensors were placed on top and bottom each between the bottom and top loading rollers, and between the top loading rollers, respectively, i.e., a total of six AE sensors, and coupled with a silicone-free vacuum grease and mounted with metal springs (see Fig. 1 for details). For assessing the delamination length as a function of time, linear AE signal source location has been performed with three sensors mounted on the bottom side of the joint (there were additional AE sensors mounted on the top side of the beam, see Fig. 1). The location accuracy was checked via the so-called autocalibration for which each sensor in turn was used as emitter of elastic waves recorded by the other sensors.

Derivation of G_{II}

The setup used for this experiment is schematically shown in the Fig. 2. Please note that the distance between the supports and the loading points differs from the standard setups (1/3–1/3–1/3) and (1/4–1/2–1/4) for 4-point bending tests. This arrangement was chosen to allow the positioning of the acoustic emission sensors on selected samples. An overview of the acoustic emission results was published in (Brunner et al. 2018). A schematic representation of the test setup is shown in Fig. 2 where P is the load, PL and PR the relative load under both loading points V_l and V_r are the displacements under the loading points. Due to the pinned configuration, the force PL is equal to PR. The following system of differential equations (3) was derived using the Euler-Bernoulli equation. This system of Eq. (3) was then used to derive energy release rate and crack

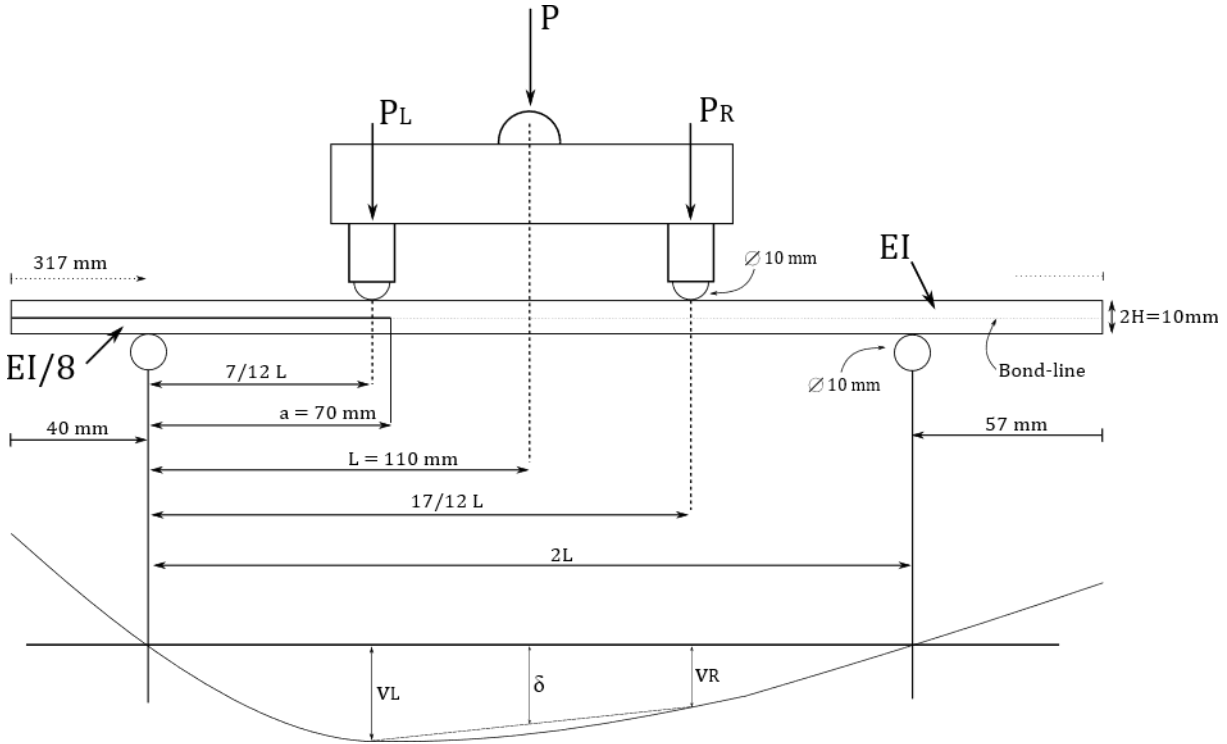


Figure 2 – Schematic representation of the test setup drawn to scale – With theoretical deformation line – support and loading noses diameter of 10 mm.

length.

$$\begin{cases} \frac{EI d^2 y}{8 dx^2} = -\frac{1}{4} P x & (0 \leq x \leq \frac{7}{12} L) \\ \frac{EI d^2 y}{8 dx^2} = -\frac{1}{8} P x & (\frac{7}{12} L \leq x \leq a) \\ EI \frac{d^2 y}{dx^2} = -\frac{1}{4} P x & (a \leq x \leq \frac{17}{12} L) \\ EI \frac{d^2 y}{dx^2} = -\frac{1}{2} P x - PL & (\frac{17}{12} L \leq x \leq 2L) \end{cases} \quad (3)$$

where E is the Young's modulus in the longitudinal axis and I is the moment of inertia in the crack-free region. Solving these equations for the displacements of both loading points, the displacement at the center of the beam δ is obtained according to Eq. (4):

$$\delta = \frac{|v_l - v_r|}{2} = \frac{49L^2 P(L + 54a)}{10368EI} \quad (4)$$

The compliance of the setup was measured by loading a steel bar from 0 to 700 N. The deformation vs force data were then fitted through a linear model. The Eq. (5) was then

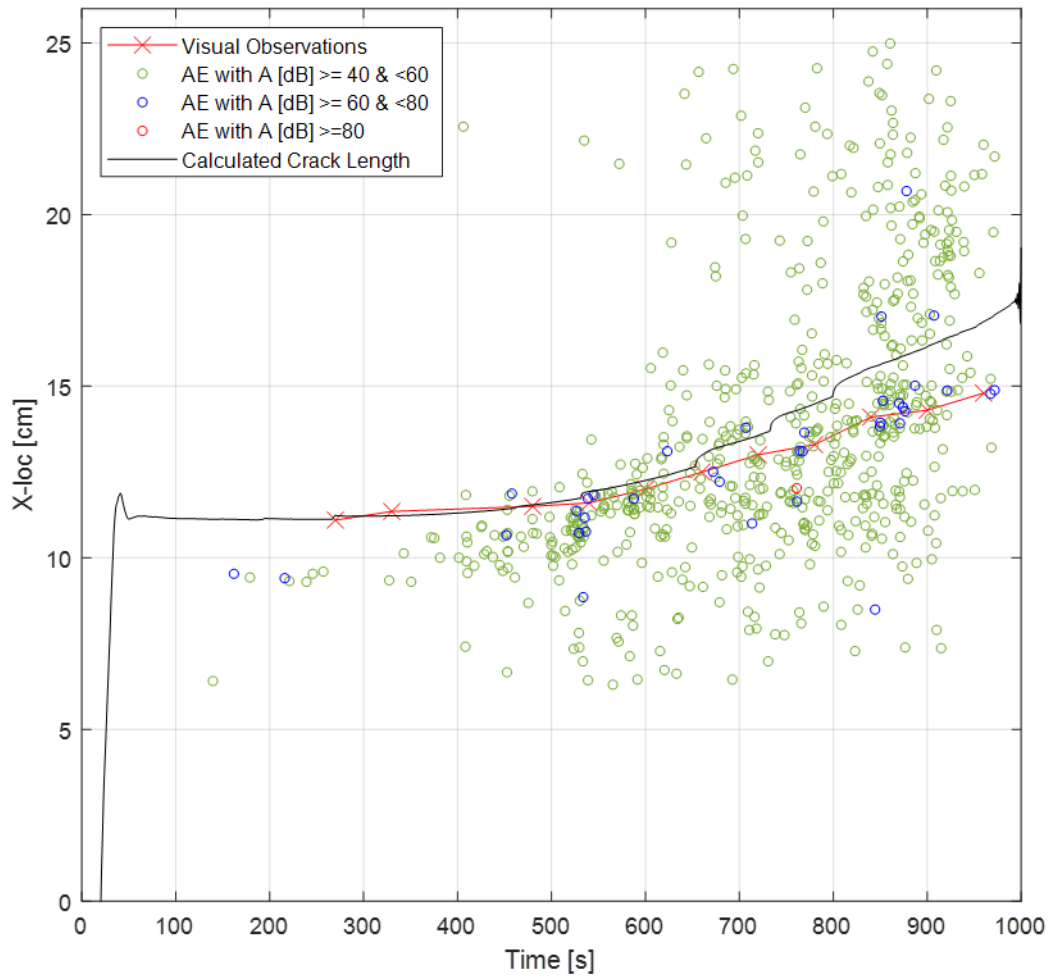


Figure 3 – Comparison of different methods for determination of the delamination length in quasistatic tests: Visual observation (red x, line drawn to guide the eye), calculated from change in compliance (black line), and from linear AE signal source location (open blue circles), see text for discussion. (For interpretation of the references to color in this figure legend, the reader is referred to the web version of this article.)

used to correct the deformation data for each sample.

$$\delta_c = \delta - 0.0003P + b \quad (5)$$

It appears that the value b , the offset in deformation, is varying with each sample and cannot be obtained from calibration measurement. Therefore, the value b was successfully estimated from the load-displacement curve by determining the crossing point of the extended theoretical elastic zone with the deformation axis. This correction

is critical for determining the effective crack length of the sample. The compliance at the loading point is then defined as the ratio of displacement to the applied force which correspond to the Eq. (6):

$$C_c = \frac{\delta_c}{P} = \frac{49L^2(L + 54a)}{10368EI} \quad (6)$$

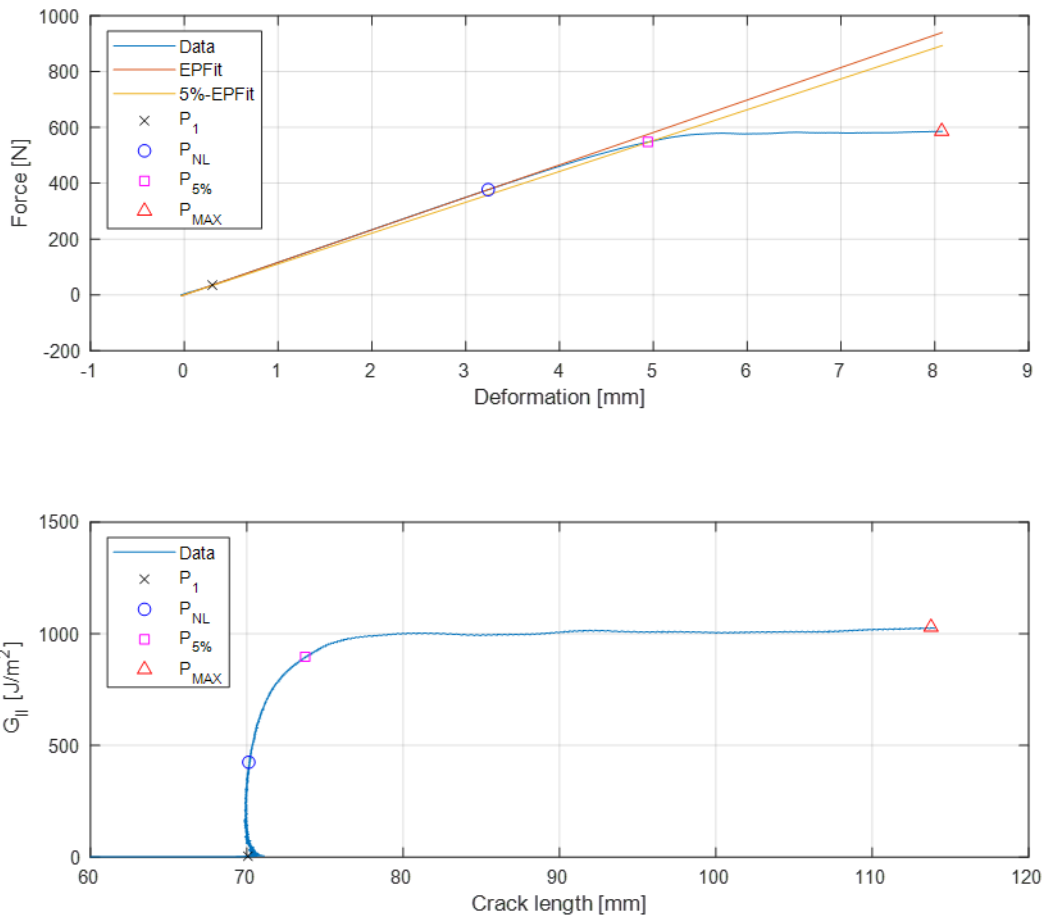


Figure 4 – Position of the point P_1 (corresponding to a load of 20 N to eliminate initial play), P_{NL} (Non-Linear Point), $P_{5\%}$ (5% reduced rigidity Point) and P_{MAX} (maximum force value).

The energy release rate G_{II} is calculated according to Eq. (7):

$$G_{II} = \frac{P^2}{2b} \frac{dC}{da} = \frac{49}{384} \frac{P^2 L^2}{BEI} \quad (7)$$

The theoretical crack length was calculated from the compliance Eq. (8)

$$a = \frac{C_c 10368EI - 49L^3}{2646L^2} \quad (8)$$

The Modulus of Elasticity was calculated according to Eq. (9) at a load of P=200 N (force higher than the initial deformation of the setup and lower than the crack start).

$$E = \frac{49L^3 + 2646L^2 a_0}{10368C_0 I} \quad (9)$$

Validation of the Method: To verify the delamination lengths calculated from the machine compliance data (solid black line in Fig. 3 for one quasi-static test), the delamination lengths from the quasi-static and cyclic fatigue fracture tests were compared with visual observation of the delamination propagation on the edge of the joint using a travelling microscope with magnification between 10x and 16x (red crosses in Fig. 3). For this measurement, the cyclic fatigue fracture tests were briefly stopped, since visual observation during cycling at 5 Hz was not feasible. A second, independent verification of the calculated delamination lengths was obtained from linear Acoustic Emission (AE) source location along the length of the beam (green, blue and red open circles in Fig. 3). The different colors of the AE signal source locations represent different ranges of AE signal amplitude (green between 40 and 60 dBAE, blue between 60 and 80 dBAE and red higher than 80 dBAE). If the AE signal source locations with intermediate amplitudes (40–60 dBAE) are taken as an indication of the tip of the delamination (e.g., similar to the amplitude range found for delamination in fiber reinforced polymer composites (Bohse et al. 2000)) these tend to slightly exceed the visual observation, while the calculated values (black line) indicate a larger delamination length, and this difference is even increasing with time. However, within a margin of about ± 1 cm, all three measures agree and indicate the same non-linear trend with time.

That visual observation on the edge yields the lowest value is reasonable in view of the fact that it is difficult to distinguish shear displacement from real delamination under mode II loading in adhesively bonded joints as discussed in detail, e.g., by Blackman et al. (2005). Comparing calculated delamination lengths with those from AE source location, it has to be noted that the accuracy of AE source location is limited to about 1 cm at best (as verified by simulating AE sources via pulsing the transducers before the start of the test and locating the signal sources), essentially due to the finite sensor diameter of 20 mm. Further, AE source location, in principle, highlights the size or

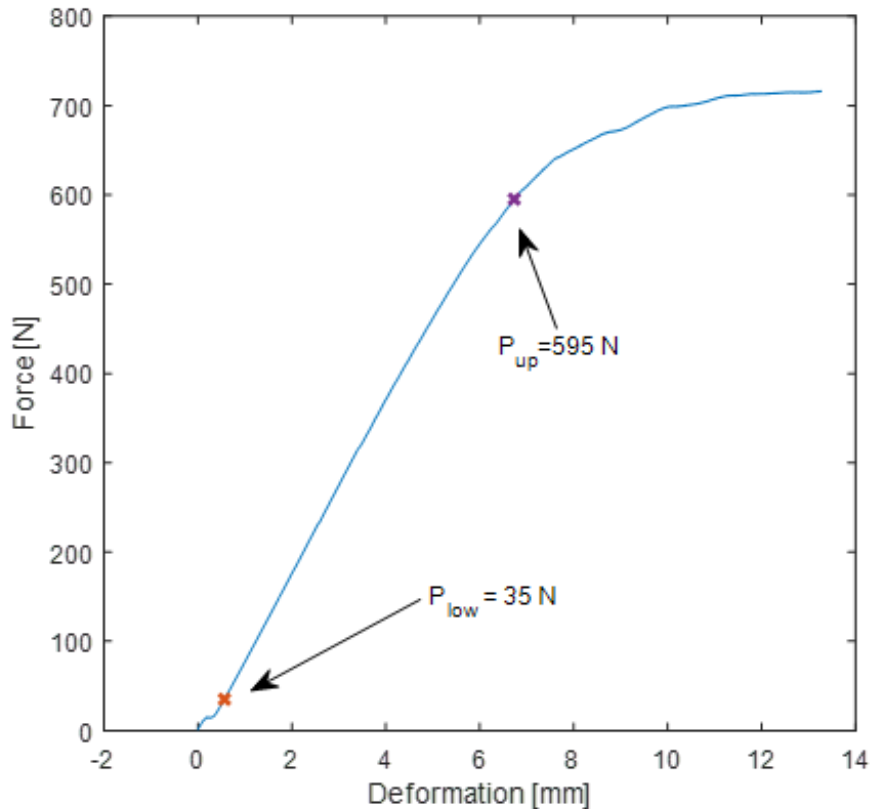


Figure 5 – Position of the point P_{low} and P_{up} for determining the position of P_{NL} .

extent of the fracture process zone around the delamination tip, and hence the accuracy also depends on the choice of the amplitude criterion to distinguish delamination from fracture process zone beyond the delamination tip. If the amplitude range is, e.g., reduced to 45–65 dBAE (instead of 60–80 dBAE), the delamination length indicated by the open blue circles would move closer to the black line. Damage accumulation in the fracture process zone around the tip of the delamination also explains the AE signal source locations far beyond the tip of the delamination observed in the last 300 s of the test. There, the adhesive joint beam shows significant bending and that induces distributed damage in the adherends and possibly in the adhesive beyond the delamination tip. It seems hence likely that the calculated delamination lengths from compliance may also tend to slightly overestimate the effective delamination lengths, since in that approach, all damage created in the specimen increasing its compliance is attributed to increasing delamination length, even if the damage is possibly created in the fracture process zone and/or in the adherends. In any case, the time-resolution of the compliance-based delamination propagation is higher (machine data sampling rate

of 5 Hz) than that of the other two methods (visual and AE) which explains why the observed step-like increases in delamination length at about 650, 730, and 800 s (Fig. 3) are not detected by the other two methods. Overall, it can be concluded that three independent methods do yield consistent delamination length measurements within the respective experimental resolution and that the compliance-based delamination lengths can be used for comparing the quasi-static and cyclic fatigue mode II fracture performance of the different adhesives.

Evaluation of the quasi-static samples

The ERR was evaluated at three different points. The first non-linear point on the load-displacement (P_{NL}) is interpreted as the onset of the crack propagation, it is defined as the limit of the elastic range. The slope of the elastic part is calculated between this point and the point P_1 (corresponding to a load of 20 N to eliminate initial non-linear play). The crossing point between the slope of a 5% more compliant sample and the load-deformation curve is then obtained ($P_{5\%}$). The third point corresponds to the maximum force obtained during the test. Fig. 4 shows an example of a typical test result. The linear-elastic part of the test is defined between the point P_1 and the P_{NL} . As mentioned by ASTM (E399-17) if the point where the maximum force is obtained (P_{MAX}) occurs later than the point $P_{5\%}$, then the point P_{MAX} shall be discarded. For all the tested samples, the P_{MAX} point occurred later than the point $P_{5\%}$, as it can also be seen in Fig. 4. Point P_{MAX} generally appears at a relatively arbitrary position once the plateau force value is reached. For these reasons, the P_{MAX} values were not further considered in the analysis. Also, the speed of the crack propagation was computed between P_{NL} and $P_{5\%}$.

Derivation of the Non-Linear (NL) point

The P_{NL} point is the position at which the force-displacement curve is not linear anymore and begins to curve due to the onset of damage. Defining this point accurately on the load-displacement plot is rather difficult. The normal procedure e.g. described in ISO 15024 is a subjective task which can produce a variability of approximately 10% between different examiners (Simon et al. 2017). Therefore, a procedure is proposed in this paper to calculate automatically the non-linear offset point using a simple algorithm avoiding subjective interpretation of the data. First, a force range is defined which contains the linear-part of the test. In this range, the value P_{low} and P_{up} are defined

corresponding respectively to the start of the linear range (force high enough to avoid effects from initial non-linearity due to play in the setup) and to a force clearly higher than the NL-point (loading curve should already be clearly curved at this point), as shown in Fig. 5. The algorithm will process the data only between these two points. To explain the principle of the method, three points (A, B and C) are considered as shown in Fig. 6. For the complete analysis, every recorded point between P_{low} and P_{up} will be considered. The next step of the algorithm is to draw a linear fit starting from P_{low} to point A and to calculate the fit parameter according to a linear polynomial. This line is named “Fit line A” in Fig. 6. Then, a goodness of fit test is done between the Fit line A and the data from P_{low} until Point A using the normalized root mean square error test. The goodness of fit is calculated and plotted versus the position of the point A. This step is then repeated for point B and C as illustrated in Fig. 6. To improve the accuracy of the algorithm, this procedure is repeated for each measured point between P_{low} and P_{up} . An example of the obtained goodness of fit coefficients is shown in Fig. 7. The position of the best fit corresponds to the point where the data approach best a straight line. It is therefore the most realistic point for the position of the P_{NL}

Evaluation of the cyclic fatigue fracture loaded samples

A similar evaluation method as for the quasi-static tested samples was used for the cyclic data as well. As suggested by Simon et al. (2017) the compliance of the samples was calculated with:

$$C = \frac{\delta_{max} - \delta_{min}}{P_{max} - P_{min}} \quad (10)$$

where δ_{max} and δ_{min} correspond to the maximum and minimum displacement, and P_{max} and P_{min} to the maximum and minimum force value per cycle, respectively.

The main difficulty regarding the analysis of the samples consists of the smoothing of the data affected by experimental scatter. During the test, maximum and minimum force and displacement values for each cycle were recorded. The data were then smoothed using a so-called “logarithmic fitting” algorithm. For example, data-points are averaged every 200 cycles until 1000 cycles then every 500 cycles until 10,000 then every 1000 cycles until the end of the test ($N_{max} \leq 10^6$). These “cycle range” parameters were adjusted according to the different samples to obtain regularly spaced points over the test and a comparative number of data-points between the different samples. The

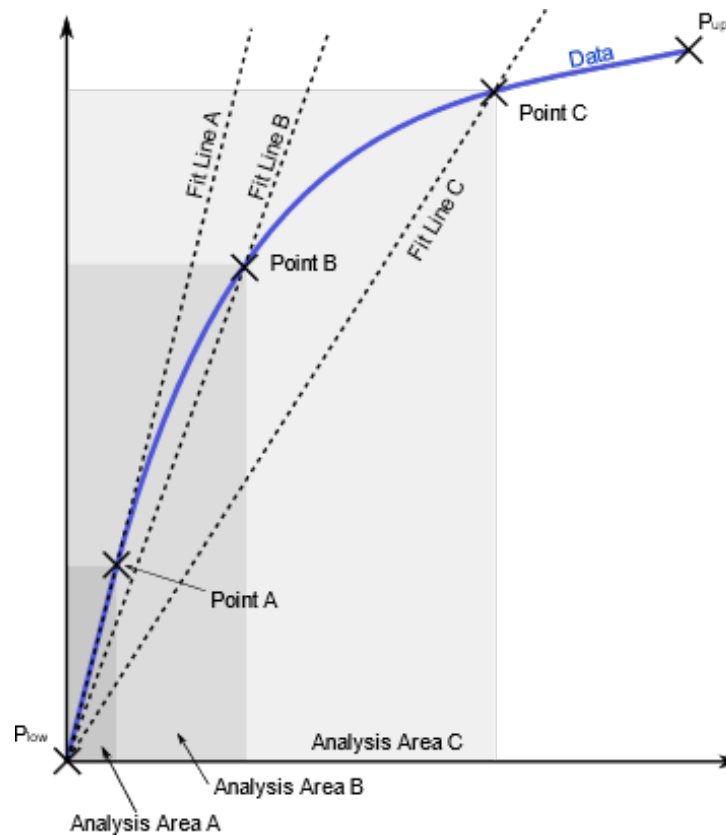


Figure 6 – Schematic representation of the procedure for determining the position of the Non-Linear (PNL) Point – the point A, B and C are representing different exemplary step of the algorithm.

compliance-data calculated according to Eq. (10) was log-fitted before calculating the crack length and its corresponding derivative. In comparison, a simple fitting of the data using a power model is shown in Fig. 8. As shown by the curve in Fig. 8, the log-fitting algorithm allows to follow exactly the raw data structure in comparison with the power model fitting which averages the data over the complete data-range. Also, as visible from the insert in Fig. 8, the power model is less precise at the beginning of the test for short crack lengths. The ERR data, calculated according to the Eq. (7) was also log-fitted with the same “log-fitting” parameters as the compliance data.

Results

Quasi-static mode II fracture

The obtained results for quasi-static mode II fracture are shown in Fig. 9. The ERR value at the P_{NL} and $P_{5\%}$ points ($G_{II,NL}$ and $G_{II,5\%}$ respectively) are shown respectively

for the three tested adhesives. Relatively similar results are obtained between the PRF and HB 110 adhesive with an ERR at P_{NL} of approximately 380 J/m^2 and 1000 J/m^2 at $P_{5\%}$. In comparison the VN 3158 adhesive show a higher ERR at PNL but a similar ERR at $P_{5\%}$. A two samples t-test (5% significance level) was used to find significant differences between the variables. Despite the lower ERR at $P_{5\%}$ for the HB 110 value no significant difference exists between the three adhesives at $P_{5\%}$. However, at P_{NL} the ERR value for the adhesive VN 3158 is significantly higher. These results seem to indicate that a higher energy is needed for the VN 3158 adhesive for the crack to initiate. However, despite this difference the crack reached a similar propagation value for the three tested adhesives (measured at $P_{5\%}$ which is in this case close to the average propagation values).

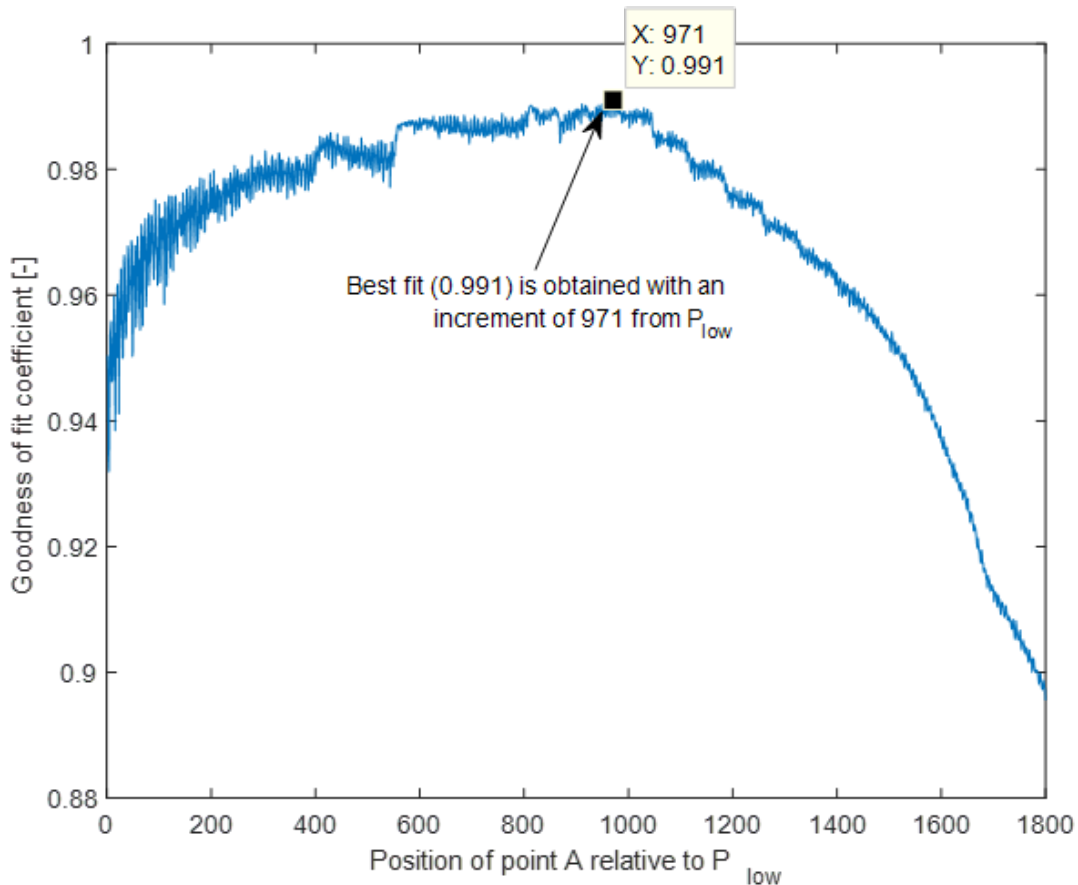


Figure 7 – Goodness of fit versus number of measured values for finding the position of the Non-Linear (NL) Point.

Table 2 gives the average value, the standard deviation, the coefficient of variation and the number of tested samples for the three-series shown in Fig. 9. The coefficient of

variation for the $G_{II,NL}$ and $G_{II,5\%}$ is lower for the PRF adhesive than for the 1C-PUR adhesives.

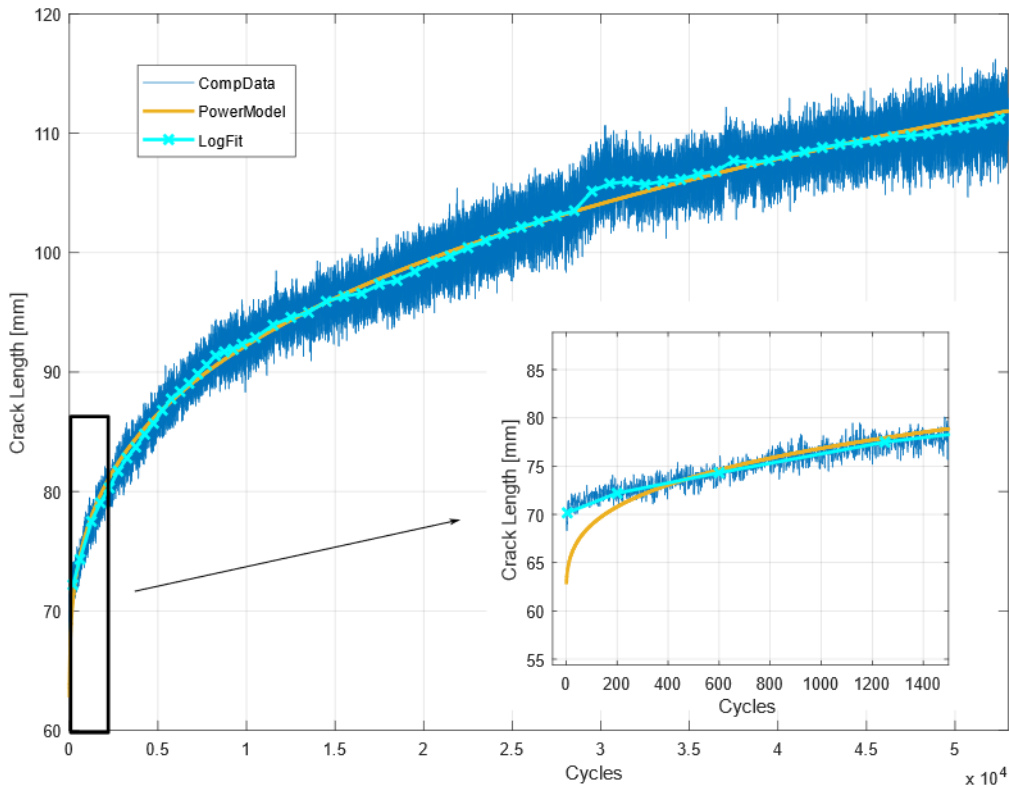


Figure 8 – Comparison between data-fitting method: Power model fitting versus Log fitting model and raw Compliance data – with extended view of the start of the experiment in the insert.

Both 1C-PUR have similar coefficients of variation. It shall be noted as visible in Fig. 9, that for the VN 3158 adhesive the ERR-value decreased shortly after reaching $G_{II,5\%}$ and reached a plateau of approx. 900 J/m^2 . For the HB 110 and PRF adhesive a more continuous increase was seen until reaching a plateau ERR of 1550 J/m^2 for the PRF and 1250 J/m^2 for the HB 110 always higher than the $G_{II,5\%}$ -value.

The values of the average speed of crack propagation are shown in Table 3. Despite the slightly lower values for the PRF, no significant differences could be observed between the three different adhesive systems under quasi-static loading.

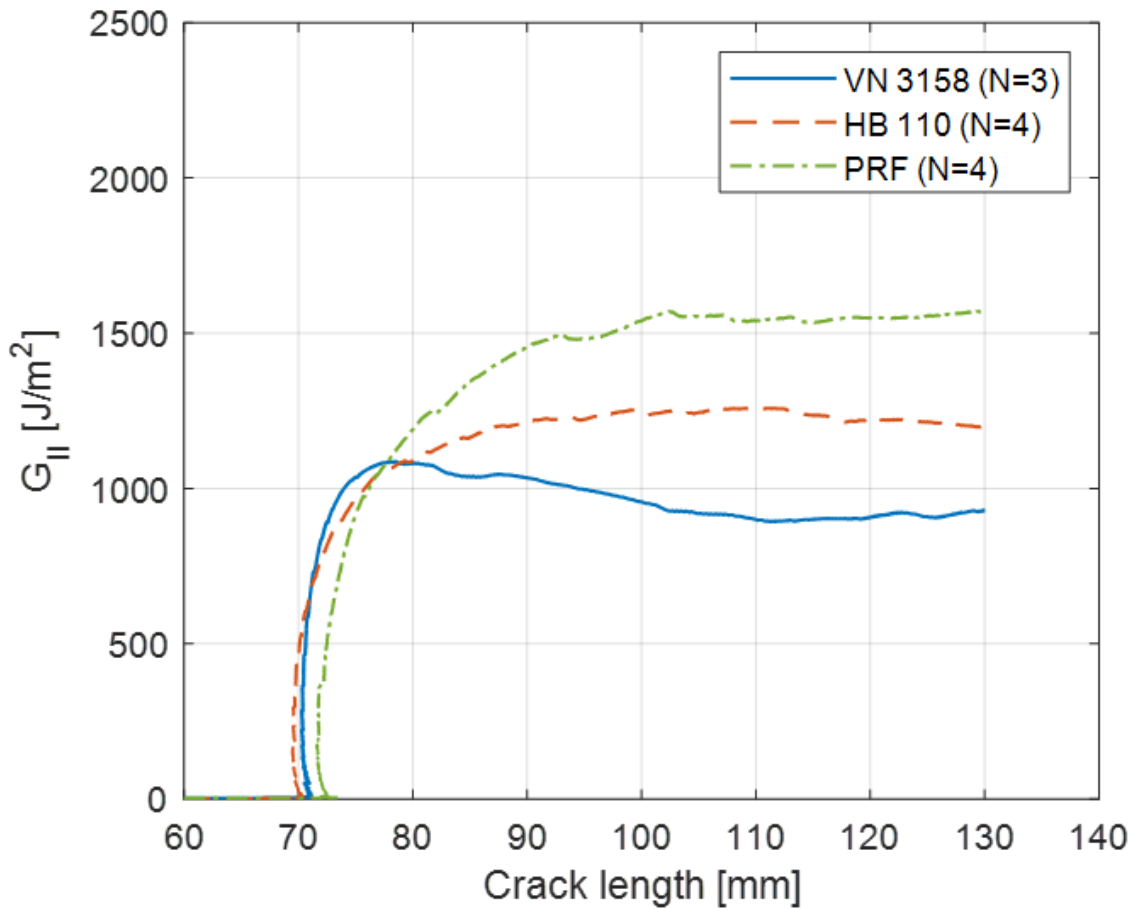


Figure 9 – Average G_{II} Resistance-curve for the three tested adhesives.

Cyclic fatigue fracture tests

Influence of the log-fitting method

The ERR values and the crack length were directly calculated out of the load and displacement machine-data according to Eqs. (7) and (8) respectively. Due to the high signal noise of the machine-data, an additional fitting phase was included. This fitting step was done using the log-fitting algorithm described above. Three different log-fitting parameters were tried out to determine the influence of the data point on the fitting quality. The parameters described in Table 4 were tested. The same number of points for averaging was used until 1000 cycles as 10 points was considered a minimum for the first part of the test. As can be seen in Fig. 10, the general trend of the Paris fitting line remains the same. Only a slight deviation can be seen between the fit in the lower G_{II} range. This difference is mainly due to the inaccuracy of the last data

points. Indeed, for the last data points, the G_{II} value remains almost constant with a very small increase in crack length, resulting in additional data-scatter. Therefore, a higher number of data points resulting from smaller step parameter in the log-fitting algorithm, as shown in Table 4 does not necessarily modify the fit line. For further analysis, the parameters were adjusted to obtain a similar number of points between the samples and to achieve a homogenous distribution of data-points over the complete data range.

Table 2 – Energy release rate numerical values and its scatter at the NL Point and at P5 for the HB 110, PRF and VN 3158 adhesive.

	HB 110 (N=4)		PRF (N=4)		VN 3158 (N=3)	
	$G_{II,NL}$	$G_{II,5\%}$	$G_{II,NL}$	$G_{II,5\%}$	$G_{II,NL}$	$G_{II,5\%}$
Average [J/m^2]	329	896	377	1004	539	1023
St-dev [J/m^2]	79	120	39	77	117	131
Coeff. Of. Var.	24%	13%	10%	8%	22%	13%

Table 3 – Average speed of crack propagation between P_{NL} and $P_{5\%}$ for the HB 110, PRF and VN 3158 adhesive.

	HB 110 (N=4)	PRF (N=4)	VN 3158 (N=3)
Average [mm/min]	1.8	1.7	2.1
St-dev [mm/min]	0.6	0.3	0.5

Comparison between different adhesive types

The crack propagation rate versus the ERR of the three samples glued with the VN adhesive are shown in Fig. 11. The obtained fitting coefficients are shown in Table 5.

Table 4 – Influence of the number of points for averaging on the fit quality.

	Until 1000	Until 10'000	Until 100'000	Num. of points
Fit1	100	250	500	120
Fit2	100	500	1000	65
Fit3	100	100	2000	37

The samples VN-2 and VN-3 show a very similar behavior. In comparison, the sample VN-1 has a similar slope but a higher ERR. Also, the crack propagation seems to stop earlier for the VN-1 sample at around 300 J/m^2 . For the samples VN-2 and VN-3, the crack propagation continues until an ERR of approximately 180 J/m^2 .

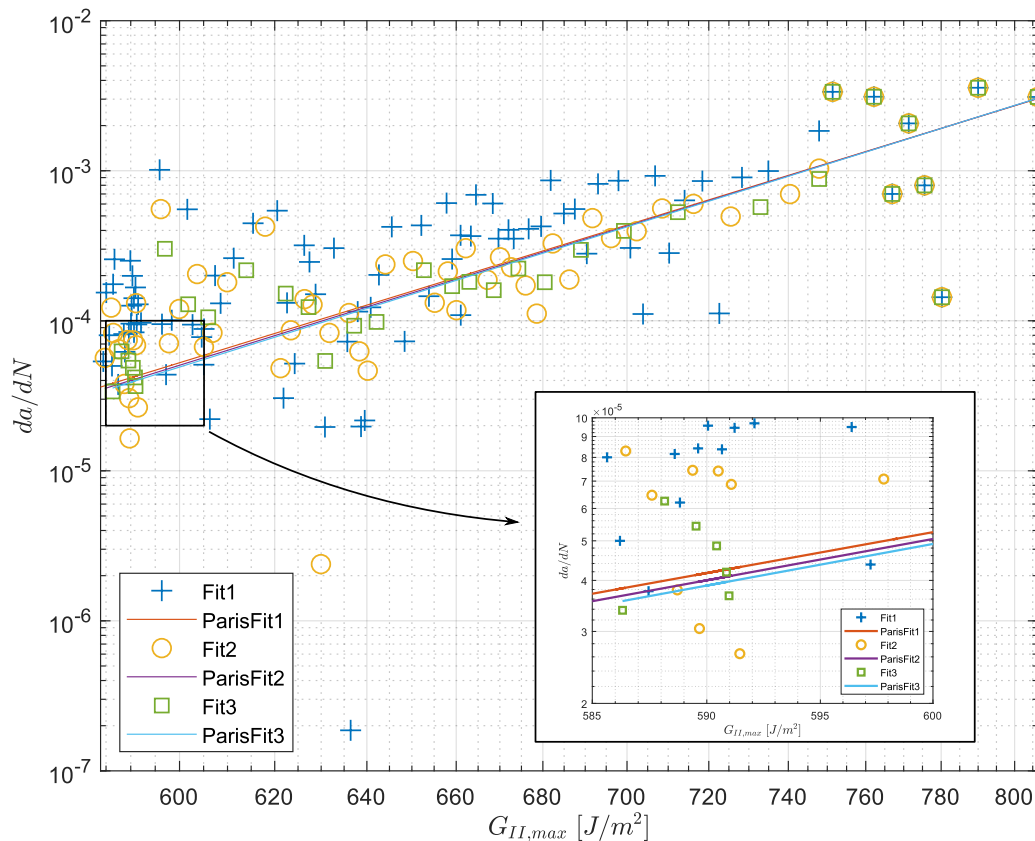


Figure 10 – Influence of number of data points described in Table 4 on the fit quality with extended view of the low ERR data.

The crack propagation rate versus the ERR of the three samples glued with the HB 110 adhesive are shown in Fig. 12. The obtained fitting coefficients are shown in Table 5. The three tested samples have similar slope and fitting coefficients. In comparison with the VN 3158 adhesive, it seems here that the crack propagation stops around an ERR value of 330 J/m^2 for the samples HB 110-1 and HB 110-2 and around 450 J/m^2 for the sample HB 110-3. The crack propagation rate versus the ERR of the three samples glued with the PRF adhesive are shown in Fig. 13. The obtained fitting coefficients are shown in Table 5. The sample PRF-1 show a much shorter data range than the other samples. This is due to the smaller crack length growth obtained during the

test, i.e. to the smaller crack growth range. The slope is relatively similar between the three samples. The crack propagation seems to stop around a value 600–660 J/m^2 , which is much higher than the observed value for the adhesives VN 3158 and HB 110, respectively.

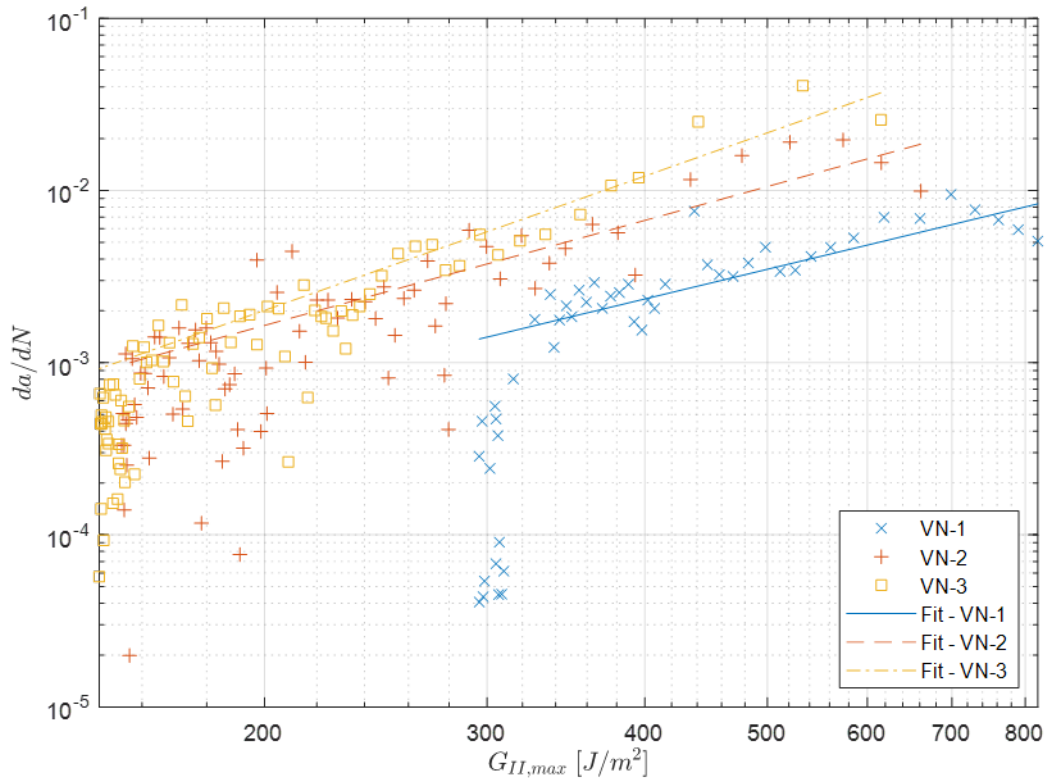


Figure 11 – Paris-plot for the three samples glued with the adhesive VN 3158.

For a better comparison, the Paris-plot of all samples tested with the three different adhesives is shown in Fig. 14, the respective Paris coefficients are given in Table 5. The fitting line shown in Fig. 14 for each adhesive was calculated by combining all the samples from one adhesive into a single data set. These coefficients correspond to the average behavior of one adhesive and are also given in Table 5. It could seem reasonable to estimate the behavior of one adhesive by averaging the Paris coefficients for each adhesive, but it appears that the fitting line calculated from these coefficients is generally clearly deviating from the data-points. From Fig. 14 and Table 5 three different groups can be distinguished. The PRF samples show a clearly distinct behavior compared to the 1C-PUR adhesive. The obtained m -fitting parameter is significantly higher than the same fitting coefficient for the VN and HB 110 adhesives. Both 1C-PUR adhesives are also displaying a different behavior. The VN adhesive has the lowest

Table 5 – Resulting fitting coefficient for the Paris model and all tested samples from the three different adhesives. The fitting coefficient were obtained by combining all data from one adhesive into a single data set.

Sample	C	m
VN-1	5.60E-06	1.78
VN-2	3.56E-08	2.03
VN-3	2.19E-09	2.59
MS-fit-VN	5.76E-07	1.51
HB-1	1.34E-12	3.32
HB-2	2.92E-16	4.73
HB-3	1.84E-13	3.53
MS-fit-HB	5.51E-13	3.44
PRF-1	3.02E-53	17.25
PRF-2	5.04E-39	12.27
PRF-3	5.58E-42	13.30
MS-fit-PRF	4.37E-42	13.33

C-coefficient and m-coefficient, which result in a comparatively fast crack growth rate as visible in the Fig. 15. The HB 110 is showing a behavior in between the VN adhesive and the PRF. The fitting lines for the HB 110 are steeper than for the VN samples and the average crack growth rate is lower. The higher ERR threshold values observed for the PRF adhesive imply that the crack growth will become very slow for a higher ERR than for 1CPUR adhesive. The difference between both 1C-PUR is smaller but it seems that the HB 110 has a higher ERR threshold value than the VN 3158 adhesive.

Discussion

The obtained results from the QS tests are showing that a higher ERR is obtained for the VN adhesive, meaning that a higher energy is needed to start the crack propagation. Yet, it was not possible to identify significantly different rates of crack propagation between the adhesive systems under static loading as shown in Table 3. Indeed, the crack-growth rate is higher for the VN 3158 adhesive than for the HB 110 and PRF adhesive. This implies that for the VN 3158 adhesive, once the crack is started the propagation will consume little energy. In comparison the HB 110 adhesive performs

clearly better. This is an interesting finding as the HB 110 adhesive and the VN 3158 adhesive are composed of the same polymer, with the only difference being that the HB 110 adhesive contains small (0.1 mm) polyamide fibers. These fibers seem to increase the energy needed for the crack to grow, and to slow the crack-growth rate of the HB 110 adhesive compared to the VN 3158 adhesive.

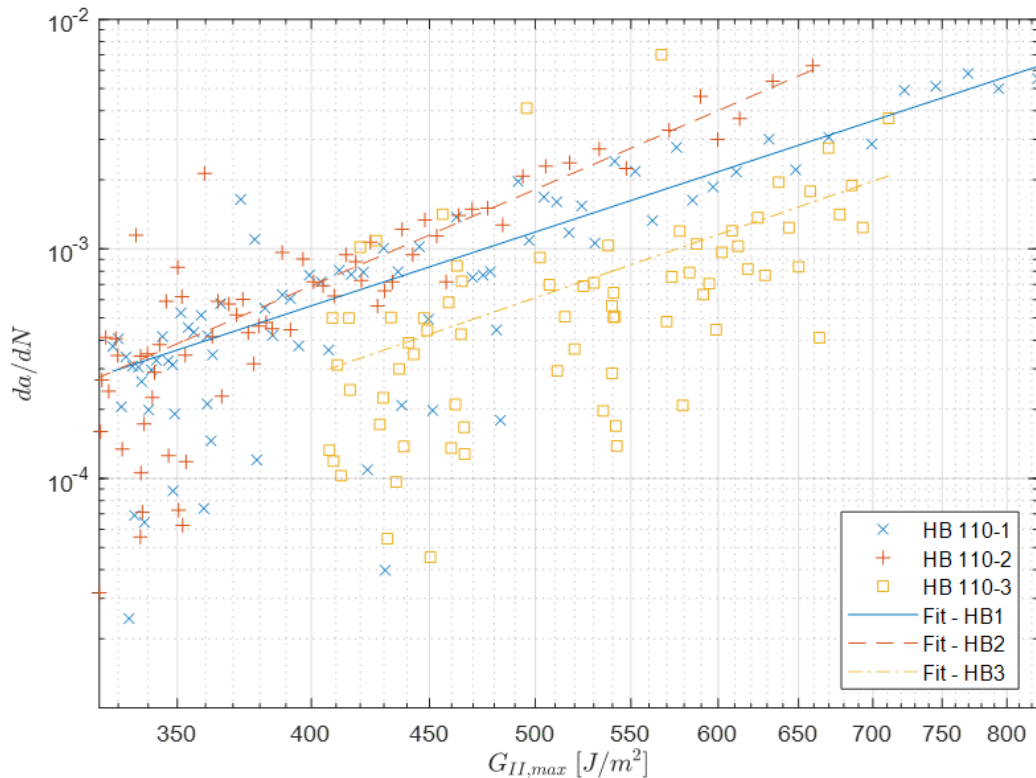


Figure 12 – Paris-plot for the three samples glued with the adhesive HB 110.

In comparison, the better performance of the PRF adhesive is probably due to wood fibers bridging effect through the better adhesion between the wood and the adhesive. Indeed, the propagation of the crack for the PRF samples was generally in the wood or at the wood adhesive interface (layers 4–9 as described by Marra (1992)).

Examples of wood-adhesive fracture surfaces for one PRF-sample are shown in Fig. 15, revealing several wood fibers and adhesive fragments. In comparison, for the 1C-PUR adhesive, the layer of crack propagation was mainly the adhesive interface (layers 1–3 (Marra 1992)). Fracture surface of one HB 110 sample reveals an overall smooth surface (compared to the PRF fracture surface) with a few polyamide fibers embedded in the adhesive. In comparison the fracture surface of the VN 3158 adhesive reveals a homogenous and smooth surface. Both 1C-PUR fracture surfaces show no sign of wood

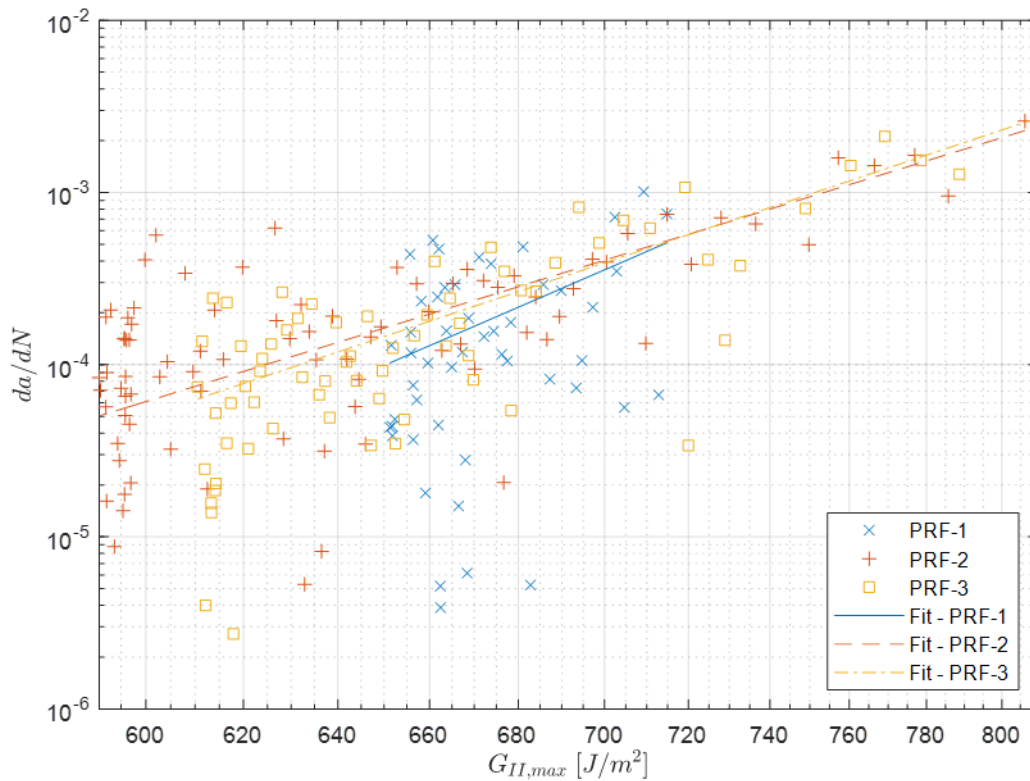


Figure 13 – Paris-plot for the three samples glued with the adhesive PRF.

fracture. It is however interesting to notice, that no plain wood failure was observed for the cyclic fatigue fracture loaded PRF samples, but only wood-adhesive interface failure as shown in Fig. 15. Only during quasi-static loading plain wood failure was observed for this adhesive type. This difference is yet not completely understood and could be due to the higher loading-rate in the cyclic tests and to a hypothetical different stress distribution.

It is interesting to notice that due to the viscoelastic properties of the adhesives and to the different loading rate between the QS and cyclic fatigue fracture tests, the respective performances of the adhesives are varying considerably. Indeed, despite having the highest $G_{II,NL}$ value in QS test, the VN adhesive has a higher speed of crack propagation at comparable lower ERR-level than the other adhesive systems. Also, the fatigue threshold of the VN adhesive is lower than the $G_{II,NL}$ value even though the opposite is observed for the other adhesive systems. Similar observations were done on unidirectional fiber reinforced composites by Stelzer et al. 2012. A possible explanation is, that the energy needed to start the crack is higher than the energy to propagate the crack, possibly due to the non well-defined crack-tip prior to the

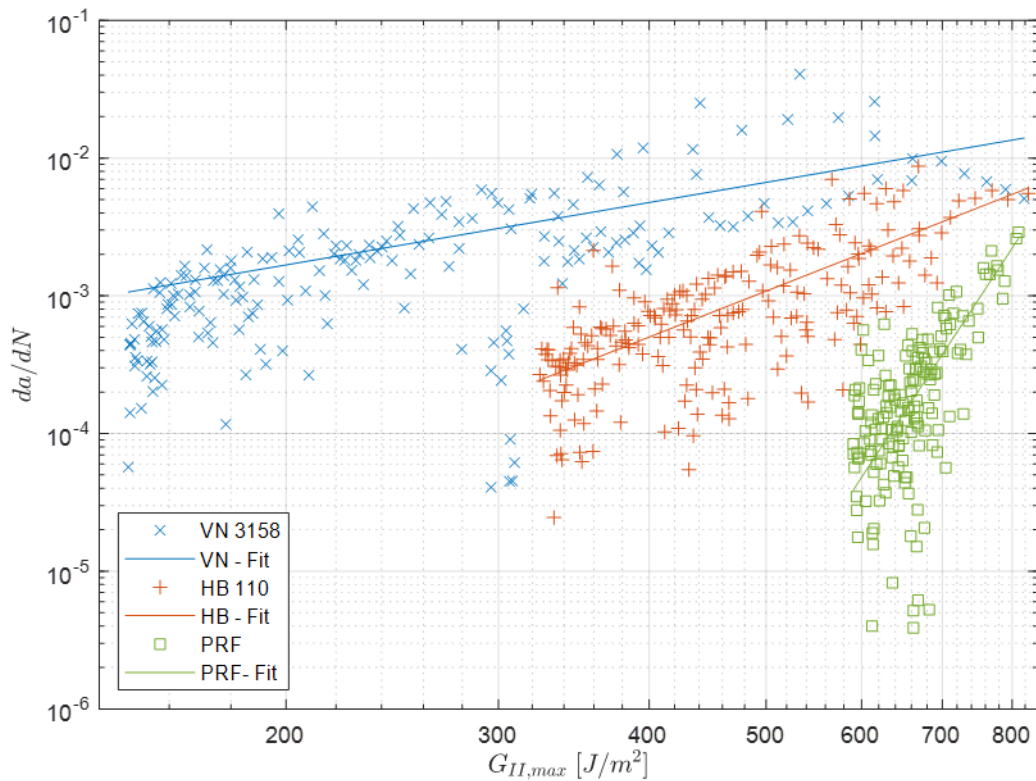


Figure 14 – Paris plot for all tested samples from the three different adhesives. Each fitting line was calculated by combining all data from one adhesive into a single data-set.

test. Also, it is possible, as visible on the fracture surfaces of the PRF samples, that different failure behaviors are encountered between the static and cyclic fatigue fracture test due to the different loading rate. Additional (unpublished) tests have shown that with samples with a low annual angle ($< 5^\circ$), it is difficult to achieve crack growth in the bondline before the bending failure of the lower lamella. This can be due to the different properties of wood crack propagation (Kretschmann 2010) and wood bending (Schneeweiß and Felber 2013). As a function of the annual ring angle. It shall also be noted, that for a horizontal ring orientation, the medullary rays are perpendicular to the bond line and could act as a reinforcement in the wood radial direction. Furthermore, the medullary rays could improve the adhesion of the adhesive with the wood through a better adhesive penetration in the wood. It is, therefore, likely, that the variability of the wood annual ring angle in the tested samples (and generally the variability of the wood properties) could explain the relatively large scatter of the results. Also, the exact crack-tip geometry is depending on the adhesive dispersion during the pressing and cannot be exactly reproduced from one sample to another. However, despite the

large scatter, the trends observed for the three tested adhesive systems can be well distinguished.

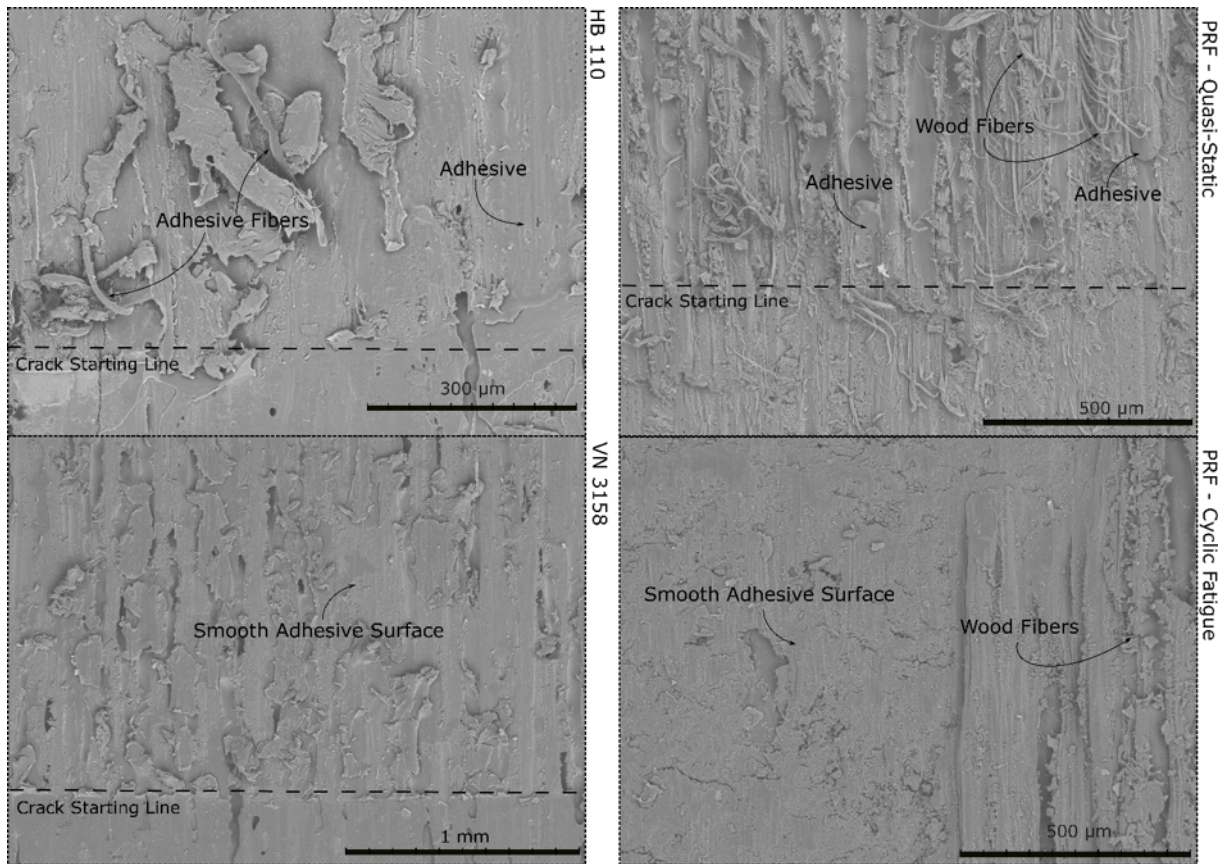


Figure 15 – REM images of the different fracture surfaces observed between the three-different adhesives – Note the different scale of the images – All images are from quasi-statically loaded samples except the last which is issued from a cyclic fatigue test.

The crack propagation for the tested brittle adhesive showed a slower delamination propagation at higher energy level than the more ductile 1C-PUR. These findings are contradictory with the conclusions presented by (Bachtiar et al. 2017) for lap shear tests where the ductile adhesives seem to perform better. This is probably explained by the different testing setup. Indeed, for lap-shear tests, no cracks are a priori present in the bondline before the failure of the sample, whereas for the 4-ENF test an artificial crack tip is created and the needed propagation energy is measured. Therefore, a ductile adhesive is probably advantageous for lap-shear tests where a higher amount of energy can be dissipated per cycle, however once a crack appears, the ductile adhesive matrix offers little resistance to propagation despite the higher plasticity. In comparison, due to its denser polymer network, the brittle adhesive has a better connection to the wood where fiber bridging effects improve the fatigue resistance. These findings seem

to indicate that a modification of the wood interface would possibly be beneficial to improve the bonding of the wood with the adhesive without having to use highly-polymerized-brittle adhesives. However, further testing is needed to verify the here presented hypothesis for the tested adhesives. It was shown, that the method for calculating the crack length gives accurate results compared to visual observations and determination of the position of the crack-tip using acoustic emission. As this model neglect the influence of shear stresses on the total deformation, the obtained crack length is slightly overestimated due to an overestimation of the MOE. Several models exist (Yoshihara and Ohta 2000 and de Moura et al. 2004) where the effects of shear stress on the deformation are considered. The model developed by de Moura et al. (2006) was used for the QS test in comparison with the developed Compliance-based model. As the differences between both models were confirmed to be small, the simpler compliance based model presented here was chosen for the analysis.

Conclusion

This paper presents a simple method to determine the mode-II inplane shear delamination resistance for adhesively bonded wood. This method is based on the simple beam theory for calculating the relevant fracture mechanics parameter directly out of the test data without additional measurements. In addition, an automated and systematic method was presented to simplify the estimation of the NL-point from quasi-static test. Using these methods, it was shown that the performances of three types of adhesives are very similar under quasi-static Mode II fracture loading. However, the crack growth rate between the adhesive under Mode II cyclic fatigue fracture is showing clear differences. The PRF adhesive displays the best fatigue behavior with a slow crack growth rate for relatively high ERR level in comparison to the 1CPUR adhesives. These good performances are probably due to the high adhesion between the wood and the PRF adhesive. It was shown that between the two 1C-PUR adhesives, the HB 110 is performing better under cyclic fatigue fracture loading than the VN 3158 adhesive. This difference is probably explained through the addition of small polyamide fibers in the adhesive matrix of the HB 110 adhesive, likely preventing rapid crack propagation. Yet, even the performance of the modified 1C-PUR adhesive remains below that of the PRF adhesive. Therefore, further testing is needed to better estimate the fatigue performance of glued wood specimens on non-precracked wood samples. The obtained findings can be used to modify the properties of the adherends to improve the fatigue

resistance of the wooden adhesive joint and to improve the design and prediction of the lifetime of structural adhesive joints subjected to cyclic fatigue fracture.

Acknowledgement

The authors thank the Swiss Innovation Agency for the financial support (Project 18958.1), as well as Henkel AG for providing 1C-PUR adhesive. Furthermore, the assistance of Mr. Daniel Völki for the test machine setup and data acquisition is gratefully acknowledged.

References

1. Vallée T, Tannert T, Fecht S (2016) Adhesively bonded connections in the context of timber engineering – a review. *J Adhesion*;93:257–87.
2. Bachtiar EV, Clerc G, Brunner AJ, Kaliske M, et al. (2017) Static and dynamic tensile shear test of glued lap wooden joint with four different types of adhesives. *Holzforschung*;71:391–6.
3. Tannert T, Vallée T, Hehl S (2012) Experimental and numerical investigations on adhesively bonded hardwood joints. *Int J Adhes Adhes*;37:65–9.
4. Barrett JD, Foschi RO (1977) Mode II stress-intensity factors for cracked wood beams. *Eng Fract Mech*;9:371–8.
5. Ammann S, Niemz P (2015) Specific fracture energy at glue joints in European beech wood. *Int J Adhes Adhes*;60:47–53.
6. Martin RH, Davidson BD (2013) Mode II fracture toughness evaluation using four point bend, end notched flexure test. *Plast Rubber Compos*;28:401–6.
7. Watson P, Clauss S, Ammann S, Niemz P (2013) Fracture properties of adhesive joints under mechanical stresses. *Wood Res*;58:43–56.
8. Niemz P, Sonderegger W (2000) *Holzphysik*. München: Carl Hanser Verlag GmbH & Co. KG.
9. Yoshihara H, Ohta M (2000) Measurement of mode II fracture toughness of wood by the end-notched flexure test. *J Wood Sci*;46:273–8.

10. Yoshihara H (2004) Mode II R-curve of wood measured by 4-ENF test. *Eng Fract Mech*;71:2065–77.
11. de Moura MFSE, Silva MAL, de Morais AB, Morais JJJ (2006) Equivalent crack based mode II fracture characterization of wood. *Eng Fract Mech*;73:978–93.
12. Jia J, Davalos JF (2004) Study of load ratio for Mode-I fatigue fracture of wood-FRP bonded interfaces. *J Compos Mater*;38:1211–30.
13. Qiao P, Hu G (2004) Mode-II fatigue fracture of wood-composite bonded interfaces. *J Compos Mater*;38:453–73.
14. Hsieh TH, Kinloch AJ, Masania K, Sohn Lee J, et al. (2010) The toughness of epoxy polymers and fibre composites modified with rubber microparticles and silica nanoparticles. *J Mater Sci*;45:1193–210.
15. Paris P, Erdogan F (1963) A critical analysis of crack propagation laws. *J Basic Eng*;85:528–33.
16. Pascoe JA, Alderliesten RC, Benedictus R (2013) Methods for the prediction of fatigue delamination growth in composites and adhesive bonds – a critical review. *Eng Fract Mech*;112–113:72–96.
17. Kim H-B, Naito K, Oguma H (2018) Mode II fatigue crack growth properties of adherends bonded with DP8005: end-notched flexible tests. *Int J Fatigue*;111:333–44.
18. Kläusler O, Clauß S, Lübke L, Trachsel J, et al. (2013) Influence of moisture on stress–strain behaviour of adhesives used for structural bonding of wood. *Int J Adhes Adhes*;44:57–65.
19. Brunner AJ, Clerc G, Niemz P (2018) Acoustic emission monitoring of adhesively bonded wood joints under quasistatic and cyclic fatigue mode II flexure loads using end notch flexure specimens. *Proceedings 33rd Acoustic Emission Conference (EWGAE)*; p. 116–25.
20. Bohse J, Krietsch T, Chen JH, Brunner AJ (2000) Acoustic emission analysis and micromechanical interpretation of Mode I fracture toughness tests on composite materials. Williams JG, Pavan A, editors. *Proceedings ESIS conference on fracture of polymers, composites and adhesives, vol. 27. ESIS Publication*; p. 15–26.

21. Blackman BRK, Kinloch AJ, Paraschi M (2005) The determination of the mode II adhesive fracture resistance, G_{IIC} , of structural adhesive joints: an effective crack length approach. *Eng Fract Mech*;72:877–97.
22. Davies P. Round Robin analysis of G_{Ic} interlaminar fracture test (1996) *Appl Compos Mater*;3:135–40.
23. Simon I, Banks-Sills L, Fourman V (2017) Mode I delamination propagation and R-ratio effects in woven composite DCB specimens for a multi-directional layup. *Int J Fatigue*;96:237–51.
24. Marra AA. *Technology of wood bonding: principles in practice* (1992) New York: Van Nostrand Reinhold
25. Stelzer S, Brunner AJ, Argüelles A, Murphy N, Pinter G (2012) Mode I delamination fatigue crack growth in unidirectional fiber reinforced composites: development of a standardized test procedure. *Compos Sci Technol*;72:1102–7.
26. Kretschmann DE (2010) *Wood handbook*. Chapter 05: mechanical properties of wood. General Technical Report FPL-GTR-190. Madison, WI: U.S. Department of Agriculture, Forest Service, Forest Products Laboratory; p. 1–46 [chapter 5].
27. Schneeweiß G, Felber S (2013) Review on the bending strength of wood and influencing factors. *Am J Mater Sci*;3:41–54.

3.4 Paper IV - Feasibility study on Hartman-Schijve data analysis for mode II fatigue fracture of adhesively bonded wood joints

Paper IV

International Journal of Fracture

Feasibility study on Hartman–Schijve data analysis for mode II fatigue fracture of adhesively bonded wood joints

Gaspard Clerc^{a,d}, Andreas J. Brunner^b, Peter Niemz^a, Jan Willem G. van de Kuilen^d

a. Bern University of Applied Sciences

Architecture, Wood and Civil Engineering

Solothurnstrasse 102

CH-2500 Biel

b. Empa, Swiss Federal Laboratories for Materials Science and Technology

Mechanical Systems Engineering

Überlandstrasse 129

CH-8600 Dübendorf

c. Henkel & cie. AG

Industriestrasse 17a

CH-6203 Sempach Station

d. Technical University of Munich

Wood Technology Munich

Winzererstrasse 45

DE-80797 München

Abstract

The feasibility of using the modified Hartman–Schijve (HS) equation to analyze the fatigue fracture performance of adhesively bonded wood specimens under cyclic mode II loading was investigated in comparison with the Paris crack growth equation. Wood joints prepared with three different adhesives have been subject to cyclic Mode II testing at room temperature (23°C and 50% relative humidity) in a four-point End-Notched-Flexure configuration, determining the crack length from specimen compliance. It was shown, that the HS-equation can be successfully applied to adhesively bonded wood and that it successfully estimates threshold and maximum energy release rate (ERR) values for three different adhesive systems. Since a limited number of tests were performed for investigating the feasibility, scatter sources and possible scatter reduction methods are analyzed and discussed in detail. Also, a new, automated data reduction method was developed for estimating the maximum and the threshold ERR (G_{thr}) values. The main advantage of the HS-equation appears to be the application in design standards. However, before the maximum ERR and G_{thr} values derived here can be used in design applications or for drafting a design guideline, additional testing is required for understanding how the number of cycles, the related measurement resolution; the corresponding ERR value influence the threshold value G_{thr} and how and to what extent its scatter can be reduced; and to further explore the link between cyclic ERR and the critical ERR value measured during quasi-static fracture tests.

Keyword

Wood adhesive, Fatigue fracture, 4-ENF, Paris-plot, Hartman-Schijve equation

Introduction

Timber as a renewable carbon-neutral material is gaining interest in the field of construction trying to reduce its ecological impact. To assure the future of timber as construction material, a good understanding of its mechanical behavior is required to obtain design rules that are not too conservative. In this matter, the design rules considering the fatigue behavior of timber generally are based on an extremely conservative design (Lewis 1960). Furthermore, the influence of adhesive on the fatigue life generally is not considered due to the lack of research in this domain (Kyanka 1980). Also, most

of the research considering the fatigue life of wood (Aicher 2015; Smith et al. 2003), or bonded wood (Bachtiar et al. 2017) is based on stress-cycle (S–N) tests, the aspect of crack propagation under fatigue loading of wood or bonded wood has received scant attention at best. Recently, Clerc et al. (2019a, b) showed that the fatigue crack-growth of adhesively bonded wood joints is successfully described by the Paris equation (Paris and Erdogan 1963) in the linear part of a fatigue test. Further, the type of adhesive has an influence on the crack growth rate, with ductile adhesives showing typically a faster delamination propagation compared to brittle adhesive systems. Since the Paris equation was originally developed to describe fatigue phenomena in metallic material, the stress intensity factor K was used. For composite materials, the use of the energy release rate (ERR), i.e., the G -value, is preferred over the stress intensity factor due to the material anisotropy. There is, however, still no consensus on whether it is more appropriate to use G_{max} , Δ or \sqrt{G} or a combination thereof (Alderliesten et al. 2018). However, as the Paris-equation (in a double-logarithmic presentation) can only be used to describe the linear range of crack growth during a fatigue test, it does not provide direct information for estimating a threshold energy release rate (G_{thr}) or the maximum energy release rate. These values, however, constitute essential information for the future development of a design standard considering the behavior of adhesively bonded wood over the complete fatigue crack propagation range. To extend the Paris-equation beyond the linear fatigue crack growth range, Hartman and Schijve (1970) proposed a new equation for the study of aluminum alloys which was adapted by Jones et al. (2012) as modified Hartman–Schijve (HS) equation to represent Mode I, Mode II, and later Mode I/II delamination growth in composites, as shown in Eq. (1).

$$\frac{da}{dN} = D \left(\frac{\sqrt{G_{max}} - \sqrt{G_{thr}}}{\sqrt{1 - \sqrt{G_{max}/A}}} \right)^\beta \quad (1)$$

where a is the crack length, N the number of cycles, G_{max} the maximum ERR measured during one cycle, G_{thr} the threshold ERR value, A the maximum ERR value and D , β being fit parameters. The advantage of the HS-equation is that it describes the full fatigue life of the specimen in a single, roughly linear equation whereas the Paris-equation describes only a limited part of crack growth (Jones et al. 2012). Furthermore, the HS-equation is capable of accounting for R-ratio effects. The HS-analysis uses a transformation of the x-axis where two additional parameters are introduced, $G_{II,thr}$ a threshold ERR value and A the maximum ERR value for Mode II, the latter roughly corresponding to the critical ERR obtained during quasi-static tests. One further advantage of using the

HS-equation is that the complete data set can be directly used for analysis. In comparison, data analyzed with the Paris equation should be carefully chosen so that only the linear part of crack growth is analyzed. Despite these advantages, a more refined data reduction method is needed to be able to estimate the four parameters needed for the HS-equation with sufficient accuracy (instead of two for the Paris equation). Of the four parameters in the HS-equation, two are fitting constants, i.e., D and β that are analogous to the C and m coefficients of the Paris-equation as described by Clerc et al. (2019a, b) and two are constants that each can be associated with a physical phenomenon. As explained previously the A value can be associated with the onset of crack growth corresponding approximately to the critical ERR obtained during quasi-static test ($G_{5\%}$). The $G_{II,thr}$ value, in principle, corresponds to the minimum ERR below which no crack growth should happen. It, together with the associated scatter, represents therefore a very important quantity for design purpose (Jones et al. 2017). Several different methods exist to determine these values (Yao et al. 2018), which are generally based on the same idea, i.e., obtaining a linear ‘master’ relationship between the ERR and da/dN values by adjusting the A and $G_{II,thr}$ values. This can be easily accomplished for data with comparatively low scatter as it is generally the case in polymer composites. But for adhesively bonded wood specimens, due to higher scatter of the data, a new automated method was developed in this paper. Beside the limited number of specimens tested in the feasibility study, the underlying reasons for the relatively high scatter observed in the results are not yet completely understood. Likely, these are due to a number of factors. Alderliesten et al. (2018) classify these into intrinsic and extrinsic factors (cite): “Examples of the latter are test set-up (e.g., compliance or play in the load-introduction, or load cell range with insufficient measurement resolution), operator experience (e.g., learning curve for proper test set-up as well as visual observation during testing), but also machining variation in specimen width and cutting quality, or variation in laminate plate thickness (e.g., near the edges) affecting the individual specimens’ compliance which should be limited or excluded by proper test specification. The intrinsic scatter, i.e. due to processing variability and inhomogeneous material morphology, should be considered relevant for design purposes and shall not be excluded nor underestimated.” In addition to the extrinsic scatter observed during fatigue fracture testing, wood itself is known to have a higher variability in morphology and hence yields higher intrinsic scatter in properties and fracture behavior than polymer composite materials. During a real fatigue test, the crack growth does not always follow a continuously increasing path. During short time intervals, the crack can quickly grow and then stabilize before

following the same tendency again. During these sporadic events, the crack growth rate and the energy level will change abruptly. If plotted chronologically in a double logarithmic plot, the obtained energy level and crack growth rate during these sporadic events strongly deviate from the average as their values are much higher and lower, respectively. This problem is generally best solved by fitting the crack length and the ERR data using an equation such as a second order power model (Stelzer et al. 2014). This, however, has the effect where all the sporadic events are smoothed to some extent by the fitting procedure, allowing, on the other hand, the scatter to be drastically reduced. It is, however, questionable to eliminate a source of scatter without determining its origin. Indeed, if the irregular crack growth events are due to material heterogeneity or non-uniform adhesive distribution, these shall be considered as intrinsic scatter and not be eliminated. Furthermore, as shown by Clerc et al. (2019a, b), the fit quality of a second order power model at the beginning and at the end of the test is generally low. This may not be an issue if the data are represented using the Paris-equation, where the main interest lies in the linear part of the test and the fit of the power model is generally good. However, if the data are plotted using the HS-equation, the test behavior should be accurately described, also for low and high ERR in order to be able to reliably determine the values of A and G_{thr} . Clerc et al. (2019a, b) present a simple method based on a moving average (on a logarithmic scale) of the crack growth rate and maximum ERR per cycles to estimate the Paris coefficient. This method is developed further in this paper to allow for an automatic estimation of the HS-parameters. A specific focus was given to the estimation of the ERR threshold and maximum value (A and $G_{II,thr}$), as they correspond to physical quantities which can be used for development of a future design standard. The goal of this article is to examine if the HS equation can be successfully applied to adhesively bonded wood and to compare the analysis of mode II fatigue crack growth data using the Paris-equation and the HS-equation in order to establish the strengths and weaknesses of both approaches as well as to validate approaches for reducing extrinsic scatter in the data. In Sect. 2, the preparation of the samples and the testing method will briefly be summarized. Then the data reduction method and the method used to determine the A and G_{thr} value are presented in detail. These methods then are applied in Sect. 3 to adhesively bonded wood glued with three different adhesive systems and tested with the four point End-Notched Flexure (4-ENF) specimen in constant amplitude cyclic fatigue. In Sect. 4, the sources of scatter will be discussed, and a different method will be presented with the potential of reducing the scatter of the data. Finally, in the conclusion, the main findings in this article will be

summarized and a brief outlook will be given on how to improve the results presented here and how they can possibly be used in a design guideline.

Material and methods

Preparation of the samples

A detailed description of the samples' preparation and the testing method can be found in Clerc et al. (2019a, b). Only the main steps will be described here. Beech wood (*Fagus sylvatica* L.) with a mean density of 714 kg/m^3 at a wood moisture content of 12% was used for the tests. The wood had no defects such as knots and grain deviation, the boards were planed prior to bonding to avoid the migration of wood extractives on the surface and to guarantee their planeness. Before the adhesive bonding, a $15 \text{ }\mu\text{m}$ thick fluoropolymer (ETFE230N) foil was applied between the lamellae on the first 120 mm to simulate a starter crack. Three adhesives are compared in the tests, one relatively brittle phenol resorcinol formaldehyde (PRF, trade name «Aerodux 185») with a Young's modulus of approx. 2750 MPa and two ductile one component polyurethane (1C-PUR) adhesives with a low Young's modulus (approx. 1000 MPa for the VN3158 and 500 MPa for the HB 110). These two 1C-PUR adhesives are based on the same polymer, with the difference that additional small polyamide fibers were introduced in the adhesive matrix of the LOCTITE HB 110 PURBOND and not in the LOCTITE VN 3158. The adhesives were pressed during 10 hours at a pressure of 1 MPa and at a temperature of approx. 20°C . Once cured, the front-position of the foil was referenced as position of the crack tip and the crack length was set to 110 mm. The samples were then cut to a width of 20 mm and a length of 317 mm. The adhesively bonded wood joints were stored for several days in the test climate of 23°C and 50% relative humidity before testing. The setup used for this experiment is schematically shown in Fig. 1. In Fig. 1, P is the load, PL and PR the relative loads under both loading points. Vl and Vr are the displacements under both loading points. Due to the pinned configuration, the force PL is equal to PR . The compliance at the loading point is then defined as the ratio of displacement to the applied force, which corresponds to Eq. (2). Only the main equations are summarized here, a detailed derivation can be found in Clerc et al. (2019a, b).

$$C_c = \frac{\delta_c}{P} = \frac{49L^2(L + 54a)}{10368EI} \quad (2)$$

The energy release rate G_{II} is calculated according to Eq.(3):

$$G_{II} = \frac{P^2}{2b} \frac{dC}{da} = \frac{49P^2L^2}{384BEI} \quad (3)$$

The crack length is calculated from the compliance Eq. (4)

$$a = \frac{C_c 10368EI - 49L^3}{2646L^2} \quad (4)$$

The MOE was calculated according to Eq. (5) at a load of $P = 200$ N (higher than the initial deformation of the setup and lower than the crack start, and hence in the elastic range).

$$E = \frac{49L^3 + 2646L^2a_0}{10368C_0I} \quad (5)$$

Evaluation of the quasi-static samples

The ERR was computed at two different load points. The first point (P_{NL}) corresponds to the point of initiation of the crack propagation, it is defined as the limit of the elastic range. With this point, the slope of the elastic part is calculated. The crossing point between a 5% more compliant slope and the load-deformation curve is then obtained as a second point ($P_{5\%}$).

Evaluation of the cyclic fatigue loaded samples

A similar evaluation method was used as for the quasistatic tested samples. As suggested by Simon et al. (2017) the compliance of the samples is calculated with:

$$C = \frac{\delta_{max} - \delta_{min}}{P_{max} - P_{min}} \quad (6)$$

where δ_{max} and δ_{min} correspond to the maximum and minimum displacement, and P_{max} and P_{min} to the maximum and minimum force value per cycle, respectively. The main difficulty regarding the analysis of the samples consists of the smoothing of the data affected by experimental scatter. During the test, maximum and minimum force and displacement values were recorded. The data were then smoothed using the “logarithmic fitting” algorithm described by Clerc et al. (2019a, b). For example, data-points are averaged every 200 cycles until 1000 cycles then every 500 cycles until 10,000 then every 1000 cycles until the end of the test. These “cycle range” parameters were adjusted according to the different samples to obtain regularly spaced points over

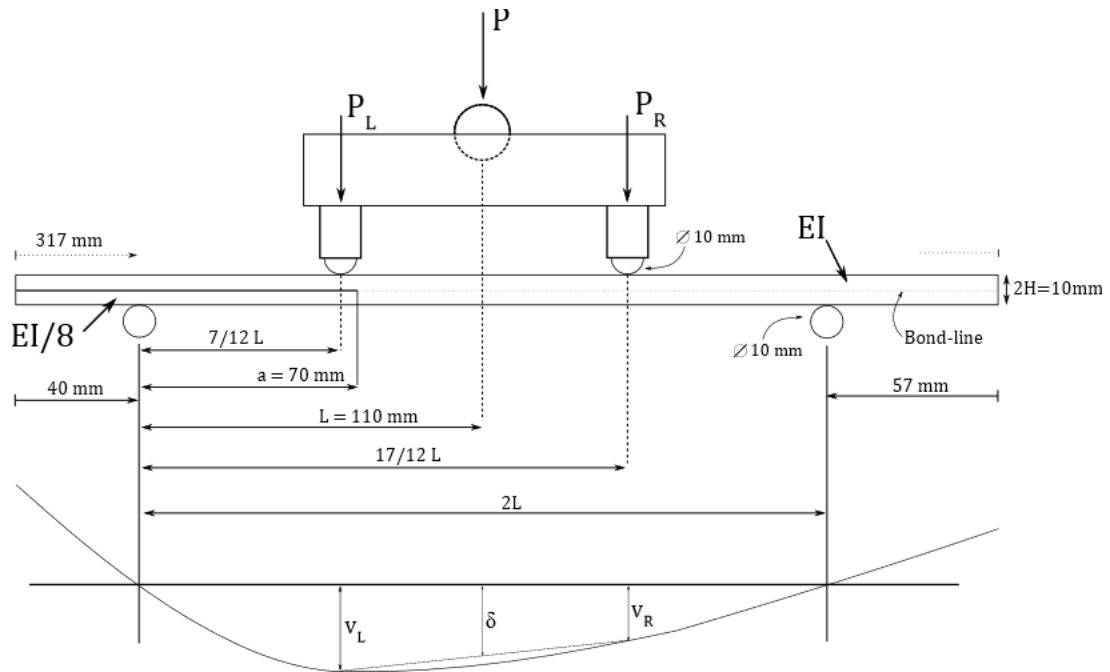


Figure 1 – Schematic representation of the test setup drawn to scale with theoretical deformation line, the total crack length is 110 mm measured from the left side of the specimen— an hinge was used to distribute the force equally between P_L and P_R – testing setup according to (Clerc et al. 2019)

the test and a comparable number of data points between the different samples. The compliance data calculated according to Eq. (6) were log-fitted before calculating the crack length and its corresponding derivative. The ERR data, calculated according to Eq. (3) was also log-fitted with the same parameters as the compliance data.

Testing procedure

The machine used for the test was a servo-hydraulic test machine (type 1237 Instron) equipped with a 1 kN load cell. The head of the support was fully articulated to prevent any bending moment in the fixture apparatus. The quasi-static tests were performed under displacement control at 1 mm/min. For the cyclic loaded samples, three samples for each adhesive were tested at a frequency of 5 Hz under displacement control until reaching 40,000 cycles or until a very slow crack growth was reached. The average machine displacement value was fixed to 13.36 mm corresponding approximatively to the average force observed at the PNL-point. The displacement amplitude was set to ± 2.1 mm corresponding approximatively to a force of ± 200 N. A few extra supports were placed to prevent the sample from sliding during the test and Teflon was sprayed on the sample for assuring a low friction between the sample and the machine support.

Source of extrinsic scatter

The load and displacement were measured with an accuracy of 1% of the measured value, meaning that the force was measured with an accuracy of at least 5N and the displacement with an accuracy of 0.1 mm. The compliance of the setup was corrected using a stiff steel bar for calibration (Clerc et al. 2019a, b). The non-linear initial play in the setup was corrected by extending the linear elastic part of the load–displacement curve to the crossing point with the deformation axis. During the test, only the maximum and minimum displacement and load values per cycle were recorded to limit the data file size. In order to check the accuracy of the maximum and minimum values preliminary tests were recorded during a few cycles with a 1 kHz sampling rate, meaning that on average 200 data points were recorded per cycle. An average step of 4 N (and 0.042 mm) between two successive data points was observed over the complete cycle, but well below that near the maximum and minimum value (Fig. 2). This inaccuracy was estimated to be below 0.1 N and 0.01 mm. A potential source of systematic error could be the fact that the maximum and minimum force and displacement values per cycle were not necessarily recorded at the same time. As shown in Fig. 2, there is a phase difference between the force and deformation data. Where the maximum deformation appears before the maximum force, the difference is less for the minimum value per cycle. By averaging the behavior of the specimen over one cycle and using only the maximum and minimum value, a time difference of approximately 0.004 s could be observed between the maximum values of the displacement and force data. This means, that the compliance is not necessarily estimated at the exact same time, the influence of this systematic error on the result is however difficult to estimate. Using these rough estimates, the accuracy of the compliance is estimated to be 2.3% if the compliance is calculated as $C = \delta_{max}/P_{max}$ and 4.3% if the compliance is calculated using Eq. 6. In both cases, the accuracy of the load cell is dominant accounting for 80% of the inaccuracy.

Fitting process for samples tested under cyclic fatigue loading

General procedure

The fitting procedure consisted of two steps, a first fit was done to calculate the value of A and $G_{II,thr}$, without considering the influence of D and β . Then, using the values of A and $G_{II,thr}$, a second fit was done to obtain the value for D and β . One can see

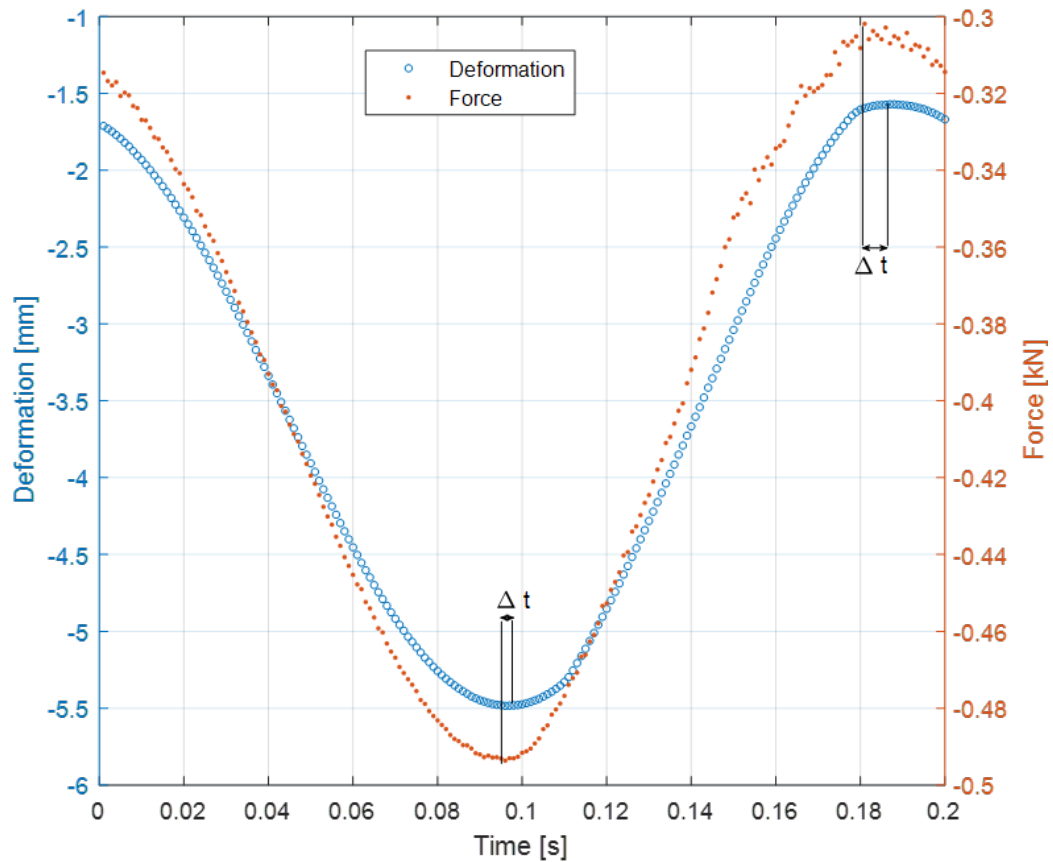


Figure 2 – Phase difference between the force and deformation measurement during one cycle illustrating that there is a time delay between the maximum and minimum force and deformation values, meaning that they are not necessary measured at the exact same time

in Eq. 1 that for G_{II} term near $G_{II,thr}$, the x-axis will tend to zero crack growth rate. Additionally, $G_{II,max}$ values smaller than $G_{II,thr}$ are resulting in a negative crack growth rate. A $G_{II,max}$ value near the A value will tend to infinity, meaning a virtually infinite crack growth rate. Therefore, as first estimation the $G_{II,thr}$ value should be lower than the maximum ERR value obtained for each cycle ($G_{II,max}$) and the A value should be higher than the $G_{II,max}$ values. Furthermore, as the HS-equation (1) is covering the entire fatigue-life of the sample, all the data points shall be displayed on a straight line. This can be achieved, as suggested by Jones et al. (2014), by plotting the da/dN values and the term $\left(\frac{\sqrt{G_{max}} - \sqrt{G_{thr}}}{\sqrt{1 - \sqrt{G_{max}/A}}} \right)$ on a double logarithmic scale as shown in Fig. 3 and by adjusting the A and $G_{II,thr}$ coefficients. By choosing the appropriate value of $G_{II,thr}$, the non-linearity of the data in the threshold domain can be reduced. For example, in Fig. 3, a $G_{II,thr}$ value of 100

J/m^2 is too low as the data-points are shifted on the right-side of the line. The contrary is observed for a $G_{II,thr}$ value of $350 J/m^2$ as this time the data are shifted to the left-side of the line. A $G_{II,thr}$ value of approximately $250 J/m^2$ seems here a reasonable estimate as the data are following a fairly linear trend.

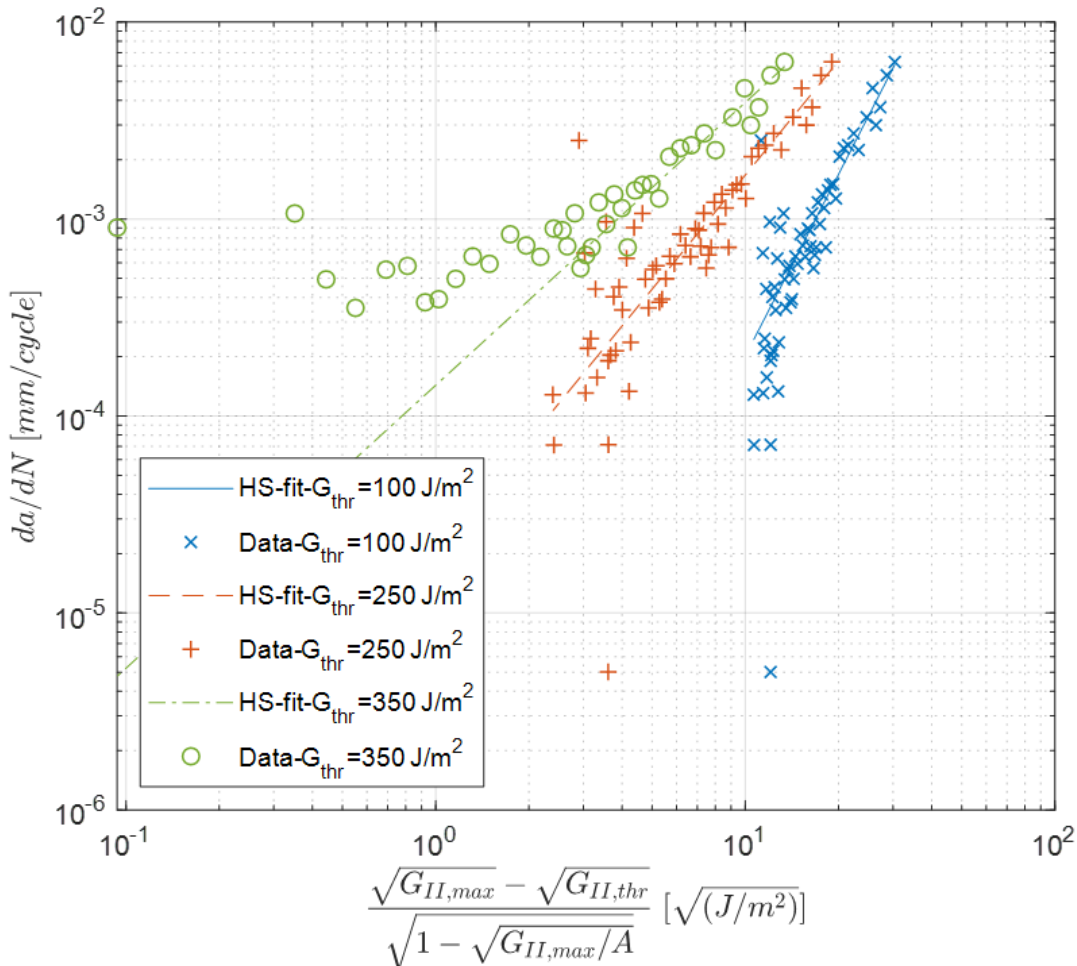


Figure 3 – Influence of the variation $G_{II,thr}$ value for one sample glued with the adhesive HB 110 using the HS-analysis – a $G_{II,thr}$ value of $100 J/m^2$ is too low as the data-points are shifted on the right-side of the line. The contrary is observed for a $G_{II,thr}$ value of $350 J/m^2$ as this time the data are shifted to the left-side of the line. The most representative $G_{II,thr}$ value should result in the data point being plotted along a straight line as shown with $G_{II,thr} = 250 J/m^2$

The starting value of A is based on the ERR measured at $P_{5\%}$ under quasi-static loading. The upper bound for estimating the A value was fixed at two standard deviations from the average $G_{II,5\%}$ value, the lower bound was fixed to be the maximal ERR release rate measured during the fatigue cyclic tests (as theoretically the A value cannot be smaller than the maximum ERR measured during the test). The lower bound for estimating the

G_{thr} value was set to zero and the upper bound to the minimum ERR value measured during the test.

Automatic method for estimating the A and G_{thr}

Using the above-mentioned procedure to estimate “manually” the value of A and G_{thr} is a rather cumbersome and subjective process as due to the scatter of the data it is difficult to judge if the data are forming a straight line. For this reason, a simple procedure was proposed to automatically estimate the value of A and G_{thr} . Using the above-mentioned assumption, it is possible to design an algorithm generating random values (from a uniform distribution) of A and G_{thr} which control if the data are forming a straight line. For each random pair of A and $G_{II,thr}$ the term $\left(\frac{\sqrt{G_{max}} - \sqrt{G_{thr}}}{\sqrt{1 - \sqrt{G_{max}/A}}}\right)$ is computed and fitted using the HS-equation (3). As evaluation criteria, the coefficient of determination (CoD) is calculated for each pair. Then the highest CoD values, and the corresponding A and G_{thr} values are selected as they should represent the best fit. An example of the A and G_{thr} value obtained with this method is shown in Fig. 4. In this contour plot, the coefficients are shown in a color scale on the right of the picture (the scale is truncated to show only high CoD values). Even though the differences in the CoD are relatively small, a clear tendency can be seen leading to a best fit in this example of $706.2 J/m^2$ for A and $261.2 J/m^2$ for G_{thr} with a CoD of 0.8209. Due to the random nature of the estimation, the best fit is not always located exactly at the same place. To estimate the variability of the best fit, ten different random initialization (with 2500 A and G_{thr} pairs each) are done and the average and standard deviation of the best fitting A and G_{thr} values are calculated. Using this method for each tested sample, 25,000 pairs of A and G_{thr} are randomly generated giving a coefficient of variation of approximately 5% for the A and G values. The average coefficient of variation for the CoD value was below 0.1%.

The contour plot shown in Fig. 4, can also be used as sensibility analysis tool for estimating the influence of a relative change in the A and G_{thr} values. In Table 1, the influence of a 5% and 10% higher or lower A or G_{thr} value (keeping respectively the G_{thr} or A value constant) can be seen. It appears that a relative change of the A value has more influence than of the G_{thr} value. This can also be observed in Fig. 4, where all the range of the tested G_{thr} value can give a CoD higher than 0.81 (if the appropriate A value is chosen). Whereas, a small decrease of the A value promptly results in a low CoD.

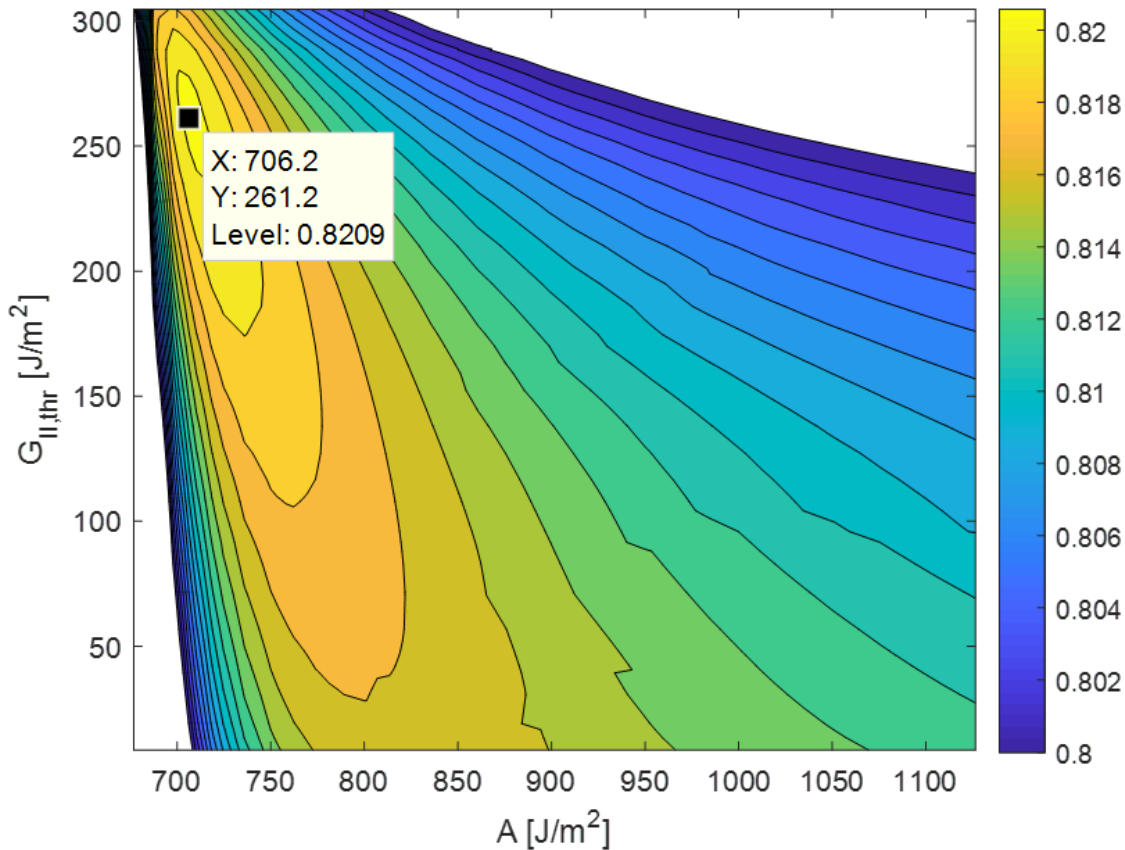


Figure 4 – Contour plot of the Coefficient of Determination corresponding to different A and G_{thr} values. For this sample glued with the adhesive HB 110, the best CoD (0.8209) is obtained with a value of 706.2 J/m^2 for A and 261.2 J/m^2 for $G_{II,thr}$. The color-scale is truncated to show only the high CoD values.

Influence of the data-reduction method on the A and G_{thr}

To evaluate the influence of the number of data points on the estimation of the A and G_{thr} values, two different data reduction methods were compared. The first data set (labeled “LogFit1”) is obtained by averaging the data every 100 cycles until 1000, every 200 cycles until 10,000 and every 400 cycles until the end of the test, giving a total data set of 161 data points. Clerc et al. (2019a, b) provide a more detailed description of the data reduction method. The second data set (labeled “LogFit 2”) is obtained by averaging the data every 100 cycles until 1000 cycles, every 300 cycles until 10,000 and every 600 cycles until the end of the test giving a total data set of 110 data points. For the data set LogFit 1 and LogFit 2 the above described procedure (Sect. 2.7.2) was used to estimate the value of A and G_{thr} . The numerical values obtained with a 95 confidence interval are shown in Table 2.

Table 1 – Influence of a variation of $\pm 5\%$ and $\pm 10\%$ on the value of G_{thr} and A on the CoD—data set obtained from one sample glued with the adhesive HB 110—*A-10% would be lower than the maximum ERR measured during the test hence resulting in a negative value and was therefore not calculated

	$A [J/m^2]$	$G_{thr} [J/m^2]$	CoD
Ref.	723	246	0.8205
$A + 5\%$	760	246	0.8166
$A - 5\%$	687	246	0.8109
$G_{thr} + 5\%$	723	258	0.8200
$G_{thr} - 5\%$	723	234	0.8204
$A + 10\%$	795	246	0.8141
$G_{thr} + 10\%$	723	271	0.8193
$G_{thr} - 10\%$	723	221	0.8204

The difference between both A and G_{thr} values estimated from different LogFit data set, are in the 95% confidence interval (see Fig. 5). However, the A value is slightly higher in the LogFit1 data-set whereas the G_{thr} value from Logfit1 is slightly lower. This is probably explained by the non-equivalent weighting of the different parts of the test. For both data sets the moving average parameters were equivalent until 1000 cycles, only after that were the number of data points reduced in the LogFit2 data set. This implies, that the data set Log- Fit1 has proportionally more data in the upper part of the test than the logFit2 data set. This probably explains why, having relatively more data in the upper range of the test, the A value is higher (and the G_{thr} value lower) in the LogFit1 Data Set. Despite these small differences, the fits are considered similar between both data sets with a CoD of 0.7022 for the Data set “LogFit1” and 0.8039 for the data set “LogFit2”. The parameters corresponding to this data set were chosen for further analysis due to the higher CoD.

Results

Quasi-static loading

The ERR measured at the $P_{5\%}$ points under quasi-static loading was $896 \pm 120 J/m^2$ for the samples glued with the HB 110 adhesive, $1004 \pm 77 J/m^2$ for the PRF adhesive and $1023 \pm 131 J/m^2$ for the VN 3158 adhesive (from Clerc et al. (2019a, b)).

Table 2 – Numerical values of A , G_{thr} , D and β values for two different LogFit data sets obtained from one sample glued with the adhesive HB 110 - Range is given with a 95% confidence interval

		Mean	Lower bound	Upper bound
Data Set "LogFit1"	$A [J/m^2]$	894	876	912
	$G_{thr} [J/m^2]$	307	297	317
	$D [mm/cycle]$	1.331E-03	8.207E-05	1.842E-04
	$\beta [-]$	0.995	0.8833	1.107
Data Set "LogFit2"	$A [J/m^2]$	879	865	894
	$G_{thr} [J/m^2]$	313	301	325
	$D [mm/cycle]$	1.596E-03	1.019E-04	2.174E-04
	$\beta [-]$	0.9271	0.8264	1.028

Cycle-fatigue loading

The above-mentioned method will be tested on adhesively bonded specimen bonded with different types of adhesive. In Fig. 6, the fatigue test results of all samples glued with the adhesive HB 110 are presented. The fit parameters obtained for each sample are shown in Table 3. The general slope is very similar between the three samples but still, significant scatter can be noted for the sample HB3. The cause for this scatter will be further discussed. The obtained HS parameters are relatively similar, with an average A value of $785 J/m^2$ and an average G_{thr} value of $285 J/m^2$.

For the VN adhesive, the samples VN2 and VN3 show a very similar behavior (see Fig. 7). However the sample VN-1 presents a different slope and a comparatively higher G value as the other samples glued with the VN adhesive. The same tendency could be observed for this sample in Clerc et al. (2019a, b). For all samples glued with the VN, an important scatter is also observed. It shall also be noted that the average slope for the VN samples is similar to the HB 110 samples. However, the average value of A ($1228 J/m^2$) is significantly higher for the VN adhesive than for the HB 110 adhesive. The same tendency was observed during the quasi-static test where a higher maximum ERR value was measured for the VN samples. In comparison, the average threshold ERR value ($192 J/m^2$) is clearly lower than for the HB 110 samples.

Only two samples glued with the adhesive PRF could be successfully analyzed with the above-mentioned method. For the sample PRF1, no satisfying results could be obtained using the random estimation of the A and G value. This is probably due to the short

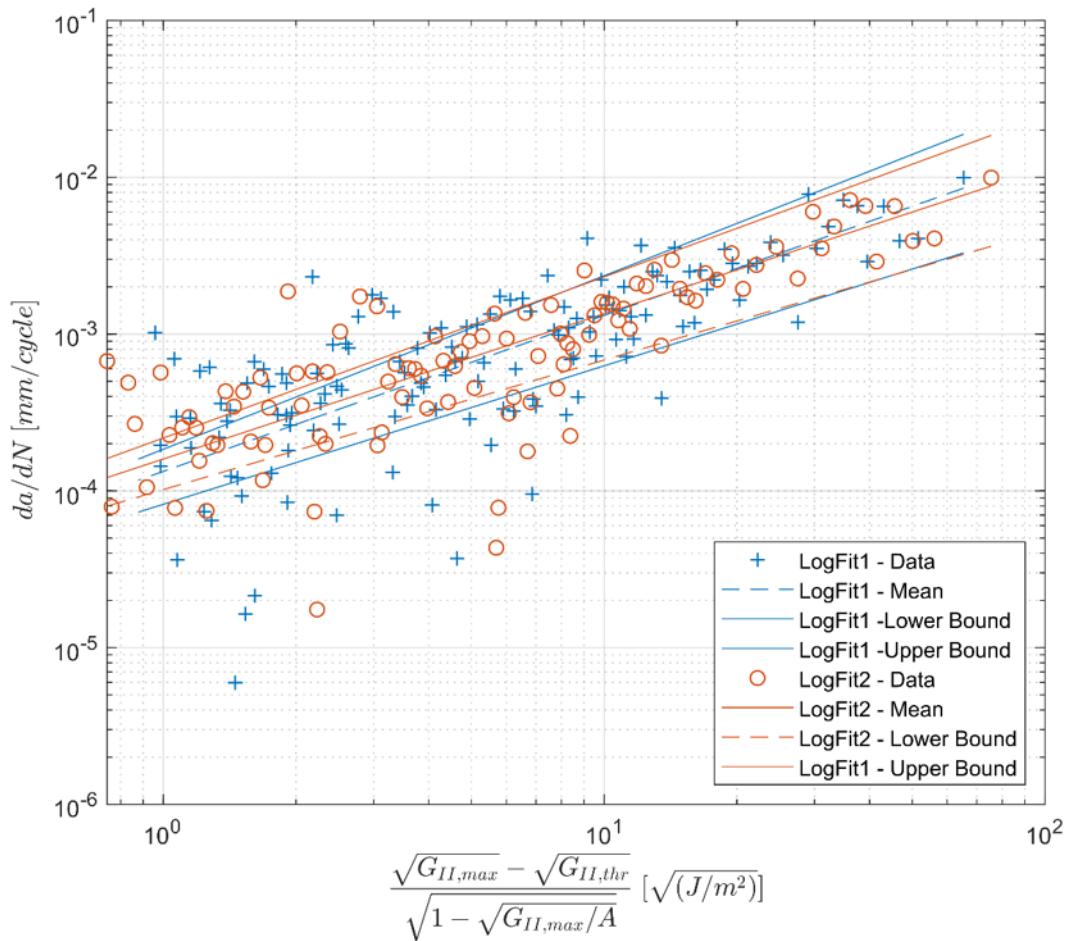


Figure 5 – Comparison of the same sample with two different LogFit parameters (see text) to illustrate the influence of the number and repartition of data points on the determination of the A and G_{thr} values – the upper and lower bound for each LogFit are given with a 95% confidence interval

delamination (only 16,000 cycles compared to the 40,000 cycles for the other samples). Indeed, if too few points are available for the fitting algorithm, no CoD can successfully be calculated resulting in a failed estimation. Increasing the moving average filter parameters to obtain more data points, was in this case not successful as this tended to increase the scatter even more. It can, however, be seen in Fig. 8 that the data points are matching relatively well the other tested PRF samples. The average A ($880 J/m^2$) and G_{thr} ($552 J/m^2$) values obtained for the PRF2 and PRF3 samples were used to plot the data of the sample PRF1. For the PRF samples, the average A value is similar to the one obtained for the HB 110 samples but clearly lower than for VN samples. The PRF samples are showing the highest G_{thr} and A values in comparison with both 1C-PUR adhesives. Meaning that in average, a slower crack growth will be observed for specimen

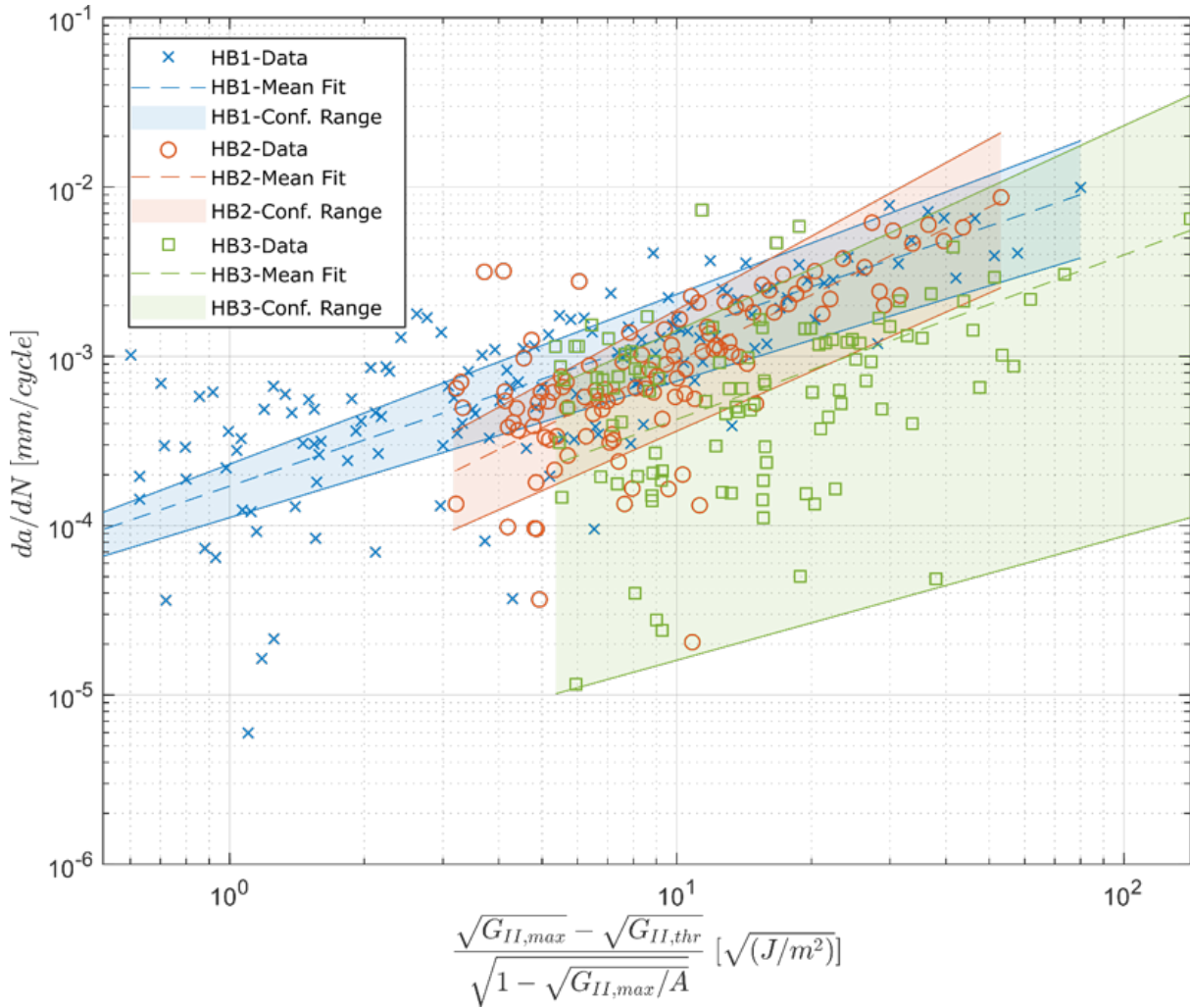


Figure 6 – Data points of the three samples glued with the adhesive HB 110 are plotted in comparison with the mean fit obtained with the HS-analysis – The Confidence Range is given with 95% Confidence Interval

glued with this adhesive, and that the crack growth will become infinitely small at a higher energy than for the other adhesives tested in this study.

In order to allow for a better comparison between the adhesive performances, all the data samples are plotted together in Fig. 9. Each sample was plotted using the value of A and G_{thr} determined in Table 3. Then, all the data for one adhesive system are combined in one data set and the coefficients D and β are calculated for the complete data set. The coefficients obtained from the HS-equation are compared with those obtained using the Paris equation in Table 4 (Clerc et al. (2019a, b)). Generally, the β coefficient is much smaller than the m coefficient and the relative difference of the coefficient between the adhesive system is also less. Meaning, as explained by Jones et

Table 3 – Hartman–Schijve coefficient for all tested samples - *Average value from PRF2 and PRF3

	Sample	$A [J/m^2]$	$G_{thr} [J/m^2]$	D	β
HB 110	HB110-1a1	874 ± 9	315 ± 5	8.54E-06	1.73
	HB110-1a5	723 ± 9	246 ± 13	7.80E-06	1.95
	HB110-3a2	727 ± 18	306 ± 19	4.26E-05	1.71
PRF	PRF-3B3	885 ± 21	555 ± 10	5.81E-06	1.92
	PRF-3B4	876 ± 23	550 ± 6	4.94E-06	1.95
	PRF	880*	552*	N.A.	N.A.
VN 3158	VN1B4	1275 ± 8	287 ± 5	9.86E-04	0.64
	VNS2-2	1275 ± 14	145 ± 2	3.27E-04	1.26
	VNS2-3	1151 ± 5	134 ± 6	3.23E-04	1.45

al. (2015) that if the data are used for design purposes, the error bound to the power coefficient by extrapolating remains relatively similar between samples or adhesive systems. The coefficients obtained for adhesively bonded wood are relatively similar to the one obtained by Jones et al. (2015) for composites in Mode II. Generally, slower crack growth is observed as the D coefficient is lower and the β coefficient higher for the several tested composites, but the A and G_{thr} remain relatively similar.

Table 4 – Comparison between Multi-sample fit (MS-fit) of the power-model coefficient between the Paris- and Hartmann–Schijve equations

	Sample	C for Paris equ. D for HS equ.	m for Paris equ. β for HS equ.
Paris-equ.	MS-fit-VN	5.76E-07	1.51
	MS-fit-HB	5.51E-13	3.44
	MS-fit-PRF	4.70E-42	13.33
Hartman-Schijve equ.	MS-fit-VN	4.94E-04	1.09
	MS-fit-HB	1.38E-04	0.83
	MS-fit-PRF	3.41E-06	2.08

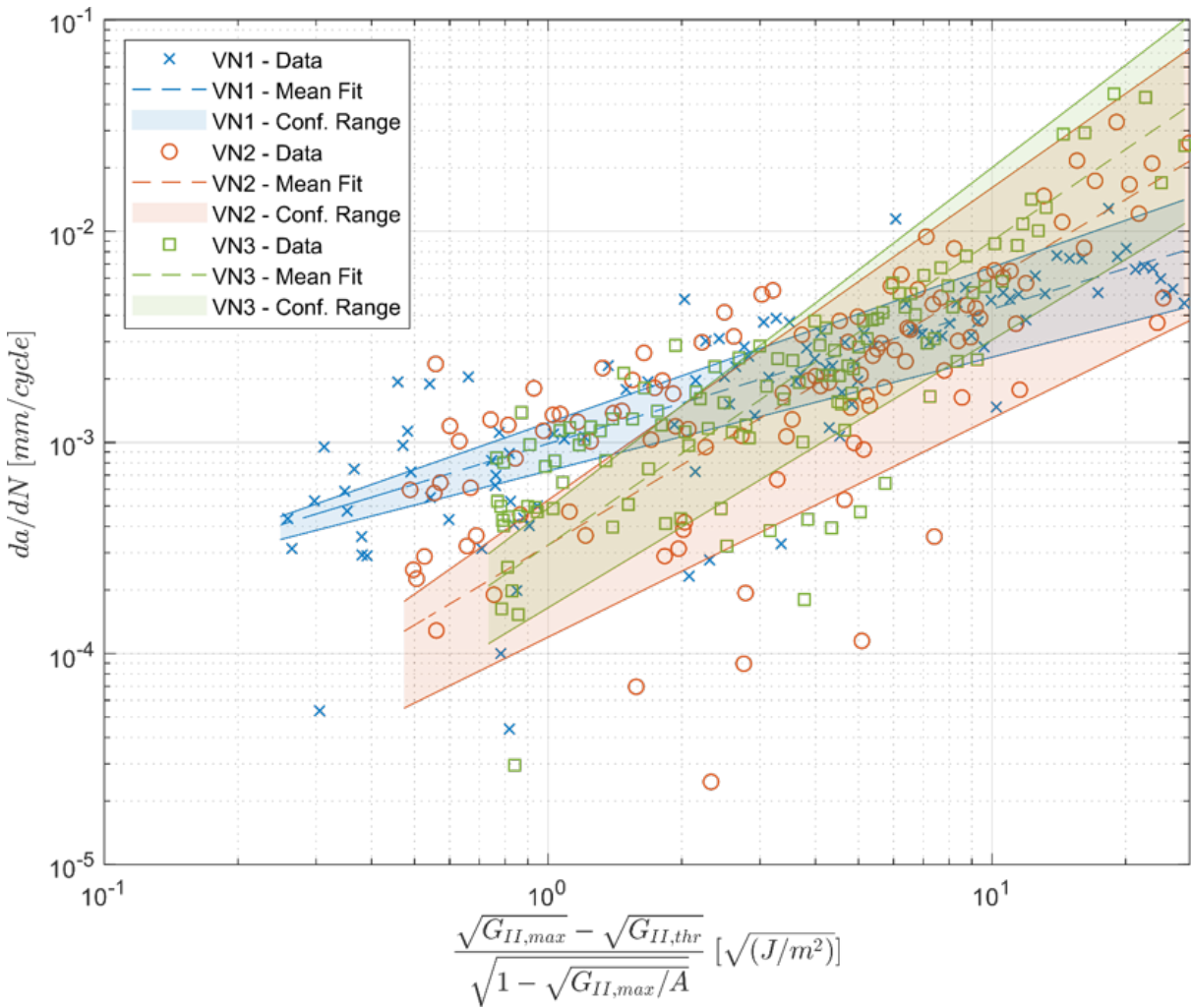


Figure 7 – Data points of the three samples glued with the adhesive VN 3158 are plotted in comparison with the mean fit obtained with the HS-analysis – The Confidence Range is given with 95% Confidence Interval

Discussion

Sources of scatter

As shown in Fig. 9, the crack growth data and ERR data are associated with a relatively constant scatter over the complete duration of the fatigue test. For the crack length a variation of approximately 5% of the average value is observed, for the ERR value a variation of below 2% of the average values is observed. These observations confirm the estimation of the measurement accuracy presented in 2.6. Indeed, as the crack length is directly calculated from the compliance according to Eq. 4, the same accuracy can be expected. In comparison, the ERR values are calculated (according to Eq. 3) using

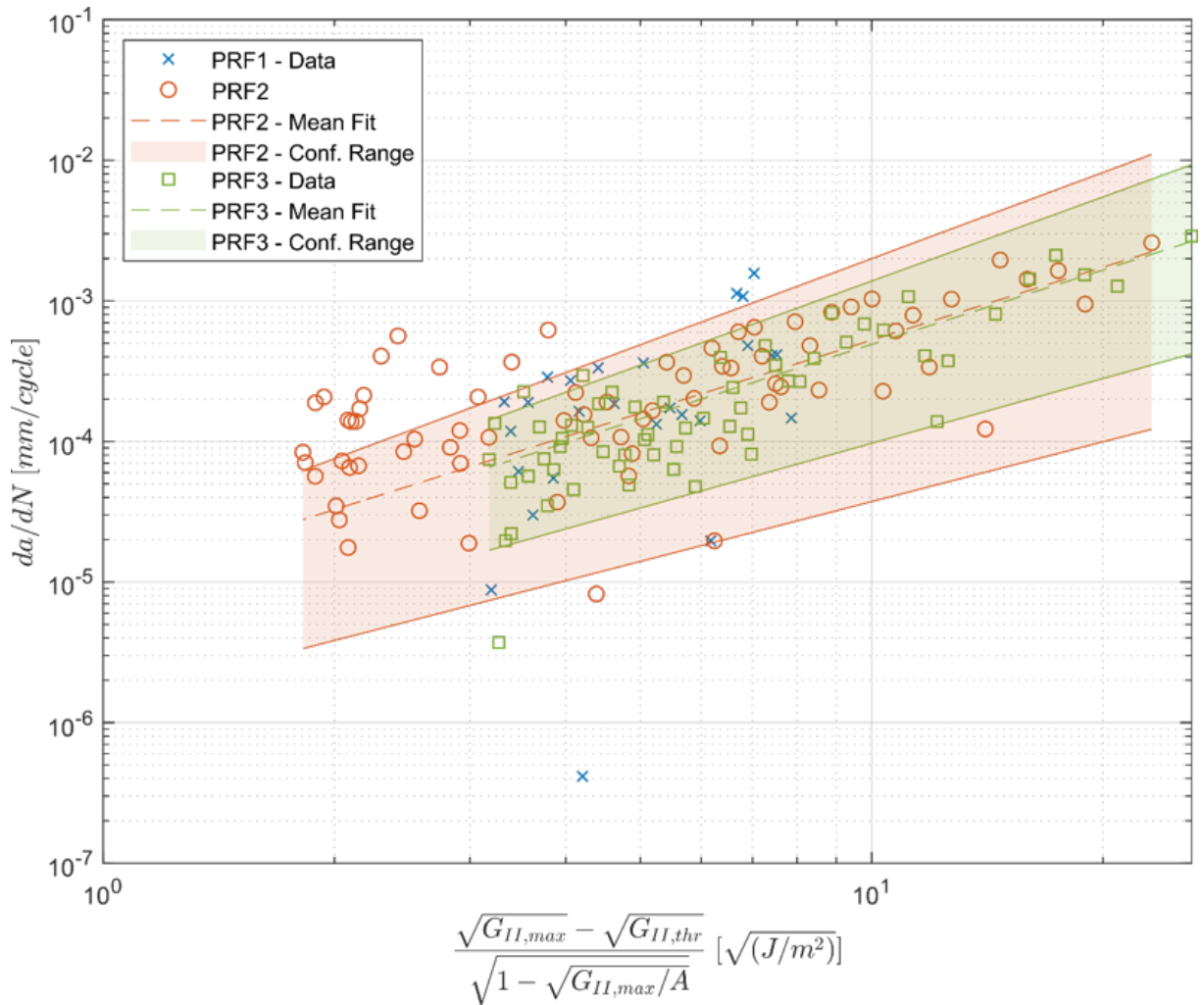


Figure 8 – Data points of the three samples glued with the adhesive PRF are plotted in comparison with the mean fit obtained with the HS-analysis, the Confidence Range is given with 95% Confidence Interval.

only the maximum force per cycle. Therefore, the scatter of the results in this case is lower. This also confirms that the main cause of measurement inaccuracy is due to the load and displacement measurement and the related measurement resolution. In addition to this relatively homogenous scatter, strong deviation of the crack length and ERR during a short amount of cycle can be observed. As these events are sporadic and associated to deviation higher than the measured extrinsic scatter, they can realistically be associated with intrinsic scatter due to the material heterogeneity. For example, as can be seen in Fig. 6, the sample HB3 has a much higher scatter than the other HB samples. This higher scatter is probably due to two isolated non-homogenous crack growth events, one of them resulting in a significant spike in the data during the fatigue test. As visible in Fig. 10, at 8000 and 18,000 cycles approximately, a sudden crack

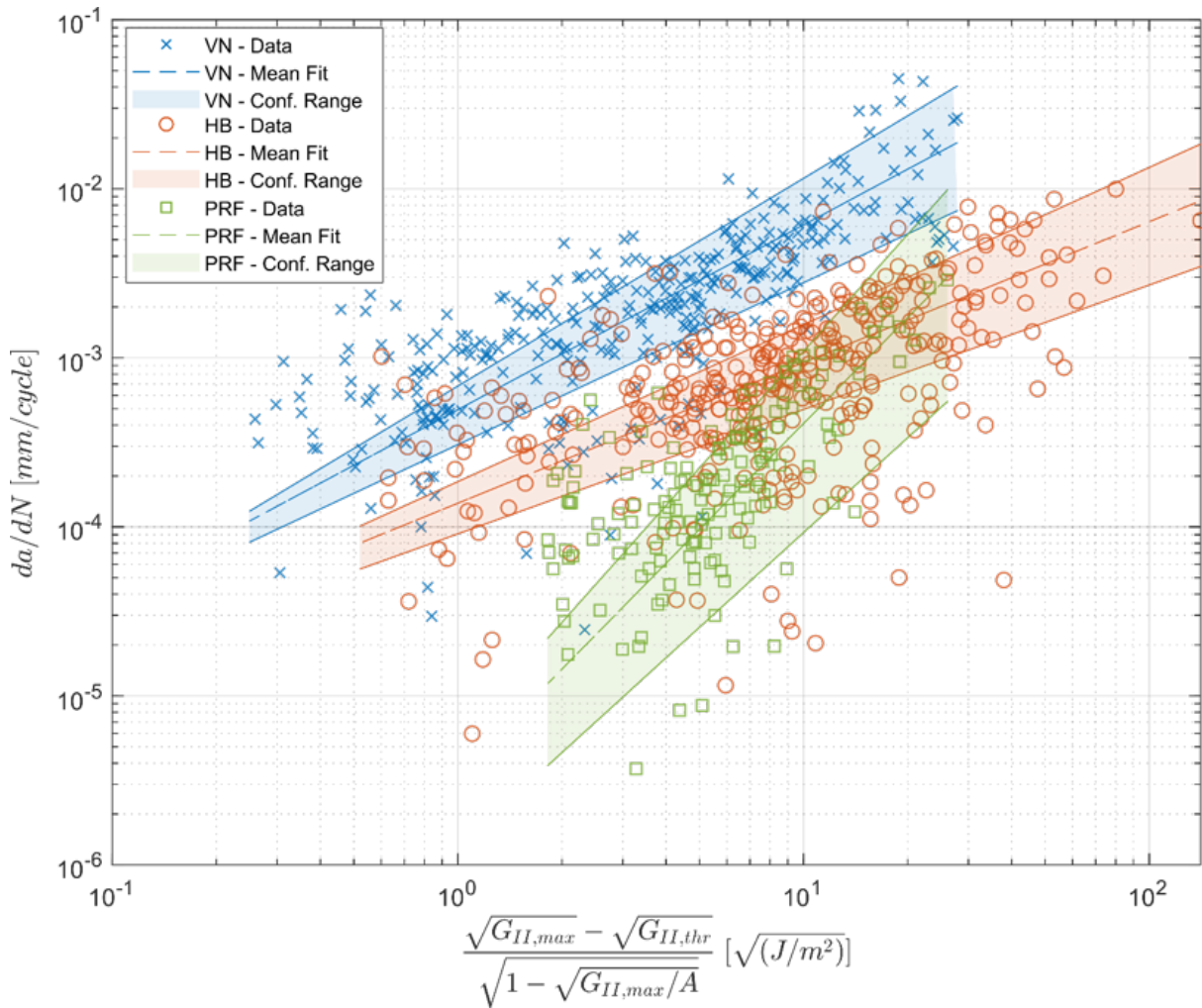


Figure 9 – All data points from one adhesive system were plotted together with the corresponding fit using the HS-analysis - The Confidence Range is given with 95% Confidence Interval

growth and decrease of the ERR is observed for the sample HB3. Following the fast growth of the crack, the delamination length remains constant until the ERR needed for the further crack growth is reached. During this event, the crack growth increment per cycle becomes very small, and as the data are plotted chronologically; this very slow crack growth is associated with scatter. In comparison, the sample HB2 shows a much more regular crack growth as visible in Fig. 10, hence the reduced scatter observed for these samples.

During the experiment, the machine had to be stopped for a short period, mainly to export results and hence free the memory of the acquisition system. It could be that these short interruptions may have influenced the compliance of the specimen through relaxation effects. For example, the machine was stopped at 22,000 cycles for

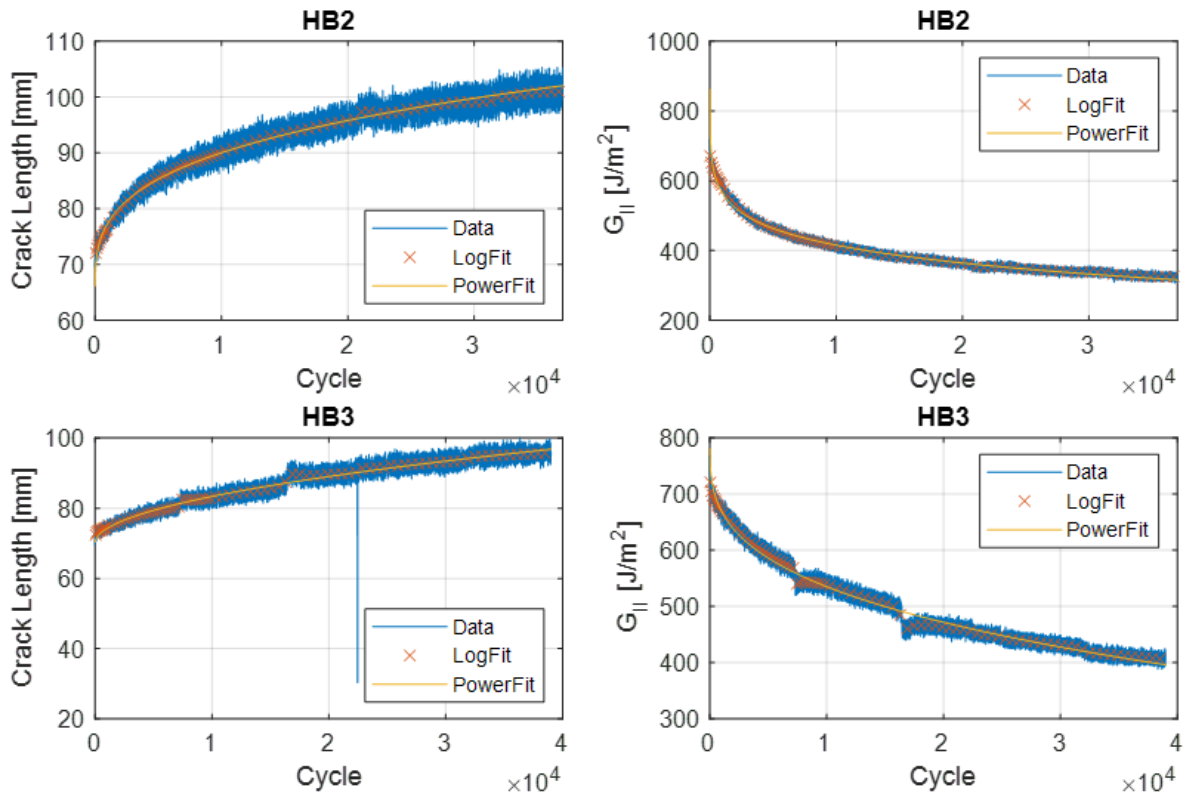


Figure 10 – Comparison of the crack growth and ERR values during the fatigue test of two different samples glued with adhesive HB 110 illustrating the non-regular behavior of the sample HB3 due to fast crack growth events (observed at 8000 and 18000 cycles)

the sample HB3 to export the preliminary results. In Fig. 10, at 22,000 cycles a small increase in the crack length and a very small decrease of the G_{II} value can be observed for the sample HB3. These modifications are however much smaller than the sporadic crack growth events at 7500 and 16,570 cycles presented before. The reasons for these sporadic events are not yet completely understood but could be due to non-uniform adhesive application and/or to heterogeneity in local morphology of the material. They are therefore associated with intrinsic scatter and should be considered in the safety factors determined from these tests in order to account for the specimen variability. It should, however, be recognized that the above mentioned factors influencing the scatter are obtained from laboratory test series and that these sources of scatter do not necessarily occur in service, where other sources may be present (Schijve 1994).

Further consideration for reducing the scatter

The problem of scatter is a frequent topic in fatigue testing. (Schijve 1994) mentioned that scatter encountered in S-N data is often a “nuisance” which can prevent the fitting

of the data. An interesting solution to this was proposed by Gatto (1956) which consists in arranging the strength (S) values in descending order and the cycle (N) values in ascending order as ideally expected and to plot the obtained pairs as (S,N) values. Using this method, the scatter could be drastically reduced and the centroidal line could be localized immediately without “mathematical treatment” of the data, which was probably appreciated at a time where computer usage was relatively scarce, but also to limit the risk of overfitting the data. This method also estimates the random variability of the population around its centroidal line by computing the difference between the experimental values and value of the rearranged coordinate. Hence, this is offering a new statistical variable for estimating the scatter of S–N curves. To the authors’ knowledge this method was never applied to fatigue crack growth data. Instead of the strength and cycle data, the crack growth rate and ERR could be plotted in ascending order as theoretically expected. This rearrangement method was compared to the power model fitting (fitting the crack growth and ERR with a power model of first order) in Fig. 11.

A very similar fit is observed between the rearranged data and the power model fit in the linear range of Fig. 11, between 470 and 700 J/m^2 . Outside this range, the deviations are important between both data reduction methods, as the power model is extrapolating the data along the same tendency whereas the rearranged data are showing an asymptotic decrease in the low ERR and increase for the high ERR, as ideally expected from a fatigue fracture test. The Paris fit determined using the data reduction method presented by Clerc et al. (2019a, b) seems to match the rearranged data better than the power model fit. As the average difference between the rearranged points and the original points is near zero for the crack growth and ERR values, it seems more appropriate to compute the absolute difference instead. This yields a value of 151 J/m^2 for the ERR values and 0.0013 mm/cycle for the crack growth rate. As mentioned by Gatto (1956), these values can be used as estimation of the scatter of the data. The rearranged data plotted in Fig. 11 seem to follow the expected typical fatigue crack growth behavior. It is therefore interesting to investigate how the rearranged data are displayed using the HS-analysis.

It is possible to plot the rearranged data in a straight line that matches quite precisely the HS-fit line obtained from the LogFit Data by adjusting the G_{thr} and A values as shown in Fig. 12. However, it needs to be mentioned that the obtained A and G_{thr} values are different from those computed using the method described in Sect. 2.7. For example, Fig. 12 was plotted using a A -value of 730 J/m^2 and 430 J/m^2 for G_{thr} . In

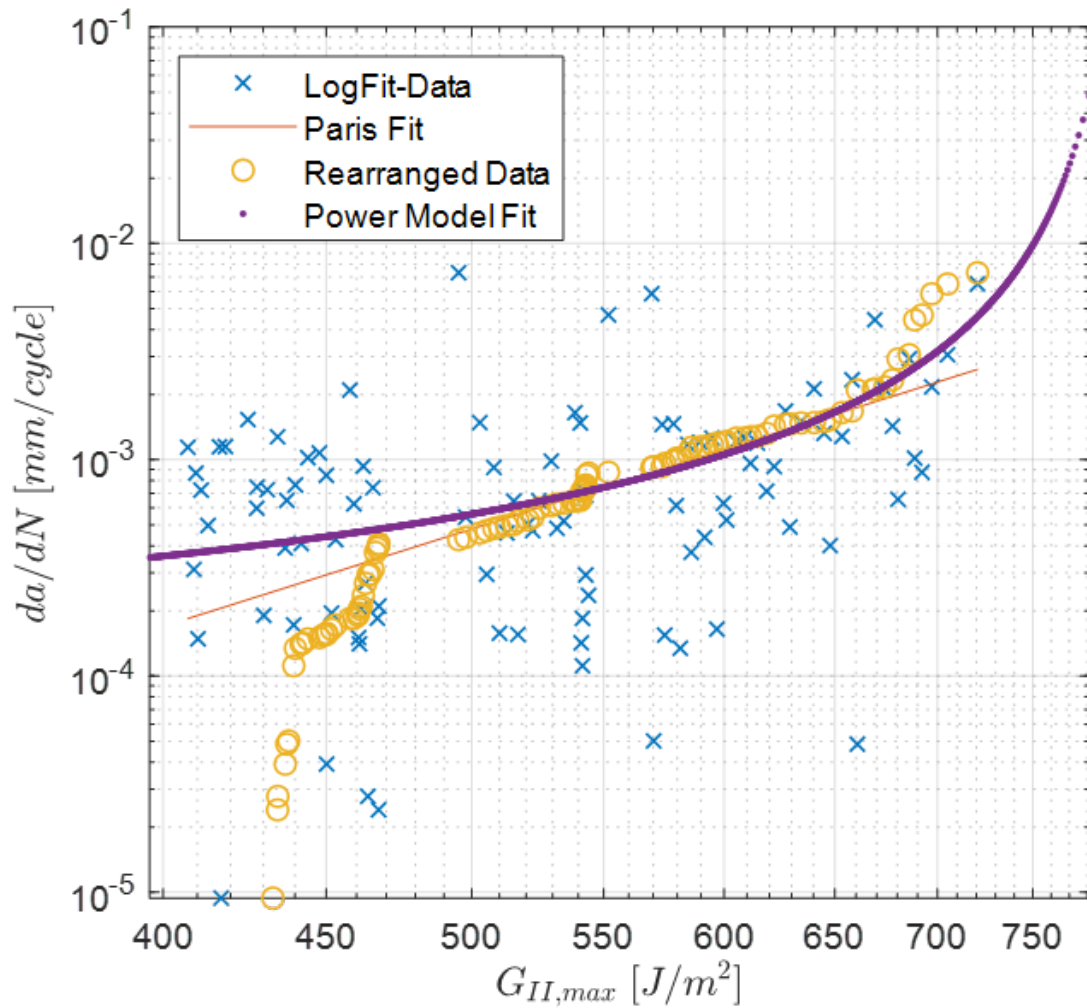


Figure 11 – Comparison between the rearranged method and the Power Model fit on one data set plotted using the Paris Analysis illustrating the good correspondence of the three data reduction method between 470 J/m^2 and 700 J/m^2 .

comparison, the A-value computed with the method described in 3.2 was $727 \pm 18 \text{ J/m}^2$ and $306 \pm 19 \text{ J/m}^2$ for G_{thr} . As the difference between both A-values is below the standard deviation of 18 J/m^2 they can be considered similar. However, the difference between both G_{thr} values is much higher than the standard deviation of 19 J/m^2 . To the question of which estimation of G_{thr} is the most accurate, several points need to be considered. The value of 430 J/m^2 is actually higher than the minimal recorded ERR during the test, in fact 15% of the data points displayed an ERR value lower than 430 J/m^2 . Also, after sorting the data in ascending order there is not necessarily a match corresponding to the real behavior of the specimen for each recorded value. Indeed, if a high crack growth is observed due to a hypothetical material heterogeneity

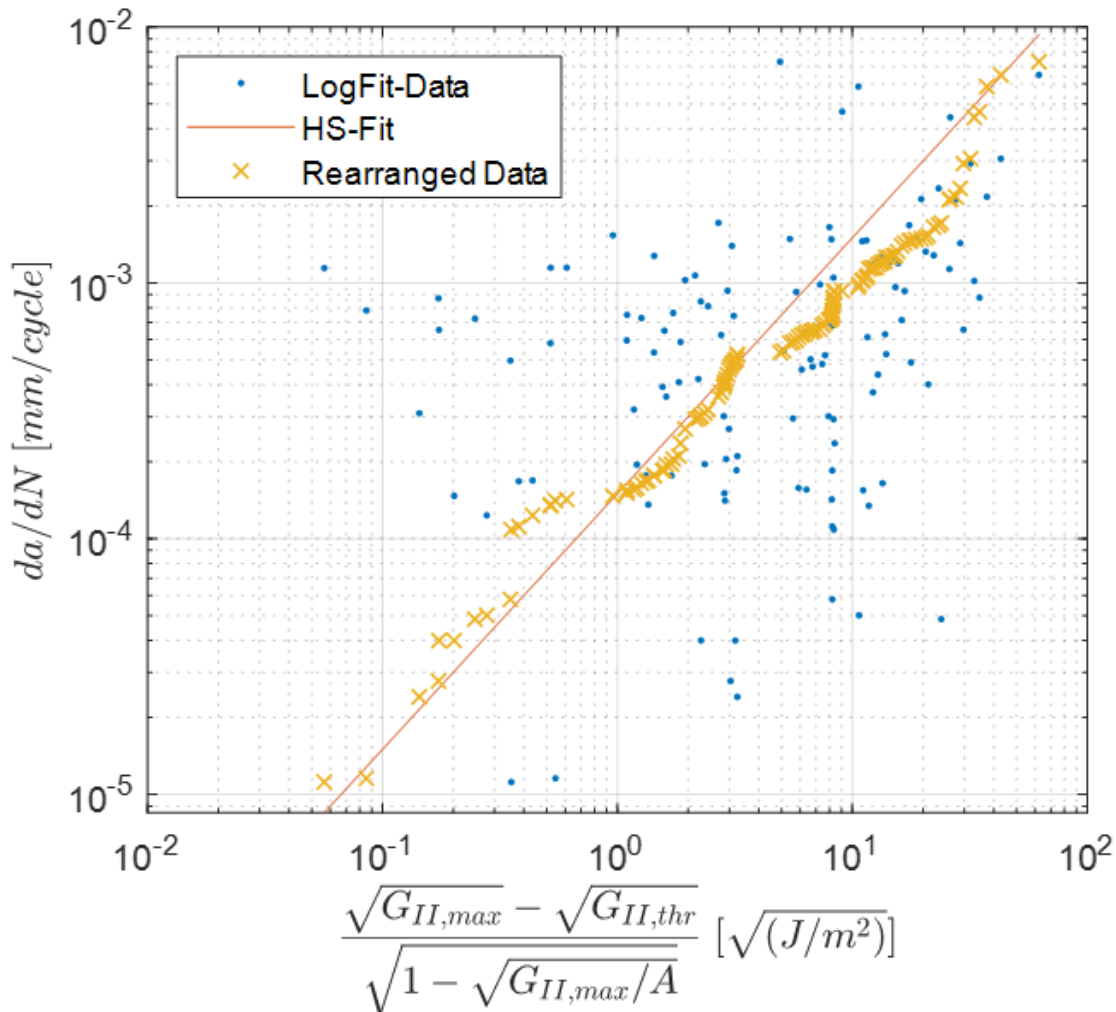


Figure 12 – Application of the rearranged data reduction method to the HS-analysis illustrating the potential of the this data reduction method to reduce the scatter and estimate the A and $G_{II,thr}$ values.

or non-uniform adhesive application as discussed above, the theoretical high ERR corresponding to this crack growth rate does not necessarily exist in the data set. Instead, this crack growth rate will be plotted with an ERR value corresponding approximately to the same rank, leading therefore to a possible underestimation of the A value. After the fast crack growth, a slower delamination increase will be observed associated with low ERR until the general trend of the data is reached again. In this case, the slow crack growth rate will not necessarily be associated with the corresponding low ERR value leading this time to an overestimation of the ERR threshold value. Similar critics were formulated by Schijve (1994) considering the application of the method to S–N data. Nevertheless, it was shown that the rearrangement method proposed by Gatto (1956)

can be successfully applied to fatigue crack growth data to reduce the scatter and obtain easily the centroidal line of the data. If this method is used to estimate the fatigue behavior outside the linear range, i.e. using the HS-analysis, the ERR threshold value will likely be overestimated, and the A value underestimated.

Application of the HS-equation to a design guideline

One of the advantages of the HS-equation, is that the ERR threshold value is an explicit parameter of the equation and can be estimated. The ERR threshold value presented in this study was obtained for long crack and under constant amplitude loading. The influence of possible short crack effects, where a short crack (in comparison with a relevant microstructural scale of the material as defined in (ASTM E647)), grows at an unexpected high rate as discussed by Jones et al. (2014) for polymer composites should be investigated. To date and to the best knowledge of the authors, such effects have not been reported for wood materials or adhesively bonded wood joints. However, in analogy with fiberreinforced polymer composites, this can a priori not be excluded and may effectively occur, even though its existence may be difficult to prove, among others, simply because of the large variability in wood morphology and properties. In order to estimate a valid value of the threshold below which no significant fatigue crack growth occurs, the conservative design approach discussed in detail by Jones et al. (2017) could be used. This approach, based on the (modified) Hartman– Schijve equation, consists of estimating an upper bound fatigue crack growth curve which encompasses all the experimental data. At the same time, a realistic experimental scatter can be determined. The ERR threshold value associated with this conservative fatigue crack growth curve could then be reduced by two or three standard deviations depending on the required safety level. The value chosen for the safety factor would also have to accommodate the intrinsic scatter in the data due to limited measurement resolution (load and displacement from test machine) in the low load regime typically associated with near threshold delamination tests. Therefore, the consistency of the ERR threshold value should be verified as it can typically be expected that at low loads the extrinsic scatter will increase due to the uncertainty of the load and displacement measurements. However, even in this approach there is a further issue: for fiber-reinforced polymer composites, where specimens with unidirectionally aligned fibers are used in testing for design values, the safety factor may be overestimated due to effects of large-scale fiber bridging (as recently discussed by Yao et al. and Alderliesten et al.). In multidirectional

fiber composites (mostly used in structural applications) the effective fiber-bridging may be significantly less than in the test coupons for determining the fracture behavior of the laminate and the design limits. The only exception noted in literature are wind rotor blades that consist of mainly unidirectional lay-up, where the large-scale fiber-bridging is effectively exploited in the design. In the adhesively bonded wood joints, fiber bridging does not occur as long as the delamination runs in the adhesive layer or at the adhesive-wood interface. If, however, the delamination fully or partially deviates into the wood layer adjacent to the adhesive bond-line, as observed for some types of adhesives (Clerc et al. 2019a, b), the same argument as for the wind rotor blade could be used, i.e., fiber bridging in the wood would contribute to slowing delamination propagation and this would be captured by the respective Hartman– Schijve data analysis (as shown by the Mode II fatigue fracture data presented in the manuscript). Therefore, the HS-type data analysis provides data (G_{thr} and ERR values with respective scatter) that can be used in the development of a future design guideline.

Conclusion

It was shown that the use of the HS-equation, despite the low number of samples analyzed in this feasibility study, yields plausible results for describing mode II fatigue fracture of wood adhesively bonded joints and that it represents a viable alternative to the Paris equation. Indeed, the advantages of the HS-equation are the following:

- Allows to estimate the ERR threshold and maximum values directly from fitting the data with the HS-equation
- The description is more physics-based as da/dN is proportional to a \sqrt{G} -term (i.e., directly proportional to K) instead of to G and quasi-static critical ERR and threshold values are explicit parameters in the HS-equation
- For data plotted using the Paris-equation, it is difficult to estimate precisely whether the test data are all obtained from the linear crack growth part of the fatigue fracture test. This does not matter for data plotted using the HS-equation as the complete data-set is linearized by the equation.
- The lower power-law coefficient in the HS-equation (compared to the Paris-equation) and, in addition, having a similar exponent coefficient between different

adhesive systems means that the same design methodology can be used, as the errors will remain in the same range.

Despite these advantages, the fitting process needed to determine the four parameters of the HS-equation is relatively cumbersome and somewhat subjective for data showing a large scatter. To simplify the fitting process, an automatic method which can be used even if significant scatter of the data is seen was successfully applied to wood specimens bonded with three different adhesives types. Additionally, an analysis a posteriori of the scatter origin has shown that it can differentiate between extrinsic and intrinsic scatter. The main cause of extrinsic scatter is attributed to limited measurement resolution at low levels of load and displacement. The intrinsic scatter for adhesively bonded wood is likely due to sporadic events where a sudden faster crack growth was observed, probably caused by a nonuniform adhesive application or heterogeneity in local morphology of the adherends. The main advantages of the HS-equation appear for an application in design guidelines. However, before the A and G_{thr} values presented here can be used in design applications, several issues should first be investigated. One such question is, how the number of cycles and the corresponding ERR value influence the calculated G_{thr} value. Also, further tests would be necessary to explore the link between the A -value and the ERR measured during quasi-static test, the influence of possible short crack effects on the measured threshold ERR and the variation and intrinsic scatter of the G_{thr} -value.

Acknowledgements

The authors thank the Swiss Innovation Agency for the financial support (Project 18958.1), as well as Henkel AG for providing 1C-PUR adhesive. Furthermore, the assistance of Mr. Daniel Völki for the test machine setup and data acquisition is gratefully acknowledged.

References

1. Aicher S, Christian Z (2015) Fatigue behavior of wood and glued wood components. 21. Internationales Holzbau-Forum IHF
2. Alderliesten RC, Brunner AJ, Pascoe JA (2018) Cyclic fatigue fracture of composites: what has testing revealed about the physics of the processes so far? Eng Fract

- Mech 203:186– 196.
3. Bachtiar EV, Clerc G, Brunner AJ, Kaliske M, Niemz P (2017) Static and dynamic tensile shear test of glued lap wooden joint with four different types of adhesives. *Holzforschung* 71:2751.
 4. Clerc G, Brunner AJ, Josset S, Niemz P, Pichelin F, van de Kuilen JWG (2019a) Adhesive wood joints under quasi-static and cyclic fatigue fracture Mode II loads. *Int J Fatigue* 123:40– 52.
 5. Clerc G, Sause MGR, Brunner AJ, Niemz P, van de Kuilen JWG (2019b) Fractography combined with unsupervised pattern recognition of acoustic emission signals for a better understanding of crack propagation in adhesively bonded wood. *Wood Sci Technol* 53:1235-1253
 6. Gatto F (1956) New statistical methods applied to the analysis of fatigue data. In: Weibull W, Odqvist FKG (eds) *IUTAM Colloquium on Fatigue*, pp 66–77
 7. Hartman A, Schijve J (1970) The effects of environment and load frequency on the crack propagation law for macro fatigue crack growth in aluminium alloys. *Eng Fract Mech* 1:615– 631.
 8. Jones R, Pitt S, Brunner AJ, Hui D (2012) Application of the Hartman–Schijve equation to represent Mode I and Mode II fatigue delamination growth in composites. *Compos Struct* 94:1343–1351.
 9. Jones R, Stelzer S, Brunner AJ (2014) Mode I, II and mixed Mode I/II delamination growth in composites. *Compos Struct* 110:317–324.
 10. Jones R, Hu W, Kinloch AJ (2015) A convenient way to represent fatigue crack growth in structural adhesives. *Fatigue Fract Eng Mater Struct* 38:379–391.
 11. Jones R, Kinloch AJ, Michopoulos JG, Brunner AJ, Phan N (2017) Delamination growth in polymer-matrix fibre composites and the use of fracture mechanics data for material characterisation and life prediction. *Compos Struct* 180:316–333.
 12. Kyanka GH (1980) Fatigue properties of wood and wood composites. *Int J Fract* 16:609–616
 13. Lewis WC(1960) Design consideration of fatigue in timber structures. *Am Soc Civ Eng* 86:15–23

14. Paris P, Erdogan F (1963) A critical analysis of crack propagation laws. *J Basic Eng* 85:528–533.
15. Schijve J (1994) Fatigue predictions and scatter. *Fatigue Fract Eng Mater Struct* 17:381–396
16. Simon I, Banks-Sills L, Fourman V (2017) Mode I delamination propagation and R-ratio effects in woven composite DCB specimens for a multi-directional layup. *Int J Fatigue* 96:237–251.
17. Smith I, Landis E, Gong M (2003) *Fracture and fatigue in wood*. Wiley, Winchester
18. Stelzer S, Brunner AJ, Argüelles A, Murphy N, Cano GM, Pinter G (2014) Mode I delamination fatigue crack growth in unidirectional fiber reinforced composites: results from ESIS TC4 round-robins. *Eng Fract Mech* 116:92–107.
19. Yao L, Alderliesten RC, Jones R, Kinloch AJ (2018) Delamination fatigue growth in polymer-matrix fibre composites: a methodology for determining the design and lifing allowables. *Compos Struct* 196:8–20.

3.5 Paper V - Fractography combined with unsupervised pattern recognition of acoustic emission signals for a better understanding of crack propagation in adhesively bonded wood

Paper V

Wood Science and Technology

Fractography combined with unsupervised pattern recognition of acoustic emission signals for a better understanding of crack propagation in adhesively bonded wood

Gaspard Clerc ^{a,d}, Markus G. R. Sause ^b, Andreas J. Brunner ^c, Peter Niemz^a, Jan Willem G. van de Kuilen^d

a. Bern University of Applied Sciences

Architecture, Wood and Civil Engineering

Solothurnstrasse 102

CH-2500 Biel

b. Institute of Materials Resource Management

University of Augsburg

Universitätstrasse 1

DE-86159 Augsburg

c. Empa, Swiss Federal Laboratories for Materials Science and Technology

Mechanical Systems Engineering

Überlandstrasse 129

CH-8600 Dübendorf

d. Technical University of Munich

Wood Technology Munich

Winzererstrasse 45

DE-80797 München

Abstract

In this paper, acoustic emission (AE) signals obtained during quasi-static crack propagation in adhesively bonded beech wood were classified using an unsupervised pattern recognition method. Two ductile one-component polyurethane (1C-PUR) adhesives with the same formulation except for one system being reinforced with short polyamide (1 mm long) fibers were compared to a relative brittle phenol–resorcinol– formaldehyde (PRF) adhesive. Using only localized AE signals, it was shown that the signals originating from the crack propagation could be classified into two different clusters. Comparing the AE signals with a new fractography method, it was estimated that different clusters are due to distinct failure mechanisms, with signals of cluster 1 being associated with wood failure and signals of cluster 2 with adhesive failure. The obtained results suggest that for the PRF adhesive the wood fibers help to slow down the crack propagation. A similar but lesser effect was noted for the polyamide fibers added to the 1C-PUR adhesive matrix.

Introduction

The current development of adhesives for timber load-bearing structures must meet the performance requirements and at the same time reduce the ecological and health impact of the adhesives used. Thus, the adhesive industry is trying to develop new adhesives as an alternative to the PRF adhesive system, which have, despite their high mechanical performance, the disadvantage of containing a significant proportion of formaldehyde, a substance known to be cancerogenic. One of the best currently available alternatives to these systems are 1C-PUR systems, but despite encouraging results (Lehringer and Gabriel 2014), the performance of 1C-PUR adhesives is still below that of long-used commercial systems such as the PRF. The exact reason explaining why the PRF system is generally performing better in terms of strength and delamination resistance is still not completely understood. One possible explanation could originate from the fracture behavior. Generally, a rupture of the bond line in the wood layer is preferable (and recommended by the EN 14080 standard, for example) as it implies that the adhesive is stronger than the wood. However, it was shown that the proportion of the fracture surface occurring in the wood layer, i.e., the wood fracture percentage (WFP), does not correlate with the strength of the bond line and that depending on the wood origin, strong variations can be observed (Hass et al. 2014). Typically, lap shear samples of

adhesively bonded wood show no strength differences between 1C-PUR and PRF (in dry climate), but PRF-bonded samples generally have a higher WFP than 1C-PUR-bonded samples (Kläusler et al. 2014). Clerc et al. (2019) have shown that under cyclic loading, crack propagation under Mode II 4-ENF is slower and demands higher energy for PRF samples than for 1C-PUR samples despite showing a relatively similar energy release rate (ERR) under quasi-static loading. Here, too, 1C-PUR adhesives typically show a failure at the interface between the wood and the adhesive, whereas PRF generally shows a higher wood fracture percentage. The question is, therefore, whether the better performance of PRF adhesive can be partly explained by the failure layer located in the wood, where its fibrous nature helps to reduce the crack propagation speed compared to a propagation in the adhesive interface. Typically, a crack stopped by a fiber during its propagation will branch (supposing that the fracture toughness of the crack propagation domain is lower than that of the fibers) to overcome the obstacle. Due to the branching of the crack, more surface is created, and an on average smaller damage size can be expected. It is, however, difficult to know whether the wood fibrous structure is really reducing the rate of crack propagation as the observation of the fracture surface is only possible a posteriori. The use of AE to monitor damage accumulation in wood material in situ (Aicher et al. 2001; Jakiela et al. 2008; Reiterer et al. 2000) is a suitable method to complement common mechanical tests as it permits the detection of the associated accumulation and interaction of damage in the full specimen volume with sub-microsecond time resolution. One difficulty of the AE method is the identification of the AE signal origin, with respect to both the microscopic source mechanism and its exact location and orientation. Concerning this issue, fractography combined with AE-based parameter analysis has been used to identify microscopic failure mechanism in wood (Ando et al. 2006) and in bamboo (Chen et al. 2018). Unsupervised pattern recognition (UPR) methods based on AE frequency and/or AE time domain features have been successfully used to characterize wood failure (Baensch et al. 2015a; Diakhate et al. 2017; Najafi et al. 2017). These methods seek the numerically best partition of signals according to selected features into different clusters to possibly identify different natural classes of AE signals (Sause et al. 2012a). To associate these natural classes with physical features, a detailed analysis of the fracture surface/volume should be conducted using for example multiphysics finite element method (Sause et al. 2012b), nondestructive testing (Baensch et al. 2015b) or fractography. In wood under tensile stress, Baensch et al. 2015b could combine AE with in situ synchrotron X-ray micro-computed tomography to determine the main failure mechanisms were interwall cracks

(cell wall debonding) and cell wall cracks. However, the use of UPR and X-ray CT on plywood miniature specimens yielded the same two AE clusters as obtained for clear wood (Brunner et al. 2015); no separate AE cluster could be assigned solely to the adhesive. One possible explanation could be that for the chosen sample geometry (dog-bone tensile sample), the maximal stresses generally do not occur in the bond line but rather in the wood. In this paper, AE was used to monitor the damage accumulation of adhesively bonded wood under quasi-static Mode II 4-ENF loading. Using this test setup, the maximal shear stresses are occurring in the bond line of the sample. The AE signals were recorded from three wood adhesives (two relatively ductile 1C-PURs and one relatively brittle PRF system). This setting was chosen to better understand how the structure of the wood adhesive compound influences the crack propagation and how damages evolve for each adhesive system. For this reason, small polyamide fibers were added to the matrix of one of the 1C-PUR adhesives, being otherwise identical. AE signals obtained during the test were then analyzed with an unsupervised pattern recognition to identify natural clusters. A new fractography method is presented to potentially explain the microscopic origin of these different clusters.

Material and methods

Experimental setup

Mechanical test setup

Beech wood (*Fagus sylvatica* L.) with a mean density of 714 kg/m^3 at a wood moisture content of 12% was used for the tests. The wood had no defects such as knots or grain deviation. Prior to the adhesive bonding, a $15\text{-}\mu\text{m}$ -thick fluoropolymer (ETFE230N) foil was applied between the lamellae on the first 120 mm to simulate a starter crack. Three adhesives are compared in the tests: The first is a relatively brittle phenol–resorcinol–formaldehyde (PRF, trade name (Aerodux 185) and two are ductile one-component polyurethane (1C-PUR) adhesives with a low modulus of elasticity (MOE). These two 1C-PUR adhesives are based on the same polymer, with the difference that additional small polyamide fibers (1 mm length and 0.1 mm diameter) were introduced into the adhesive matrix of the LOCTITE HB 110 PURBOND (short name HB 110), but not into the LOCTITE VN 3158 (short name: VN 3158). Once cured, the front position of the foil was referenced as position of the crack tip, and the pre-crack length was set to 110 mm. The samples were then cut to a width of 20

mm, a crack length of 110 mm and a length of 317 mm. The adhesively bonded wood joints were stored for several days at 23°C and 50% relative humidity prior to testing. The end-notched flexure (ENF) specimens were loaded under quasi-static displacement control at 1 mm/min in 4-point bending Mode II. The test was performed on a servo-hydraulic test machine (type 1237 Instron) equipped with a 1 kN load cell with a load and displacement accuracy of at least 1% of the measured value.

AE test setup

AE equipment (type AMSY-6) and preamplifier (type AEP-3 with a hardware bandpass between 30 and 1000 kHz from Vallen Systeme GmbH) with 150 kHz resonant sensors (type SE-150 M from Dunegan Engineering Corp.) and one broadband sensor (type S9208 from Physical Acoustics Corp.) were used. Data acquisition settings were: acquisition threshold 40 dBAE, duration discrimination time 400 *mus* and a rearm time of 1 ms. Two SE-150 M AE sensors were placed on top and bottom each between the bottom and top loading rollers, and between the top loading rollers, respectively. In addition, one S9208 sensor was placed on the bottom side between the top loading rollers (see Fig. 1 for details). All sensors were coupled with a silicone-free vacuum grease and mounted with metal springs. For assessing the delamination length as a function of time, linear AE signal source location was performed with the four sensors mounted on the bottom side of the joint. The signal sources were localized using two different 1-D localization processors to find signals, which were correctly identified by the four sensors 2–7–4–6 (see Fig. 1). Using this method, only AE wave propagation in the longitudinal direction was considered, meaning that only one speed of propagation ($v = 4250$ m/s) could be used. The AE source location accuracy was checked via the so-called autocalibration for which each sensor in turn was used as emitter of elastic waves, which were recorded by the other sensors and localized.

Unsupervised pattern recognition (UPR) methodology

The UPR used in this work was adapted from earlier researches on composites (Sause et al. 2012a) and has been previously applied to wood failure (Baensch et al. 2015a). The algorithm is based on an exhaustive search procedure of AE features and identifies the most suitable partition without initial assumptions regarding the number of AE features used and the number of clusters. To this end, a list of $K = 9$ frequency-based AE features were defined to use for the investigation (see Table 1). The selection of the

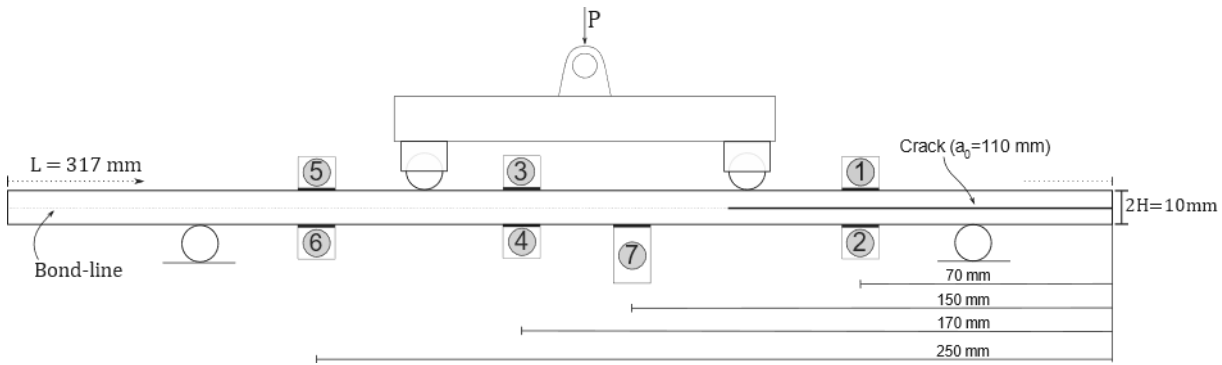


Figure 1 – Scaled schematic representation of the test setup, with the type and position of each AE sensor— the type of sensor for sensors 1–6 is SE-150M and S9208 for the sensor 7

number of partial powers (6 in this case) in the AE feature set, in principle, is arbitrary, but experience has shown that 6 is a reasonable choice in terms of computational effort and results (Sause et al. 2012a; Sause and Horn 2013). Boundary constraints for the algorithm were chosen as $M = 3$ minimum number of features to use for a partition and $P = 10$ as maximum number of clusters expected. Based on these boundary constraints, the algorithm investigates all $\binom{n}{k}(P - 1)$ partitions and ranks the obtained result using cluster validity metrics (Sause et al. 2012a). For this investigation, Gaussian mixture models were chosen as clustering algorithm with normalization of features using their unit variance.

Fractography

It is hypothesized that different AE signal clusters revealed by UPR are representing different fracture layers in or near the bond line. The distinction between the different fracture layers on the fracture surface is relatively easy for PRF adhesive as the contrast between the wood and the adhesives' dark color allows distinguishing fracture of the wood and of the adhesive. However, for the 1C-PUR adhesive, this is more challenging due to the transparency of the adhesive. To simplify the distinction (step 1 in Fig. 2), a chemical treatment of the samples using a reacting product was used (a solution of hydrochloric acid and phloroglucinol). This reagent colors the lignin in red allowing a better contrast between adhesive and wood, hence allowing distinguishing between adhesive and wood fracture. Approximately one hour after applying the reagent, images of both fracture surfaces were taken with a digital single-lens reflex (DSLR) camera (24.2 megapixel APS-C 22.3×14.9 mm sensor) and a 100 mm macrolens. The final image resolution was one pixel ≈ 0.01 mm. Using the color difference (step 2

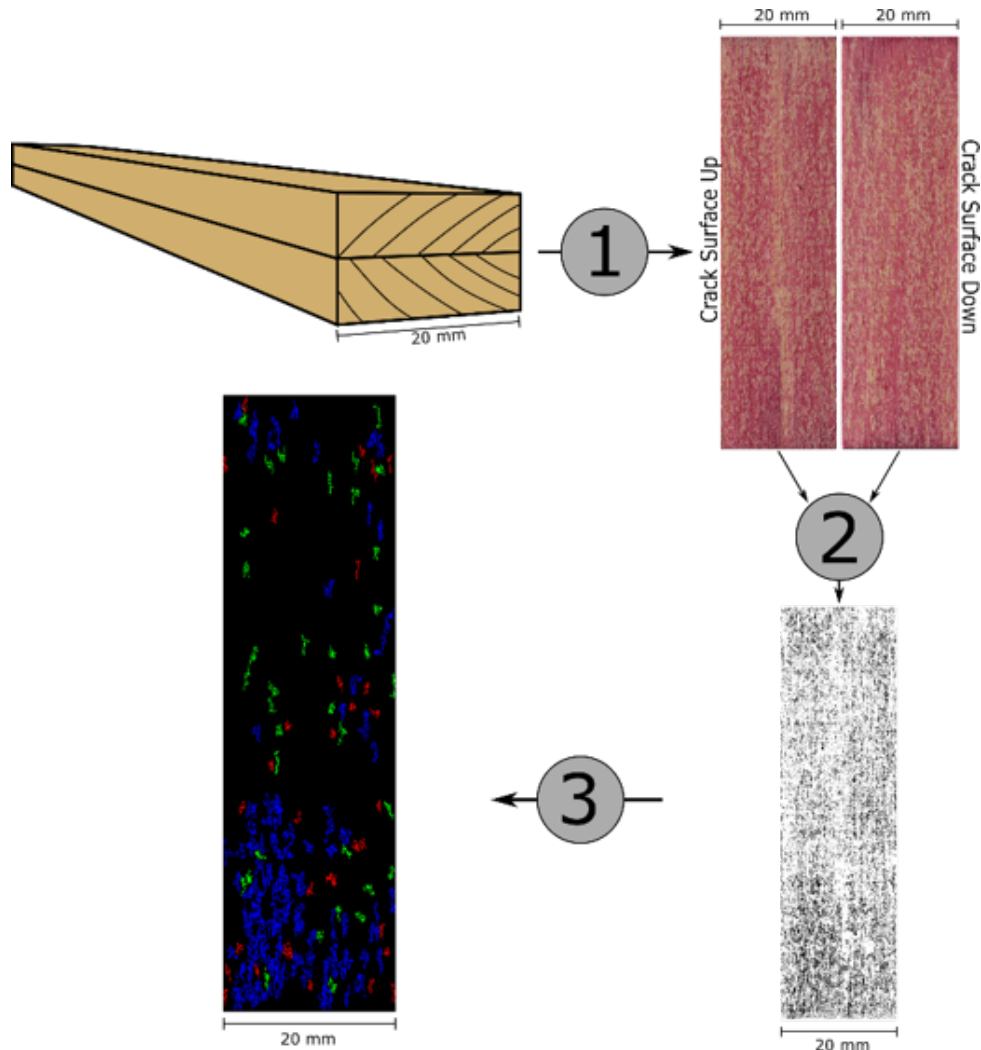


Figure 2 – Schematic of the main steps of the fractography analysis method—see text for a detailed description of the method

in Fig. 2), a color mask was applied using HSV color space to differentiate between the wood and adhesive fracture. Both images were then binarized according to the color masks so that a black pixel ($= 0$) corresponds to wood failure and a white pixel ($= 1$) to adhesive failure. Both images were then superposed to obtain a map of the fracture surface using an OR filter so that if a pixel appears black ($= 0$) it means that this pixel is black on both images, and hence indicates wood failure. This allows to distinguish between interface failure (one fracture surface fails in the wood and the opposite side in the adhesive) and wood failure. However, the distinction between wood and adhesive rupture based on color difference is not always exact, especially between zone boundaries. In addition, it is difficult to superpose and align both surfaces exactly. Both errors will overestimate the wood fracture percentage. To limit this error (step 3

Table 1 – AE features used for the investigation

Peak frequency	f_{peak}	[Hz]
Frequency centroid	$f_{centroid} = \frac{\int f \cdot U(f) df}{\int U(f) df}$	[Hz]
Weighted peak frequency	$f_{peak} = \sqrt{f_{peak} \cdot f_{centroid}}$	[%]
Partial power	$\int_{f_1}^{f_2} U^2(f) df / \int_{f_{start}}^{f_{end}} U^2(f) df$ $f_{start} = 0 \text{ kHz}$ $f_{end} = 1200 \text{ kHz}$ PP1: $f_1 = 0 \text{ kHz}; f_2 = 150 \text{ kHz}$ PP2: $f_1 = 150 \text{ kHz}; f_2 = 300 \text{ kHz}$ PP3: $f_1 = 300 \text{ kHz}; f_2 = 450 \text{ kHz}$ PP4: $f_1 = 450 \text{ kHz}; f_2 = 600 \text{ kHz}$ PP5: $f_1 = 600 \text{ kHz}; f_2 = 900 \text{ kHz}$ PP6: $f_1 = 900 \text{ kHz}; f_2 = 1200 \text{ kHz}$	

in Fig. 2), only groups of interconnected black pixels which surfaces correspond to the different crack size estimation were considered in the calculation of the WFP. The main steps of the fractography method are summarized in Fig. 2.

Results and discussion

Estimation of the sensitivity of the acoustic emission measurements

Recent developments in the analysis of acoustic emission measurements (Brunner 2016) have shown that it is possible to establish an estimated correlation between crack area and the recorded linear AE signal amplitude (after amplification, measured in μV). A similar method is used here to estimate the damage size depending on the adhesive system. For each sample, the sum of the signal peak voltage is divided by the cracked surface. The cracked surface is estimated by multiplying the width of the specimen by the crack length increment measured during the test. This number is an estimation of the sensitivity and is given in ($\mu V/\mu m^2$). The crack length is measured on both lateral sides of the specimen, and the average value is taken for the calculation of the cracked surface. However, the exact crack tip position between these points is not known; therefore to consider a nonlinear crack tip position, upper and lower bounds are estimated by adding and, respectively, subtracting a half circle (with a diameter

equal to the width of the specimen) to or from the cracked surface. Additionally, the surface roughness is considered by adding an arbitrary amount of 20% to the upper bound surface value. Using these estimations, lower and upper bounds are estimated for the sensitivity. Finally, the typical damage surface is computed by dividing the average amplitude of the signals (for one adhesive system) by the estimated sensitivity. Then, the square root of this surface is calculated to obtain the typical damage size (considering a quadratic or equivalent circular crack shape). The average sensitivity and expected crack size are given in Table 2 for the different adhesive systems. The influence of the material damping (with a measured far-field damping value of 0.22 dBAE/cm) on the estimated sensitivity was found to be less than 10% (estimated only from localized signals). Since attenuation was hence neglected, no AE signal amplitude correction as a function of distance was applied. In the next section, the UPR analysis was applied on the sample bonded using the HB 110 and PRF adhesive, respectively. Due to the few signals ($n = 2$) obtained for the samples glued with the adhesive VN 3158, no further analysis was considered in this case.

Table 2 – Estimated sensitivity and estimated crack size for a nonlinear crack tip propagation and for the different adhesive systems based on the AE signals amplitude — each value is given with upper and lower bounds

	Estimated sensitivity [$\mu V/\mu m^2$]			Estimated crack size [μm]		
	Mean	Upper bound	Lower bound	Mean	Upper bound	Lower bound
Hb 110	7.5E-04	5.3E-04	9.4E-04	714	850	631
PRF	3.4E-03	2.4E-03	4.3E-03	363	466	321
VN 3158	2.3E-04	1.6E-04	2.9E-04	863	1028	763

UPR on HB 110 adhesively bonded samples

The partition of all AE localized signals ($n = 380$) obtained for the four different samples glued with the HB 110 adhesive are shown in Fig. 3. The best partition is obtained with a direct use of the classifier algorithm with two clusters resulting in an uncertainty of classification (UoC) of 0.97 (Sause and Horn 2013), meaning that only 3% of the signals are potentially classified in the wrong cluster. In Fig. 3, marginal histograms are shown for both variables and both cluster data with a fitted line represent the data distribution. The number of bins was computed based on the sample standard deviation using Scott's

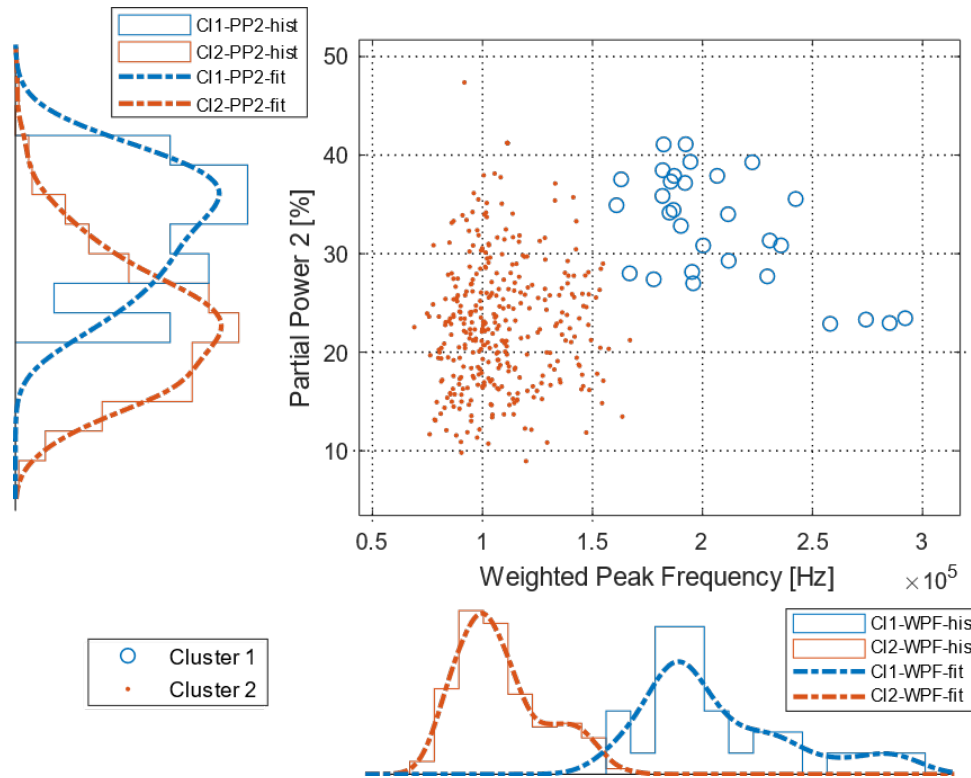


Figure 3 – Resulting partition of the AE signals in 2 clusters for the samples glued with the adhesive HB 110 according to the UPR method—C11: cluster 1, C12: cluster 2

rule. In further plots, only the fitted line was plotted to show the data distribution. In Fig. 4, the relative timescale is compared with the estimated AE source position. The general tendency shown in Fig. 4 is that the position of the signal is increasing with the time duration and that it follows the approximate position of the crack tip. The signals from clusters 1 and 2 have a comparable temporal distribution. On average, the energy of the signals from cluster 2 is higher than for cluster 1. However, no significant difference between the true energy distribution in clusters 1 and 2 was found (at a 5% significance level). In Figs. 3 and 4, all four HB 110 samples are shown in the same plot. However, the proportion for each sample was different as shown in Table 3. The main difference between the clusters lies in their frequency characteristics, as the weighted peak frequency is clearly higher for cluster 1 compared to cluster 2. The physical meaning of different high-frequency proportions between clusters could be interpreted as originating from different microscopic sources, i.e., fracture mechanisms (Baensch et al. 2015a). To examine this hypothesis, an analysis of the fracture surface was conducted.

Prior to the analysis of the fracture surfaces, the estimated damage size was calculated

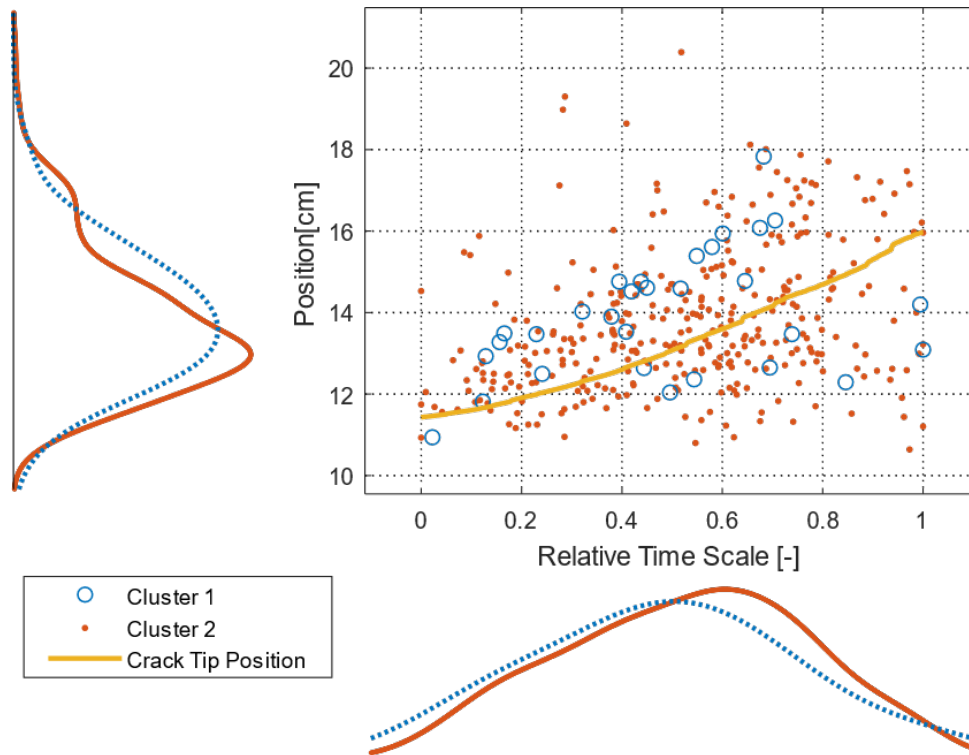


Figure 4 – Linear AE signal location, time and average crack tip position (calculated according to Clerc et al. 2019) for the four samples glued with the adhesive HB 110. Signals of both clusters follow the direction of the crack propagation

(according to the above procedure) for each sample. These values were then used as lower, mean and upper range for estimating the crack size in the fractography analysis. The average wood fracture percentage is calculated by summing all the black pixel groups with a group size higher than the estimated lower crack size. Without lower limit, the estimated wood fracture percentage would be overestimated due to a high number of small pixel groups. Indeed, if all pixel groups are considered, the average group size is 0.03 mm^2 . Given the size of these groups, they are probably due to the difficulty in superposing exactly two different images and to select the appropriate color filters to obtain the best distinction between wood and adhesive failure. Both phenomena will lead to a superposition of the same color area, interpreted as wood failure if black pixels are superposed. The average wood fracture percentage obtained using the fractography analysis reveals a rough correlation between the number of signals associated with cluster 1 and the average WFP (Table 6). For example, it was noted that sample HB3a-1 had only 2 signals associated with cluster 2 (3%), whereas sample HB3a-3 had around 12% of its signals associated with cluster 2. The fractography analysis reveals that the average wood fracture percentage is below 0.1% for the HB3a-1 and around 7% for the

Table 3 – Absolute and relative number of the signals for the adhesive HB 110 classified in clusters 1 and 2—the number of signals identified in cluster 1 is ranging from 0 to approximatively 10%

Sample	Signals from cluster 1	Signals from cluster 2
HB1a-2	4(7%)	54 (93%)
HB3a-1	2(3%)	60 (97%)
HB1a-1	7(7%)	96 (93%)
HB3a-3	17(11%)	138 (89%)

HB3a-3. The number of groups and their size is significantly higher for the HB3a-3 sample compared to the HB3a-1 sample (Fig. 5). In comparison, both other samples (HB1a-1 and HB1a-2) show a relatively similar average wood fracture percentage (0.8% and 1.6%, respectively) and also a relatively similar percentage of signals associated with cluster 2 (7%). Considering the four samples, a correlation can be seen between the WFP and the number of signals associated with cluster 1. The higher weighted peak frequency observed in cluster 1 can be partly explained by the higher rigidity of the wood compared to the adhesive. Typically, cracks occurring in a brittle medium are expected to deliver a broad frequency spectrum. Defect-free beech as used here has a MOE of about 13 GPa, whereas adhesive stiffness is approximatively 1–4 GPa (with 1C-PUR ranging from 1 to 2 GPa and PRF from 3 to 4 GPa; Kläusler et al. 2013). Therefore, failure of the adhesive interface or cohesive failure is expected to result in AE signals with less broad frequency spectra. This translates into the different weighted peak frequencies found for the two clusters.

PRF adhesive

The partition of all localized AE signals ($n = 1927$) obtained for the four different samples glued with the PRF adhesive is shown in Fig. 6. The best partition is obtained with a direct use of the classifier algorithm with two clusters with an UoC of 0.91. The number of signals obtained from the PRF samples is much higher than for the HB 110 samples. This could be an indication of a larger effective fracture surface due to higher roughness or due to a smaller crack increment per AE signal due to the more brittle PRF adhesive. The average energy per hit for cluster 1 of the PRF (Table 7) is very similar to cluster 1 of the HB 110 adhesive (Table 4). On average, a higher number of signals is classified in cluster 1 (Table 5) in comparison with the HB 110 adhesive, the

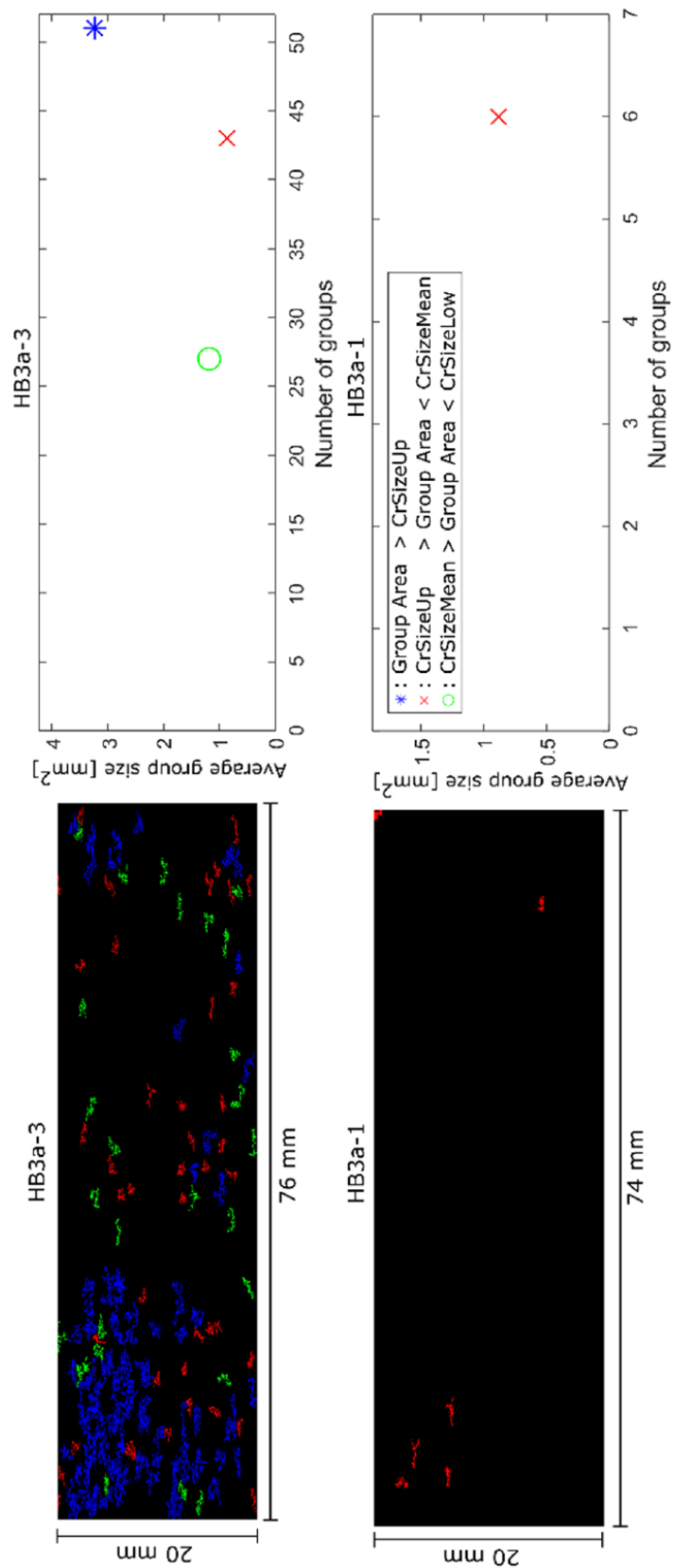


Figure 5 – Fractography results for the sample HB3a-3 (top) and HB3a-1 (bottom) showing the different groups of pixels associated with wood fracture according to the estimated crack size

majority being still classified into cluster 2 (Table 6). On average, a higher weighted peak frequency is obtained for cluster 1 than for cluster 2 (Table 7). In comparison with the adhesive HB 110, the average weighted peak frequency from clusters 1 and 2 is higher for the PRF adhesive (approx. 20%) (Table 7). Contrary to the samples glued with the adhesive HB 110, the number of signals associated with cluster 1 tends to increase nonlinearly with the test duration (Fig. 7). In comparison, the number of signals from cluster 2 increases gradually until the end of the test, but the number of signals from cluster 1 increases significantly only after 50% of the relative timescale.

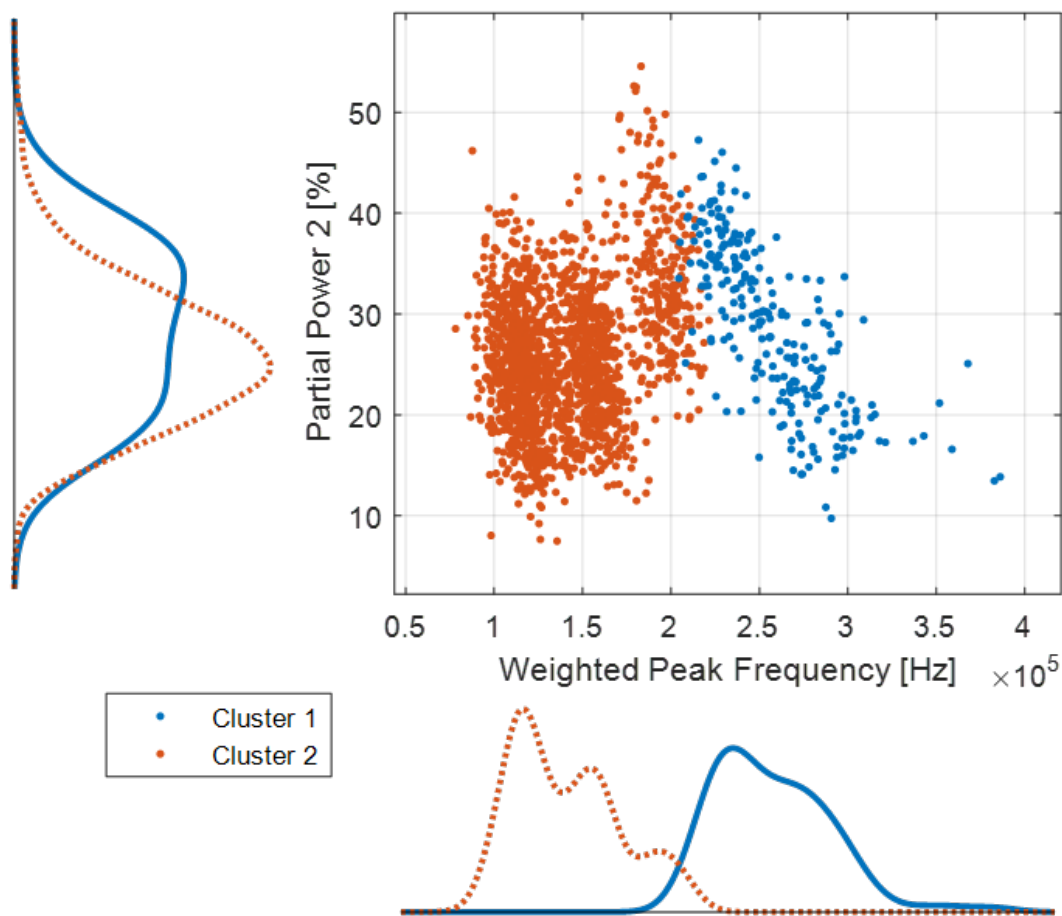


Figure 6 – Resulting partition of the AE signals in 2 clusters for the samples glued with the adhesive PRF according to the UPR method

Using the fractography method as described above, it is possible to distinguish between wood fracture and adhesive failure (using the natural contrast between the wood and the dark brown PRF adhesive). Summing the number of pixels associated with wood failure

Table 4 – Main differences between the signals associated with cluster 1 and cluster 2

Sample	Cluster 1	Cluster 2
Number (quota)	30(80%)	348 (92%)
Energy sum (quota)	2.5860E-15 (1%)	4.9583E-13 (99%)
Energy per hit (J) (median)	1.9831E-17	5.5038E-17
Partial power 2 (%)	32.7	22.8
Weighted peak frequency (kHz)	207.3	108.3

Table 5 – Absolute and relative classification of the signals in cluster 1 and cluster 2 for the PRF samples—the number of signals identified in cluster 1 ranges from 10% to approximately 20%

Sample	Signals from cluster 1	Signals from cluster 2
PRF3B-1	93(14%)	590 (86%)
PRF2B-1	44(11%)	351 (89%)
PRF2B-2	44(18%)	205 (82%)
PRF2B-5	62(11%)	494 (89%)

over the cracked surfaces reveals that the crack is generally starting as an interface failure but evolves gradually into wood failure as shown in Fig. 8.

Influence of the adhesive system of the cluster features

It has been shown that for both adhesive systems, it was possible to roughly correlate the signals from the lower-frequency cluster 1 with wood failure. It was also noted that for the samples glued with the PRF adhesive, a higher number of signals were recorded than for the HB 110 adhesive. Furthermore, the estimated average crack increment is smaller for the PRF system than for the HB 110. One further difference is that for the PRF adhesive, the crack is growing into the wood and propagates into the wood for most of the samples, whereas for the HB 110 samples, the crack propagates at the interface essentially due to an adhesive failure. Only a small fraction of the fracture surface corresponds to wood failure. This could indicate that the propagation medium of the HB 110 is more homogenous and fewer obstacles have to be overcome during the crack growth, whereas for the PRF samples, the crack has to propagate through the highly fibrous environment of the wood. This hypothesis seems to be confirmed by the very low number of signals obtained from the VN adhesive, which is even more

Table 6 – Average wood fracture percentage (WFP) obtained from the cluster analysis and corresponding estimated crack size, mean and upper and lower bounds for the samples glued with the adhesive HB 110

Sample	Average WFP	Crack size mean value [μm]	Crack size up. Bound value [μm]	Crack size low. Bound value [μm]
HB1a-2	1.6	663	788	590
HB31-1	< 0.1	721	859	637
HB1a-1	0.8	510	603	457
HB3a-3	7	656	775	568

Table 7 – Main differences between the signals associated with cluster 1 and cluster 2 for the PRF samples

Sample	Cluster 1	Cluster 2
Size (quota)	243(13%)	1640 (87%)
Energy sum	3.81E-14	4.96E-13
Energy per hit (J) (median)	1.9453E-17	2.527E-17
Partial power 2 (%)	28.6	26.0
Weighted peak frequency (kHz)	257.6	141.3

homogenous (due to the absence of polyamide fibers in the adhesive matrix but also due to the more ductile behavior of the adhesive). For the PRF samples, even though the number of signals associated with cluster 1 tends to correlate with the wood fracture percentage, the majority of the signals are still associated with cluster 2 even when the crack is mostly propagating into the wood. The exact reason for this is not yet completely understood, but it may be that since beech stiffness perpendicular to the grain is around 1 GPa, if the crack follows a path under an angle with the grain, the stiffness may well be in the same range as that of PRF. It may also be that this difference is due to different failure mechanisms occurring in plain wood. As shown in Fig. 9, the fracture surface is a complex patchwork of different wood anatomical features. It can be expected that failures of different anatomical features have different acoustic patterns and that some failure mechanisms have a similar acoustic pattern to interface failure, which would lead to classification in the same clusters. In addition, as shown in Fig. 6, it is possible that more clusters exist than those investigated in this study. However, partitions with more than two clusters results in a lower UoC, meaning that potentially more signals would be classified into the wrong clusters. For this reason, this was not

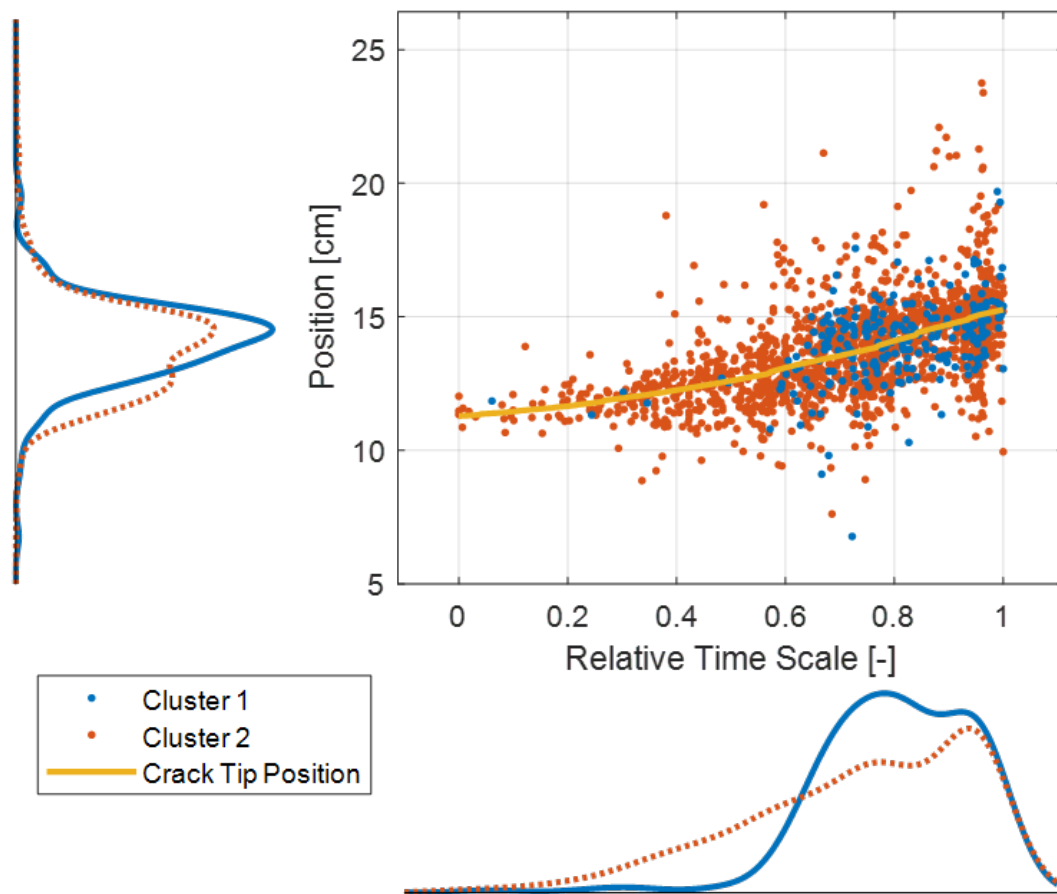


Figure 7 – AE signal location, time and average crack tip position for the four samples glued with the adhesive PRF. Signals of both clusters follow the direction of the crack propagation

further considered.

It seems therefore that crack propagation into the wood is advantageous as the crack has a higher number of obstacles (or obstacles that yield higher energy dissipation) to overcome in order to propagate, hence generating AE signals. This hypothesis corresponds to the results obtained by Clerc et al. (2019), where in quasi-static 4-ENF Mode II tests PRF samples had typically a slower crack propagation compared to the HB 110 adhesive, which itself had a slower crack propagation than the VN 3158 adhesive. For further adhesive development, an optimal adhesive system would need to have a low MOE for absorbing the damages, but a high cohesive and adhesive strength so that the easiest growth path for the crack is in the wood. It is, however, questionable whether it is possible to obtain an adhesive with a low MOE and a high

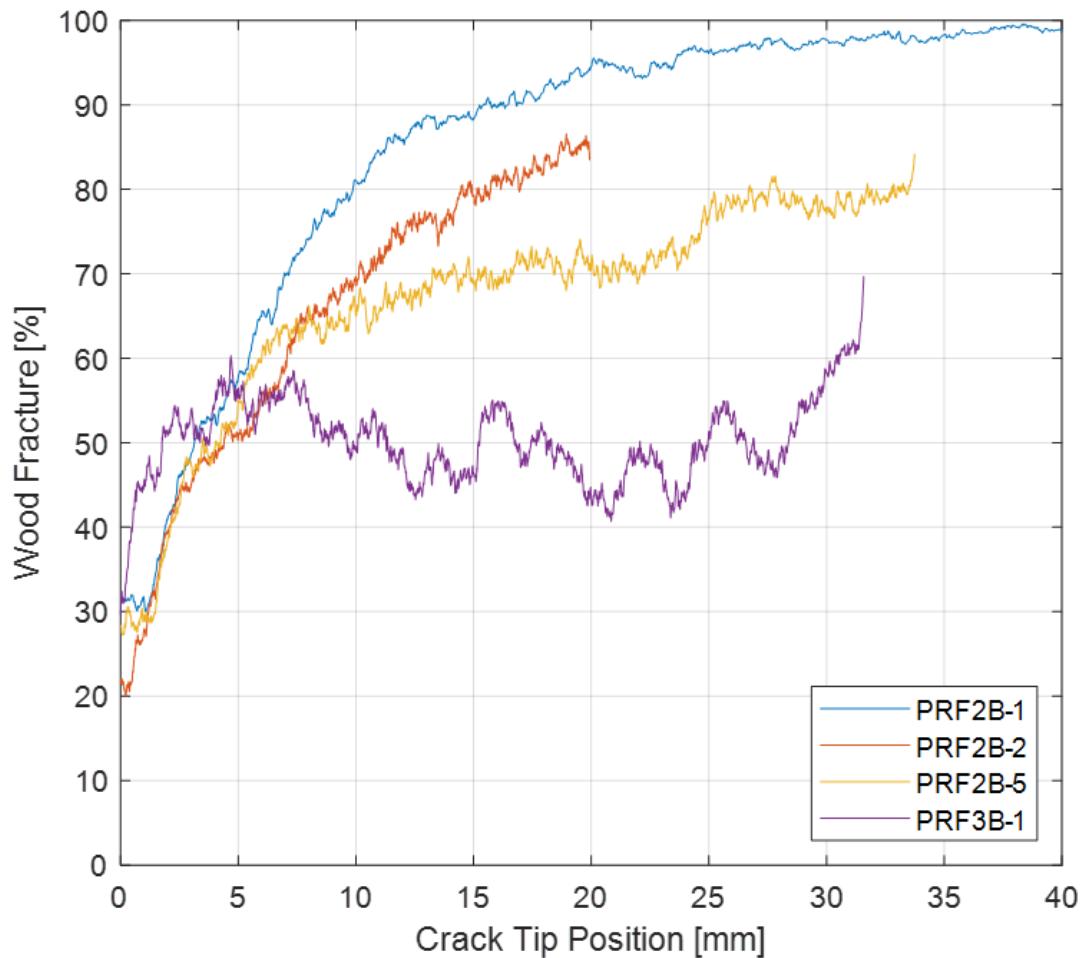


Figure 8 – Increase in the wood fracture percentage with increasing crack length for the samples glued with the PRF adhesive

cohesive/adhesive strength as generally a highly cross-linked polymer has a high MOE and a high cohesive/adhesive strength due to the greater number of links available for bonding with the adherent. During shear loading, the main causes of rupture in the wood are probably associated with interwall (middle lamella) cracks (Fig. 9). The average weighted peak frequency of cluster 1 of both adhesives is around 200–250 kHz, which corresponds approximatively to cluster A presented by Baensch et al. (2015a). Vergeynst et al. (2014) have shown, by using FEM modeling of signal propagation in wood, that the brittle rupture phenomenon will generate signals with a higher WFP, whereas the ductile rupture phenomenon will result in signals with a lower WFP. It should, however, be added that, even though the speed of the mechanism leads to a shorter or longer rise time of the source (voltage/load build-up), this will influence

the rise time of the signals, but also the frequency spectrum. The higher-frequency components of the signals will be more attenuated in the material than low-frequency components. Therefore, this will also depend on the source–sensor distance and its material properties. With an average WFP of 600 kHz, the signals of cluster B found by Baensch et al. (2015a) have a much higher WFP than the signals obtained in the present study. This could be due to the more brittle rupture of the wood obtained under tension loading and/or to different rupture phenomena occurring between softwood (spruce in the case of Baensch et al. 2015b) and hardwood in the present study. Cluster B in Baensch et al. (2015b) was associated with the transversal cell wall cracks in the RT plane, a type of rupture which was not observed on the tested samples. As shown in Fig. 9, the main type of wood rupture was interwall/cell wall cracks in the LT/LR plane. This confirms the results obtained by Ando et al. (2006), where under shear loading, mainly interwall (middle lamella) failure of wood was observed.

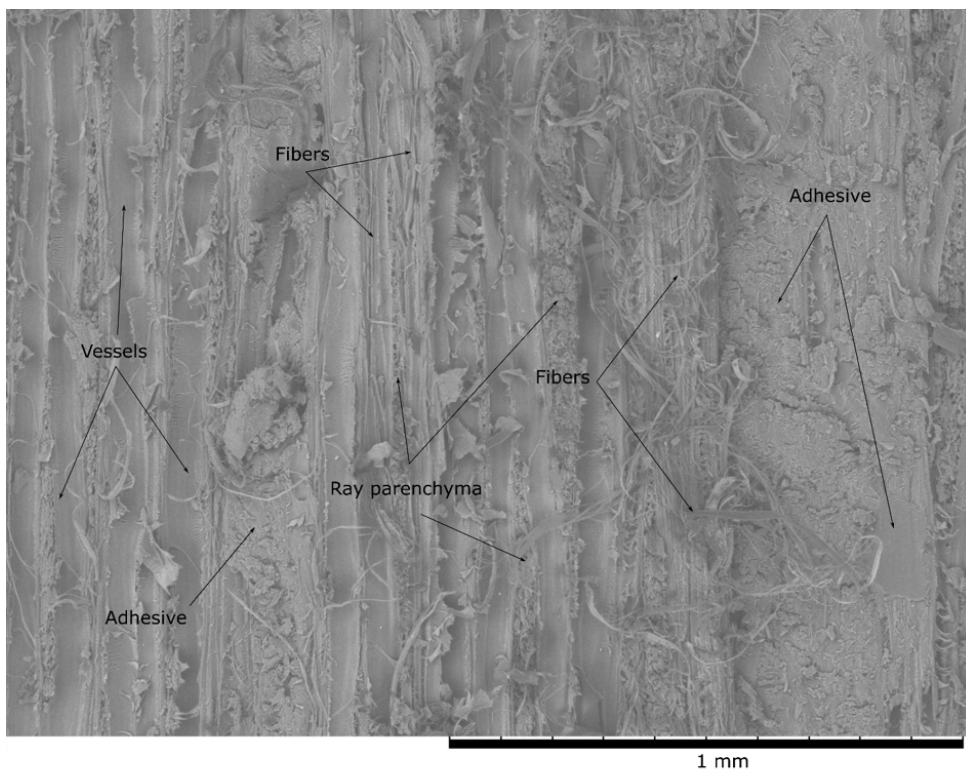


Figure 9 – SEM image of the fracture surface of one PRF sample showing the different anatomical features failing during the crack propagation —each feature with a possible distinct AE pattern

One further point to discuss is that the present analysis was specifically conducted on samples tested under quasi-static loading. AE measurements were also taken on samples tested under cyclic loading but were not analyzed as the signal/ noise ratio

was too high for dedicated AE analysis. Further, as noted by Clerc et al. (2019), cyclic loaded PRF samples had a lower wood fracture percentage as typically observed under quasi-static loading. However, the average wood fracture of these samples remains higher than for 1C-PUR-bonded samples. It can therefore be assumed that the presented hypotheses are still valid (but probably to a lesser extent) in case of cyclic fracture loading. Nevertheless, this should be confirmed with additional tests.

Conclusion

For both adhesive systems, PUR and PRF, it was possible to show that the AE signals associated with cluster 1 correspond to wood fracture. The proposed method of associating fractography with acoustic emission allows estimating even a very small percentage of wood failure through a higher resolution of the cracked surfaces. The following points can be summarized:

- Two types of clusters could be identified for two different types of adhesive; these clusters seem to correspond to different failure mechanisms in the bond line, cluster 2 being associated with crack propagation in the interface and cluster 1 being associated with crack propagation in the wood layer near the interface.
- By using fractography, it was shown that the size and number of pixel groups associated with wood failure reflect the number of signals corresponding to cluster 1 for the adhesive HB 110.
- It was shown for the adhesive PRF that the number of signals associated with cluster 1 is increasing with the test duration. Comparing the fracture surface, it was shown that the crack is starting from an adhesive failure type and propagates into the wood, hence reflecting the signal classification into cluster 1.

The presented results suggest that the addition of short fibers (< 1 mm) in an adhesive helps slowing down the crack propagation. The addition of fibers in the adhesive may, however, be limited for practical reasons (viscosity too high, agglomeration of fibers and difficulty in obtaining a uniform application). In addition, it seems that the wood structure is more efficient in slowing the crack than the modified 1C-PUR adhesive. Further research on adhesive development should focus on obtaining a transition of the fracture surface away from the interface into the wood to improve the crack propagation resistance of relatively ductile wood adhesives.

Acknowledgements The authors thank Dr. Sébastien Josset (Henkel AG) for providing 1C-PUR adhesives as well as the Swiss Innovation Agency (Innosuisse) for the financial support (Project No. 18958.1).

References

1. Aicher S, Höfflin L, Dill-Langer G (2001) Damage evolution and acoustic emission of wood at tension perpendicular to fiber. *Holz Roh Werkst* 59:104–116.
2. Ando K, Hirashima Y, Sugihara M, Hirao S, Sasaki Y (2006) Microscopic processes of shearing fracture of old wood, examined using the acoustic emission technique. *J Wood Sci* 52:483–489.
3. Baensch F, Sause MGR, Brunner AJ, Niemz P (2015a) Damage evolution in wood-pattern recognition based on acoustic emission (AE) frequency spectra. *Holz-forschung* 69(3):357-365.
4. Baensch F, Zauner M, Sanabria SJ, Sause MGR, Pinzer BR, Brunner AJ, Stampanoni M, Niemz P (2015b) Damage evolution in wood: synchrotron radiation micro-computed tomography (SRuCT) as a complementary tool for interpreting acoustic emission (AE) behavior. *Holz-forschung* 69:1015–1025.
5. Brunner AJ (2016) Correlation between acoustic emission signals and delaminations in carbon fiberreinforced polymer-matrix composites: a new look at mode I fracture test data. In: 32nd European conference on acoustic emission testing Czech society for nondestructive testing, Prague
6. Brunner AJ, Baensch F, Sause MGR, Zauner M, Niemz P (2015) Schallemissionanalyse und Synchrotron-basierte Mikrotomografie an verklebten Miniatur-Zugprüfkörpern aus Fichtenholz. *DGZfP* 20. Kolloquium Schallemission, Garmisch-Partenkirchen [Acoustic emission analysis and synchrotronbased microtomography on glued shear strength samples from spruce solid wood]
7. Chen G, Luo H, Wu S, Guan J, Luo J, Zhao T (2018) Flexural deformation and fracture behaviors of bamboo with gradient hierarchical fibrous structure and water content. *Compos Sci Technol* 157:126–133.

8. Clerc G, Brunner AJ, Josset S, Niemz P, Pichelin F, van de Kuilen JWG (2019) Adhesive wood joints under quasi-static and cyclic fatigue fracture Mode II loads. *Int J Fatigue* 123:40–52.
9. Diakhate M, Bastidas-Arteaga E, Moutou Pitti R, Schoefs F (2017) Cluster analysis of acoustic emission activity within wood material: towards a real-time monitoring of crack tip propagation. *Eng Fract Mech* 180:254–267.
10. Hass P, Kläusler O, Schlegel S, Niemz P (2014) Effects of mechanical and chemical surface preparation on adhesively bonded wooden joints. *Int J Adhes Adhes* 51:95–102.
11. Jakięła S, Bratasz Ł, Kozłowski R (2008) Acoustic emission for tracing fracture intensity in lime wood due to climatic variations. *Wood Sci Technol* 42:269–279.
12. Kläusler O, Clauß S, Lübke L, Trachsel J, Niemz P (2013) Influence of moisture on stress–strain behaviour of adhesives used for structural bonding of wood. *Int J Adhes Adhes* 44:57–65.
13. Kläusler O, Hass P, Amen C, Schlegel S, Niemz P (2014) Improvement of tensile shear strength and wood failure percentage of 1C PUR bonded wooden joints at wet stage by means of DMF priming. *Eur J Wood Prod* 72:343–354.
14. Lehringer C, Gabriel J (2014) Review of recent research activities on one-component PUR-adhesives for engineered wood products. In: Aicher S, Reinhardt HW, Garrecht H (eds) *Materials and joints in timber structures*. RILEM Bookseries, vol 9. Springer, Dordrecht
15. Najafi SK, Sharifnia H, Najafabadi MA, Landis E (2017) Acoustic emission characterization of failure mechanisms in oriented strand board using wavelet based and unsupervised clustering methods. *Wood Sci Technol* 51:1433–1446.
16. Reiterer A, Stanzl-Tscheegg SE, Tscheegg EK (2000) Mode I fracture and acoustic emission of softwood and hardwood. *Wood Sci Technol* 34:417–430.
17. Sause MGR, Horn S (2013) Quantification of the uncertainty of pattern recognition approaches applied to acoustic emission signals. *J Nondestruct Eval* 32:242–255.
18. Sause MGR, Gribov A, Unwin AR, Horn S (2012a) Pattern recognition approach to identify natural clusters of acoustic emission signals. *Pattern Recognit Lett* 33:17–23.

19. Sause MGR, Müller T, Horoschenkoff A, Horn S (2012b) Quantification of failure mechanisms in mode-I loading of fiber reinforced plastics utilizing acoustic emission analysis. *Compos Sci Technol* 72:167–174.
20. Vergeynst LL, Sause MGR, Ritschel F, Brunner AJ, Niemz P, Steppe K (2014) Finite element modelling used to support wood failure identification based on acoustic emission signals. In: Franke S, Franke B, Widmann R (eds) *COST timber bridge conference*. Bern University of Applied Sciences, Bern, pp 141–146

4. Additional Investigations

4.1 Modification of the surface properties to improve the fatigue resistance

As noted in paper V, a possible way to improve the fatigue performance of the bond line would be to modify the surface properties of the wood/adhesive interface using a ductile adhesive with a low modulus of elasticity. This would allow to have a higher amount of energy dissipated per cycle and a fracture at the wood interface. Generally, ductile 1C-PUR adhesives with a low elastic modulus also had a low wood fracture percentage. Several methods for modifying the wood surface properties were investigated by (Kläusler et al., 2013) to increase the wood fracture percentage (WFP). For example, applying a solution of Di-methyl Formaldehyde on the wood prior to bonding typically increases the WFP (Kläusler et al., 2013). These results were later used to develop a primer based on a tenside, which modifies the affinity of the wood with the urethane groups of the adhesive (Casdorff et al., 2018). An increase of the WFP using this primer is observed by (Clerc et al., 2018) on ash wood glued laminated timber. Additional experiments on three different 1C-PUR adhesives using the same sample geometry as described in paper III tested under 3-points ENF showed that samples treated with the PR3105 Primer from Henkel had systematically a slower crack propagation at a similar ERR level than non-treated samples, as shown in Figure 4.1.

4.2 Influence of the sample size on the fatigue life

Two types of samples are tested in this thesis, the size of which is convenient for lab testing but may not be representative for full scale timber members. The question therefore arises if the obtained results are verified on full scale timber members. To answer this question, a new sample geometry is developed with a volume approximately 30

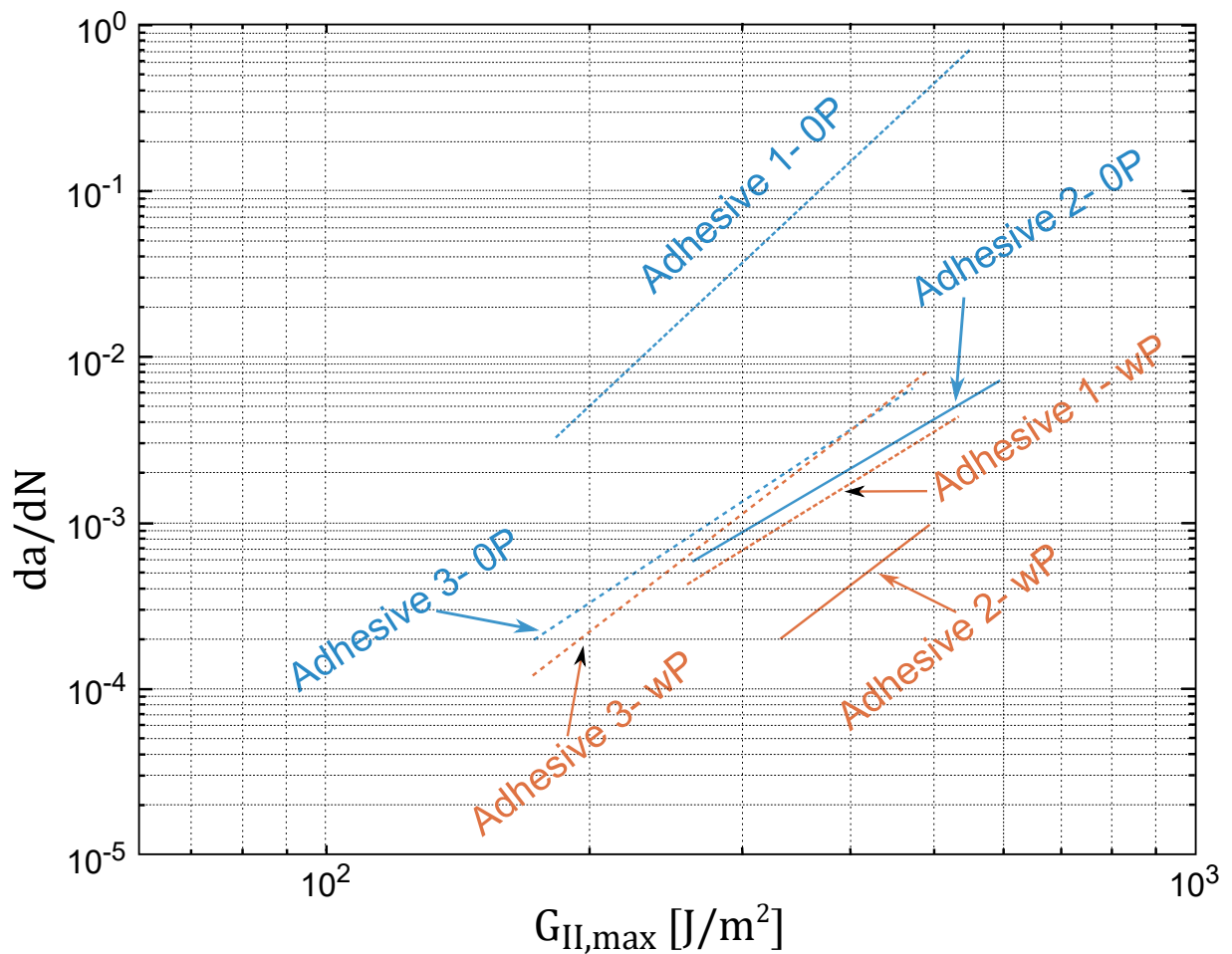


Figure 4.1 – Influence of wood surface modification using the Primer PR3105 on 3-ENF wood samples tested using the same method as described in paper III. Each line represents the average behavior of a set of 3 samples. Primer-treated samples are noted *wP*, while non-treated samples are noted *OP*. On average, a slower crack growth could be observed for samples treated with the Primer.

times bigger than the samples tested in paper III. The wood volume of these "upscaled" samples is increased while assuring that the samples will still fail using the available testing setup. The resulting geometry is described in Figure 4.2.

The same three adhesives as the ones described in the main investigation sections of this thesis are tested. The samples are tested in 3 points flexure under cyclic loading at a frequency of 2 Hz. The crack propagation was indirectly estimated from the change in compliance of the samples. It is indeed not possible to derive the crack length from the compliance of the specimen using the Bernoulli beam theory. The reasons for this are not completely understood but it seems that the Bernoulli beam theory is not applicable in this case due to the central crack causing abrupt changes in the moment of inertia of the beam. Another weak point of this sample geometry is that the crack growth is

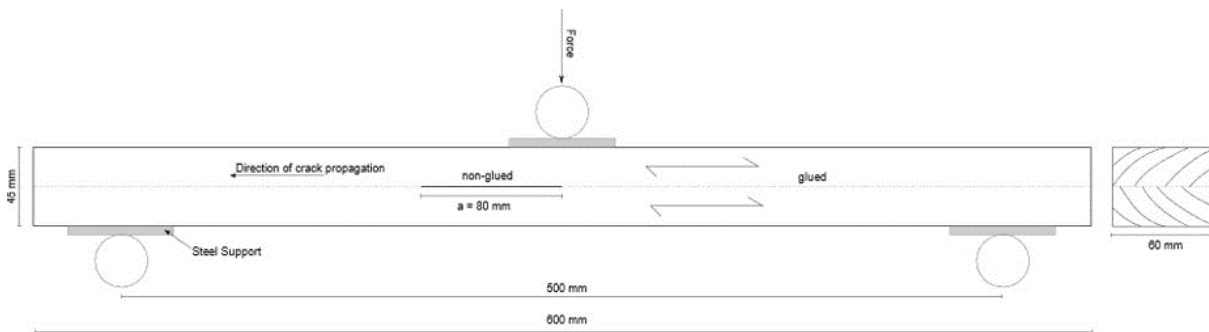


Figure 4.2 – Sample geometry developed to extrapolate the obtained results to full-size timber members

often unstable, meaning that once the critical ERR was reached, the crack propagated almost instantaneously on the complete half-length of the sample. To simplify the analysis of the results, only the number of loading cycles until failure of the sample are noted. On average, it is shown that the PRF adhesive glued samples failed after a significantly higher number of loading cycles than samples glued with the HB 110 and VN 3158 1C-PUR adhesive. Also, samples glued with the HB 110 adhesive fail after a higher number of cycles than those glued with the VN 3158 adhesive. Hence, the obtained results confirm the results presented in paper III and IV on a larger scale. This experiment should be improved to calculate the crack length according to the change in compliance of the specimen. This relatively simple example shows how complex the application of basic fracture mechanics concepts to a sample with well defined geometry can be, hence, this emphasizes the need of research in this topic.

4.3 Use of fracture mechanics for design of bonded joints

In timber construction standards, there are few design problems which require a fracture mechanics approach. One example of fracture mechanics in timber construction is found in EC5, where the design of connections loaded perpendicular to the grain are done according to Linear Elastic Fracture Mechanics (LEFM) (Jockwer and Dietsch, 2018). (Gustafsson et al., 2001) proposed a design approach based on fracture mechanics for the design of glued-in-rods. This approach is however not yet implemented in design standards. Other authors (Bengtsson and Johansson, 2002), (Gustafsson, 1987) proposed to use fracture mechanics for the design of bonded glue line instead of using strength/stiffness criteria. The general issue with fracture mechanics based design is

that despite a more sound physical basis, it is complex to acquire reliable Energy Release Rate values. Probably this is due to the difficulty to determine such values, to the relatively scant available literature on the topic compared to strength values and to the large scatter. For the design of a GLT, the type of adhesive is not considered. The glulam manufacturer may choose from different adhesives which are certified (according to EN 15425 and EN 301) for a given application. The tests required in order to obtain the certification, different for each country, are generally strength based. For example, EN 15425 requires that a set of 10 samples has at least a shear-strength of 10 MPa in order for the adhesive to be used in load bearing structure. The problem with this approach is that the obtained strength value cannot be used in a design standard as it is specific to the test specimen and conditions (as shown in paper II). A further problem with a stress based approach, is that it is not possible to accurately predict what happens once a non-homogeneous stress distribution is encountered, as for example in the case of crack propagation. This is relevant for wood structures where small cracks or delamination develop during service due to the constant swelling/shrinking of the wood. Using the fracture mechanic approach presented in papers III and IV, the obtained G value are material characteristics and less dependent on the sample geometry, which would allow for a possible application in a design guideline. A better knowledge of crack growth over time in GLT could be for example useful in inspection work for determining if a delamination is critical.

4.4 Application of the fatigue model on additional data sets

4.4.1 Comparison with fatigue design according to EC5

In this section, the fatigue model developed in paper II is used to analyze different sets of fatigue data found in the literature and to compare them with the existing design procedure in Eurocode 5 for fatigue. According to EC5, a fatigue design is needed for structures or parts of structures and connections that are subject to frequent stress changes due to traffic or wind loads. Furthermore, a design is needed if the ratio κ exceeds a given values noted in EC5. For example, κ is 0.15 for timber members loaded under shear, 0.1 for nail joints and 0.15 for all other type of joints, but no mention of adhesive joints is made. The κ value can be expressed as an endurance limit value

according to the following equation using a relative stress scale:

$$\sigma_{0,EC5} = \frac{\kappa}{(1 - R)} \quad (4.1)$$

where R is the R-ratio. If the calculated κ value is bigger than the value given in EC5, the reduction factor k_{fat} has to be calculated according to equation 4.2 (adapted from EC5):

$$k_{fat} = 1 - \frac{1 - R}{a(b - R)} \log(N) > 0 \quad (4.2)$$

where a and b are coefficients given in EC5 considering different structure loading configurations.

The first data set was obtained from finger-joints glued with an 1C-PUR adhesive and tested under cyclic fatigue bending four-points loads. In Figure 4.3, the data from (Aicher and Stapf, 2010) are plotted with the corresponding S-N curve calculated according to the method described in paper II. Additionally, the endurance limit σ_0 calculated according to the method shown in paper II is compared to the one obtained according to formula 4.1.

From Figure 4.3 the rate of damage accumulation is similar. The main difference between the EC5 and the model from paper II, is the higher endurance limit of 0.4 obtained using EC5 compared with the 0.18 obtained using the paper II model. The majority of the data tested below 0.4 are run-outs except one sample which failed before the run-out limit. However, according to the model these samples would have failed eventually so that a fatigue design should have been done depending on the required life period of the construction. It should be pointed-out that the configuration tested by (Aicher and Stapf, 2010) corresponded to samples with only one finger joint exactly placed in the middle of the timber beam, i.e. at the zone with the highest stress. Such a configuration would be rare to encounter in practice.

4.4.2 Application of the fatigue model on glued in rods fatigue experiment

The fatigue of glued-in rods is a relevant topic for the study of the the fatigue of adhesive connections in the timber industry. Several studies have investigated the fatigue phenomenon on glued-in rods. In the GIROD project, (Bengtsson and Johansson,

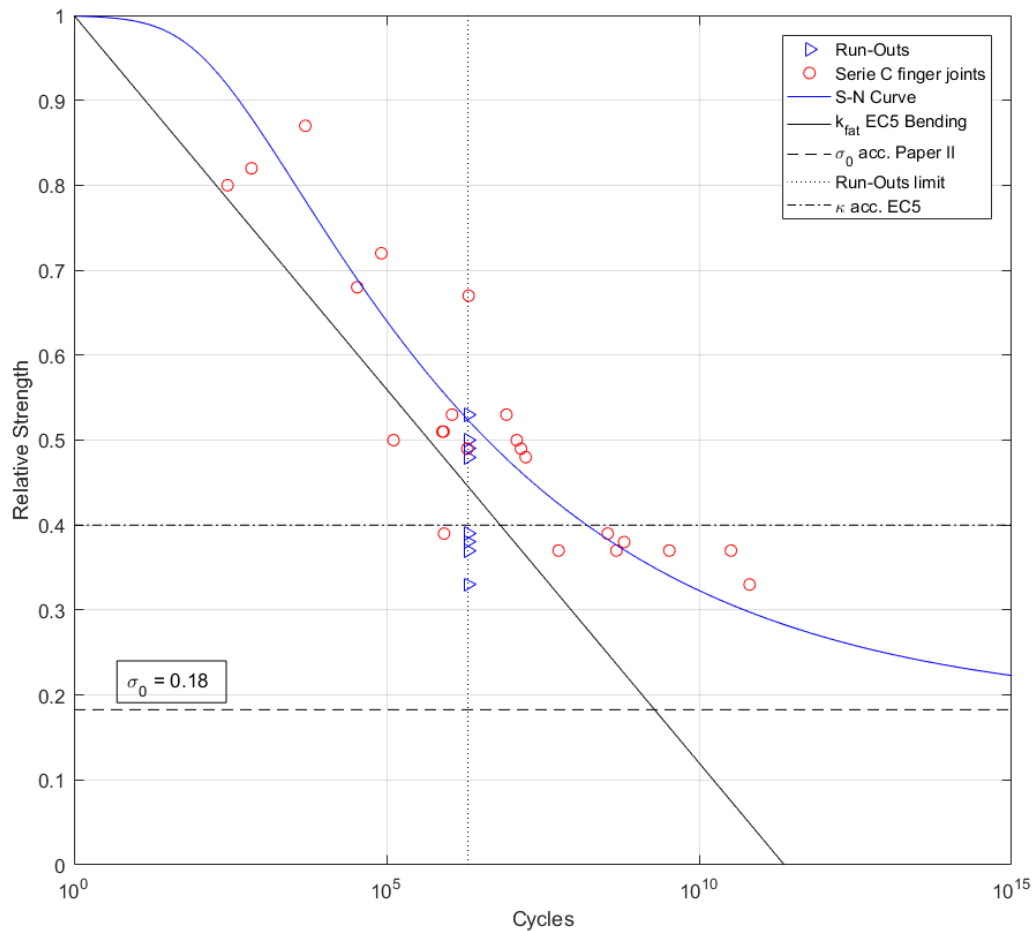


Figure 4.3 – Difference between the reduction factor k_{fat} calculated for bending with a R-factor of 0.5 according to EN 1995-1 and the Fatigue model developed in paper II for the data set C from (Aicher and Stapf, 2010),

2002) investigated the influence of different adhesives on the fatigue of GIR showing that different adhesive types behave in fundamentally different ways with respect to the fatigue performance and the eventual mode of failure at the ultimate fatigue limit state. In comparison with the samples tested in the main investigation section of this thesis, Glued-in rods are generally glued with adhesives able to fill the cavity between the wood and the rods, i.e. 2K-PUR and Epoxy. Also, these adhesives are bonding two different materials with different mechanical properties. (Myslicki et al., 2019) tested the influence of different types of rods glued with several adhesives on Oak and Beech GLT. Different types of fracture were encountered for the same type of specimen depending on the relative load level. For glued-in threaded rods and rebars

wood/adhesive failure occurred in the quasi-static and LCF-range tests, failure shifted towards rod fracture in the HCF-range. For glued-in rebars composed of stainless steel, no change of failure mode was observed, and failure repeatedly occurred at the wood-adhesive interface. This added complexity to the analysis of fatigue tests, as two different models are needed to analyze first the possible rupture of the wood/adhesive, followed by the rupture of the rod. Using the model developed in paper II, it is possible to describe both failure phenomena with the same model. The influence of the R-ratio (between R=0.1 and R=0.5) can be seen in the data from (Myslicki et al., 2019) shown in Figure 4.4. With increasing R-ratio, the S-N curve shifts to the right. This corresponds to a change of the Φ component of the model parameter. In Figure 4.4, it can be seen that the endurance limit σ_0 does not depend on the R-ratio, and that its value is much lower than the κ factor given in EC5.

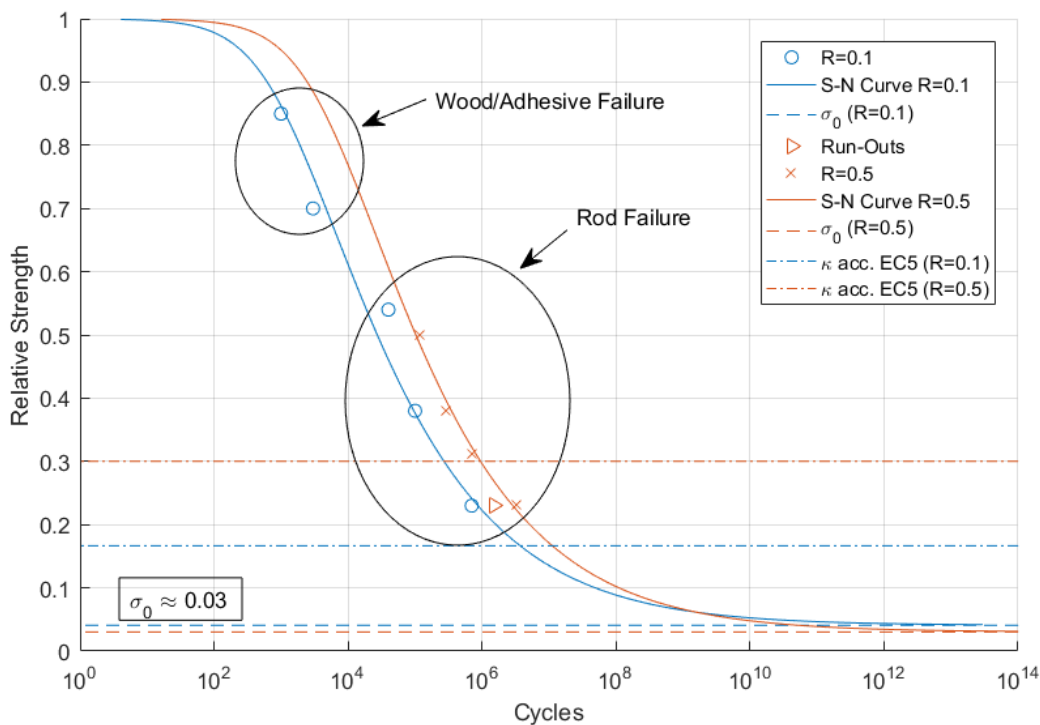


Figure 4.4 – Influence of the R-ratio (0.1 and 0.5) tested at a frequency of 5 Hz for Beech GLT glued-in threaded rods - Data adapted from (Myslicki et al., 2019)

In Figure 4.5, the influence of different glued rod lengths are analyzed using the model described in paper II. GiR glued with a length of 6 times the diameter of the rod are compared with GiR glued with a length of 10 times the diameter of the rod. For a longer glued length, the quasi-static strength is also higher (130 kN for 10d and 80 kN

for 6d), this does not appear in Figure 4.5 as the strength is plotted on a relative scale. Compared on a relative strength axis, the damage accumulation is much faster for the 10d GiR than for the 6d. The endurance limit is 2.6 MPa for the 10d GiR and 12 MPa for the 6d GiR. The damage accumulation, visible through the steeper slope of the S-N curve is faster for the 10d GiR. The main difference between the two S-N curves seems to be the parameters Λ and σ_0 . From the two examples shown in Figure 4.4 and Figure 4.5, the model parameters Φ , Λ and σ_0 could be correlated with physical parameters, i.e. the GiR gluing length and the R-ratio. Further experiments on a bigger data set are needed to verify this correlation and obtain a better understanding of the physics of the fatigue process.

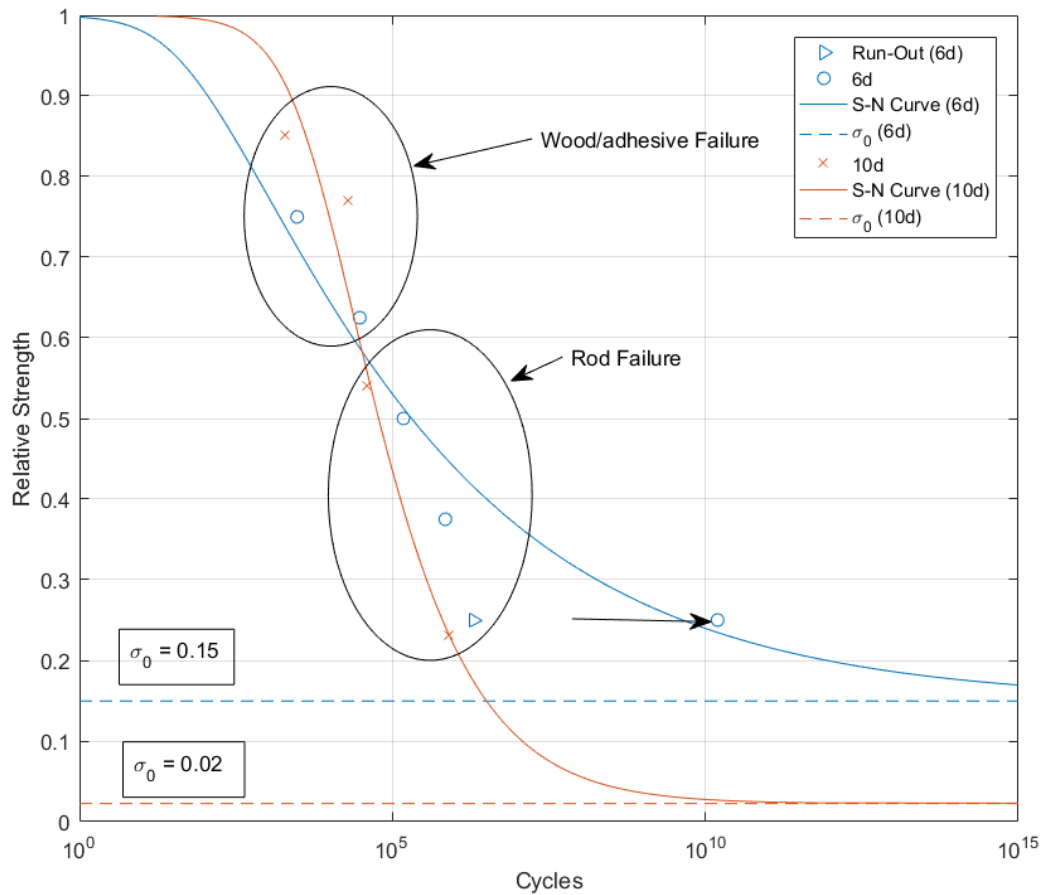


Figure 4.5 – Influence of the glued rod length tested at a frequency of 5 Hz for beech LVL glued-in threaded rods - Data adapted from (Myslicki et al., 2019)

5. Synthesis

5.1 Main findings

The following points have been shown:

- The strength of adhesively bonded wood joints is influenced by the fatigue phenomenon (it is reduced with increasing number of cycles of loading). Fatigue leads to failure at lower load levels than long term static loads, confirming 0.3 as average endurance limit
- The properties of the adhesive influence the fatigue performance of the wood joints
- Brittle and rigid adhesives such as PRF have a slower crack propagation at comparable ERR than ductile adhesives with a low modulus of elasticity (paper III and IV). For lap-shear samples loaded under cyclic fatigue loading, the opposite is observed, i.e. the ductile adhesives can sustain a higher number of cycles at a similar relative stress level than brittle and rigid adhesives
- With increasing humidity, the energy dissipation of adhesive film samples increases. This does not result in an improvement of the fatigue life as the strength degradation under cyclic fatigue loading also increases. This is probably due to a degradation of the adhesion between the wood and the 1C-PUR adhesive under high moisture conditions
- The addition of fibers in the 1C-PUR adhesive helps reducing the speed of crack propagation and increases service life at the given load level
- A new fatigue model combining an empirical model with a probabilistic model is developed to describe the fatigue life at all relative load levels

- The crack propagation in adhesively bonded wood samples can be described using the Paris equation. The application domain of the Paris equation can be expanded using the modified Hartman-Schijve equation, which, for the first time, is successfully applied to describe the fatigue fracture of adhesively bonded wood joints
- A new fractography technique is combined with an unsupervised pattern recognition of AE signals with source location to study the influence of the wood/adhesive morphology on the crack propagation path
- A crack propagating through the wood interface is slower and requires more energy than through the adhesive interface

5.2 Potential for future research

In this thesis two different aspects were investigated:

- Understand the influence of the adhesive properties on the performance of the bond line under cyclic fatigue or fatigue fracture loading at 1 Hz and 5 Hz and R.H. of 35, 50 and 85 %
- Develop or adapt test methods or procedures to study the fatigue phenomenon on adhesively bonded wood samples

For future research these two different aspects can be investigated as follows:

- Only three adhesives (from two different adhesive systems) are studied in this thesis. To better understand the influence of the adhesive properties on the cyclic fatigue performance of the bond line, several other adhesives with different properties should be tested, for example brittle adhesive systems such as MUF, UF or ductile two components PUR with a thick adhesive layer. These adhesive systems would result in different stress distributions in the bond line and possibly to different damages accumulation. An interesting alternative research path could be to modify the wood surface properties to improve the adhesion while maintaining a high ductility of the adhesive. For example by using a tensioactif to provide a link between the urethane bond of the adhesive and the hydroxyl bond in the wood. Or by increasing the surface roughness prior to bonding which should increase the total gluing surface and generate semi-detached wood fibers

which could have a similar effect as the fibers added directly to the adhesive. Only a limited number of fibers was investigated, it was shown that the addition of fibers helps reducing the speed of crack propagation. Other types of fibers such as composed of different material, or different shape might be increasing the performance even more. A further potential domain of application would be to investigate whether the results presented here are valid outside the scope of surface gluing, i.e. for Glued-in rods or end-grain gluing.

- The feasibility of using the different testing methods developed in this thesis in a design guideline, should be investigated. A fracture mechanics approach is promising as it would allow to obtain material characteristics theoretically independent from the sample geometry. This would then allow to design bonded connections for a given loading condition, an approach which is not yet possible with the available lap-shear and delamination tests. Those tests could be used for quality control as their results are highly dependent on the sample geometry. Also, the model developed in paper II was successfully used for analyzing the fatigue data set. To obtain a better understanding of the role of the different model parameters, this model should be used on other data sets to examine the influence of the testing methods and sample type on the model parameters.

5.3 Recommendation for fatigue testing

Due to high scatter generally encountered in fatigue testing, a careful planned experiment is necessary in order to obtain satisfying results. For the determination of S-N curves using the model developed in paper II, it is necessary to have sufficiently different last level. Indeed, an optimal sample distribution would be to test 3 samples for 4 different load levels. The time needed to test HCF samples is generally underestimated, resulting in not enough samples tested at low last level. Generally, a reduction of the testing variables could be recommended to increase the significance of the results.

5.4 Closing words

The results of this thesis help understanding how the properties of the adhesive influence the fatigue performance of adhesively bonded wood joints. It has been shown that ductile adhesives tend to reduce the accumulation of microdamages due to a more homogeneous stress distribution. However, once a crack appears and propagates a stiff adhesive is favorable as the crack propagates slower in the wood layers than at the adhesive interface. Further experiments investigating the influence of surface modification should be conducted in order to understand how to combine a crack propagation in the wood layer with a ductile adhesive in order to design new adhesives with improved fatigue performance. Another potential domain of application of the results obtained in this thesis, is the development of a new design method. Two different aspects could be investigated. First, the fatigue model presented in paper II for predicting the strength degradation. This model could be implemented in the design of fatigue exposed timber-members and for different types of connections. Further research is needed, to be able to understand how different samples' or structures' parameters influence the fatigue stress-life curves. A second point is the use of the Paris or Hartmann-Schijve equation to be able to predict whether a crack will propagate or not given a specific loading condition. The potential of such a method is important as nowadays the prediction of the crack propagation is done according to the experience of the inspector in the case of partial delamination in glued laminated timber. This approach requires further research to better understand the influence of several parameters on the Energy Release Rate values under quasi-static and fatigue-cyclic loading and how the delamination develops with respect to the length and depth of the crack in the longitudinal and transversal direction respectively.

6. References

Bibliography

- Aicher, S. and Stapf, G. (2010). Fatigue behaviour of finger jointed lumber. *International Council for research and innovation in building and construction Working commission W18 - Timber Structures*, CIB-W18/43-12-1.
- Ammann, S. and Niemz, P. (2014). Fibre and adhesive bridging at glue joints in european beech wood. *Wood Research*, 59(2):303–312.
- Ammann, S. and Niemz, P. (2015a). Mixed-mode fracture toughness of bond lines of prf and pur adhesives in european beech wood. *Holzforschung*, 69(4):415–420.
- Ammann, S. and Niemz, P. (2015b). Specific fracture energy at glue joints in European beech wood. *International Journal of Adhesion & Adhesives*, 60:47.53.
- Ando, K., Hirashima, Y., Sugihara, M., Hirao, S., and Sasaki, Y. (2006). Microscopic processes of shearing fracture of old wood, examined using the acoustic emission technique. *Journal of wood science*, 52:483–489.
- Bach, L. (1975). Frequency-dependent fracture in wood under pulsating loading. *FRPS-Annual meeting Proceedings*, June 1975:Portland, Oregon, USA.
- Bachtiar, E., Clerc, G., Brunner, A. J., Kaliske, M., and Niemz, P. (2017). Static and dynamic tensile shear test of glued lap wooden joint with four different types of adhesives. *Holzforschung*, 71(5):391–396.
- Baensch, F. (2015). *Damage evolution in wood and layered wood composites monitored in situ by acoustic emission, digital image correlation and synchrotron based tomographic microscopy*. Diss. ETH No. 22372.

BIBLIOGRAPHY

- Bengtsson, C. and Johansson, C.-J. (2002). *GIROD - Glued in Rods for Timber Structures*. SP Swedisch National Testing and Research Institute, Report: 2002:26.
- Bertolin, C., de Ferri, L., Grottesi, G., and Strojceki, M. (2020). Study on the conservation state of wooden historical structures by means of acoustic attenuation and vaccum microbalance. *Wood Science and Technology*, 54:203–226.
- Bohse, J. and Brunner, A. J. (2008). *Delamination Behaviour of Composites - Acoustic emission in delamination investigation*, volume 25. Woodhead Publishing Series in Compistes Science and Engineering.
- Casdorff, K., Kläusler, O., Gabriel, J., Amen, C., Lehringer, C., Burgert, I., and Keplinger, T. (2018). About the influence of a water-based priming system on the interactionsbetween wood and one-component polyurethane adhesive studied by atomic force microscopy and confocal raman spectroscopy imaging. *International journal of adhesion and adhesives*, 80:52–59.
- Clauss, S., Dijkstra, D. J., Gabriel, J., Kläusler, O., Meckel, W., and Niemz, P. (2011). Influence of the chemical structure of pur prepolymers on thermal stability. *Internation Journal of Adhesion and Adhesives*, 31:513–523.
- Clerc, G., Brülisauer, M., Affolter, S., Volkmer, T., and Pichelin, F. (2017). Characterization of the ageing process of one-component polyurethane moisture curing wood adhesive. *International journal of adhesion and adhesives*, 72:130–138.
- Clerc, G., Lehmann, M., Gabriel, J., Salzgeber, D., Pichelin, F., Strahm, T., and Niemz, P. (2018). Improvement of ash (*fraxinus excelsior* l.) bonding quality with one-component polyurethane adhesive and hydrophilic primer for load-bearing application. *International Journal of Adhesion and Adhesives*, 85:303–307.
- Clorius, C. O. (2002). *Fatigue in wood*. Danmarks Tekniske Universitet, PhD Thesis.
- Clorius, C. O., Hoffmeyer, M. U., and Damkilde, L. (2000). Compressive fatigue in wood. *Wood science and technology*, 34:21–37.
- Forest Products Laboratory (1989). *Handbook of wood and wood-based materials for engineers, architects, and builders*. Forest, U.S. Departement of Agriculture. Hemisphere Publishing Corporation, New York, NY, USA.

BIBLIOGRAPHY

- Griffith, A. A. (1921). The phenomena of rupture and flow in solids. *Philosophical Transactions of the Royal Society of London*, 221:163–198.
- Gustafsson, P. J. (1987). Analysis of generalized volkersen-joints in terms of non-linear fracture mechanics. *International council for building research studies and documentation working commission W18A - Timber Structures*, CIB-W18A/20-18-2.
- Gustafsson, P. J., Serrano, E., Aicher, S., and Johansson, C.-J. (2001). A strength design equation for glued-in rods. *Symposium, Joints in Timber Structures; 2001; Stuttgart, Germany*, RILEM:323–332.
- Habenicht, G. (2009). *Applied adhesive bonding: A practical guide for flawless results*. Wiley.
- Hartman, A. and Schijve, J. (1970). The effects of environment and load frequency on the crack propagation law or macro fatigue crack growth in aluminium alloys. *Engineering Fracture Mechanics*, 1:615–631.
- Hass, P., Wittel, F. K., Mendoza, M., Herrmann, H. J., and Niemz, P. (2012). Adhesive penetration in beech wood: experiments. *Wood Science and Technology*, 46:243–256.
- Hirsch, G. and Bachmann, H. (1995). *Wind-induced vibrations, In Vibration Problems in Structures: Practical Guidelines*, chapter 3. Eds. Birkhäuser Basel.
- Ingólfsson, E., Georgakis, C., and Jönsson, J. (2012). Pedestrian-induced lateral vibrations of footbridges: A literature review. *Engineering Structures*, 45:21–52.
- Jockwer, R. and Dietsch, P. (2018). Review of design approaches and test results on brittle failure modes of connections loaded at an angle to the grain. *Engineering and Structures*, 171:362–372.
- Jones, R., Pitt, S., Brunner, A. J., and Hui, D. (2012). Application of the Hartman-Schijve equation to represent Mode I and Mode II fatigue delamination growth in composites. *Composite Structures*, 94:1343–1351.
- Kamke, F. A. and Lee, J. N. (2007). Adhesive penetration in wood - a review. *Wood and Fiber Science*, 39:205–220.
- Kläusler, O., Clauss, S., Lübke, L., Trachsel, J., and Niemz, P. (2013). Influence of moisture on stress-strain behaviour of adhesives used for structural bonding of wood. *International Journal of Adhesion and Adhesives*, 44:57–65.

BIBLIOGRAPHY

- Kläusler, O., Hass, P., Amen, C., Schlegel, S., and Niemz, P. (2014). Improvement of tensile shear strength and wood failure percentage of 1c pur bonded wooden joints at wet stages by means of dmf priming. *European Journal of Wood and Wood Products*, 72(3):313–354.
- Kollmann, F. F. P. (1968). *Principles of wood science and technology*. Springer-Verlag Berlin Heidelberg.
- Luedtke, J., Amen, C., van Ofen, A., and Lehringer, C. (2015). 1c-pur-bonded hardwoods for engineered wood products: influence of selected processing parameters. *European Journal of Wood and Wood Products*, 73:167–178.
- Madhousi, M. and Ansell, M. (2004). Experimental study of static and fatigue strengths of pultruded gfrp rods bonded into lvl and glulam. *International Journal of Adhesion and Adhesives*, 24:319–325.
- Marra, A. A. (1992). *Technology of wood bonding, Principles in practice*. Kluwer Academic.
- Martin, R. H. and Davidson, B. D. (1999). Mode II fracture toughness evaluation using four point bend, end notched flexure test. *Plastics, Rubber and Composites*, 28:401–406.
- Müller, U., Müller, H., and Teischinger, A. (2004). Durability of wood adhesives in 50 year old aircraft and glider constructions. *Wood Research*, 49(3):25–33.
- Myslicki, S. (2016). Short-time procedure for fatigue assessment of beech wood and adhesively bonded wood joints. *Materials and Structures*, 49(6):2161–2170.
- Myslicki, S., Bletz-Mühldorfer, O., Diehl, F., Lavarec, C., Vallée, T., Scholz, R., and Walther, F. (2019). Fatigue of glued-in rods in engineered hardwood products — part i: experimental results. *The journal of adhesion*, 95:675–701.
- Niemz, P. and Sonderegger, W. (2017). *Holzphysik - Physik des Holzes und der Holzwerkstoffe*. Hanser.
- Okuyama, T., Itoh, A., and Marsoem, S. N. (1984). Mechanical responses of wood to repeated loading i; tensile and compressive fatigue fractures. *Journal of Japanese Wood Research Society*, 30(10):791–798.
- Ota, M. and Tsubota, Y. (1967). Studies on the fatigue of 2-ply laminated wood, parts iv. *J. Japan Wood Res. Soc.*, 13:131–137.

BIBLIOGRAPHY

- Paris, P. and Erdogan, F. (1963). A critical analysis of crack propagation laws. *Journal of Basic Engineering*, 85:528–533.
- Pérez-Galmés, M., Renart, J., Sarrado, C., Brunner, A. J., and Rodríguez-Bellido, A. (2018). Towards a consensus on mode II adhesive fracture testing: Experimental study. *Theoretical and Applied Fracture Mechanics*, 98:210–219.
- Ren, D. and Frazier, C. E. (2012). Wood/adhesive interactions and the phase morphology of moisture-cure polyurethane wood adhesives. *International Journal of Adhesion and Adhesives*, 34:55–61.
- Rhême, M., Botsis, J., Cugnoni, J., and Navi, P. (2013). Influence of the moisture content on the fracture characteristics of welded wood joint. part 1: Mode I fracture. *Holzforschung*, 67:747–754.
- Schuecker, C. and Davidson, B. D. (2000). Effect of friction on the perceived mode II delamination toughness from three- and four-point bend end-notched flexure tests. *Composite Structures: Theory and Practice*, pages 334–344.
- Smith, I., Landis, E., and Gong, M. (2003). *Fracture and Fatigue in Wood*. Wiley.
- Sterr, R. (1963). Investigation of the fatigue properties of laminated wood beams. *Holz als Roh- und Werkstoff*, 21(2):47–61.
- Tsai, K. T. and Ansell, M. P. (1990). The fatigue properties of wood in flexure. *Journal of Materials Science*, 25:865–878.
- van der Put, T. A. C. M. (2007). A new fracture mechanics theory for orthotropic materials like wood. *Engineering Fracture Mechanics*, 74:771–781.
- Weaver, F. W. and Owen, N. L. (1995). Isocyanate - wood adhesive bond. *Applied Spectroscopy*, 49:171–176.
- Xavier, J., Morais, J., Dourado, N., and de Moura, M. F. S. F. (2011). Measurements of mode I and mode II fracture properties of wood-bonded joints. *Journal of Adhesion Science and Technology*, 25:2881–2895.
- Yelle, D. J. and Ralph, J. (2016). Characterizing phenol formaldehyde adhesive cure chemistry within the wood cell wall. *International Journal of Adhesion and Adhesives*, 70:26–36.

BIBLIOGRAPHY

- Yoshihara, H. (2005). Examination of the 4-enf test for measuring the mode III r-curve of wood. *Engineering and Fracture Mechanics*, 73(1):42–63.
- Yoshihara, H. and Satoh, A. (2007). Shear and crack tip deformation correction for the double cantilever beam and three-point end-notched flexure specimens for mode I and mode II fracture toughness measurement of wood. *Engineering Fracture Mechanics*, 76:335–346.

7. Acknowledgment

This dissertation was mostly accomplished at the Bern University of Applied Science in Biel (CH). The financial support of this work by the Swiss Innovation Agency (Innosuisse) under grant 18958.1 is gratefully acknowledged.

First of all, I would like to thank Prof. Dr. Peter Niemz who rendered this thesis possible with his personal and scientific support during the last years. Also, many thanks are due to my supervisor Prof. Dr. Jan Willem van de Kuilen (TUM, Holzforschung) and to Dr. Andreas J. Brunner (Empa, Switzerland) for his precious help. I am also grateful to Prof. Dr. Markus Sause (Uni. Augsburg) for his support. Special thanks go to Dr. Sebastian Josset and his team at Henkel for supporting this project.

I am also grateful to Martin Lehmann and Frédéric Pichelin from the BFH for their support. My thank also go to Martin Otti, Bruno Salzmänn from the BFH, Daniel Völkli from Empa and Thomas Wasenegger from Henkel for their support in specimen preparation and testing.

8. Curriculum Vitae

Gaspard Clerc

- Date of birth: 18.09.1988
- Place of birth: Aigle, Switzerland
- Nationality: Swiss/French
- E-mail adress: gaspard.clerc@gmail.com

Education

- 2015-2018 **Master in wood technology-part time study**, *Bern University of applied sciences*, Option: complex timber structures, Biel
- 2011-2015 **Bachelor of science in wood technology**, *Bern University of applied sciences*, Option: Timber structure and technology, Biel
- 2007-2011 **Federal Diploma of Vocational Education and Training in Violin Making**, *Swiss school of violin making*, Brienz-Switzerland.
- 2004-2007 **High School Diploma**, *Gymnase de Burier*

9. List of Publications and Conference Papers

Publications (Peer-reviewed)

G. Clerc, M. Brülisauer, S. Affolter, T. Volkmer, F. Pichelin and P. Niemz Characterization of the ageing process of one-component polyurethane moisture curing wood adhesive; *International Journal of Adhesion and Adhesives*; 72, 130-138, 2017

E.V. Bachtiar, G. Clerc, A.J. Brunner, M. Kaliske and P. Niemz; Static and dynamic tensile shear test of glued lap wooden joint with four different types of adhesives; *Holzforschung*; 71(5), 391-396, 2017

G. Clerc, M. Lehmann, J. Gabriel, D. Salzgeber, F. Pichelin, T. Strahm and P. Niemz; Improvement of ash (*Fraxinus excelsior* L.) bonding quality with one-component polyurethane adhesive and hydrophilic primer for load-bearing application; *International Journal of Adhesion and Adhesives*; 85, 303-307, 2018

G. Clerc, A.J. Brunner, S. Josset, P. Niemz, F. Pichelin and J-W. van de Kuilen; Adhesive wood joints under quasi-static and cyclic fatigue fracture Mode II loads; *International Journal of Fatigue*; 123, 40-52, 2019

T. Künniger, G. Clerc, S. Josset, P. Niemz, F. Pichelin, J-W. van de Kuilen; Influence of humidity and frequency on the energy dissipation in wood adhesives; *International Journal of Adhesion and Adhesives*; 92, 99-104, 2019

G. Clerc, M.G.R Sause, A.J. Brunner, P. Niemz and J-W. van de Kuilen; Fractography combined with unsupervised pattern recognition of acoustic emission signals for a better understanding of crack propagation in adhesively bonded wood; *Wood Science and Technology*; 53(6), 1235-1253, 2019

G. Clerc, A.J. Brunner, P. Niemz and J-W. van de Kuilen; Feasibility study on Hartman–Schijve data analysis for mode II fatigue fracture of adhesively bonded wood joints; *International Journal of Fracture*; 221(2), 123-140, 2020

G. Clerc, T. Lüthi, P. Niemz and J-W. van de Kuilen; Reaction kinetics investigation in relation to the influence of humidity on fatigue behavior of wood lap joints, *Holzforschung*, published online, doi.org/10.1515/hf-2019-0136

Conference Papers

G. Clerc, T. Volkmer, F. Pichelin, P. Niemz; Characterization of the ageing process of one component polyurethane moisture curing wood adhesive; *World Conference Timber Engineering*, 2016, Vienna

A.J. Brunner, G. Clerc and P. Niemz; Acoustic emission monitoring of adhesively bonded wood joints under quasi-static and cyclic fatigue mode II flexure loads using end-notch-flexure specimens; *Conference proceedings EWGAE 2018*, Senlis

G. Clerc, A.J. Brunner, P. Niemz, and J-W. van de Kuilen; Anwendung geführter Wellen aus der Überprüfung der Sensorkopplung für die Bestimmung von Prüfkorpereigenschaften und Schädigungsgrad; 22. Kolloquium Schallemission DGZfP 2019, Karlsruhe

G. Clerc, M.G.R Sause, A.J. Brunner, P. Niemz and J-W. van de Kuilen; Unsupervised Pattern Recognition of Acoustic Emission Signals of Adhesively Bonded Wood; 21st International Nondestructive Testing and Evaluation of Wood Symposium, 2019, Freiburg